Laminate Zeolite Structure prepared using Papermaking Techniques for Carbon Dioxide Capture: Synthesis, Characterisation and Performance

Sigappi Narayanan

Bachelor of Chemical and Materials Engineering (Honours)

University of Auckland

Submitted in fulfilment of the requirements for the

Degree of Doctor of Philosophy

Australian Pulp and Paper Institute

Department of Chemical Engineering

Monash University

April 2014

This page is intentionally blank

Declaration

This thesis contains no material which has been accepted for the award of any other degree or diploma in any university. To the best of my knowledge and belief, it contains no material previously written or published by another person, expect where due reference is made in the text.

Sigappi Narayanan

This page is intentionally blank

TABLE OF CONTENTS

Dedicated to my family and friends

Acknowledgements

It is a great privilege to use this opportunity to thank everyone who has been instrumental in the completion of my thesis.

I would like to express my heartfelt appreciation and gratitude to my supervisors Dr. Warren Batchelor and Professor Paul Webley for their constant encouragement, valuable advice and unwavering support throughout my candidature. Warren and Paul have been exceptional individuals and have guided me patiently throughout my candidature. The excellent working atmosphere and motivation they provided have helped me complete this project. They are also very resourceful and innovative and without them this project would not be possible.

I would like to thank all the academic staff members at APPI and the Department of Chemical Engineering at Monash University. My special thanks to Dr. Emily Perkins, Dr. Penny Xiao and Dr. Ranjeet Singh from Warren's and Paul's group for their guidance, encouragement and friendship throughout my project. I would like to thank Professor Gil Garnier and Professor Wei Shen for their advice during my time at APPI.

I would like to acknowledge Dr. Aidan Sudbury from the School of Mathematical Sciences for his help with devising a statistical plan to test my structures. I would like to thank the Monash Centre for Electron Microscopy for giving access to their advanced Scanning Microscopy equipment and their ever helpful staff mainly Dr. Flame Burgmann and Dr. Xi-Ya Fang.

I would like to thank all the administrative and technical staff at APPI and Chemical Engineering. My thanks go to Janette Anthony, Lilyanne Price, Jill Crisfield, Chloe Priebee and Gary Thunder for their assistance with administrative matters. I would also like to acknowledge the support of Kim Phu, Ron Graham, Gamini Ganegoda, Martin Watkins, Harry Bouwmeester and Ross Ellingham for all their technical help.

I would like to thank Hui Hui Chiam, Rosiana Lestiani and Matthew O'Connor for being great friends and making my time at APPI enjoyable. I would like to thank Xu Li, Miaosi Li, Tina Arbatan, Liyuan Zhang, Sharmiza Adnan, Galuh Yuliani, Scot Sharman, Purim Jarujamrus, Jielong Su, Lizi Li, Varanasi Swambabu, David Ballerini, Whui Lyn Then, Azadeh Nilghaz, Natasha Yeow and Heather McLiesh for their friendship during my project.

Lastly, I would like to thank my mother, father and sister for their love, understanding and support in the completion of my PhD study. Without their encouragement, this study would not have been possible.

Abstract

Carbon capture and storage technology has become a possible solution to address the problem of global warming due to the increasing use of fossil fuels. The application of this technology by many carbon dioxide emitting industrial units is still hindered by the process and equipment cost associated with the capture of carbon dioxide. Zeolites have become a major player in this field due to their high adsorption capacity for carbon dioxide. Traditional use of zeolites in the form of pellets or beads has issues relating to high mass transfer resistance and increased energy consumption required to overcome high pressure drop for such systems. Novel structured adsorbents have been developed to manage these problems but they require high precision and cost for their manufacture. Although they are superior to beads/pellets in terms of breakthrough characteristics, they have very low loading of adsorbent.

To overcome the limitations of high cost and low loading of non-particulate structures and the disadvantages of the conventional adsorbent structures, new preparatory techniques for adsorbent structures are being researched. For more practical applications, a zeolite structured adsorbent needs to be created that has high adsorption capacity, low pressure drop, high mass transfer and provides overall high system efficiency. In addition, the very large scale of the flue gas capture application demands that the adsorbent structure should be made using low cost materials and processes. Motivated by the low cost of papermaking technology, we have studied and adapted this technique to create a highly loaded, large surface area sheet structure. Zeolites have already found use in the paper industry as fillers and retention aids and can therefore be easily adapted to current paper mills to create structured laminate adsorbents.

This project looks towards creating zeolite laminate structured adsorbent using papermaking techniques for carbon dioxide capture. The selection of materials for the preparation of laminate

structures is initially done to create structures that are strong and have high porosity with high loading of zeolite. An easy method of preparing laminate zeolite sheet structures is also outlined. This leads to the next part of the project which is characterisation of the zeolite laminate sheet structures. Although few materials were used in preparation of the sheets, the many variables involved in sheet forming would make it very time consuming to create each unique sheet structure and characterise the properties. Hence, to speed up the process, a partial factorial design method was used to characterise the laminate sheets. 16 experiments were completed.

SEM and mercury porosity methods were used to characterise the porosity of the sheet structures. These results show that porosity of the structure is mainly affected by the amount of silica present in the structure. Nitrogen adsorption and carbon dioxide adsorption measurements were studied to determine the loading in the laminate sheet structures, since the adsorption capacity is completely dependent on the zeolite. The strength of the laminate structures were measured using a novel testing method as it was difficult to apply the routine strength measurement methods to some of the weak laminate samples. Considering the application of the laminate structures, a vibratory sieve was used to determine the comparative strength of the different structures from the partial factorial design. It was found that laminate structures with either 40-55wt% micron zeolite or 30wt% nano zeolite had adequate strength for breakthrough testing. Structures with higher loading of zeolite fell apart very easily. The kinetics of the laminate samples were also measured using the Rate of Adsorption software in ASAP 2010. These results show that the presence of nano zeolite increases the adsorption kinetics of the laminate structures and on the whole the laminate structure had higher kinetics when compared to powder or beads due to overcoming macropore diffusion resistance.

The structures which had the best characteristics from the partial factorial design were used for breakthrough testing. Testing for different porosities, it was found that structures with high porosity i.e. samples having 40wt% zeolite had higher effective diffusivities and lower pressure drop when compared to structure with low porosity i.e. samples having 20wt% zeolite. Other methods of increasing spacing between the folds of the laminate structures were also tested and using a wire to create spacing was found to be the best method to lower pressure drop. In some instances, the effective diffusivities were reduced while in other instances they were the same. But the method of winding to produce laminate structures for breakthrough testing produced highly variable results.

An idea of printing hydrophobic channels on the paper samples was considered to improve breakthrough characteristics of the laminate structures. Since printing is easy, cheap and can be adapted to a large industrial setting, this method of creating channels for gas flow in the laminate structures has many advantages. An initial assessment of this method showed that using AKD to create hydrophobic patterns on the sheet was successful as different levels of depth were observed between the AKD treated and untreated sections in the final laminate structure. To create distinguishable regions of AKD treated and untreated sections, the amount of the zeolite loading and ceramic loading were also fixed at 8g zeolite and 6.5g ceramic fibres. A method of printing parallel hydrophobic channels was established and the sheets were coated with two different weight % of colloidal silica (40wt% and 20wt%). These differing amounts of colloidal silica create laminate structures with different depths of channels as seen from SEM imaging. Breakthrough assessment of the printed laminate structures show that the structures with 20wt% silica have higher effective diffusivities and lower pressure drop when compared to structures with 40wt% silica or structures without hydrophobic printing, showing that laminate structures with printed channels is a very attractive adsorbent structure for CO_2 capture.

This page is intentionally blank

List of Figures

List of Tables

Abbreviations

AKD - Alkyl Ketene Dimer

APPI - Australian Pulp and Paper Institute

ASAP - Accelerated Surface Area and Porosimetry Analyser

BDF - Backward Differentiation Formula

CCS - Carbon Capture and Storage

CHA - Chabazite

CPAM- Cationic Polyacrlyamide

ESA - Electrical Swing Adsorption

FAU - Faujasite

GCC - Ground Calcium Carbonate

gsm - grammage/ grams per square metre

HCl - Hydrochloric acid

HNO_3 - Nitric acid

LTA - Linde Type A

MBSF - Moving belt Sheet former

MC - Methyl cellulose

MCEM - Monash Centre for Electron Microscopy

MTZ - Mass Transfer Zone

NaOH - Sodium hydroxide

NO_x - Nitrogen oxides

OD - Outer diameter

PCC - Precipitated Calcium Carbonate

PDADMAC - Poly diallyldimethlylammonium chloride

PSA - Pressure Swing Adsorption

SEM - Scanning Electron Microscopy

SSA - Specific Surface Area

SO_x - Sulfur oxides

TiO_2 - Titanium dioxide

TMP - Themomechanical Pulp

TSA - Temperature Swing Adsorption

VOC - Volatile Organic Compounds

XRD - X-Ray Diffraction

Nomenclature

a- Final weight proportion that the sample reaches

b- adsorption constant

c- Degradation rate

d- adsorption constant

h_w – Heat transfer co-efficient from bed to the wall

k – Rate of adsorption

l –Characteristic dimension of laminate sheet (thickness)

m_1 and **m_2** – Maximum amount adsorbed

n- Instantaneous adsorption loading of the sample

n_{eq}- Equilibrium amount adsorbed

n_i- Amount of component i adsorbed

q_i- Isosteric heat

t- Time

u- Interstitial velocity

w- Spacing between the sheets

y- Weight loss %

z- Bed length

C- Total gas concentration

$\mathbf{C_{ads}}$- Adsorbent heat capacity

$\mathbf{C_{gas}}$- Gas heat capacity

$\mathbf{C_i}$- Concentration of component i

D – Diameter of a cylindrical pore

$\mathbf{D_{ei}}$- Effective diffusivity parameter

$\mathbf{D_p}$- Average diameter of the beads

P – Pressure

$\mathbf{P_{eq}}$- Gas pressure corresponding to equilibrium amount adsorbed

ΔP- Pressure drop

Q- Heat of adsorption

R- Ideal gas constant

T- Temperature

$\mathbf{T_w}$- Wall temperature

γ – Surface tension of mercury

θ – Contact angle mercury forms against solid

ε_B- Bed voidage

ρ_{ads}- Adsorbent density

ρ_{bed}- Bed density

μ- Viscosity of the gas mixture

v_0- Superficial velocity of the gas mixture

ϕ_b- Sphericity of the beads

Chapter 1

Introduction

This page is intentionally blank

1.0 Introduction

Zeolites are hydrated, microporous, alkali alumino-silicates with applications in many fields*[1-21]*. Synthetic zeolites are currently being used in high end applications as molecular sieves, ion exchangers, adsorbents and catalysts. Many more applications in other industries are anticipated with the discovery of larger deposits of natural zeolites*[16]*.

Zeolites play a dominant role as physical adsorbents owing to their ability to adsorb large quantities of material thereby achieving extremely low mole fractions of these adsorbed compounds in the product gas. Their internal porosity is high and the majority of the adsorption takes place internally. Physical adsorption takes place where the cavities fill and desorb by emptying reversibly and the mechanism is generally considered to be one of pore filling*[9, 22-25]*. Large pores in the zeolite structure act as passageways for molecules to diffuse from the surrounding environment into the interior of the particle. Once inside the particle, the molecules will diffuse into the interior of the microparticle. The pore size of the microparticle is of the order of molecular dimensions and molecules inside the micropores never escape the attraction potential of the pore walls.

The use of papermaking techniques to create structured adsorbents is an important new area of zeolite application. Current adsorbent structures such as beads and pellets have high mass transfer resistance and pressure drop while pre-formed monolith structures have a high cost associated with their preparation and low adsorbent loading present in the structure*[22, 26, 27]*. Papermaking is a highly developed field, the methods of which may be used in creating thin, high density adsorbent sheets that will have improved mass transfer and reduced pressure drop. The preparation of zeolite filled sheets is made much easier as they already play a role in the paper industry as fillers and retention aids in areas where natural zeolite is available in

abundance*[28, 29]*. Zeolite is an unconventional product owing to its characteristic three dimensional channel shape which influences many of its properties. Fillers are used in the pulp and paper industry mainly to reduce production costs, to improve printability and runnability, for mechanical and chemical retention and to improve optical properties*[30]*. While fillers have various benefits, their addition to the pulp slurry reduces mechanical strength and stiffness while increasing dusting tendency. The addition of fillers can also increase deposits in the papermaking machine and provide additional components in the white water circulation loop. Zeolites not only work well as fillers but due to their action as adsorbents and ion exchangers, they can be used to create value added paper products and help in dealing with some of the problems associated with fillers. This opens up many avenues for the paper industry to explore.

Motivated by the low cost of papermaking technology, the application of the papermaking technique to create a highly loaded, large surface area sheet structure is considered. The zeolite sheets created by this method are required to be thin, lightweight, have a homogenous distribution of zeolite, be easy to handle, flexible to process and have microporosity, mesoporosity and macroporosity due to the addition of different components*[31, 32]*. It is believed that by incorporating a zeolite adsorbent structure with macropores and mesopores, the properties of the micro, meso and macropores can be exploited simultaneously. By creating a structure with varying pore size distributions, channels of appropriate dimensions are formed for gas flow leading to lower pressure drop and easier transport through the structure while maintaining sharp breakthrough fronts and high mass transfer coefficients*[22]*.

The goal of this research is to use simple papermaking techniques to create zeolite laminate sheet structures with high porosity for better adsorption performance of capturing carbon dioxide. Chapter 2 in this thesis reviews relevant literature on zeolites and adsorption processes in carbon capture applications to overcome global warming, the current structures available as adsorbents

and the role of papermaking as an approach to solve the limitations of the current adsorbent structures. Chapter 3 discusses the materials and methods used in this study to create laminate structured adsorbents. The synthesis condition affects the structure and the performance of the sheets. Hence, the synthesis conditions were varied and studied systematically to understand the relationship between synthesis, structure and properties. The different synthesis conditions to perform a systematic study are also described in Chapter 3. Chapter 4 and Chapter 5 present the results of the characterisation of the sheet made using the varying synthesis conditions. Chapter 4 uses well established methods for characterisation of the laminate structures while Chapter 5 develops novel methods that can be particularly used to characterise the prepared laminate structures. Chapter 6 combines the results from all the characterisation techniques and considers which structures will be useful for carbon dioxide capture. Chapter 7 utilises the best structures from optimisation and tests the performance of these structures for the carbon capture application. Chapter 8 presents a hydrophobic printing technique on the laminate structures to provide even channels for gas flow and provides the results from using these structures in a carbon capture application. Finally, the conclusions from this study and suggestions for future work are summarised in Chapter 9.

This page is intentionally blank

Chapter 2

Literature Review

This page is intentionally blank

2.0 Literature Review

2.1 Overview

This literature review deals briefly with adsorption processes as a potential solution to mitigate global warming. The application of zeolites as adsorbents is also discussed. The problems associated with commercial adsorbents and the non-particulate structures are highlighted and the possibility of using papermaking to overcome the limitations of these structures is considered. The previous use of zeolites in the papermaking process is extensively reviewed along with the use of papermaking techniques to create adsorbent structures. Lastly, the format of the thesis along with the scope of the project is presented.

2.2. Global Warming

The anthropogenic forcing of increased carbon emissions is essentially through fossil fuel burning and deforestation*[33]*. The feedback mechanism between carbon dioxide and temperature is stable and self regulating. However, increasing carbon dioxide concentration through human activity might destabilize the equilibrium and turn the stable system to an unstable one with typical run away behaviour*[34]*. A possible mechanism is that increasing the atmospheric carbon dioxide concentration will add to the greenhouse effect, thus causing warming on a global scale. The major effects that global warming is expected to cause are sea level rise and climate changes. Both the effects of sea level rise and climate change effects are expected to be highly regional*[35]*. Although the effects may be regional, the frequency and intensity of extreme weather events like hurricanes, tsunamis, cyclones and heat waves are expected to increase. Other problems that are expected to arise are changes in agricultural yields, glacial retreat, species extinction and increased diseases*[33]*.

2.3 Carbon Capture and Storage Technologies

Many possibilities are being considered to overcome the issues related with global warming. These include i) energy conservation technologies ii) clean energy technologies and iii) CO_2 fixation technologies*[36]*. It is likely that all these options will need to be applied simultaneously in order to radically lower carbon dioxide emissions and stabilise carbon dioxide levels. Other than developing renewable energy sources which are slowly being adapted as it is more difficult for them to supply the baseline power, more immediate solutions need to be found. For steady decarbonisation, intermediate technologies must be available in the next 10-20 years which are technologically easily accessible and low cost while maintaining energy security*[37]*.

Carbon capture and sequestration (CCS) from point source emissions is considered an important strategy in mitigating the release of greenhouse gases into the atmosphere. This technology is used to capture CO_2 from large point sources, and inject it into geological formations such as depleted oil and gas fields, saline formations and unmineable coal seams*[38]*. Separation techniques for separating the CO_2 from the other gases include chemical absorption, physical absorption, physical adsorption, cryogenics and membrane technology.

Capture of carbon dioxide contributes to over 75% of the overall CCS costs*[39]* and implementing CCS technology could potentially increase electricity production costs by about 50%. Hence reducing the capture costs is the most important issue for CCS technology to become acceptable to the energy industry*[40]*. Choosing the right carbon capture scheme is determined by analyzing the costs and the context for power generation. To choose the required capture technology, it is necessary to take into account factors such as the carbon dioxide concentration and pressure of the gas stream and fuel type i.e. solid or gas*[40]*.

2.4 Fundamentals of Adsorption Processes

Adsorption is one possible carbon capture process. Adsorption is the thermodynamic property of a substance to shift from the fluid phase and attach itself to a solid material. It is the result of affinity between the surface of a porous solid and component molecules being removed from a bulk phase which leads to the concentration of component molecules at the surface*[25]*. Gas adsorption occurs when a solid surface is exposed to a gas and undergoes an interaction with gas molecules, thereby temporarily removing them from the gas phase. Gas adsorption on solid surfaces and in pore spaces is a complex phenomenon involving mass and energy interaction and phase changes.

The adsorption of gases on solids increases with increasing pressure and decreasing temperature. The adsorption process is exothermic in nature i.e. energy is released and the process is represented using an adsorption isotherm. The adsorption isotherm is a measure of the molar quantity of gas adsorbed or desorbed at a constant temperature as a function of gas pressure*[41]*.

For microporous adsorbents, the adsorption isotherm is quite different to the other adsorbents*[41]*. The increased adsorption capacity can be attributed to the enhanced adsorption in the micropores and is not a surface phenomenon. The initial rise takes place by micropore filling and this continues progressively until the larger micropores fill in order of increasing size, all under a driving force of quite low relative pressure. Once the micropores are filled, very little adsorption takes place thereafter as there is no space remaining on which adsorption can occur*[42]*.

Adsorption can be either a physical or chemical adsorption process.

Physisorption or physical adsorption is the weak interaction where the trapped adsorbate molecule diffuses across the potential energy wells on the surface of an adsorbent molecule before acquiring the energy to return to the gas phase. The forces involved in physisorption are attractive dispersion forces, short range repulsive forces and electrostatic forces which are responsible for adsorption of polar molecules or for the adsorption by surfaces with permanent dipoles. The attractive dispersion forces arise from the rapid fluctuations in electron density in one atom which induces an electrical moment in the neighbouring atom. The short range repulsive forces are the result of the interpenetration of the electron clouds. These forces are collectively called "Van der Waals forces". Physical adsorption is a reversible process and of low selectivity. Relatively low levels of adsorption energy are involved*[23]*.

Chemisorption or chemical adsorption is caused by stronger interactions due to deeper potential energy wells. Chemical bonds are formed by overcoming the activation energy and electron transfer occurs between the surface and the adsorbed molecules. Here the wells are harder to escape and the adsorbed molecule requires a much greater energy to return to gas phase when compared to physisorption*[43]*.

2.4.1 Phenomena of Gas Separation

Gas separation via adsorption can occur in an adsorbent because of equilibrium separation, molecular sieving or kinetic selectivity.

Equilibrium separation is the interaction between the dipole moments of the gas molecules with the electrical field inside the pores of the adsorbent, as the porous solids have different affinities for different species; the strongly adsorbing species is preferentially adsorbed on the solid. Molecular sieving refers to the separation of gas components in terms of size or steric exclusion of components which are too large to enter pores of a given dimension. Kinetic selectivity is

based on the ability of some components to enter pores faster than others. Hence, by controlling the time of exposure, the faster diffusing species can be selectively removed*[16, 24]*.

The adsorption/desorption process is achieved by pressure swing (PSA), temperature swing (TSA), electrical swing (ESA) adsorption or through process hybrids.

The TSA and PSA processes have different methods of regenerating the adsorbent. In TSA, increasing temperature acts as the driving force for desorption of the adsorbed compound while in PSA, decreasing pressure acts as the driving force for desorption*[44]*. In TSA, energy is added to the adsorbent in order to heat the bed and the gas surrounding the adsorbent. The resulting change in the adsorbent equilibrium promotes a change in the loading state. The energy required for the heat of adsorption is provided externally by thermal energy transfer and thereby, desorption of sorbates that reside on the adsorbent occurs. In PSA, a change in both total pressure of the system and the partial pressure of the adsorbed compounds is required to affect a change in the equilibrium. Molecules are desorbed because of a change in equilibrium. No heat is supplied for this change in equilibrium to occur although desorption occurs. This heat is taken from the adsorbent and the gas surrounding the adsorbent which is the local environment. This constitutes an adiabatic system which results in cooling the bed and the gas surrounding the desorbed portion of the bed. During adsorption, the heating of the bed and the gas flowing through the bed occurs from the heat liberated. This net effect of heating and cooling of the bed during the adsorption/desorption process diminishes the working capacity of the adsorbent*[45]*.

PSA has much shorter cycle times when compared to TSA as TSA has to account for the large thermal capacities of the adsorbent bed. The longer cycle times of the TSA processes are inconvenient and in some cases can be replaced by ESA processes where a low voltage current is used to heat the adsorbent, thereby speeding up the adsorption process but a disadvantage of the ESA process is that it uses electric power to increase the temperature while TSA processes use

waste heat for the same purposes*[46]*. TSA processes should be used when certain components of a mixture are strongly adsorbed and when a small change in temperature produces a large amount of desorption of the strongly adsorbed species, which makes them useful in purification processes. PSA processes on the other hand are a good choice when a weakly adsorbed species is required at high purity and since the cycle times are much shorter, greater throughput can be obtained which make them useful in bulk separation applications*[44, 47]*. PSA processes are attractive for CO_2 separation from nitrogen rich streams due to the low energy requirements*[48]* when compared to other separation technologies and with rapid PSA applications, the throughput can be considerably larger than for regular PSA applications*[3]*. The requirement for PSA processes to work in this application is that the adsorbent has high CO_2 selectivity and capacity*[48]*.

2.4.2 Adsorbents

Adsorbents are solid chemical substances that possess porous surfaces that can admit molecules to the interior surface of the structure*[9]*. Most adsorbent structures contain complex networks of interconnected micropores (pore openings < 2nm), mesopores (pore openings between 2-50nm) and macropores (pore openings > 50nm)*[49]*. Adsorption occurs when the adsorbate molecules pass through the fluid film which is external to the adsorbent particle, followed by passing through the macroporous structure into the microporous structure where the bulk of the molecules are adsorbed*[47]*, as shown in Figure 2.1.

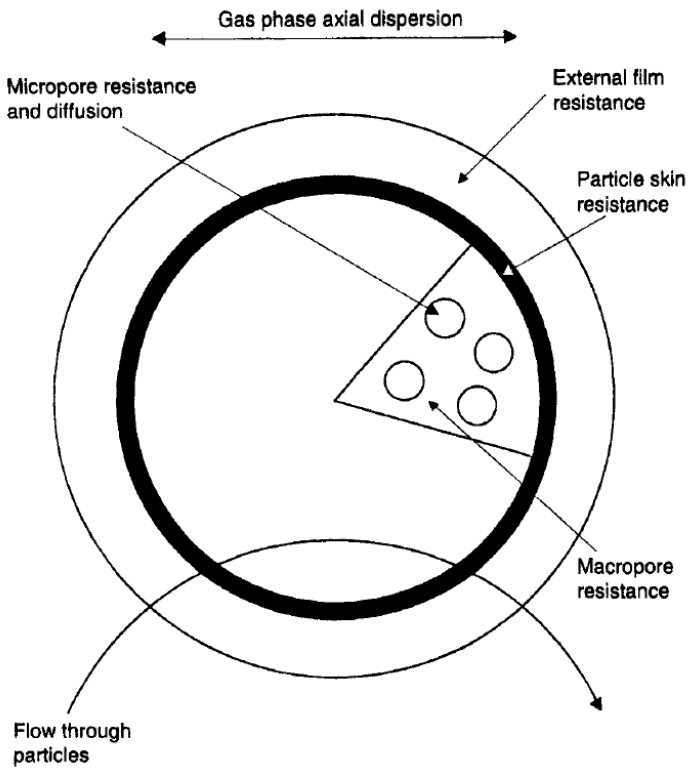

Figure 2.1: General structure of an adsorbent particle and the associated resistances to the uptake of fluid*[47]*

An adsorbent surface may be thought of as having potential wells of varying depths each of which corresponds to an adsorption site. A gas molecule may collide on the surface in two ways: i) the collision may be elastic and no energy is exchanged so the molecule can reflect back into the gas phase and the system remains unchanged or ii) the collision may be inelastic which means that the gas molecules may gain energy or lose energy. If the gas molecule loses energy, it will be unable to escape the surface potential of the well and become adsorbed for a period of time after which it returns to the gas phase. Hence, inelastic collisions have distinctly higher possibilities of leading to adsorption. The strength of the interaction will be correlated with well potential*[43]*.

Adsorbents suitable for CO_2 separation from flue gas are expected to have the following attributes which include*[50]*:

1. High CO_2 adsorption capacity with high uptake at low CO_2 partial pressures
2. Fast kinetics which results in a working capacity close to the equilibrium capacity over a wide range of operating conditions
3. High CO_2 selectivity as a purer product is obtained which makes the process more economically viable
4. Mild regeneration conditions with interactions that are neither too weak nor too strong Very weak bonds are easy to regenerate but have a low uptake of CO_2, while very strong bonds have high CO_2 uptake but are costly and have difficult desorption
5. Stability during the entire adsorption-desorption cycle which directly affects the economics of the process
6. Tolerance for the presence of impurities and moisture in the flue gas and
7. The adsorbent itself should be low cost and prepared for the adsorption process using low cost techniques*[50]*.

2.4.3 Zeolites as Adsorbents

Zeolites are comprised of hydrated aluminosilicates in a repeated crystalline structure. Further details on the structure and chemical composition of zeolites are discussed in Section 2.5.1. Zeolites play a dominant role as adsorbents owing to their ability to adsorb large quantities of material thereby achieving extremely low mole fractions of these adsorbed compounds in the product gas*[45]*. Adsorption by zeolites is a very desirable industrial separation process because of its extensive and flexible applications and also because it is a more energy efficient process when compared to more conventional separation techniques*[51]*. Zeolites have been used in

three major areas of separation applications: i) Removal of trace impurities from a gas, ii) bulk gas mixture separations and iii) gas analysis*[24]*.

Adsorption by zeolites is a physical process, which occurs mostly by Van der Waal's forces which consist of interactions between adsorbate and adsorbent by molecular forces, combining dipole, induced dipole and quadrupole electrostatic effects*[40]*. Zeolites are distinct from other adsorbents because they have no distribution of pore size. The crystal lattice into which the adsorbate molecule can enter is precisely uniform in crystal form. Hence zeolites are capable of separating effectively on size and are assigned the popular term of molecular sieves. The internal porosity is high and majority of the adsorption takes place internally. Physical adsorption takes place where the cavities fill and desorb by emptying reversibly and the mechanism is generally considered to be one of pore filling*[15]*. Although zeolites have pores and channels of precise dimensions in the microporous range, when pelletised or made to different structures, they have a pore size distribution*[16]*. Large pores in the zeolite structure act as passage-ways for molecules to diffuse from the surrounding environment into the interior of the particle. Once inside the particle, the molecules will diffuse into the interior of the microparticle. The pore size of the microparticle is of the order of molecular dimension and molecules inside the micropores never escape the attraction potential of the pore walls. This means that molecules in free form do not exist and only adsorbed molecules exist in the micropore*[16]*.

Zeolites work as molecular sieves because of their ability to separate components from gas mixture through steric exclusion but the vast majority of industrial gas separation processes using zeolites occurs via equilibrium separation. Thermodynamic selectivity works because of the preferential adsorption of a particular gas on accessible cationic sites in a zeolite cavity*[24]*. Adsorption of a gas on the aluminosilicate framework is weak and not very selective. The strength and selectivity of adsorption depends on various factors such as the shape, size and

structure of the cavity, the density and concentration of cations, polarisability and the permanent polarity of the adsorbent molecule*[24]*. Adsorption by kinetic selectivity is very rare with zeolite based gas separation*[52]*. The adsorption isotherm of a pure gas follows the type I isotherm for a microporous zeolite adsorbent*[53]*. In order to further understand zeolites, it is important to gain an understanding of zeolite structure and composition and this is discussed next in Section 2.5.

2.5 Zeolites

2.5.1 Zeolite Structure and Composition

Zeolites are complex, inorganic polymers that have uniformly sized pores of molecular dimensions. They were originally defined as structures which have aluminosilicate frameworks linked to each other by sharing oxygen atoms with loosely bonded cations and water molecules in extra- framework positions*[40]*. The more recent definition however excludes the constraints of composition and defines a zeolite as any crystalline structure that consists of specific frameworks of linked TO_4 units where T is the tetrahedrally bonded atom in the framework*[54]*. The TO_4 unit represents the basic building unit. Several basic building units are combined to form a composite building unit. These could be simple polyhedra like cubes, hexagonal prisms or cubo-octahedra. A few examples of some composite building units are shown in Figure 2.2*[15]*. The final framework is an assembly of composite building units and the pore sizes range from 3-20Å with pore volumes ranging from 0.1-0.35cm^3/g*[55]*.

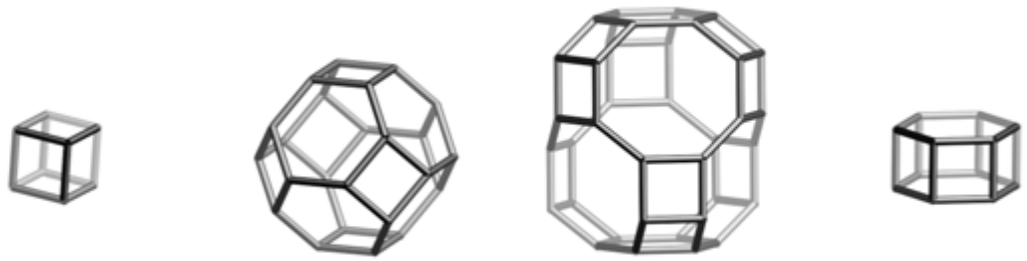

Figure 2.2: Composite building structures i) Double 4-ring ii) Sodalite Cage iii)Chabazite Cage iv) Double 6-ring*[15]*

The empirical representation of aluminosilicate zeolites, which are the most industrially and commercially useful members of the zeolite family, is $M_{y/n}[(SiO_2)_x(AlO_2)_y].zH_2O$ where M is the charge compensating cation with valency n*[56]*. These cations belong to the family of alkali and alkaline earth elements. The ratio x/y can have a value of 1 to infinity and z represents the number of water molecules that can be adsorbed or desorbed in the pores*[3]*. The AlO_2 bears a net negative charge which is balanced by an extra-framework univalent cation. The cations and the water molecules occupy the many intracrystalline channels and interconnected voids present in the framework. These molecules have considerable mobility. Ion exchange thus becomes easy for the cations and the water molecules can be removed reversibly with the application of heat. The host structure has many micropores and voids which account for almost 50% of the crystal volume. The zeolite framework is slightly flexible as the size and shape of a pore can change corresponding with the particular guest species present in the pore*[3]*.

Figure 2.3*[15]* shows the different zeolite framework types. In the diagrammatical representation of these frameworks, the nodes represent the T-atoms and the lines represent the oxygen bridges*[48]*.

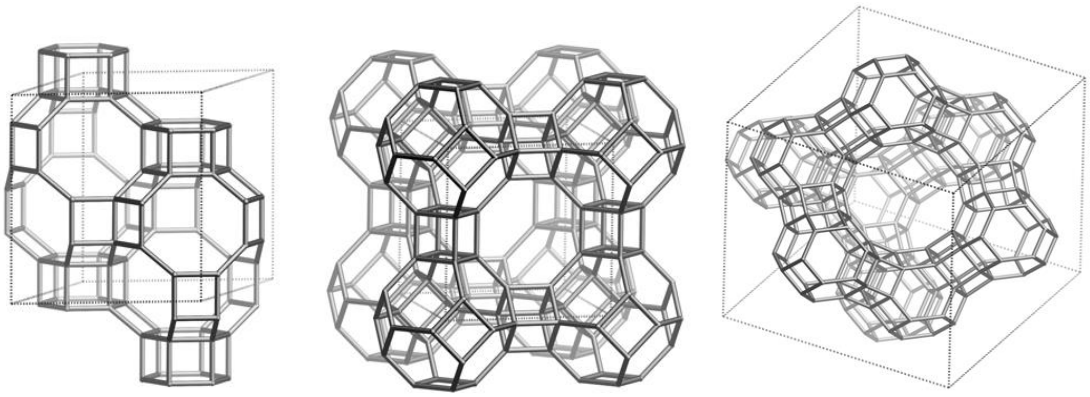

Figure 2.3: Different zeolite frameworks a)Chabazite (CHA) framework type b)Linde Type A (LTA) framework type c)Faujasite (FAU) framework type*[15]*

2.5.2 Zeolite Classification

Zeolites do not come under an easily definable family of crystalline solids and can be differentiated from denser tectosilicates by the framework density (the number of tetrahedral atoms per 1000Å)*[57]*. Zeolites now include structures that also have Ga, P and Ge as the tetrahedrally bonded atom.

Zeolites are primarily classified based on their framework topology (most accepted classification) with distinctive frameworks assigned three letter codes*[58]*. The framework type describes the connectivity of the framework tetrahedral atoms in the highest possible symmetry without reference to chemical composition, dimensions of the channels system, size and shape of pore openings and the type of cation sites available, although all of these properties are very important when determining the properties of the zeolite*[48]*. As of Oct 2011, The International Zeolite Association has 201 framework type codes defined*[15]*.

Aluminosilicate zeolites are divided into four categories by Si/Al composition. They are low, intermediate, and high silica zeolites as well as silica molecular sieves. Low silica zeolites have a

Si/Al ratio of 1 to 1.5, intermediate silica zeolites have a Si/Al ratio of 2 to 5, high silica zeolites have a Si/Al ratio of 10 to 100 and silica molecular sieves have a Si/Al ratio > 100. The low silica zeolites are thermally stable to 700^0C and are highly hydrophilic in nature while the silica molecular sieves are thermally stable to 1300^0C and are hydrophobic in nature*[55]*. With increasing Si/Al ratio, the cation concentration and ion exchange capacity decreases and acidity increases. Low silica zeolites give optimum adsorption properties in terms of capacity, pore size and three dimensional channel systems. Low and intermediate silica zeolites find good use in removal of water from organics and in separation and catalysis of dry streams, while high silica zeolites and silica molecular sieves find use in the removal of organics from water and in separation and catalysis of wet streams*[55]*.

2.5.3 Natural and Synthetic Zeolites

Zeolites can be naturally occurring or synthesized. Natural zeolites offer only a limited range of atomic structures and properties which prevents large scale use due to stringent product specifications. Synthetic zeolites, on the other hand offer a wide range of properties but have higher cost. The cost of natural and synthetic zeolites is compared against some materials used as fillers in the paper industry in Table 2.1*[59-61]*.

Table 2.1: Cost comparison of filler materials useful in the paper industry*[60, 61]*

Material	**Cost ($/tonne)**
Natural Zeolite	70-200
Synthetic Zeolite	430-500
Clay/PCC	130-150
Titanium dioxide	1000-3000

2.5.3.1 Natural Zeolites

Natural zeolites are known to occur in very minor quantities in vugs and cavities of basaltic and volcanic rock*[62]*. Previously, they could not be put to commercial use because of very low occurrence until large, mono-mineralic deposits were found for mining. Zeolites occur in nature as a result of a chemical reaction between volcanic glass and saline water at temperatures between 27-55°C and pH 9-10*[63]*. They are cheap and especially advantageous for bulk applications where the presence of mineral and chemical impurities is accepted to some extent*[64]*. Some of their applications are as fillers in paper, in pozzolanic cements and concrete, in fertilizer and soil as a conditioner, as a dietary supplement in animal husbandry, as sorbents or support media for the immobilization of micro-organisms, in the cleanup of aqueous streams for environmental applications and as ion exchangers for cleanup of radioactive waste*[16]*. Some

natural zeolites which play a significant industrial role are clinoptilolite, chabazite and mordenite.

2.5.3.2 Synthetic Zeolites

Synthetic zeolites have more commercial uses than their natural counterpart due to high purity of product and particle size uniformity. They can be engineered to have a range of chemical properties and pore sizes with greater thermal stability. Synthetic zeolites can be prepared from silica and alumina as starting materials, which are expensive, so other cheaper starting materials like clay minerals, coal fly ash, natural zeolites, municipal solid waste, industrial slags and incineration waste have been investigated*[65, 66]*. These materials decrease the cost of synthetic zeolite and helps mitigate environmental problems*[44]*. Synthetic zeolites have high end applications in industry such as desiccants, adsorbents, molecular sieves, ion exchangers, catalysts and detergent builders. Synthetic zeolites that have significant industrial uses are zeolites A belonging to the Linde Type A (LTA) framework, X and Y belonging to the Faujasite (FAU) framework, EMC-2, ZSM-5, and Gismondine.

In the work in this thesis, we have used zeolite 13X and zeolite 4A for adsorption applications. These zeolite structures are now discussed in more detail in Section 2.5.4 and 2.5.5 respectively.

2.5.4 Zeolite X

Zeolite X belongs to the FAU framework and the unit cell has sodalite cages which are joined to one another via double 6-rings*[57]*. Figure 2.4*[15]* shows the double 6-ring, sodalite cage and the final zeolite X structure. This creates the so called supercage with four, tetrahedrally oriented, 12-ring pore openings and a 3-dimensional channel system. The supercage has a diameter of 12.5Å and the size of the aperture of the large cavity or the pore diameter is 7.4Å.

The framework density at 12.7T atoms per 1000Å is even lower than that of LTA*[67]*. Many different cations can be present in this zeolite type such as Na^+, Li^+, Ca^{2+}, which are designated NaX, LiX, CaX, respectively. The combination of large void volume (50%), 12 ring pore openings and 3-dimensional channel system makes the thermally stable silicate materials with FAU framework type ideal for many catalytic applications.

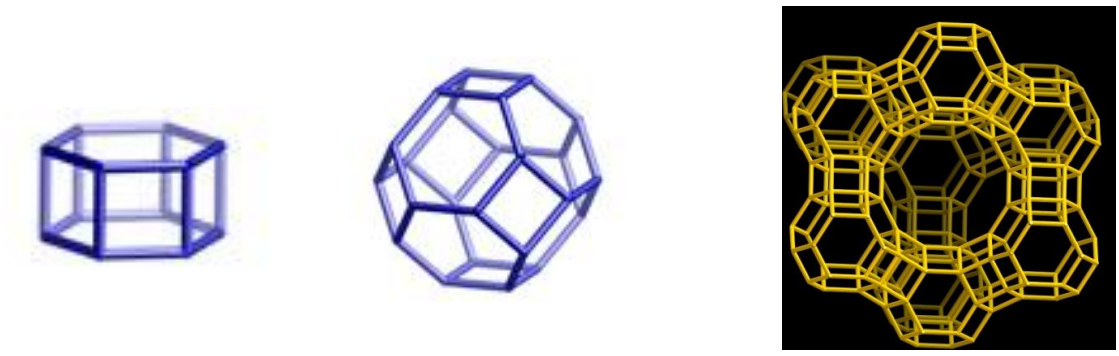

Figure 2.4: a) Double 6-ring b) Sodalite Cage c) Final Zeolite X structure*[15]*

In the Faujasite framework, zeolite X has between 96 and 77 Al atoms per unit cell (Si/Al ratio is between 1 and 1.5), while zeolite Y has less than 76 atoms per unit cell (Si/Al ratio is greater than 1.5)*[68]*. NaX also known as 13X zeolite is widely used adsorbent for CO_2 recovery due to its high working capacity, equilibrium selectivity and low purge requirement*[69]*. High purity CO_2 is adsorbed on NaX due to strong quadrupolar interaction between the CO_2 molecules and the electrical field generated by the cations inside the zeolite pores*[70, 71]*.

2.5.5 Zeolite A

Zeolite A belongs to the LTA framework and the unit cell contains sodalite cages that are joined via oxygen bridges to double 4-rings which creates an α-cavity in the centre of the unit cell and a 3-dimensional 8-ring channel system*[67]*. The diameter of the α-cavity is 11.4Å but the size of the aperture of the cavity is 5Å which represents the pore size of the unit cell*[4, 72]*. The double

4-rings and sodalite cages together with the final zeolite A structure, are shown in Figure 2.5*[15]*. The framework can also be described as a primitive cubic arrangement of α-cavities joined through common 8-rings, producing a sodalite cage in the centre.

This is one of the more open zeolite framework types with a framework density of only 12.9T-atoms per 1000Å. The Si/Al ratio is 1 which allows for strict alternation of Si and Al atoms in the structure. Based on the cation present in the framework type, three types of zeolite A are known, which are 5A, 4A and 3A with Ca^{2+}, Na^{+} and K^{+}, respectively, as the charge balancing cation. The numbers 5, 4 and 3 represent the pore size of the zeolite in Å*[73]*. Zeolite A is used as a dessicant both in the laboratory and between the panes of glass in double-glazed windows and as an ion-exchanger (water softener) in laundry detergents.

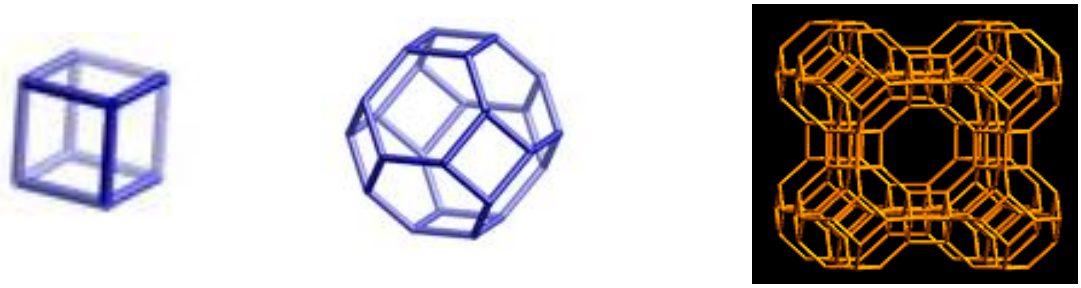

Figure 2.5: a) Double 4-ring b)Sodalite Cage c) Final Zeolite A structure*[15]*

2.6 Current Adsorbent structures

Zeolites are used as industrial adsorbents in the form of beads or pellets. These structures have various disadvantages such as high pressure drop, which increases energy consumption and high mass transfer resistance which affects overall system efficiency*[5]*. These systems are also prone to powdering when the beads rub against each other*[31]*. In applications like rapid PSA, their use is further restricted by fluidization, fluid friction and low specific surface area*[32]*. A high pressure drop in a packed bed might require high capital and operating costs for the

pressurisation/depressurisation steps in a PSA process. The long diffusion paths through meso- and macropores in the zeolite beads will produce heat and mass transfer limitations due to temperature and concentration gradients thus decreasing the overall performance of the PSA process. Reducing particle size decreases mass transfer resistance for rapid PSA applications but other problems remain or increase such as pressure drop.

Non-particulate, novel structures were created to eliminate the disadvantages of the conventional beads and pellets. In order to replace bead and pellet configurations, these structures must have high mass transfer kinetics, high volume working capacity, low voidage to create a small sized adsorber and a gas flow path that produces a low pressure drop*[22, 74]*. Although, these structures have various advantages, their use in the industry is still limited due to high preparation cost and low adsorbent loading. Novel non-particulate structures include monoliths, laminates, foam and fabric structures*[22, 74]*. The limitations and advantages of various current adsorbent structures are discussed in Table 2.2 and some examples of different adsorbent structures are shown in Figure 2.6. Monoliths have found use in PSA and rapid PSA applications, for VOC removal*[75]* and air separation*[59]*. Laminates have found use in VOC removal*[60]*, CO_2 removal*[61]* and ultra rapid PSA applications*[60]*. Foam structures have found use in heat pumps for high water uptake*[76]*, and fabric structures have found use in H_2 recovery by rapid PSA*[77]* and in air purification systems*[78]*.

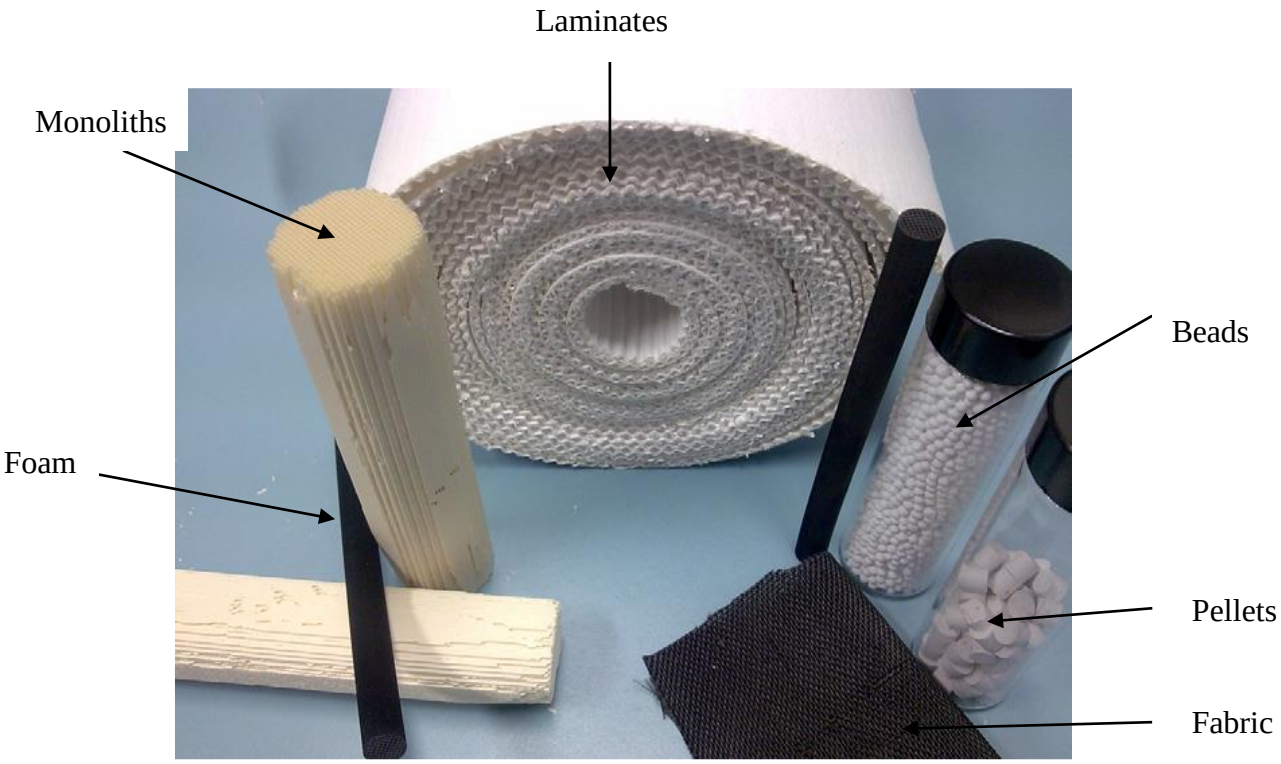

Figure 2.6: Examples of various adsorbent structures including beads, pellets, foam, fabric, monolith and laminate structures*[22]*

Table 2.2: Advantages and disadvantages of different adsorbent structures*[22]*

	Beads	Monoliths	Laminates	Foam structures	Fabric Structures
Structures	Adsorbents are usually manufactured in granular or spherical forms which sizes ranging between 0.5-8mm. They are then packed into beds.	Structured supports composed of parallel channels with a variety of cross-sectional shapes. Monoliths are created either by the extrusion process or an active film is grown on the walls of the monolithic structures by dip-coating, wash-coating, and slip-coating	These structures are considered a simpler form of monoliths where channels are replaced by 1D slits. Laminate structures can be created using support structures. They are then coated with the required zeolite. The adsorbent can be adhered to the support structure on one or both sides	These structures comprise of network of solid struts and pores.	These structures can be made as parallel sheets or spiral-wound structures.
Pros	-High adsorbent loading - Various industrial applications -Easily synthesized -Good reproducibility	-Eliminates problems of fluidization, high pressure drop and high mass transfer resistance -Efficient method to pack high adsorbent surface area into a fixed volume while still maintaining low pressure drop	-Sheets with channel width ranging from 15-75µm between adjacent sheets show superior attainable cycle frequency with reduced bed length -Modelling of thin sheets with less than 0.2mm wall thickness show sharp breakthrough fronts -Can be used in ultra rapid PSA systems - Useful in applications where pressure drop is necessary	-High geometric surface area results in increase in high external mass transfer due to large inherent porosity and tortuosity -Flow friction and pressure drop is low due to the larger flow channels and voids -Presence of macropores which are spatially connected is large enough for molecules to freely enter and leave allowing for pressure drop to be substantially reduced	-Self supporting nature provides high adsorbent loadings -Rapid mass transfer due to the thin fibres of the composed fabric -Low attrition rates and high mechanical strength - Low resistance to gas flow gives rise to low pressure drop and eliminates fluidization issues -Useful for short cycle times where kinetics is important for separation
Cons	-Large pressure drop increases energy consumption -High mass transfer resistance -Decreasing particle size, causes problems of fluidization and channelling -Powdering of the zeolite at high velocities	-Separation performance may be inferior to pellets -Active adsorbent material may be very low compared to pellets -Not all adsorbent material present in the monolith wall will be accessible to the adsorbate molecules -Manufacture of monolith structures with high cell densities is difficult and expensive	-Practical difficulties with reproducibility - Tolerance between sheets must be tight- less than 5% to avoid gas maldistribution -Presence of other material such as binder and external support creates low adsorbent loaded structures - No reports are found of real processes utilizing laminate structures	-Not suitable for cyclic processes because of high tortuosity and porosity which decreases separation performance -High internal porosity makes the amount of active material very less so volume activity very low -Application still very rare	- No advantage in longer cycle applications where separation is based on equilibrium - Hard to create such structures with zeolites.

Thus it can be seen that a trade-off between different adsorbent properties is necessary to create an optimized adsorbent structure. Important structural parameters that impact overall performance of gas separation processes include: 1) amount of adsorbent contained in a given volume (adsorbent loading) 2) pressure drop through the structure per unit length 3) external surface area per unit volume 4) total void volume and 5) channelling and dispersion characteristics*[74]*.

2.7 Zeolite applications in the pulp and paper industry

Zeolites have many possible applications in pulp and paper processes such as fillers, retention aids and in white water treatment applications.

2.7.1 Filler applications

Fillers are a necessary addition to paper to reduce production costs, increase printing quality and reduce the use of raw materials. Zeolites are mostly used as fillers for paper in Japan*[29]*. Figure 2.7*[79]* shows the distribution of filler use in North America in 2005, where alumino-silicates, such as zeolites, represent a very small fraction of the filler market.

Research in the potential use of zeolites as fillers has found them useful in the following papermaking applications: i) To improve optical properties of paper as they have high brightness ii) to improve bulkiness and printability iii) to produce specialty papers such as gas filtration, anti-tarnish and photocatalytic papers due to their open structure iv) to increase the co-efficient of friction which can decrease the misfeed to copier machines and v) to reduce print through, which allows them to be used in the production of ultra light-weight coated publication papers and newsprint and vi) to reduce problems with pitch and filler deposits due to their ion exchange ability*[80]*.

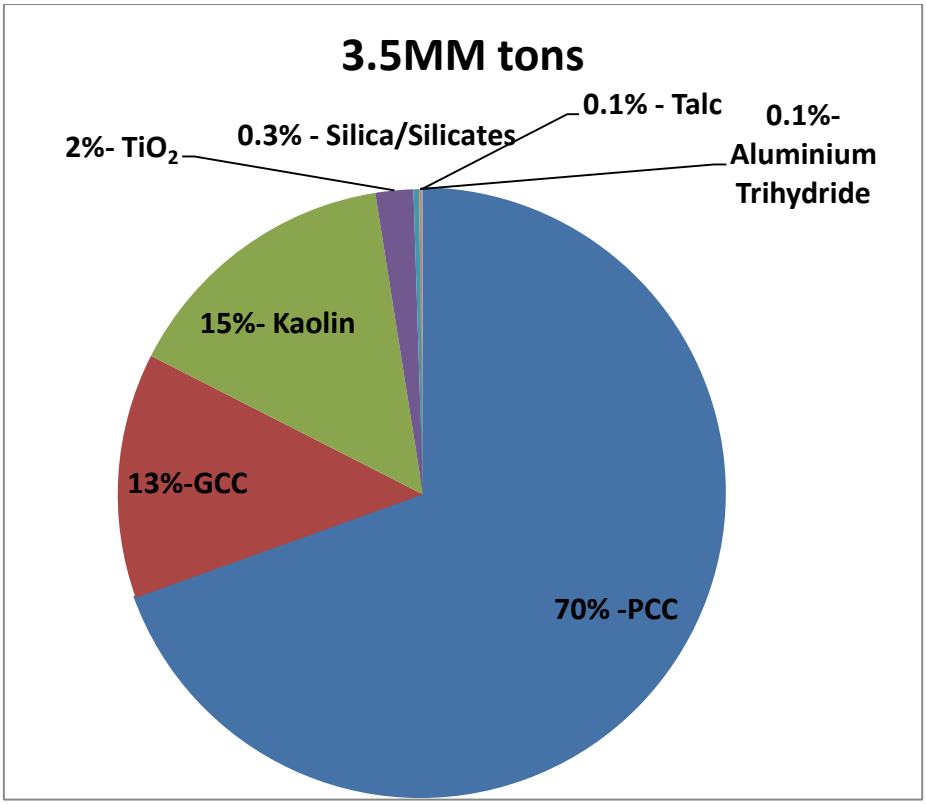

Figure 2.7: Filler use in North America (2005)*[79]*

Zeolites have properties such as high brightness, open porous structure, controllable particle size, rheology and hardness which give them the potential to replace traditional mineral fillers like bentonite (clay), GCC (ground calcium carbonate) and PCC (precipitated calcium carbonate). However zeolite filler applications must be carefully chosen as papermaking pH, temperature shocks and high metal concentrations can cause physio-chemical changes that inadvertently reduce the zeolite efficiency. Fine paper is manufactured in basic pH of 8-8.5 while mechanical grades are often produced in acidic or neutral conditions. Fine paper manufacturing shows an improvement in sheet formation, retention and optical properties with the use of zeolite fillers as compared to other mineral fillers but this is not the case with mechanical grade paper. In acidic conditions, the zeolite framework is attacked as an exchange of metal cations for hydrogen ions occur and the zeolite material starts dissolving due to dealumination by release of Al^{3+} ions. Once dissolution occurs, this reaction is

irreversible. Other effects due to pH variation on zeolite properties include changes to zeta potential and degree of flocculation*[28]*.

Brouillette et al.*[28]* demonstrated this effect of pH by measuring conductivity with the addition of HCl. With decreasing pH, neutralization of the zeolite particle occurs and after the isoelectric point (the pH where the streaming potential becomes 0 due to the addition of acid) is reached, dealumination immediately starts occurring. For the zeolites used in this particular study, the isoelectric point occurred between pH 7.2 and pH 7.8 while the clay particles had their isoelectric point occur below pH 5. Hence, zeolite particles are not as stable when there are pH fluctuations in the pulp slurry*[28]* and thus, zeolite is more useful for fine paper production. To be used at low pH, the zeolite surface should be modified to resist dissolution. The zeolite can be made more acid resistant by increasing the salt concentrations as selectivity for the hydronium ions decreases*[28]*.

Klass et al.*[80]* filed a patent that showed that zeolites (clinoptilolite of size 0.5-2μm) when used as fillers without retention aids perform admirably when compared against PCC, even at high shear rates. Zeolite retention was 2.5 to 4 times higher than PCC and the sheet formation was more uniform exhibiting improved optical properties. Since the retention of the zeolite was higher, the wet end of the machine was much cleaner. With the zeolite filled paper (45 kg per ton), no print-through was observed when compared to PCC filled paper (113 kg per ton) which still showed severe print-through. This superior performance indicates that zeolite filled paper would be useful in the production of lightweight coated publication paper.

Quanchang et al.*[29]* have investigated replacing talc with zeolite (clinoptilolite) for filler applications in the production of machine glazed paper, writing paper, and newsprint while at the same time reducing production costs. Although the authors claim that in most applications the zeolite filled paper showed better properties than talc, the claim is not supported by the data provided. Even for experiments where the authors claim that the talc performs better, the results were statistically similar. The major conclusion is that the zeolite-filled paper

conformed to the industry standard. The clinoptilolite filled paper had similar whiteness to talc filled paper even though the whiteness of clinoptilolite is much less than that of talc. This is useful because talc might be more expensive than clinoptilolite due to its higher whiteness, although the quality of the final paper product is the same. The print quality of the zeolite filled paper was higher than the talc filled paper as shown by increased legibility of the picture and print with no picking and dusting. So in areas where natural zeolite occurs in abundance, zeolite can replace talc without additional equipment or changes to the process being required, therefore without extra cost*[29]*.

Ivanov et al.*[81]* have shown that since zeolites have a more open structure than other fillers they can have significant additional benefits when used in filler applications as a carrier for basic dyes. Basic dyes adsorb strongly on zeolites compared to other fillers due to their large surface area, as shown in Table 2.3*[79]*, and reduce the sensitivity of the dye to UV radiation.

Table 2.3: Specific surface area of different filler types*[79]*

Filler types	**SSA(m^2/g)**
Kaolin (hydrous)	10-25
Kaolin (calcined)	15-25
Calcium Carbonate (ground)	2-12
Calcium Carbonate (precipitated)	3-25
Titanium dioxide	7-12
Talc	9-20
Silica, silicates (Zeolites)	45-75

Zeolites, when used as fillers, can also help reduce the effects of aging. Oxidation and hydrolysis reactions that occur due to Cu^{2+}, Mg^{2+}, Fe^{2+} and Fe^{3+} during the process of aging can be neutralized, reducing the loss of brightness after 96 days of artificial aging by approximately 2.5%*[82]*. The same study also showed that using zeolite instead of kaolin increased retention and tensile strength and reduced water uptake.

Unconventional uses of zeolites as fillers include their use in paper phenolic laminates to improve laminate resistance to corrosion when exposed to wet conditions. Paper phenolic laminates are used in printed circuit boards and integrated circuits as insulators, but are affected by electrolytic corrosion when exposed to wet conditions. Kawamura et al.*[13]* used zeolite fillers in paper phenolic laminates to increase the resistance to corrosion by improving the tracking failure. They found that the comparative tracking index increased with increasing zeolite filler content for copper electrodes, while there was no change for platinum electrodes.

When very high quality white material that has low abrasion is needed, zeolites can be used in combination with TiO_2. TiO_2 provides very high whiteness, thereby improving optical properties. Since TiO_2 by itself is very expensive, other materials need to be added to reduce production costs. Rock et al.*[83]* have used zeolite A in combination with TiO_2 to provide paper that has similar brightness and opacity, but at lower cost when compared to the use of TiO_2 alone. The brightness of silicates (zeolites), TiO_2 and other fillers are shown for comparison in Table 2.4*[79]*. For this application, zeolites must have a crystal size of less than 1µm and a particle size of less than 3µm, along with some modifications, including partial ion exchange and pH adjustment.

Table 2.4: Filler dry brightness for different filler types*[79]*

Filler types	**% Brightness**
Kaolin (hydrous)	78-90
Kaolin (calcined)	90-95
Calcium Carbonate (ground)	80-85
Calcium Carbonate (precipitated)	95-100
Titanium dioxide	98-100
Talc	85-90
Silica, silicates (zeolite)	93-99
Alumina trihydrate	97-100

2.7.2 Microparticle retention aid

Retention of papermaking components is very important for well controlled wet-end operation. High retention levels are required to reduce product loss and pollution thus controlling costs*[84]*. Many mills are striving to reduce or eliminate their effluent. However, the small sized fines fraction readily drains through the wire and ends up in the white water*[85]*. This easy drainage of the fines fraction can be reduced by adding a retention aid which enhances the colloidal retention of the fines. The fines or filler particles can form a macroparticle by attaching to each other or by attaching to long fibres thereby increasing their chance of retention. Retention using microparticles is considered to have the greatest impact on small particle retention. Microparticle retention systems include a small highly charged

microparticle that is added in addition to the polymer to destabilize the colloidal particle suspension. Different microparticle systems have used silica and bentonite clays as they have a high surface area and high surface charge density*[86]*. Silica microparticles are expensive and the right silica particle must be chosen for differing applications. With bentonite, high purity is required for use as microparticle retention aid. Even though there are other microparticle systems being used, silica and bentonite systems have become standards for microparticle retention comparison systems*[80]*.

Klass et al.*[80]* have shown that zeolite (clinoptilolite with particle size 0.5-2µm) as a microparticle retention aid performs well against microparticle silica when similar quantities were added. This was also true with bentonite as the zeolite performed well even against a larger quantity of bentonite. The use of zeolites as fillers also eliminated the need for a retention aid system.

Ko et al.*[87]* have shown that zeolites played an important role as microparticle retention aids in increasing the retention of TiO_2 nanoparticles in the preparation of photocatalytic paper. Compared to using only starch and cationic polymer, the retention of the components with the zeolite was much higher with better formation. This is because instead of fibre-fibre flocculation occurring, fibre-microparticle-fibre flocculation occurs and the microparticle also acts as a supporting substrate for the TiO_2 nanoparticles.

2.7.3 Other uses of zeolites in the papermaking process

Modified zeolites have shown promise to chelate metal ions and stabilize peroxide during the repulping process in recycling old newspaper. Daneault et al.*[88]* have shown that zeolite-supported bleach chemicals can replace the chelants typically used to protect the peroxide from decomposition. In addition, these zeolite supported chemicals require less alkali and hydrogen peroxide to achieve the required brightness level. Conventional chemicals also perform better when attached to the zeolite thereby enhancing the bleaching performance of

peroxide during the deinking process. Selective zeolite supported chemicals also create a better chelating and stabilizing effect, which can be attributed to increased contact area of the chemical with the pulp and uniform distribution of zeolite-supported chemical in the pulp. Not only does the zeolite work for the above two processes, the zeolite can also adsorb colloidal particles during bleaching and deinking thereby lowering the dissolved solid content, which improves the waste water quality. If all these processes work when applied in a mill situation, then there are economic gains from using zeolites in the recycling process*[88]*.

Zeolites not only have the ability to adsorb colloidal particles from white water, they also have ion exchange capacity in water. Calcium carbonate use as a filler is limited to paper made from chemically pulped fibres with minimal lignin. This is because, when used in lignin containing paper, calcium carbonate causes pulp darkening due to its' high alkalinity, which activates the lignin chromophores*[89]*. When used in acidic conditions for mechanical paper, the calcium carbonate dissolves to generate free calcium ions and CO_2 gas. The free ions continue to react with the dissolved and colloidal substances present in the white water (recycled for environmental purposes), causing deposits in the paper machine which leads to reduced quality in the final product.

Chabot et al.*[90]* have investigated the use of zeolites in the white water to help use calcium carbonate as a filler in mechanical grades. The zeolite 4A used in their study has a multifunctional use. It is used for ion-exchange in the white water and as a filler replacement with similar brightness when some of the calcium carbonate dissolves. From their investigations, Chabot et al.*[90]* observed that increasing the zeolite dosage, increased the ion exchange capacity and the zeolite was unaffected by the dissolved and colloidal substances. Also the zeolite filler was easily retained and the sheet properties were only slightly altered. The brightness of the zeolite filled sheet was high, opacity was reduced, gloss was also slightly higher as this was improved by the better calendaring response, roughness was about

the same, while the porosity of the zeolite filled sheet was higher, giving higher ink penetration during printing. Strength properties were slightly reduced when compared to the PCC filled sheet.

Effects of conductivity, temperature and pH were also studied by Daneault et al.*[91]* for the same system. At higher conductivity, the residual free calcium ion concentration was lower but the zeolite efficiency was also lower. Conductivity affects the ion exchange capacity of the zeolite because a higher osmotic pressure develops in the water phase when the sodium ion concentration increases. This increased osmotic pressure makes it difficult for the sodium ion to come out of the cage, thereby lowering the efficiency of the zeolite for ion-exchange. Increasing the temperature increased the performance of the zeolite. Increasing temperature dissociates the surface hydroxyl groups on the zeolite increasing their anionic charge and dehydration makes the calcium ion smaller, which allows easy access through the zeolite cages*[91]*. The study showed that at a higher pH, no free calcium ions are generated while at a lower pH, dissociation of filler is observed. Very low pH affects the efficiency of the zeolite due to acid attack and dissolution of the zeolite framework. Therefore, it was concluded that this system is safe to use at neutral or slightly acidic conditions*[91]*.

2.8 Paper making technique for the creation of novel structured adsorbent materials

The focus of current research occurring within the adsorption field is the improvement in adsorption capacity and selectivity of the adsorbent for the molecule of interest e.g. CO_2 adsorption from CO_2/N_2 mixtures. In the context of CO_2 capture, capital cost is directly related to adsorption capacity and selectivity. In particular, system costs are affected by size of the process equipment, available product recovery and the amount of power consumed. These are controlled by parameters such as adsorbent loading per unit volume, mass transfer

kinetics, and pressure drop. Improvement of these parameters by varying the adsorbent structures may help reduce system costs*[22]*.

Figure 2.8: Pellet and Bead adsorbents*[77]*

Conventional beads and pellets (Figure 2.8*[77]*) have many limitations in adsorption applications including large pressure drop, energy consumption, mass transfer resistance as well as attrition of the zeolite and packing difficulties, as explained in Table 2.2. In applications like rapid PSA, the limitations increase because of fluidization, fluid friction and specific surface area. Other non-particulate, novel structures have been created to eliminate the disadvantages of conventional beads and pellets. These structures include monoliths (Figure 2.9*[76]*) as well as laminates, foam and fabric structures shown in Figure 2.6. In order to replace bead and pellets, these structures must have high mass transfer kinetics, high volume working capacity, and low voidage to create a small sized adsorber and a gas flow path that produces low pressure drop*[22]*.

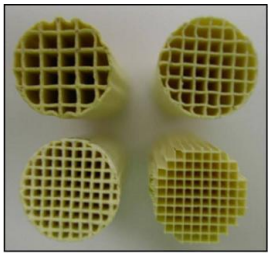

Figure 2.9: Monolith adsorbent structures with varying channel dimensions*[76]*

Monolithic adsorbents have a continuous body which is supported and have identical channels. A range of different channel sizes have been prepared, as shown in Figure 2.10. The main limitation of monoliths is that the density of the adsorbent material available is very low due to the presence of the binder and support materials and the large channel area. Also, not all the adsorbent material is accessible to the adsorbate molecules which flow past the channels. The binder material is essential as it provides an inter-particle network of bridges which bond the adsorbent particles to each other and to the substrate. Without the presence of binder material, the structure is prone to high dust production and has low strength. The fraction of active adsorbent material is decreased by the amount of non-adsorbent material*[32]*.

In order to create monolith structures, extrusion processes have been applied in which the zeolite slurry is extruded through a die. These processes can destroy the zeolite pores when high extrusion pressures are applied. The rheological properties of a dispersed zeolite slurry make it difficult to extrude and the extrusion costs can be quiet high. Channel width and wall thickness must be controlled for PSA and rapid PSA applications and this becomes very difficult with the extrusion process. Therefore, void space was either very high when narrow wall thickness was needed or the wall thickness became very thick when a small channel height was needed*[32]*.

Hence several researchers have employed the well-established papermaking process to create a large area honeycomb structure, instead of the extrusion process. The zeolite sheets created by this method are expected to be lightweight, have large surface area, have a homogenous distribution of zeolite, be easy to handle and flexible to process and can have the desired thin, uniform and narrow flow channels. These zeolite sheets can then be transformed to a honeycomb shape and used to remove large quantities of NO_x and SO_x that are present in the flue gases of the power plants, or be used in rapid PSA applications*[31]*.

A high density parallel channel laminate adsorbent structure can have advantages compared to conventional and other non-particulate adsorbent structures. This is because voidage can be controlled in these structures by controlling channel width, height and spacing, giving faster adsorption kinetics. Typical flow channel height for adsorbent structures ranges from 200-300µm and these spacers can be created by deposition, printing, extrusion or embossing as a part of sheet fabrication. These structures can also be used in systems where the velocity of the incoming gas exceeds the fluidization velocity of the traditional packed bed or extruded system as the adsorbent particles can be held more rigidly in place*[32]*.

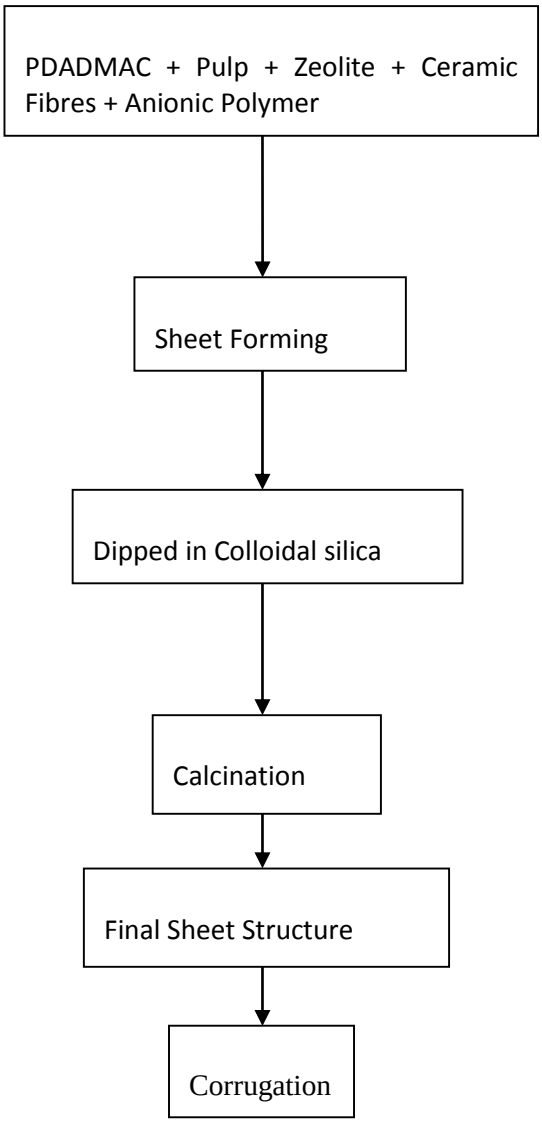

Figure 2.10: Schematic of the sheet forming process used by Ichiura et al.*[31]*

The sheet making process as described by Ichiura et al.*[31]* consists of the addition of cationic polymer (Poly diallyldimethylammonium chloride, PDADMAC) to the pulp, followed by inorganic fillers which are zeolite Y, glass fibers, ceramic fibers and kaolin and finally the addition of anionic polymer. Once the sheet is formed, it is dipped in colloidal silica and calcined at 700^0C for 20 minutes*[31]*. A schematic of the sheet forming process is shown in Figure 2.10. Here the pulp is burnt away and sintering of zeolite particles occur. The final zeolite honeycomb sheets are shown in Figure 2.11*[31]*.

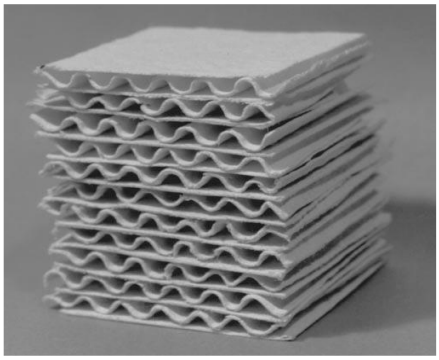

Figure 2.11: Zeolite honeycomb structures*[31]*

Ichiura et al. report that the use of the dual polymer system showed higher retention of inorganic fillers in the sheet due to the formation of comprehensive flocs. They expect that using only cationic polymer will separate the filler aggregates from the pulp preventing a high retention of zeolite. The pulp fibre was mainly used for reinforcement and for handling of the zeolite sheet to create the honeycomb structure, so a pulp content of only 5 to 10% was used. Any lower quantity of pulp used made it harder to remove the sheet from the wire. Cotton linter, unbleached softwood kraft and bleached hardwood kraft pulp were compared and linter pulp was the most favourable for sheet preparation purposes as the inorganic retention was high when a smaller quantity of pulp was used and the drainage time was also much shorter. From this study, Ichiura et al. have found that 5% linter pulp, 0.5%PDADMAC and 0.5 to 1% anionic polyacrylamide showed the highest retention and shortest drainage time*[31]*.

In a later study by Ichiura et al.*[92]*, the sheet strength was evaluated after the internal and external addition of alumina sol. The internal addition method is the addition of alumina sol to the pulp slurry before sheet casting. The external addition method is the dipping of the formed sheet in an alumina sol solution. It was found that the internal addition method was ineffective and the external addition of alumina sol showed a large improvement in sheet strength which was 8-50% higher than the sheet compressive strength when the external addition method of alumina was used. Strength was further improved by increasing the content of ceramic fibres from 10-24.5wt%. When tested against beads, the zeolite sheets showed a higher initial rate of moisture adsorption making them highly useful in practical applications. A further study by Ichiura et al.*[93]*, has shown that sheet uniformity affects the adsorption performance of the zeolite sheet. Their studies showed that the initial rate of adsorption of the more uniform sheet was much higher than the non-uniform sheet, although no comparison was made against zeolite beads. They have also acknowledged that since handsheets were prepared, the drainage was under gravity and therefore the retention was higher and would not be comparable to a commercial paper machine.

Yoo et al.*[94]* have synthesized a ceramic honeycomb rotor using papermaking techniques. No pulp was used in this preparation method. Ceramic fibres were used to prepare a sheet which was then corrugated and rolled to form a honeycomb rotor. The ceramic honeycomb rotor was heat treated at 600 ^{0}C for 5 hours to remove any organic binder. Then the rotor was soaked in a slurry of zeolite ZSM-5 and Y dispersed in silica sol, as shown in Figure 2.12. This method produced materials with a very low loading of zeolite because zeolite was not used in the sheet preparation process and added only when dipped in a zeolite-silica sol slurry, so there was not much retention of zeolite in the rotor structure. This preparation method is different from the one described by Ichiura et al.*[31, 92]*, in that pulp and zeolite were not used as a part of the papermaking furnish.

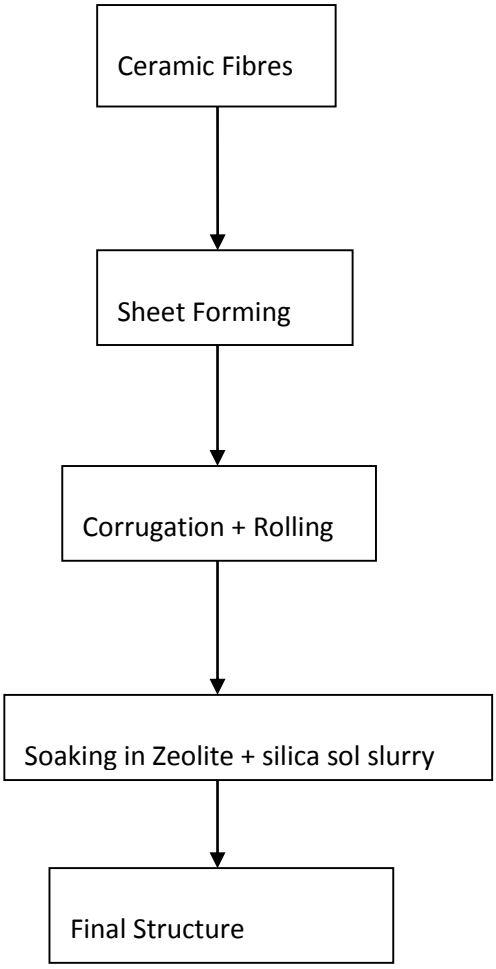

Figure 2.12: Ceramic Rotor preparation procedure used by Yoo et al*[94]*

The main drawbacks of the zeolite sheets prepared by Ichiura et al.*[31, 92, 93]*is that they are weak and brittle. They also powder easily and are difficult to handle. Too many components are added in the initial papermaking furnish for sheet preparation. As for creating a honeycomb structure for the purpose of having even flow channels, the disadvantages are that the channels are big and require intense processing of the sheet to get the required channels. Having large channels increases the voidage in the structure thereby increasing the size of the adsorption column and reducing the volumetric working capacity of the adsorbent. The ceramic rotor prepared by Yoo et al.*[94]*is stronger and more flexible but the amount of zeolite present in the structure is very low. From this previous work, it can be seen that there is an optimization between adsorbent content and strength of the sheet. Ichiura et al.*[31, 92,*

93] also show no comparison against zeolite powder or beads which would give an indication of sheet adsorption properties, while Yoo et al.*[94]* show that their structure has less than 30% adsorption capacity when compared to zeolite powder.

Another zeolite papermaking method is reported by Cecchini et al.*[5]* where handsheets were formed from zeolite NaY, ceramic and cellulose fibres and a dual polymer retention system. Depending on the end application, only cellulose fibres were used (low temperature applications) or a mixture of cellulose and ceramic fibres were used (high temperature applications). The high temperature sheets were calcined at 600°C before being used for toluene removal. The authors report that all the sheets have adequate strength before calcination, good air flow resistance and distribution of zeolite within the thickness of the sheet. Zeolite loadings of about 30% and 50% were obtained for the structures used in low temperature and high temperature applications, respectively. Both structures do not show much dispersion, as the breakthrough curves are sharp*[5]*. The dusting problem that the calcined structures often face without the addition of sintering agent was not discussed but the calcined structures are noted to be easy to handle.

In contradiction to this, in a follow up study, Cecchini et al.*[95]* mention that the structures created in the previous study are not easy to handle and improvements need to be made to the mechanical properties of the ceramic papers. They suggest the use of borate compounds as ceramic binder to improve the strength of paper. The papermaking method used a dual polyelectrolyte system to increase the retention of fine particles (Zeolite NaY and the borate compounds). The prepared sheets were fired at temperatures ranging from 600°C to 750°C to remove the pulp and increase the strength of the sheet structures. There was no clean rupture of an individual fibre break when testing the tensile strength of the ceramic papers, instead many fibres were pulled out during rupture. Having more zeolite decreased the paper strength. The maximum zeolite loading in the ceramic sheet was only 5.7%, which is very low, but since the application is for catalysis and the presence of borate increased the

mechanical strength and flexibility of the papers, this gives a new direction for the creation of structured composites. Increasing the calcination temperature from 600^0C to 750^0C, increased the strength between 5 to 17 times depending on the borate compound used. A calcination temperature of 650°C was chosen as increasing the temperature any further increased the risk of damaging the Faujasite zeolite.

2.8.1 Photocatalytic Applications of Zeolite/Titatinium dioxide filled Laminate Structures

A variation of the zeolite sheet prepared in*[31, 92, 93]*was prepared by Ichiura et al.*[96]*. A composite TiO_2- zeolite Y sheet was prepared where their combined use resulted in synergistic effects. The zeolite Y works as an adsorbent for VOCs (Volatile Organic Compounds) and the TiO_2 helps in decomposing the VOC to CO_2 by photocatalysis. The composite sheet preparatory method is similar to the zeolite sheet prepared by Ichiura et al.*[31]* with the addition of TiO_2 as an inorganic component. The adsorption and decomposition of acetaldehyde was tested on the TiO_2-zeolite sheet. The composite sheet with the help of UV-irradiation decomposed the acetaldehyde after 40 minutes and continued to do so after every run. A TiO_2: zeolite ratio of 1:4 proved to be an optimum value for the continuous removal of acetaldehyde under UV irradiation. This sheet works well when there are dilute pollutants as the adsorbing action of the zeolite concentrates the pollution for more efficient photocatalytic degradation.

Further studies by Ichiura et al.*[97, 98]* have shown the application of the composite sheets for NO_x, toluene and formaldehyde removal. With NO_x removal, the composite sheets prepared by a slightly different method seemed to produce the best results. In the final step before burning, the sheets were dipped in TiO_2 sol instead of alumina sol. The proposed mechanism of NO_x (NO +NO_2) removal from the sheet is that NO was adsorbed by the zeolite, which is then oxidized to NO_2 and then further oxidised to HNO_3 by the TiO_2 in the

sol. The HNO_3 is then fixed on the zeolite. Compared to the other sheets, the sheet prepared with TiO_2 sol was much faster with the oxidation reaction, and not much NO_2 was generated by this sheet. Toluene and formaldehyde are indoor pollutants and the composite sheet can be placed in the walls and ceilings of the houses where these pollutants are discharged from plywood, particle boards and adhesives from wallpaper.

Ko et al.*[87, 99]* have created a similar TiO_2 photocatalytic paper to Ichiura et al. where they highlight the use of zeolite not only for its adsorption of VOC but also for its role as microparticle retention aid. Ko et al. used sol-gel synthesis, where the TiO_2 nanoparticles were anchored on the zeolite particles. These particles were then used in papermaking to create a composite sheet. This composite sheet was compared with commercial photocatalytic paper and found to perform much better as higher amounts of toluene were removed.

The previous discussion clearly shows the potential of utilizing papermaking techniques in the creation of zeolite laminate structured adsorbents. Accordingly, zeolite laminate structures need to be synthesised which should be practical and suitable for adopting to large scale manufacture for use in point source capture of carbon dioxide. These structures must also have competitive advantages over beads and other non-particulate structures.

2.9 Scope of the Present Work

The literature review has highlighted the advantages of papermaking techniques in creating laminate structures using zeolites for adsorption. These structures are easy to prepare, have a large surface area and the preparation process is cheap. The drawbacks of the previous structures have also been highlighted. The structures created are weak and brittle, the process can have too many components during sheet preparation and the adsorption capacity of the laminate structures should be increased. Also, none of the studies have been conducted in a systematic manner where the relationship between the synthesis variables, the structure and characteristics and the performance of the sheet has been studied. The overall performance of

the laminate structures in an adsorbent application has also not been studied and compared against the industry standard of a fixed bed of beads. The aims of the study and the corresponding chapters are therefore:

- To develop a simple synthesis procedure to form strong, reproducible zeolite laminate structures with high internal porosity and high zeolite loading (Chapter 3).
- To identify and design a methodology to create variation in the synthesis variables in order to study the relationship between synthesis-structure-properties (Chapter 3).
- To explore the relationship between the synthesis conditions used in laminate structure fabrication and the porous structure thereby created. Creating a highly porous sheet structure has the potential to eliminate the need for creating channels for gas flow, which is a separate process to sheet forming (Chapter 4).
- To develop a new method to investigate the relationship between synthesis conditions and sheet strength (Chapter 5)
- To study the relationship between synthesis conditions and adsorption kinetics of the laminate structures (Chapter 5)
- To understand the relationship between synthesis and structure by identifying the optimal structure in terms of strength, loading, void fraction and the kinetics of adsorption (Chapter 6).
- To create an adsorbent column for the testing of the laminate structures prepared using papermaking methods that offer even gas distribution pathways (Chapter 7).
- To examine the performance of the laminate structured adsorbents in carbon capture application using pressure drop and breakthrough fronts and simulating the experimental results using modelling software to estimate the effective diffusivity of the laminate against commercial beads (Chapter 7)

- To create parallel hydrophobic channels on laminate zeolite sheets using ink-jet printing and comparing the performance of these structures against previous laminate structures and beads (Chapter 8)

Chapter 3

Synthesis of Laminate Zeolite Adsorbent Structures using Papermaking Techniques

This page is intentionally blank

3.0 Synthesis of Laminate Zeolite Adsorbent Structures using Papermaking Techniques

3.1 Introduction

As mentioned in the previous chapter, the creation of non-particulate adsorbent structures can have many advantages. But the disadvantages associated with these structures of high cost and low loading need to be reduced for use in industrial applications. Hence a structured adsorbent has to be created that has high adsorption capacity, low pressure drop, high mass transfer and provides overall high system efficiency. In addition, the very large scale of the flue gas capture application demands that the adsorbent structure should be made using low cost materials and processes. The mode of preparation for structured adsorbents using papermaking has been discussed previously in Section 2.8. Papermaking technology is low cost and can be used to create highly loaded, large surface area sheet structures. As discussed in Section 2.7, zeolites have already found uses in the paper industry as fillers and retention aids, which allows them to be easily incorporated into the papermaking process.

The zeolite sheets created by the papermaking technique are required to be thin, lightweight, have a homogenous distribution of zeolite, be easy to handle, flexible to process and have high porosity within the sheet structure. Section 2.8 shows the previous attempts at creating zeolite laminate structures using papermaking techniques. As mentioned, this technique provided sheets that had low loading of zeolite which reduced the usefulness of the sheets for bulk industrial application. Also the sheets had low internal porosity and depended on corrugation to create channels for reducing pressure drop and creating access to the zeolite within the structure. Hence the new laminate structure must have higher loading than the previously created structures with a higher internal porosity.

This chapter deals with the selection of materials for the preparation of the laminate structured adsorbent. The machine used for the formation of these laminate structures will be introduced and the differences of this machine compared to commercial papermaking machines will be explored. The initial synthesis procedure will be given along with the retention results of the zeolite in the paper structures. There are different variables that can be controlled during the sheet forming procedure. As mentioned in the scope of the project, the relationship between synthesis, structure and properties need to be studied. Therefore, six variables have been identified and a high and low factor has been established for each variable. Since, an individual study of each variable will be excessively time consuming, a partial factorial design has been established to prepare the sheets in the specified conditions for further analysis of their characteristics and properties.

3.2 Selection of Components for Laminate Structure Preparation

The fundamental goal behind the engineering of laminate zeolite sheets is to combine materials and processing steps in such a way as to provide high adsorption capacity, high strength, low mass transfer resistance and hierarchical pore network system. To accomplish this, the base ingredients are zeolites (which act as the main adsorption sites), scaffolding materials (pulp fibres) and additional inorganic materials (ceramic fibres and colloidal silica) to assist in increasing the strength of the final structure. The specific nature and content of each of these components affects the final zeolite laminate structure.

3.2.1 Adsorbent Selection

Low silica zeolites such as 13X and 4A give optimum adsorption properties for carbon dioxide capture in terms of capacity, pore size and three dimensional channel systems*[100]*. Micron zeolite NaA (1-2µm) was kindly supplied by UOP, micron sized zeolite 13X (2-4µm)

was purchased from Wholesale Group International and nano zeolite A (300-500nm) was synthesized using the procedure in the paper by Wang et al.*[48, 101]*. The method for preparation of Nano zeolite A is discussed in Section 3.2.1.1. Zeolite NaA belongs to the framework type LTA and has a mean effective aperture of 4Å. Due to the difficulty in forming nano zeolite 13X, zeolite NaA was chosen. Zeolite NaA was used for characterisation of the laminate structures as nano sized zeolite was necessary to complete preparation of the structures from the partial factorial design and Zeolite 13X was used for examining the performance of the laminate structure as zeolite 13X has previously shown to be a very suitable adsorbent for the recovery of CO_2*[69]*. Figure 3.1 shows the SEM images of micron zeolite 13X and NaA and nano zeolite NaA. The SEM images were taken according to the method described in Section 4.2.

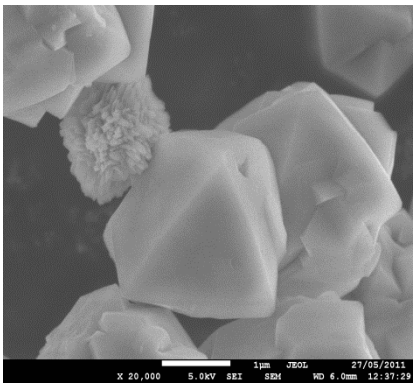

a

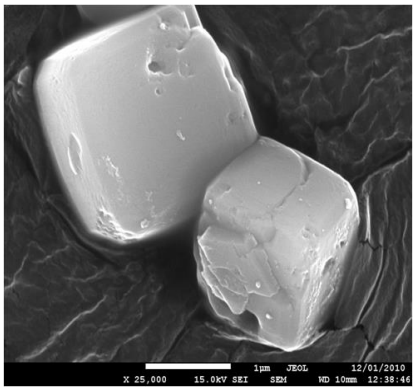

b

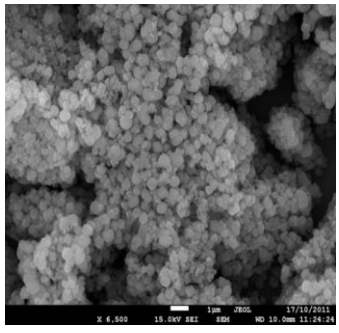

c

Figure 3.1: a) SEM of micron zeolite 13X b) SEM of micron zeolite NaA c) SEM of nano zeolite NaA

3.2.1.1 Preparation of Nano Zeolite A

The nano zeolite A is prepared using Wang's method of synthesising template free nano zeolite crystals*[101]*. The methodology reported in their supporting paper is used but since a large amount of zeolite is required, the amounts of each of the initial components were increased to five times the reported amount. The materials used include water, sodium hydroxide, sodium aluminate, aqueous 30wt% colloidal silica (Ludox HS-30) and Methylcellulose purchased from Sigma Aldrich. The methodology reported in the supporting paper was very closely followed. The nano zeolite preparation process is as follows: 805.5g deionised water, 100g sodium hydroxide and 54.5g sodium aluminate were added in that order in a polypropylene bottle and stirred vigorously until the solution became clear. Aqueous 30% colloidal silica (135g) was added to the clear solution and after addition of the colloidal silica, the solution became turbid. The synthesis gel was sealed and aged overnight under room temperature and vigorous stirring. For every 11g of aged gel, 1g of methyl cellulose powder was added. Here the weight composition was $3.56Na_2O:1.59SiO_2:1.00Al_2O_3:32.12H_2O:3.48MC$.

Since the amount made was quite large, an overhead stirrer was also employed. This was followed by continuous stirring for another 4 hours using the overhead stirrer and a magnetic stirrer. This allows the methylcellulose to dissolve. This gel was then cooked at 80°C for three hours. Finally the sample was repeatedly washed with deionised water followed by centrifugation, decanting and redispersion in deionised water until the methylcellulose is removed from the mixture. The SEM image of the nano zeolite A prepared using this method is shown in Figure 3.1C and the size of the nano crystals is shown to be between 300-500nm. XRD was also performed on the prepared nano zeolite A powder and purchased micron zeolite A powder to compare and see if there were any changes in the crystalline structure. The XRD analysis was performed according to the method described in Section 3.4.3. The XRD patterns for nano A and micron A powders are shown in Figure 3.2. As can be seen

from the figure, both the patterns show the presence of all the peaks but due to the presence of some amorphous material in the nano zeolite A powder, the peaks are broader and there is a shift from the base line.

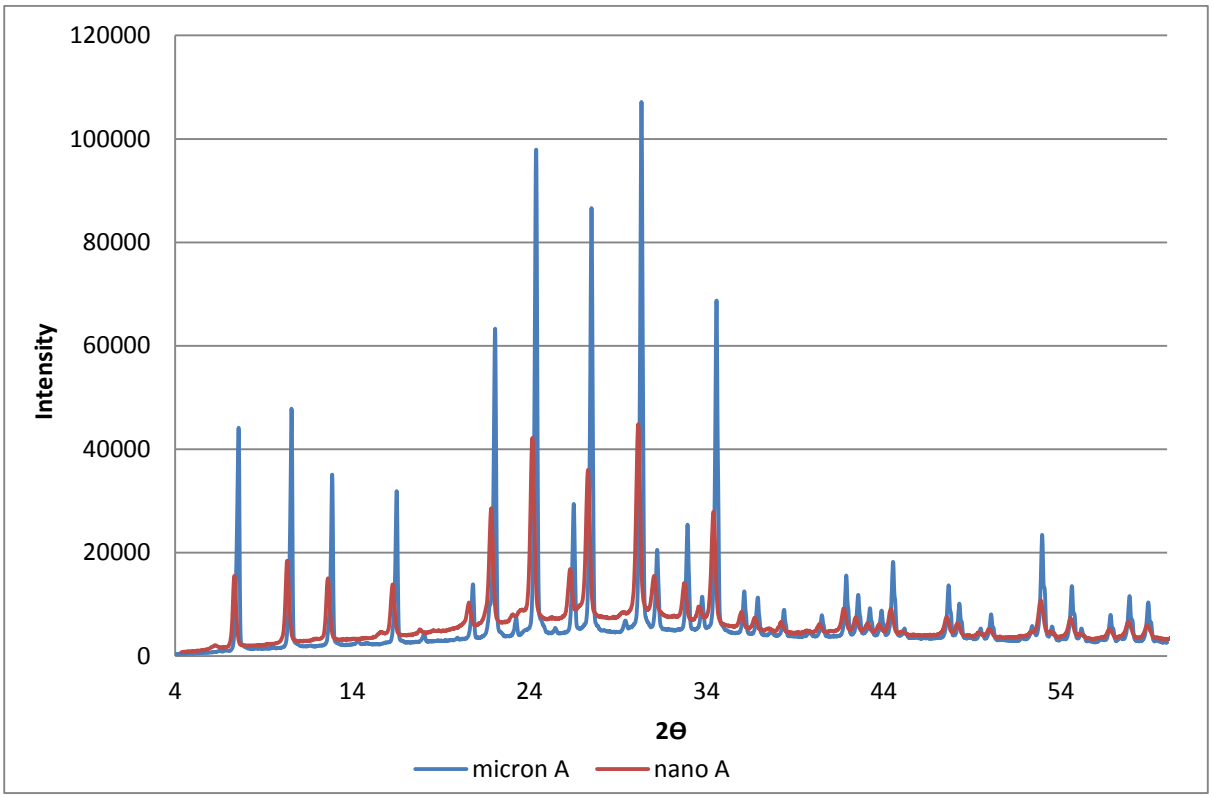

Figure 3.2: XRD patterns for purchased micron A powder and prepared nano A powder

3.2.2 Scaffolding Materials

The zeolites chosen above also unfortunately have high affinity for water and on exposure to normal atmospheric conditions, rapidly saturate all available sites leading to a dramatic drop in CO_2 capacity*[102]*. Therefore, to produce a useful structure, the persistent water must to be initially removed by heating to 350°C for about 10 hours*[100]*. This also simultaneously removes the organic content. Pulp is essentially used in the sheet forming process to retain the zeolite and in the removal of the sheet from the wire and subsequent handling. When the structure is calcined, the pulp is removed but the structure does not collapse due to the

presence of other inorganic components which helps maintain the structure. The spaces left behind by the fibres are preserved during the removal of the fibres during the calcination procedure. It is necessary to maintain the spaces left behind by the fibres as these spaces provide the internal porosity required for gas flow to reach the zeolite through the thickness of the sheet. During adsorption, it is expected that the high internal porosity allows for rapid access to the adsorption sites without any additional procedures such as corrugation.

Unbleached thermomechanical pulp (fibre diameter 30-70µm) was taken from the feed into the low consistency reject refiners of a TMP mill processing radiata pine. Unbleached radiata pine kraft pulp (Fibre diameter 20-60µm) was taken from the exit of the brownstock washers. Refer to Figure 3.3 for SEM images of TMP and Kraft fibres. Both these fibres have similar dimensions but the kraft fibres do not have many secondary fibres and the fibres are less undamaged and longer than the TMP fibres.

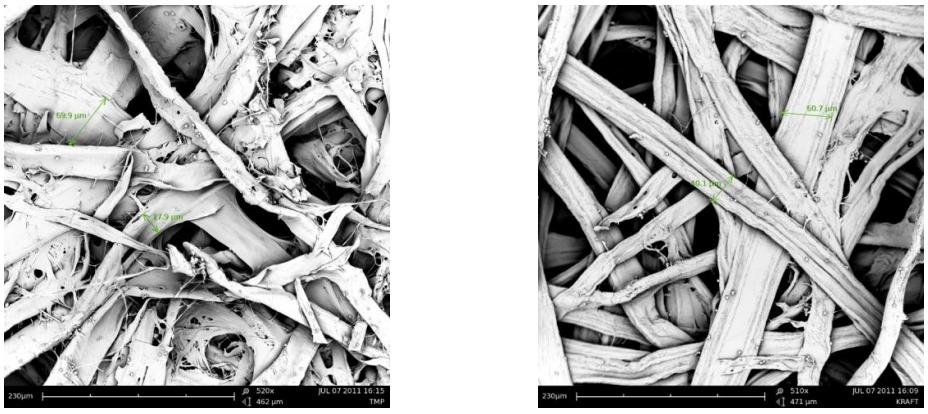

a b

Figure 3.3: a) SEM of TMP fibres b) SEM of Kraft fibres

3.2.3 Inorganic Materials

The ceramic fibres act as the reinforcement agent by holding the structure together after the removal of pulp fibres. The colloidal silica acts as the sintering agent which reduces the powdering and dust formation of the zeolite by sintering the zeolite to the ceramic fibres. The ceramic fibres were kindly given by Unifrax Australia Pty Ltd, while colloidal silica

(22nm particles) was purchased from Sigma Aldrich and colloidal silica (120nm particles) was kindly obtained from IMCD Australia Ltd. Inorganic ceramic fibres and colloidal silica are used for increasing sheet strength*[92]*. The presence of these additional components reduces the carbon dioxide adsorption capacity of the zeolite laminate structure, but enhances the strength of the structure thereby increasing applicability in different areas. Refer to Figure 3.4 for SEM images of the inorganic binders. The ceramic fibres have varying diameters with a bulbous head at one end and a thin tail at the other end. The tails can come in range between 2-50µm and the bulbous heads can come in the range of 50-250µm. The colloidal silica sols consist of extremely small, non porous amorphous particles in water stabilised by a small amount of alkali*[103]*. The 22nm colloidal silica has a very uniform particle size distribution while the 120nm silica has a varying particle size distribution ranging from 20-120nm.

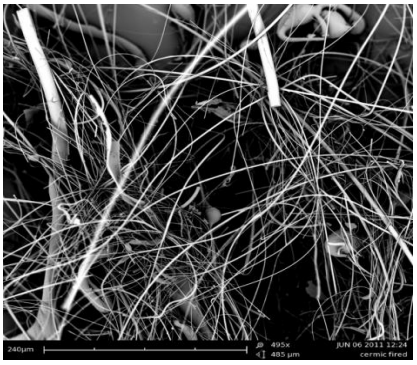

a

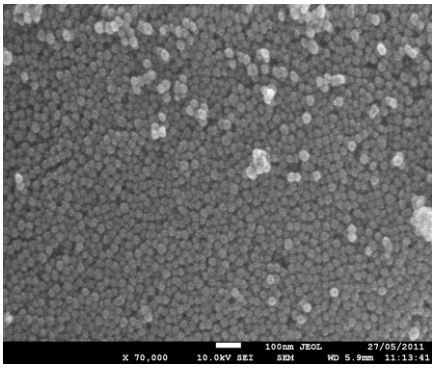

b

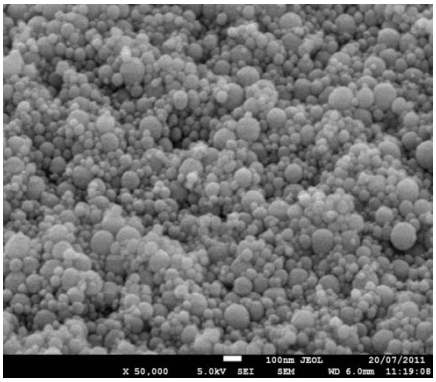

c

Figure 3.4: a) SEM of ceramic fibres b) SEM of 22nm colloidal silica c) SEM of 120nm colloidal silica

3.2.4 Cationic Polymers

Retention aids increase the percentage of filler and fibres fines retained during paper formation on a web*[78]*. Without retention aids, there is not much deposition of fillers on the cellulose fibres. Retention aids work via different means such as electrostatic attraction, charge neutralisation, formation of polymeric bridges and filtration for the deposition of fillers on the cellulose fibres. Cationic polymers are the retention aids used in this application*[104, 105]*. The zeolite was pre-flocculated with cationic polyacrylamide kindly provided by SNF Floerger, Australia. The cationic polyacrylamide has a medium charge density, high molecular weight, 39% solids content, with a bulk viscosity of 1200cps. The stability of the cationic polyacrylamide when mixed with deionised water is 1 day.

3.2.5 Table showing role of each component selected

Component	**Purpose**
Zeolite 4A and 13X	Adsorbent
Pulp	Handling purposes, physical retention of zeolite and porosity
Cationic Polyacrylamide	Retention Aid
Ceramic Fibres	Reinforcement Agent
Colloidal Silica	Sintering Agent

3.2.6 Safety Aspects of the use of Different Components

All of the components used for preparation of laminate structures are non-hazardous. General laboratory safety practices of using gloves, closed shoes, laboratory coat and goggles were used in handling all the substances. Respiratory protection was used in the handling of all powders and ceramic fibres. Since the nano zeolite is larger than 100nm in size, they can be treated like the other powder substances. The cationic polyacrylamide is non hazardous as well and general lab practices are allowed in their handling. The colloidal silica only pose a problem as they are below 100nm but they are also non-hazardous*[106]* and in colloidal form which reduces exposure to the nano particles. The colloidal silica was handled only using protective gloves and in the fume hood to reduce exposure to any airborne particles.

3.3 Sheet Forming Procedure

The formation of the adsorbent laminate structure is carried out using the Moving Belt Sheet Former. The required sheet forming components are mixed in a slurry and the components are separated from water over a wire using high vacuum conditions. The resultant sheet is coated with colloidal silica and calcined. This results in a highly porous laminate adsorbent structure which can then be used for carbon dioxide capture.

3.3.1 Moving Belt Sheet Former

The moving belt sheet former is a novel laboratory papermaking device that was developed by the Laboratory of Paper Technology at Helsinki University of Technology*[107]*. Using this machine, it is possible to reproduce certain features of a commercial paper machine such as using a commercial fabric, high frequency vacuum pulses and programmed vacuum profiles. Also the paper made from this machine can reproduce the fibre orientation of commercial papers which is not possible with general laboratory sheet formers. Hence, the moving belt sheet former has similar drainage conditions to those occurring on commercial

paper machines and can produce paper that has z-direction (through thickness) distributions of material similar to commercial paper*[108]*. The machine also produces a 22cm x 22cm square sheet of various grammages. Figure 3.5 shows an image of the moving belt sheet former with its vacuum box, stock forming chamber and the cogged belt. Figure 3.6 a shows the agitation head and forming chamber and Figure 3.6 b shows the stock in the forming chamber before sheet forming commences.

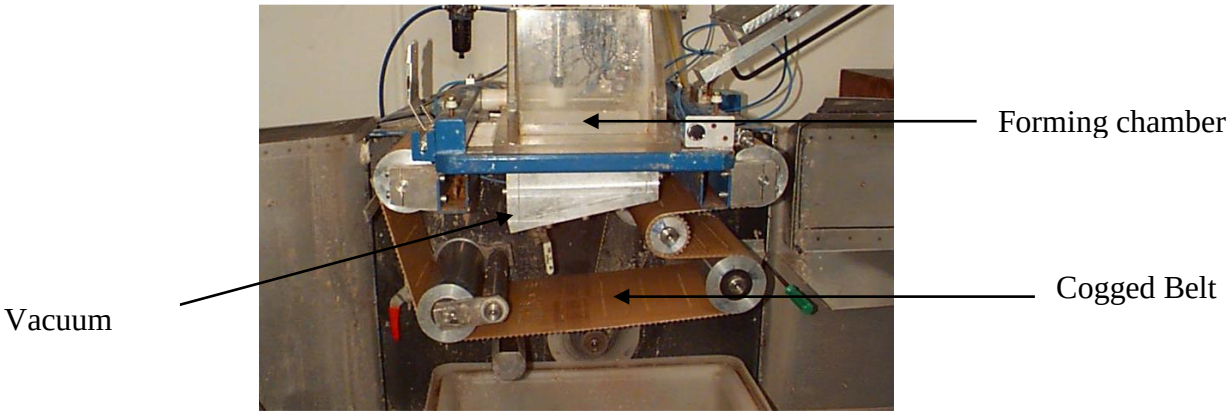

Figure 3.5: The Moving belt sheet former showing belt, vacuum box and forming chamber

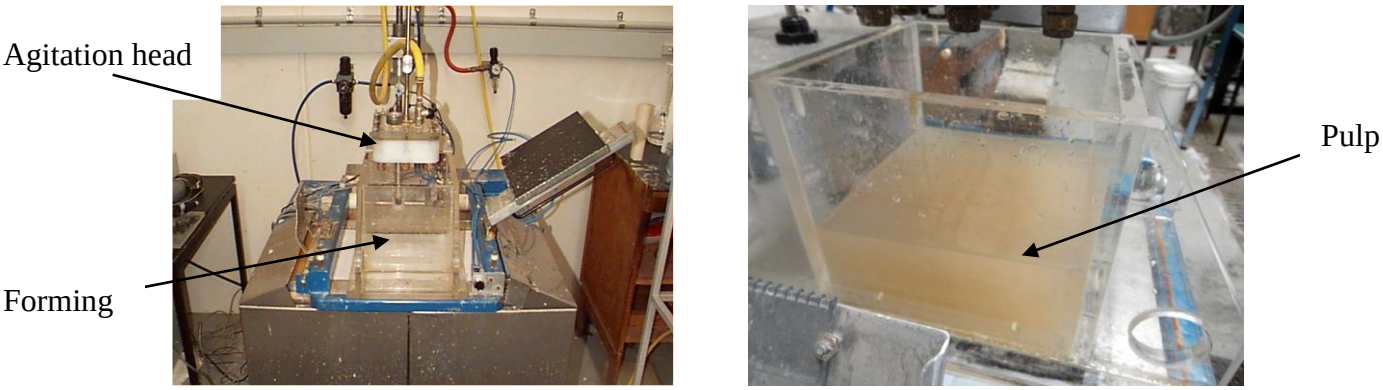

a **b**

Figure 3.6: a) Moving belt sheet former agitation head and forming chamber b) Stock in the forming chamber before sheet forming operation.

3.3.1.1 Features of the Moving Belt Sheet Former

The moving belt sheet former consists of a 9 litre stock forming chamber which sits on top of the forming fabric (wire). This forming chamber can be used to make sheets of the size 22cm x 22cm. The size of the forming chamber can be adjusted to give smaller sheet sizes. 10cm x 10cm sheets were also prepared using smaller forming chambers. A plastic sheet is placed between the chamber and wire to stop from draining of the stock before agitation. Agitation of the stock occurs using an overhead agitation head. The agitation head is initially filled with water by using a manual water inlet. Compressed air is injected into the head to push the water through the jets and ceases after the complete evacuation of the head. This agitation head evenly distributes the stock across the whole of the formed sheet. After agitation, the plastic sheet is pulled away using a hydraulic arm and drainage begins. A cogged belt sits below the forming fabric under which is a stationary suction box. The cogged belt consists of holes punched into the valleys of the cogs allowing for drainage through the belt. The suction box contains low vacuum levels (less than 15kPa) which are produced by air injectors. This aids with initial water removal. An external vacuum pump provides higher vacuum levels (up to 50kPa) which aid with sheet dewatering after formation. The formed sheet is removed using a pneumatic coaching device which helps to press the wet sheet onto a blotter. The entire sheet forming process is controlled by a computer.

3.3.2 Zeolite Laminate Formation Procedure

The first step in the sheet formation procedure is the flocculation of the zeolite particles. Since the zeolite particles have a diameter less than 2µm, they can easily pass through the wire and end up in the white water. Also both the zeolite structure and pulp have surface negative charges which reduce the physical retention of zeolite in the structure. This reduces the retention of zeolite in the adsorbent sheet to between 2-5%. Hence a flocculation step is essential to improve retention by agglomerating the zeolite particles. Since the zeolite surface

has a negative charge due to the presence of hydroxyl groups, a cationic polymer is required for flocculation to occur.

The pulp and ceramic fibres were disintegrated and the flocculated zeolite particles were then added to the pulp-ceramic slurry. Disintegration helps in dispersing the fibres through the slurry and separates interlaced fibres from one another. 100 grams per square metre (gsm) of pulp was used. The total inorganic content (ceramic fibres +zeolite particles) of the as formed sheet was 400gsm. This slurry consisting of pulp, ceramic and zeolite particles was then poured into the forming chamber of the moving belt sheet former. The vacuum ran for a total of 60s. After forming, the sheet was then removed from the former and pressed under a pressure of 350kPa for 5 minutes using a static press. The blotting paper was then changed and the sheet was further pressed for another 2 minutes at 350kPa. The pressed sheet were placed in drying racks and left overnight in a temperature and humidity controlled room at 23°C and 50% Relative Humidity. The drying racks help keep the sheet flat while it is drying and do not allow any curls to form during the drying process.

The dried sheet was then brush coated on both sides with colloidal silica and this structure was then calcined at 650°C in air. The colloidal silica was used at either 20wt% or 40wt% concentration for particular experiments and this is discussed in Section 3.5.2. At 650°C, sintering of the inorganic particles occurs, without altering the nature of the zeolite. This has been verified using XRD analysis and the results are shown in Section 3.4.3. The heating process also removes all organic materials and the final laminate structure is formed. The above procedure is the general procedure for laminate structure formation. Changes in the procedure will be elaborated closer to the sections where the changes were made.

3.4 Preliminary Results

As mentioned previously, retention of the zeolite is enhanced using cationic polyacrylamide. The variables needed to maximise retention while maintaining good formation are the amount of CPAM used and the stirring time of zeolite with CPAM.

3.4.1 Preparation of Sheets for retention and formation results

For the retention and formation experiments, 100gsm (1g) never dried unbleached kraft pulp was used to make 10 cm by 10 cm sheets using the Moving belt sheet former. 250gsm (2.5g) of zeolite 13X (particle size 2-4μm) was used for the sheet forming. The zeolite was first flocculated using Cationic Polyacrylamide (CPAM) added at the given concentration between 0-30 minutes before addition to the pulp slurry for sheet making. The sheets were then dried and photographed to capture images of the surface and see distribution of zeolite in the sheet structure. The sheets were later ashed to find zeolite retention in the sheets.

3.4.2 Formation Results

Figure 3.7 shows photographs of the sheets made from changing CPAM addition levels and stirring time. Unbleached kraft pulp was used in order to pick up visually the effects of filler distribution within the sheet. With immediate addition, large clumps are formed which reduces good sheet formation. With 5 and 10mg CPAM/g zeolite, the pulp also agglomerates creating badly formed sheets. Increasing stirring times greatly improves sheet formation and a concentration of 2mg CPAM/g zeolite with 30 minute stirring time, or 5mg CPAM/g zeolite for either 15 or 30 mins stirring time show the best formation with good distribution of small zeolite flocs. Using 10mg CPAM/g zeolite creates large zeolite flocs even with increased stirring times.

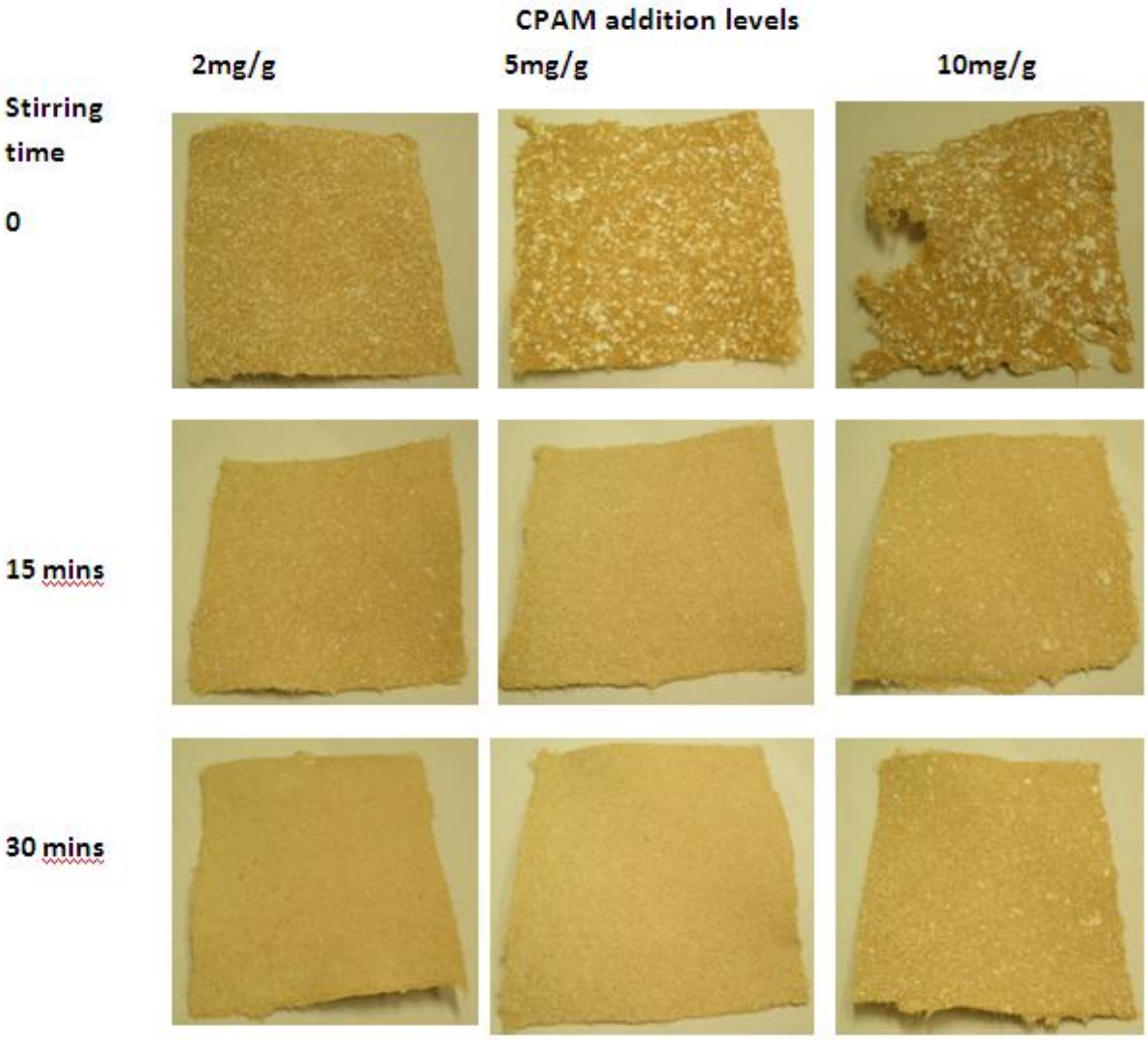

Figure 3.7: Images showing formation distribution of zeolite in the sheet structure for varying CPAM addition levels and stirring time.

3.4.3 Retention Results

Retention results (Figure 3.8) show that with CPAM addition the retention is increased to more than 80%, with 5mg CPAM/g zeolite showing the highest retention for all stirring times. From the formation results and retention experiments, a CPAM concentration of 5mg CPAM/g zeolite with a stirring time of 15 minutes is suggested and this CPAM concentration and stirring time was used for the sheets prepared in the partial factorial design and

adsorption experiments discussed in Section 3 and 7 respectively. This process had more than 95% retention of zeolite filler. These results show that with the right addition amount of polymers, the zeolite filler can be easily retained with good distribution through the sheet matrix. Depending on the polymer and the size of the zeolite particles, the retention-formation results will vary and have to be determined for each individual situation.

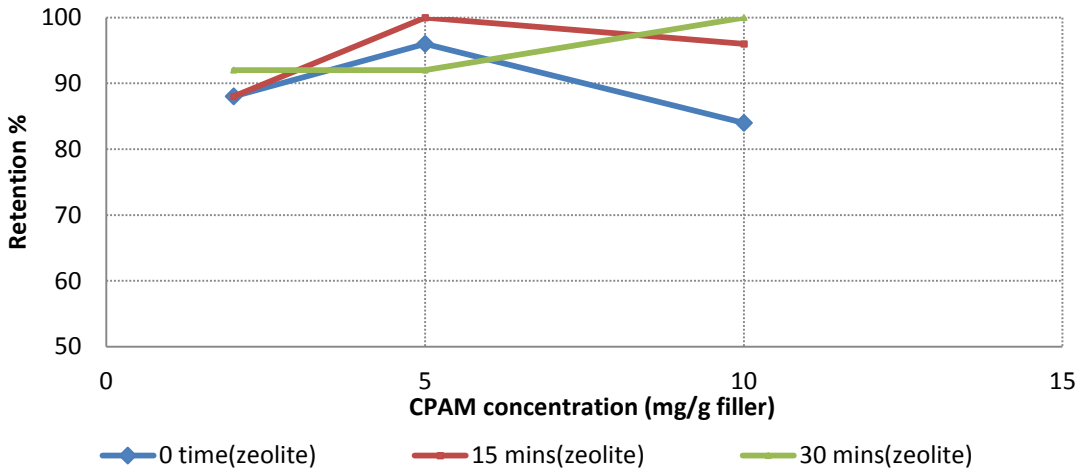

Figure 3.8: Retention results for varying CPAM concentration and stirring time

3.4.4 XRD analysis procedure

The changes in crystalline structures of the synthesised and calcined zeolite samples were characterised using powder X-ray diffraction. The wide angle diffraction patterns were recorded by a Rigaku Miniflex 600 diffractometer using Cu Kα radiation. The X-ray diffraction scanning was performed at ambient conditions at 2θ from 4-60° in steps of 0.02° at a scan rate of 2°/min.

3.4.5 Assessment for any structural changes after firing to 650°C

Since the zeolite laminate structure is fired at 650°C, it is necessary to check if any irreversible changes occur in the zeolite due to this calcination. The zeolite is the main adsorbent site and any change in its structure can reduce the amount of CO_2 adsorbed. This

assessment was made using XRD analysis described in Section 3.4.3. Figure 3.9 shows that the XRD for the zeolite 13X before and after firing to 650°C shows no changes, as the patterns are the same. Therefore, the nature of the zeolite 13X remains unaltered. The patterns for 4A micron zeolite before and after calcination to 650°C are shown in Figure 3.10. These patterns show that the micron A zeolite also remains unaltered after calcination to 650°C. The patterns for nano zeolite A before and after firing are shown in Figure 3.11 along with the pattern for micron A before firing and as expected there were no changes in the XRD patterns of the nano zeolite.

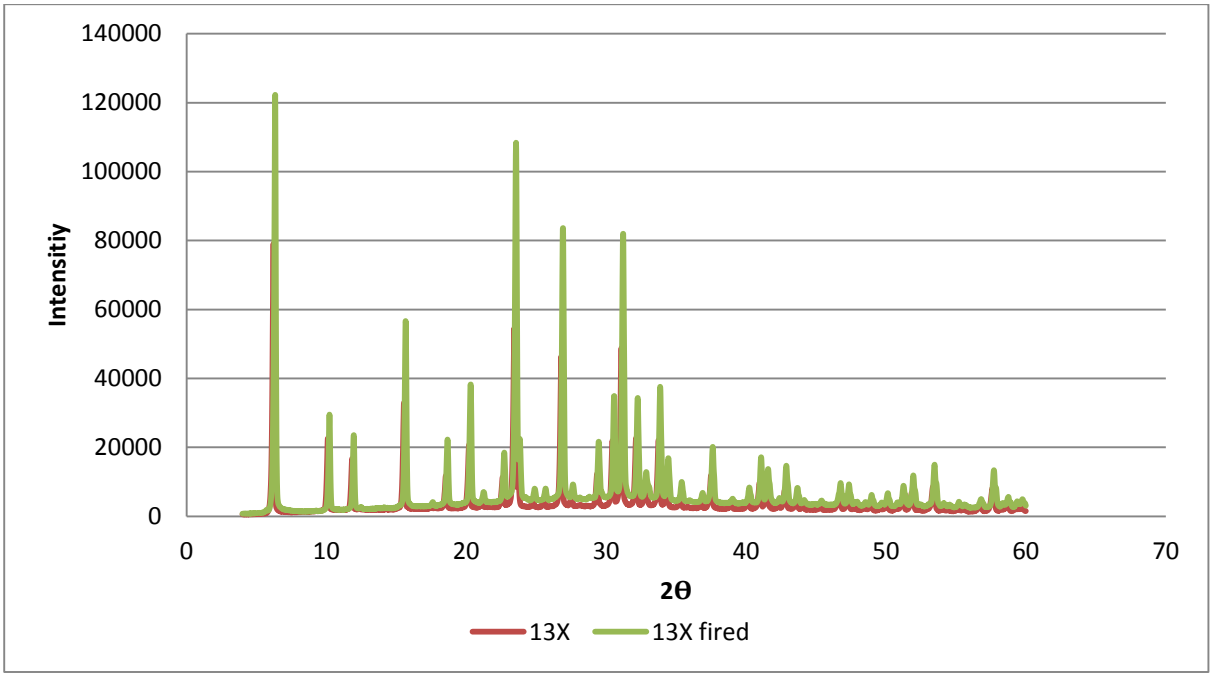

Figure 3.9: X-ray diffraction patterns for zeolite 13X before and after heating to 650^{0}C

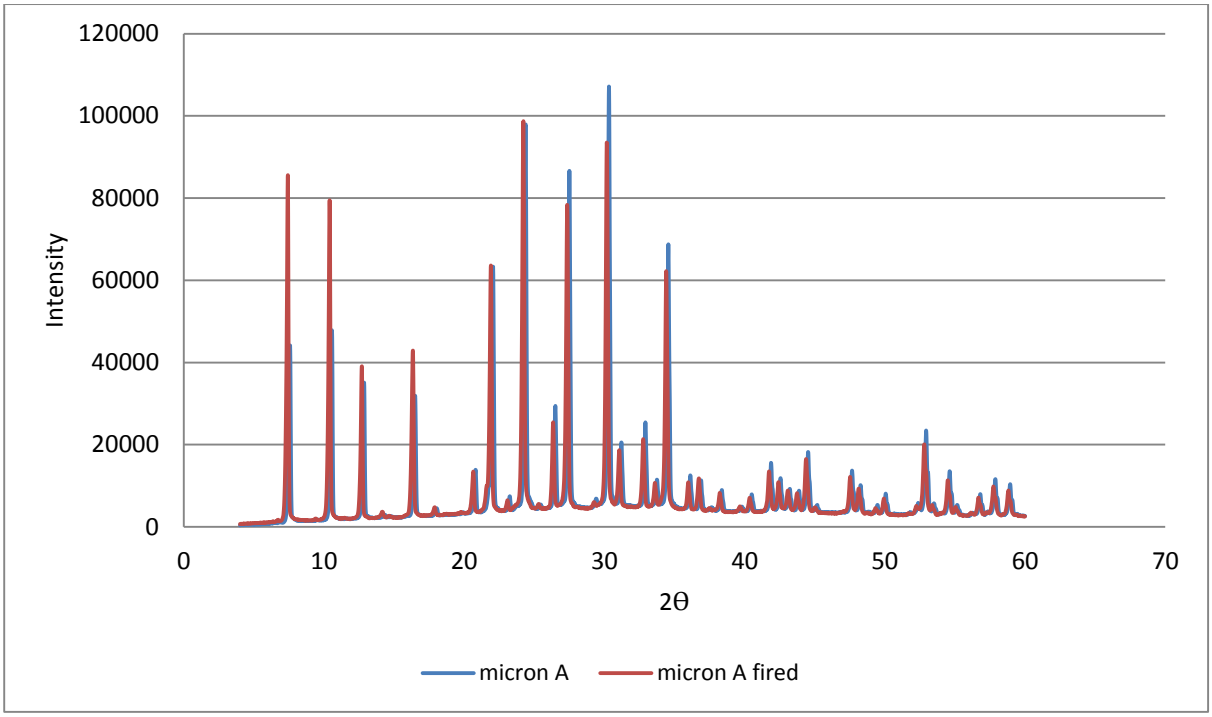

Figure 3.10: X-ray diffraction pattern for zeolite micron A before and after heating to 650°C

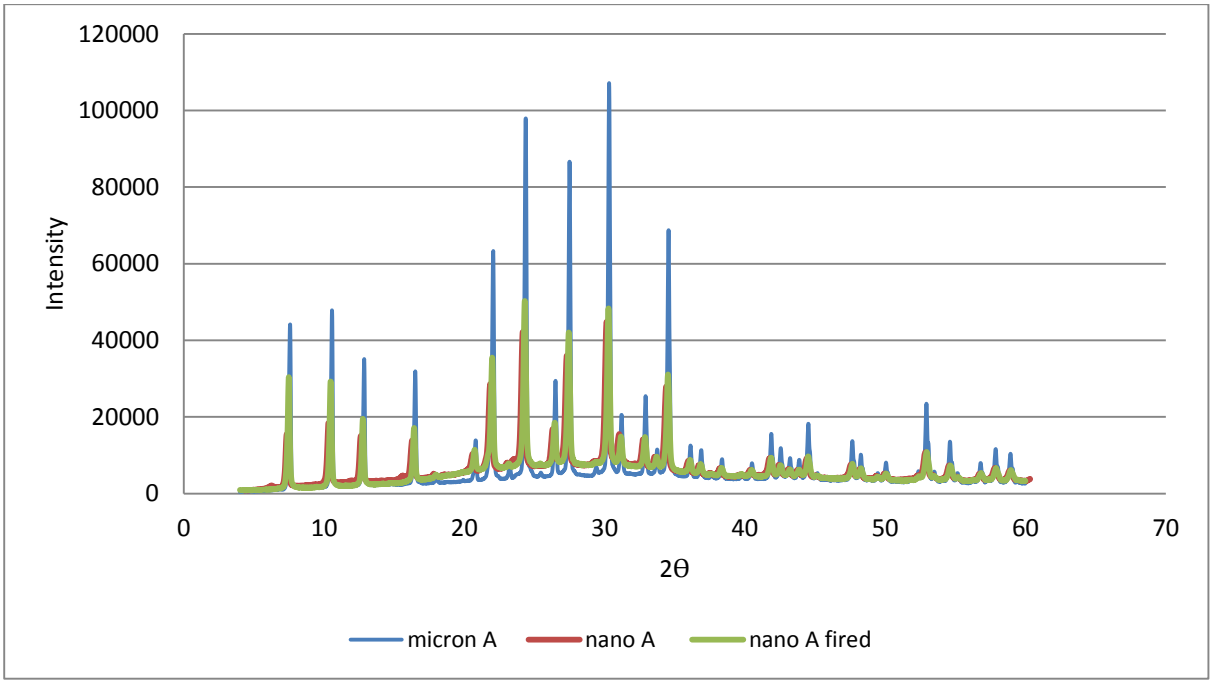

Figure 3.11: X-ray diffraction pattern for zeolite micron A before firing and nano A before and after firing

3.5 Selection of variables for partial factorial design

In order to study how the synthesis of the zeolite laminate structure affects its characteristics, the variables for synthesis that affects the characteristics have to be determined. The variables selected for this study are the ratio of ceramic fibres to zeolite particles, silica concentration in the initial suspension, the silica and zeolite particle sizes, the pulp type and the calcination rate. The preparation of the laminate structure is shown in Figure 3.12 with all the variables that were selected for this study. The characteristics that are intended to be studied are pore measurements, strength, amount of zeolite and kinetics or rate of adsorption of CO_2. For each variable, two factors are provided which are the high and low factors. These factors are meant to be very far from each other to pick up any contrasts for each variable.

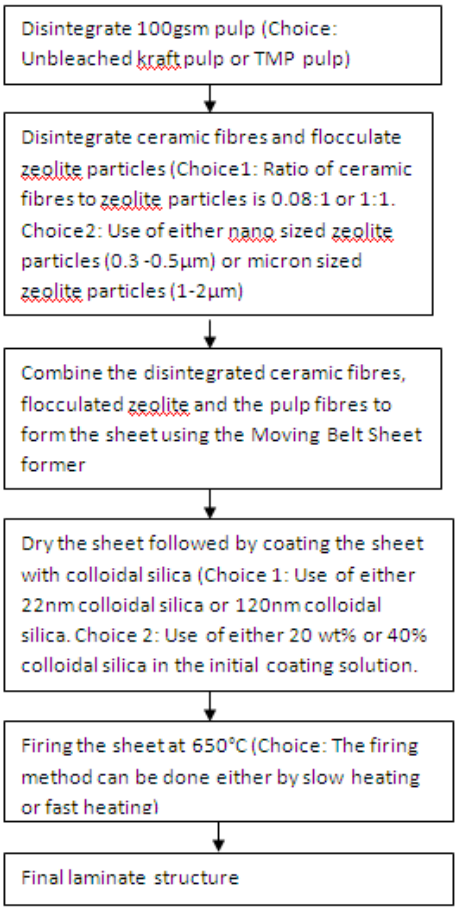

Figure 3.12: Preparation of laminate structures for the study of relationship between synthesis-structure and properties

3.5.1 Ratio of ceramic fibres to zeolite particles

The high and low factors for the ratio of ceramic fibres to zeolite particles were chosen as 1:1 and 0.08:1 respectively. The total amount of ceramic fibres and zeolite particles is kept constant at 4g or 400gsm of inorganic particles and only the ratio is varied. The concentration of zeolite and ceramic fibres in the laminate structure would then be so different that any variations in the characteristics would be easily detected.

3.5.2 Silica Concentration

This refers to the initial silica concentration in the solution which was then coated to the laminate structure. The 22nm colloidal silica contains 50wt% colloidal silica in solution. This solution was diluted to either 20wt% or 40wt% colloidal silica depending on the required amount in the laminate sample. The 120nm colloidal silica contains 40wt% colloidal silica in solution. This solution was used as is or diluted to 20wt% as required from the partial factorial design shown in Table 3.1. The 20wt% or 40wt%, 22nm or 120nm colloidal silica was coated using a paint brush on both sides of the laminate structure before calcination, as this allows the silica to penetrate through the structure. The structure was brush coated until both sides of the sheet were completely wetted.

3.5.3 Silica Particle size

Two silica particle sizes were chosen. They were 22nm or 120nm silica suspensions. Their SEM images are shown in Section 3.2.3 in Figure 3.4 B and C. As can be seen from the images, the sample that has 22nm silica particles has a very uniform distribution while the sample that has 120nm silica particles has a wide size distribution ranging from 10nm to 120nm.

3.5.4 Zeolite Particle size

Zeolite particle sizes were chosen in the micron range and nano range. The micron sized particles are 1-2µm and the nano sized particles are in the range of 300-500nm. The SEM images for these particles are again shown in Section 3.2.1, Figure 3.1 B and C. The micron zeolites were added to the pulp slurry with the addition of 5mg CPAM/g zeolite and the stirring time was 15 minutes. When nano zeolite is used, the process has to be optimised to increase retention but other issues arose with the nano zeolite. The final structures created using nano zeolite have dusting issues and hence to optimise the process, 7.5mg CPAM/g nano zeolite was used and the stirring time was kept constant at 15 minutes. These structures had high retention but the floc size was large and this reduced formation in the sheets.

3.5.5 Calcination Rate

In order for the final laminate structure to be formed, the sheet had to be heated to a temperature of 650°C for the removal of the organic pulp fibres and the sintering of the silica sol, thereby imparting the sheet with mechanical strength. The heating procedure can be completed in two ways. The first method was fast heating, which meant the furnace had to be preheated to the set temperature of 650°C, and the sheet inserted at this temperature. The sheet was held at this temperature for 2.5 hours. Slow heating corresponds to the sample being placed in a cold furnace (starting temperature around 20°C) and then heated to 650°C over 4 hours and then left at that temperature for 2.5 hours. After 2.5 hours, the furnace was cooled and the sample was removed.

3.5.6 Pulp Type

Two different pulp types were used. Thermomechanical pulping thermally softens the wood chips before mechanical refining. TMP is created using wood chips that are preheated with pressurised steam (over 3-5 bar and temperature 140-155°C) and refined under pressure at an

elevated temperature. The fibres are fatigued by using frictional forces that separate the fibres in the wood chips. The mechanical pulp is produced in harsh conditions and therefore contains less intact fibres and more fragmented fibres and fines than kraft pulp*[109]*. The TMP fibres used in the preparation of laminate structures were taken from the feed of low consistency reject refiners. As these fibres were taken from screen rejects, they do not have as many fines as normal TMP pulp. Kraft pulp is produced by chemical pulping. Chemical pulping uses chemicals for fibre liberation from the wood chips by dissolving the lignin. The fibres are therefore freed undamaged. The kraft process mainly uses NaOH and Na_2S at 160-170°C for delignification to occur*[110]*. The kraft pulp used for this project were taken from the exit of the brownstock washers. Since the preparation of the pulp fibres is so different, these fibres also have different properties. TMP pulp has fewer long fibres and more fines as compared to kraft pulp. The kraft pulp also produces easily collapsible and more flexible fibres as compared to the TMP process.

3.5.7 Partial Factorial Design

For these variables discussed above with their high and low factors, a full factorial design would have involved an impractically large number of experiments. Instead, a partial factorial design was used to investigate which of the experimental variables had a statistically significant effect on the results. This table was generated using the R project for Statistical Computing and 16 such experiments were generated. The high and low factors of each of the eight variables are listed and the number of experiments chosen was 16. The statistical package helps to randomise the high and low factors for each of the variables and come up with a table which allows the preparation of the laminate samples using the different factors of the synthesis variables, from which the different characteristics corresponding to the different synthesis conditions can be studied and the variables responsible for any of the characteristics of the samples can be evaluated. The partial factorial table is shown in Table 3.1. The first column shows the serial number for each of the experiments followed by the

either the high or the low factor of each variable discussed from Sections 3.5.1-3.5.6 for each experiment. The last column shows the sample ID. The sample ID is given by the serial number – ratio of ceramic fibres in the ceramic fibre weight to zeolite weight ratio – S and F denote whether the heating rate was either fast or slow- the silica concentration - the silica particle size – the zeolite particle size with N representing the nano sized zeolite particles between 0.3-0.5μm and M representing the micron sized zeolite particles between 1-2μm. For example, experiment 1 is denoted by 1-1-F-20-120-N as it is the 1st experiment with 1:1 ratio of ceramic fibre weight to zeolite weight, fast calcination rate, 20wt% silica concentration, 120nm silica particle size and 0.3-0.5μm zeolite particle size.

For the sheet making process, 100gsm pulp was used. The sheets were 10cm x 10cm and the total inorganic content (zeolite + ceramic fibres) of the as formed sheet was 400gsm. The proportion of zeolite in the final laminate structure is expected to be between 30-74wt%.

Table 3.1: Partial Factorial Design of the 6 variables using high and low factors for 16 experiments

	Ceramic fibre weight(g): zeolite weight(g)	Calcination Heating rate	Silica Concentration (wt %)	Silica Particle size (nm)	Zeolite Particle size (μm)	Pulp type	Sample ID
1	1:1	fast	20	120	0.3-0.5	TMP	1-1-F-20-120-N
2	0.08:1	slow	40	120	1-2	TMP	2-0.08-S-40-120-M
3	0.08:1	slow	20	22	0.3-0.5	Kraft	3-0.08-S-20-22-N
4	1:1	fast	40	22	1-2	Kraft	4-1-F-40-22-M
5	1:1	slow	20	120	1-2	Kraft	5-1-S-20-120-M
6	0.08:1	fast	20	22	1-2	TMP	6-0.0.8-F-20-22-M
7	1:1	slow	40	22	0.3-0.5	TMP	7-1-S-40-22-N
8	0.08:1	fast	40	120	0.3-0.5	Kraft	8-0.08-F-40-120-N
9	1:1	fast	20	22	0.3-0.5	Kraft	9-1-F-20-22-N
10	1:1	fast	40	120	1-2	TMP	10-1-F-40-120-M
11	0.08:1	fast	40	22	0.3-0.5	TMP	11-0.08-F-40-22-N
12	1:1	slow	20	22	1-2	TMP	12-1-S-20-22-M
13	0.08:1	fast	20	120	1-2	Kraft	13-0.08-F-20-120-M
14	1:1	slow	40	120	0.3-0.5	Kraft	14-1-S-40-120-N
15	0.08:1	slow	20	120	0.3-0.5	TMP	15-0.08-S-20-120-N
16	0.08:1	slow	40	22	1-2	Kraft	16-0.08-S-40-22-M

This page is intentionally blank

Chapter 4

Standard Characterisation Techniques

This page is intentionally blank

4.0 Standard Characterisation Techniques

4.1 Introduction and overview of the remaining chapters

Chapter 3 gave a detailed account of all the variables chosen for the study and the partial factorial table designed to understand the importance of the synthesis variables for a specified characteristic.

To optimise the properties of the zeolite sheets made as described in Chapter 3, we need to understand the relationship between structure and performance as a structured adsorbent in a breakthrough test. The performance of these materials as structured adsorbents is determined by:

1. The adsorption capacity of the material, as measured using CO_2 adsorption isotherms. These results are discussed in Section 4.3.2.
2. The internal pore volume and size distribution, which has been measured using mercury porosimetry. These results are discussed in Section 4.4
3. The rate of adsorption into the zeolite particles from the surrounding pores. This has been measured using a ROA test and the results are discussed in Section 5.5
4. The size and distribution of gas flow channels between the sheets. Several methods have been employed to add channels and the results are discussed in Chapter 8

In addition, the structures that are produced need to have a moderate strength to prevent disintegration in application. A method has been developed to assess the strength of the zeolite laminates and the results are discussed in Section 5.3 and 5.4.

This chapter deals with the standard characterisation techniques used for the sheets made in the partial factorial design and the results obtained from these characterisation techniques.

The sheets were prepared according to section 3.5.7 and followed the partial factorial design table. Zeolite A was used in these sheets as the adsorbent. The calcined structure was viewed under Scanning Electron Microscopy to obtain a qualitative understanding of the distribution of the components, the pore spaces left behind by the fibres, the openness of the structure and the surface coverage of the adsorbent with the silica. Nitrogen adsorption measurements were also performed on the samples to determine the microporous and mesoporous pore size distribution. Carbon dioxide adsorption was also performed on the samples to verify whether the calculated amount of zeolite retained on the sheets was the same as the measured amount of zeolite on the sheets. Mercury porosimetry measurements were also carried out on the samples to obtain mesoporous and macroporous pore distributions within the laminate structure. Since the mercury porosimetry measurements give a very wide range of pore measurements, these measurements have been further broken into size ranges to understand the factors controlling porosity in different ranges.

4.2 Scanning Electron Microscopy Results

Scanning electron microscopy was used to view the 2-D porous structure of the laminate sheet. This section deals with the different scanning electron microscopes used and the results obtained from these microscopes for some samples from the partial factorial design.

4.2.1 Scanning Electron Microscopes

Two different SEMs were used. The laminate structures created have components at different size ranges and all the components cannot be observed with any single magnification. Hence two different microscopes were used to accommodate the specific ranges that the components fall under. The desktop SEM was used to identify the large features while the Nano SEM was used to view very small features of the same sample. Hence, both of these instruments are necessary to understand the distribution of the sheet components. Details about each of these instruments are provided in Section 4.2.1.1 and Section 4.2.1.2. For both the SEMs used, the

samples were mounted onto a carbon taped stub. This was then coated with 1nm layer of platinum metal.

4.2.1.1 Phenom Desktop SEM

The Phenom Desktop SEM was used to clearly identify sample features with sizes ranging from 10µm to 250µm. The images produced from this microscope showed the pore spaces left behind by the pulp fibres, the distribution of ceramic fibres and zeolite particles in the structure and how the structure is held together using the silica particles. Although individual silica particles were not visible, the coating of silica over the other components was visible.

4.2.1.2 FEI Nova NanoSEM 450 FEGSEM

The FEI Nova Nano SEM 450 FEGSEM instrument was used to view the smaller particles below 10µm in size. The sample images were taken at 2kV and a spot size of 2. The immersion for ultra high resolution imaging mode was used to capture images at very high magnifications. The field emission microscope shows the distribution of the silica particles in the spaces left behind by the fibres and over the zeolite particles along with the distribution of nano zeolite particles in the laminate structure.

4.2.2 Scanning Electron Microscopy Images

The images of the starting components were shown in Section 3.2. In the current section we will present the images of the laminate structure. Four different samples will be shown at different magnifications to show how the structure is built. Cross sectional views of two samples with varying silica concentration were also taken to understand the porosity through the structure.

4.2.2.1 SEM images of Sample having Low Silica content, High Ceramic content and Nano Zeolite with 22nm Silica size

The sample shown in Figure 4.1 was made from 20wt% 22nm silica, nano zeolite and kraft pulp. The ceramic fibre to zeolite wt ratio was 1:1 and the fast heating rate was used. Figure 4.1a shows the nano zeolite interspersed between uniform silica particles of size 22nm. The silica does not seem to have fully coated the nano zeolite particles but have packed themselves around the particles instead. Figure 4.1b shows a lower magnification image of the same sample where a ceramic fibre comes into view. In this image itself the silica starts to become less visible and starts appearing almost as a coating. Figure 4.1c shows a lower magnification image where the nano zeolite also starts disappearing from view. Figure 4.1d, e and f show very low magnification images taken from the desktop SEM. Here there are large gaps shown because of the low silica amount used. While some sections of the sheet have managed to preserve the spaces left behind by the fibres, as shown by the silica taking the shape of the fibre, there are other sections where there has been insufficient silica to preserve the spaces left behind by the pulp fibres and only the ceramic fibres keeps the structure from falling apart. More images of this sample showing the larger features are available and shown in Appendix I.

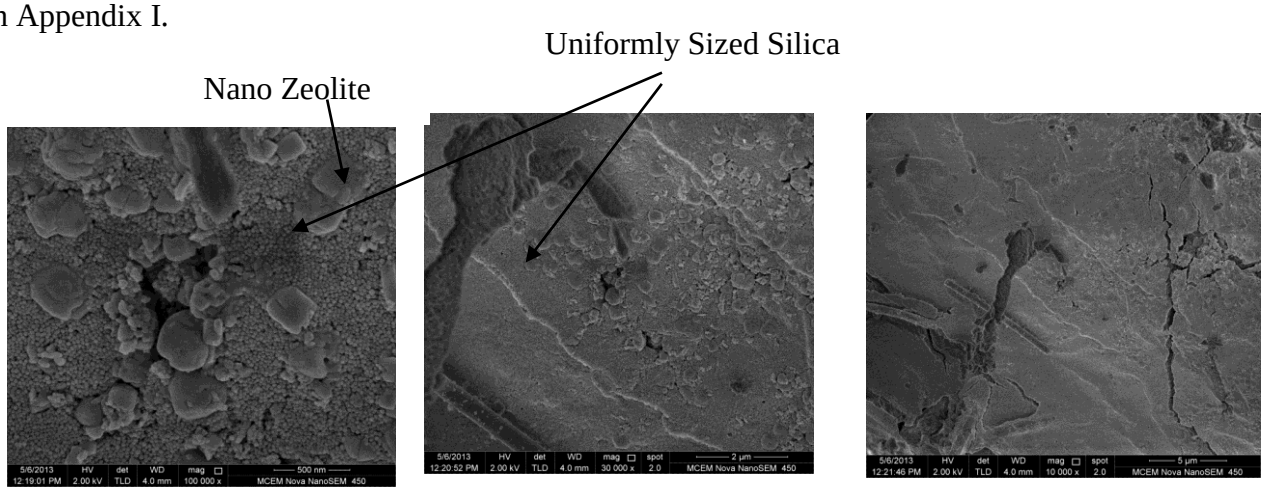

a b c

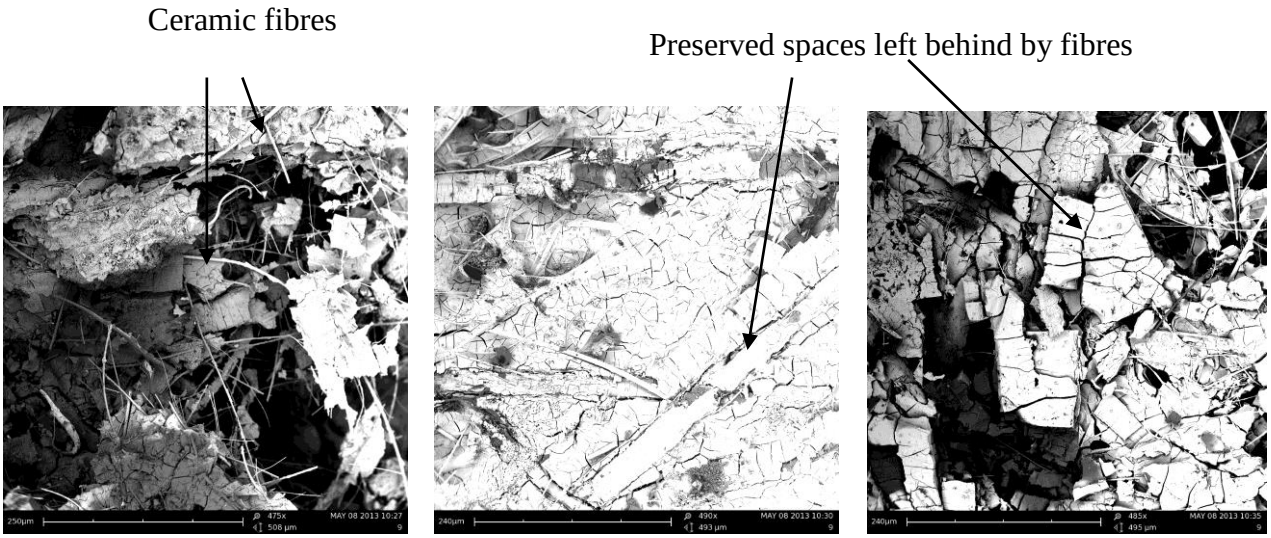

Figure 4.1: Sample made from 20wt%, 22nm silica, 1:1 ceramic to nano zeolite with Kraft pulp at a)100,000X b)30,000X c)10,000X d)475X e)490X f)485X showing different sections of the sample

4.2.2.2 SEM images of Sample having Low Silica content, High Ceramic content, Micron Zeolite and 22nm Silica size

The sample shown in Figure 4.2 was made from 20wt%, 22nm silica, micron zeolite and TMP pulp. The ceramic fibre to zeolite wt ratio was 1:1 and the heating rate used was fast. Figure 4.2 shows the sheet surface of sample 12 at various magnifications. Figure 4.2a shows some parts of the micron zeolite covered by the silica. Figure 4.2b shows the zeolite particles covered by the silica. In this image, the silica is no longer visible and can be only seen as a layer covering the zeolite particles. Figure 4.2c, d and e show that due to the low amount of silica present, the fibre spaces are not preserved in the structure. The agglomerated silica forms many chunks that are strewn all over the surface of the structure. The ceramic network with a little help from the silica holds the structure together. Additional images of Sample 12 are shown in Appendix I to get a better picture of the distribution of components.

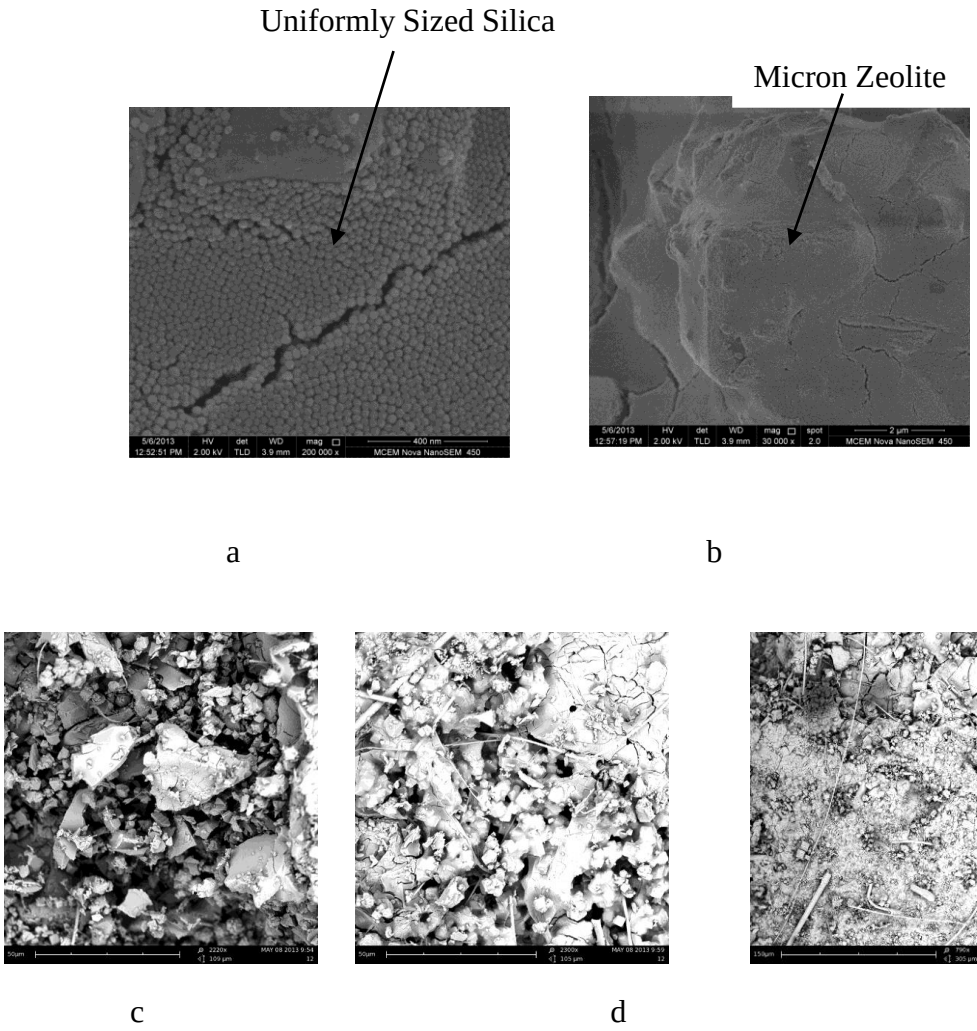

Figure 4.2: Sample made from 20wt%, 22nm silica, 1:1 ceramic fibres to micron zeolite and TMP pulp at a)200,000X b)30,000X c)2220X d)2300X e)790X showing different sections of the sample

4.2.2.3 SEM images of Sample having High Silica content, High Ceramic content, Nano Zeolite and 120nm Silica size

The sample shown in Figure 4.3 was made from 40wt%, 120nm silica, nano zeolite and Kraft pulp. The ceramic fibre to zeolite wt ratio was 1:1 and the heating rate used was slow. Figure 4.3a shows 120nm silica. As mentioned in Section 3.2.3, the silica has a varying size distribution. Figure 4.3b shows the nano zeolite surrounded by the silica particles. Although this sample contains 40wt% silica, the nano zeolite remains uncovered by the silica. This

could be due to charge repulsion between the nano zeolite and silica that does not allow coating of the nano zeolite. Figure 4.3c, d and e show the preserved spaces left behind by the fibres. Owing to the higher silica content in this structure, the fibre spaces are very well preserved. Additional images can be viewed in Appendix I.

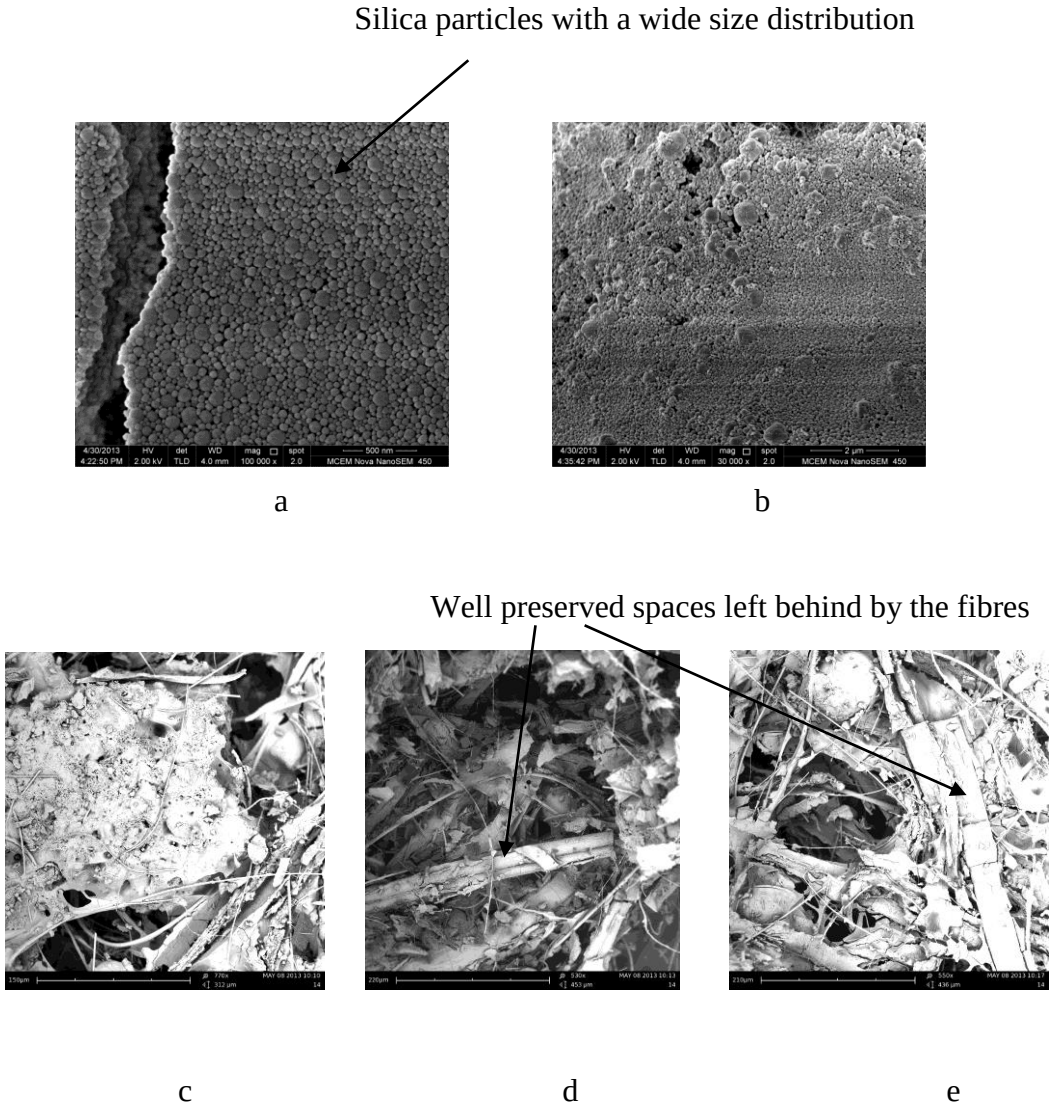

Figure 4.3: Sample made from 40wt%, 120nm silica, 1:1 ceramic fibres to nano zeolite and Kraft pulp at a)100,000X b)30,000X c)770X d)530X e)550X showing different sections of the sample

4.2.2.4 SEM images of Sample having High Silica content, Low Ceramic content, Micron Zeolite and 22nm Silica size

The sample shown in Figure 4.4 was made from 40wt%, 22nm silica, micron zeolite and kraft pulp. The ceramic fibre to zeolite wt ratio was 0.08:1 and the heating rate used was slow. Figure 4.4a shows 22nm silica distributed very evenly across the surface. Figure 4.4b shows the micron zeolite is entirely coated with silica particles. As compared to sample 12 in Section 4.2.2.2 which had only 20wt% silica and micron zeolite, this sample shows full coverage of micron zeolite particles. Again due to the presence of more silica, the fibre spaces are well preserved as shown in Figure 4.4 c, d and e. In Figure 4.4d, the silica agglomerates have fallen into a fibre space which shows that this could happen in the structure as well. The SEM images clearly show that very few ceramic fibres are present as per the synthesis conditions. Further images can be found in Appendix I.

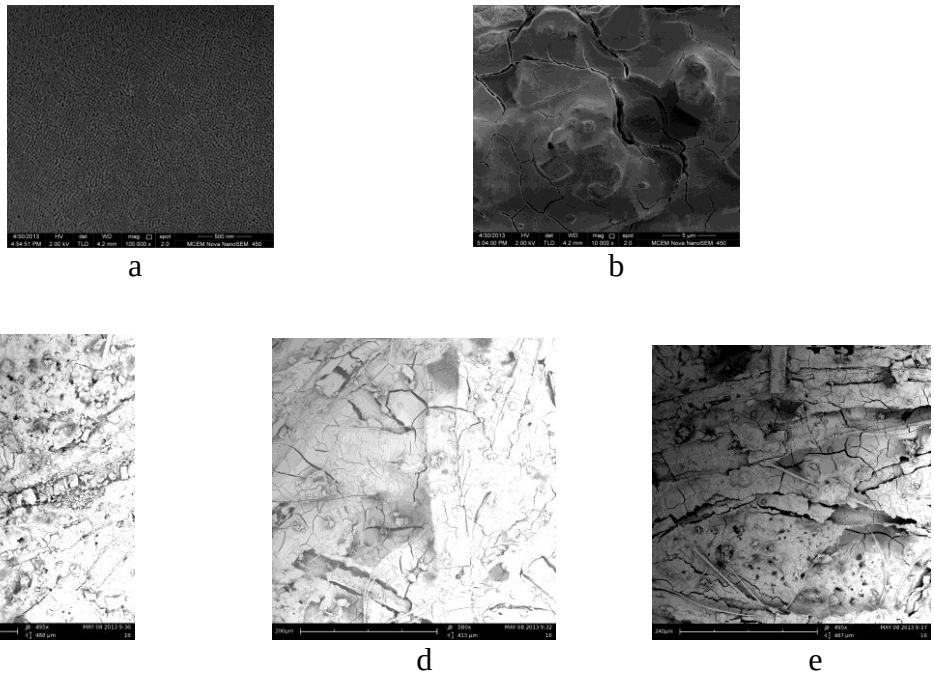

a b c d e

Figure 4.4: Sample made from 40wt%, 22nm silica, 0.08:1 ceramic fibres to micron zeolite and Kraft pulp at a)100,000X b)10,000X c)580X d)495X e)495X showing different sections of the sample

4.2.2.5 SEM images of Cross Section of Sample having Low Silica content

The sample shown in Figure 4.5 was made from 20wt%, 120nm silica, micron zeolite and kraft pulp. The ceramic fibre to zeolite wt ratio was 1:1 and the heating rate used was slow. This cross section view of this sample has been shown in Figure 4.5 a and b to show the structure density and the distribution of silica through the cross section of the structure. As can be seen from the Figure, the structure is not very dense and for gas flow, there is easy access to the zeolite within the sheet structure. The structure has a higher density of silica at the edge of the sample with the silica content reducing through the thickness. The sample also has many ceramic fibres which are responsible for holding the sheet shape and the image shows that the silica has not penetrated to the centre of the sheet. Since the sheet has many ceramic fibres, the presence of the ceramic bulbs can also be seen.

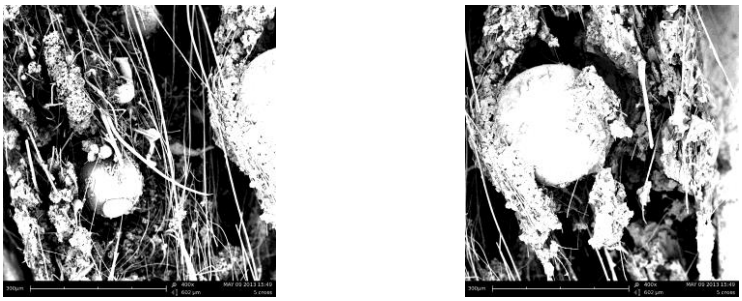

a b

Figure 4.5: Sample made from 20wt%, 120nm silica, 1:1 ceramic fibres to micron zeolite and Kraft pulp showing cross sectional view at 400X

4.2.2.6 SEM image of Cross Section of Sample having High Silica content

The sample shown in Figure 4.6 was made from 40wt%, 22nm silica, micron zeolite and TMP pulp. The ceramic fibre to zeolite wt ratio was 1:1 and the heating rate used was fast. Figure 4..6 shows the cross sectional view. This sample has more silica than the previous sample. It is very clear from Figure 4. 5 and 4. 6 that this sample is highly dense and has silica in the structure through the entire thickness of the sample.

a b c

Figure 4.6: Sample made from 40wt%, 22nm silica, 1:1 ceramic fibres to micron zeolite and TMP pulp cross sectional view at 480X

4.2.2.7 Summary of SEM images

The SEM images can be broadly divided on the basis of the initial amount of silica in the structure. The samples having 20wt% silica generally have large gaps in the sheet structure which creates high porosity and a low density laminate structure. In some parts of the laminate structure, the spaces are well preserved while in other sections, due to the low amount of silica, there is no slica holding the different components together. Hence in these sections the silica binds to itself creating chunks which are distributed through the entire laminate network. The cross sectional images also show that the silica does not penetrate to the centre of the structure and only the edges of the sheet are held by the silica. The samples having 40wt% silica on the other hand, have well preserved spaces and the laminate structure is very dense. The cross sectional views also show that the silica penetrates through the entire thickness of the sheet. The other major differences between the sheets is seen between the samples that have micron zeolite and nano zeolite. The samples with the nano zeolite have silica packed around the zeolite crystals while the samples with the micron zeolites have the silica covering the zeolite particles.

4.3 Gas Adsorption Measurements

Carbon dioxide adsorption isotherms and Nitrogen adsorption isotherms were performed using the Micromeritics ASAP 2010 instrument. The carbon dioxide adsorption isotherm shows how many moles of carbon dioxide can be adsorbed by 1g of sample. This gives a direct measurement of how much zeolite is present in the sample and can be compared against the retention measurements which were discussed in Section 3.4.2. Nitrogen adsorption isotherms on the other hand provide information on the microporosity and mesoporosity of the zeolite and silica present in the sample. Nitrogen adsorption isotherms were measured at 77K and carbon dioxide adsorption was measured at 0°C unless otherwise stated.

4.3.1 Measurement Method

For gas adsorption measurements, the sheet structure was broken into pieces to fit into the glass tube used in the Micromeritics ASAP 2010 instrument. The sample was then degassed by heating over period of 4 hours to 350°C and holding it for 10 hours under vacuum. The sample was then cooled to room temperature and analysis was performed using either nitrogen or carbon dioxide as the adsorptive gas. If nitrogen was used as the adsorptive gas, the analysis was performed at 77K using liquid nitrogen and if carbon dioxide was used as the adsorptive gas, the analysis was performed at 273K using an ice-water bath at 0°C. Although nitrogen at 77K is considered the standard adsorptive for surface area and pore size analysis, it is well known that 4A zeolites cannot be accessed with N_2 at 77K due to cations blocking the pore apertures, as the kinetic diameter of N_2 is comparable to the effective pore diameter of NaA*[8]*. Hence this methodology does not give correct pore size distributions for zeolite NaA.

4.3.2 Carbon dioxide Adsorption Results

Figure 4.7 shows the carbon dioxide adsorption isotherm at 273K of the starting components present in the structure. It can be seen that the ceramic fibres and colloidal silica have negligible adsorption capacity and hence have negligible pores and surface area. Virtually all of the adsorption capacity results from the zeolite, as expected. The micro and nano zeolite A powders have very similar adsorption capacity. This is encouraging as it indicates that the nano-zeolite prepared as part of this project has only marginally reduced the adsorptive capacity, most likely due to some amorphous material remaining in the sample after the preparation process, as seen from the XRD results in Figure 3.2.

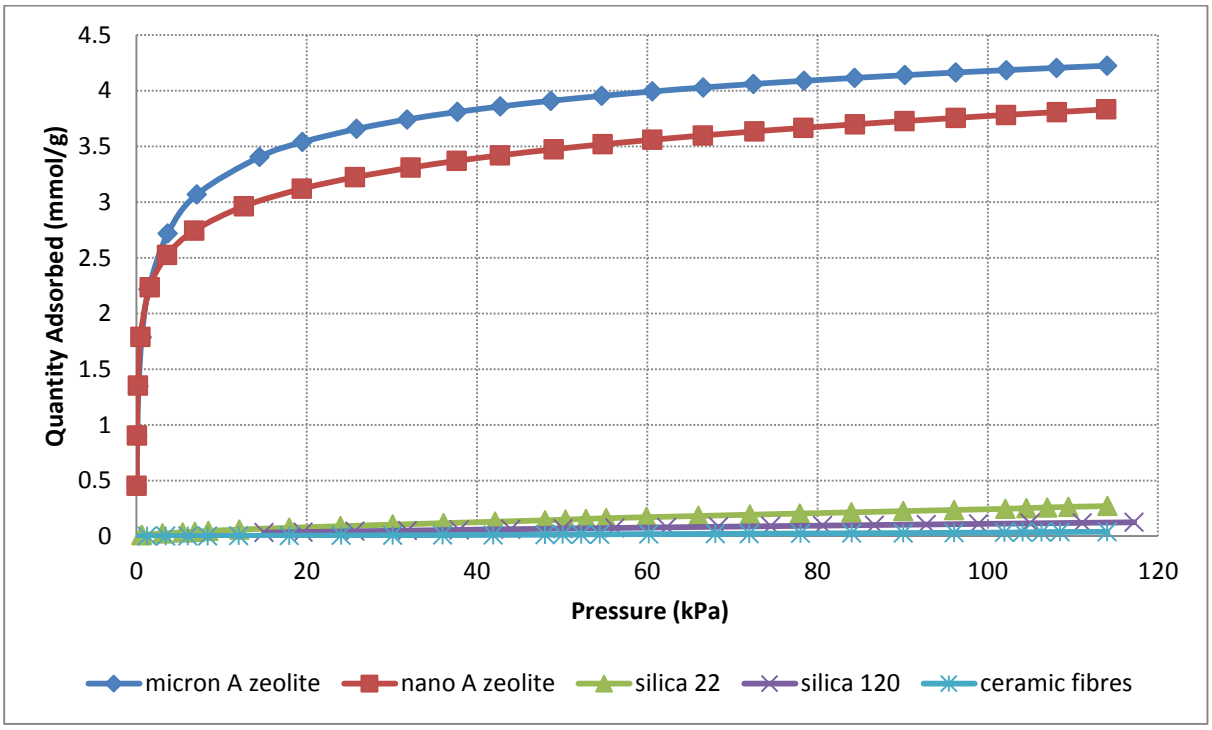

Figure 4.7: Carbon dioxide adsorption isotherms for the starting components present in sheet structure at 273K

Since the amount adsorbed by the silica and ceramic fibres is negligible, the measured CO_2 adsorption capacity of a laminate structure can be used to infer the actual amount of zeolite in the sample, by assuming all of the CO_2 adsorption capacity arises from the zeolite.

The CO_2 adsorption capacity of the zeolite laminate structures prepared from Table 3.5.7.1 for each experimental condition was measured and some examples are shown in Figure 4.8. The amount adsorbed at 120kPa gives a measure of how much zeolite is present in the structure. Only a few examples are shown to provide an estimate of the amount of zeolite in each sample. For the 16 experiments, the samples can have any of the 4 amounts as shown in Figure 4.8. Sample 6, 7, 8 and 9 are shown and they have 74, 30, 55 and 40wt% of zeolite, respectively. Also the preparation method has been shown in the sample name. For example sample 6 has the ID 6-0.08-F-20-22-M where 6 stands for sample number, 0.08 refers to ceramic weight to zeolite weight ratio of 0.08:1, F refers to fast heating, 20 is 20wt% silica, 22 is the size of the silica particles in nm and M refers to the micron sized zeolite particles. This ID system has been followed through in the coming results sections to identify the different components present in the sample and is discussed in Section 3.5.7

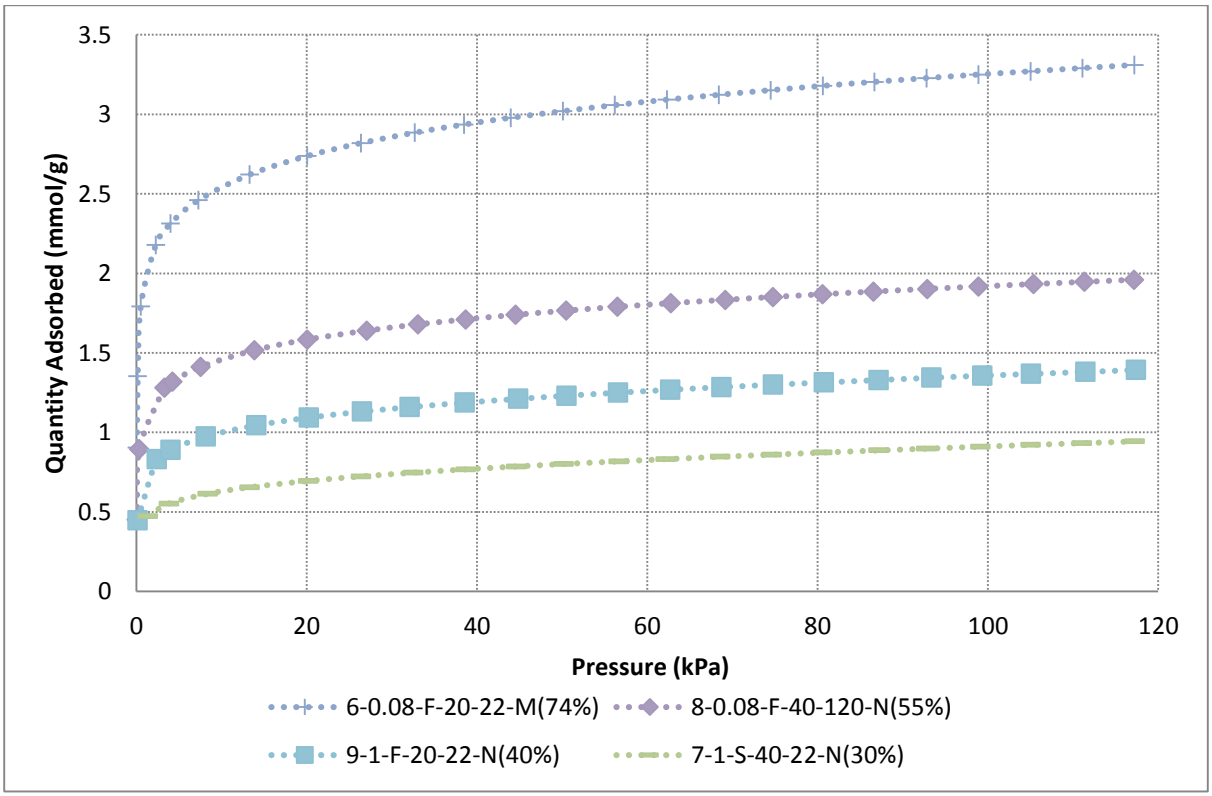

Figure 4.8: CO_2 adsorption at 0˚C for sample laminate sheet structures

Figure 4.9 shows the expected amount of zeolite in the structure (from synthesis conditions assuming complete zeolite retention) plotted against the amount of zeolite measured at P=120kPa using CO_2 adsorption for the nano zeolite A and the micron zeolite A. The line shows 1:1 correspondence between the measured and expected values. The nano zeolite shows lower zeolite present in the structure when compared to the expected value. This is because with the nano zeolite, the retention is lower and there is more dusting of the structure in general which reduced the zeolite loading. To increase the retention of nano zeolite, larger flocs were formed as discussed in section 3.5.4. This reduced their uniform distribution within the paper matrix which further reduced strength and increased dusting in the final structure as compared to micron zeolite samples.

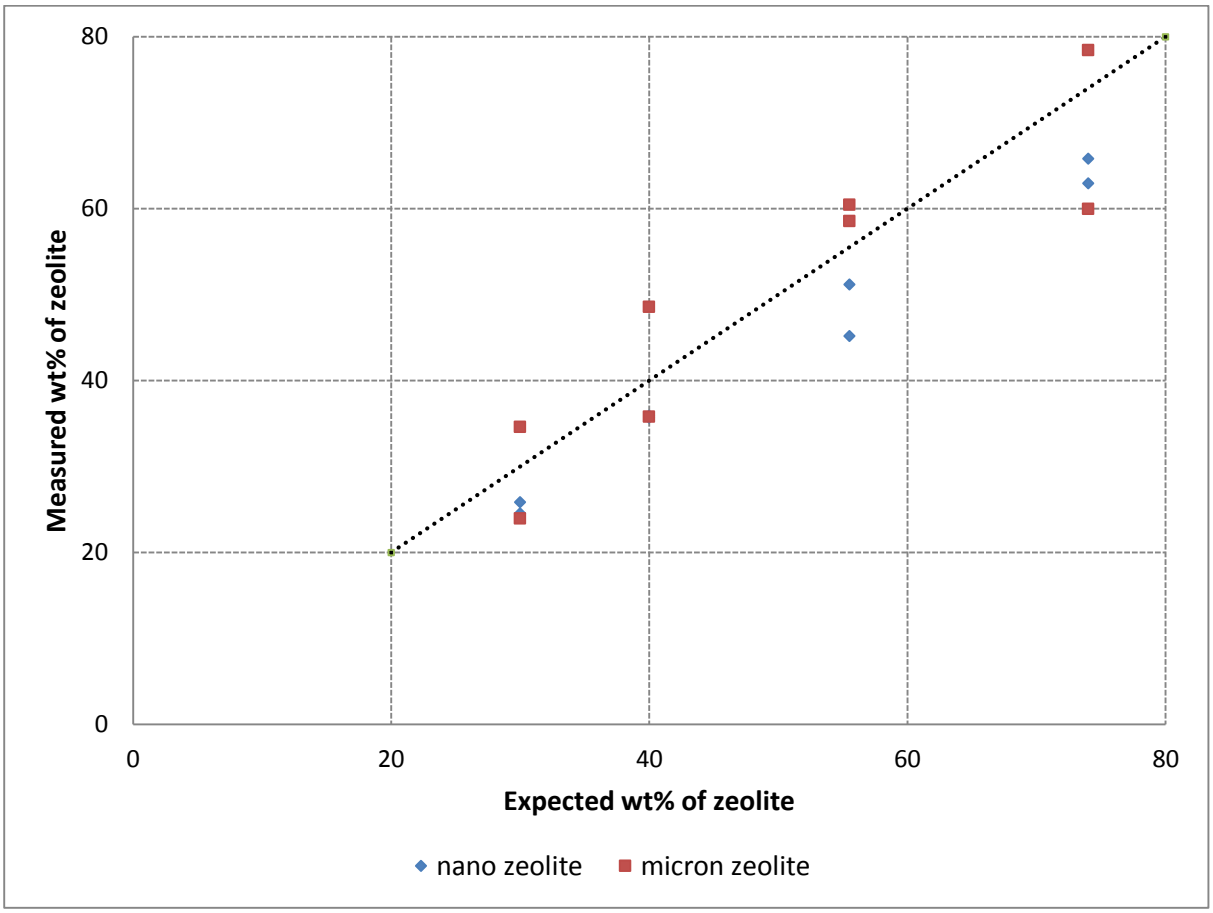

Figure 4.9: Comparison of expected and measured wt% of zeolite

4.3.3 Nitrogen adsorption for <50nm pore size distributions

The micropore and mesopore size distribution of the components of the structures was characterized with surface area analysis using liquid N_2 at 77K. This is shown in Figure 4.10 where colloidal silica shows the presence of mesopores. As expected, the 22nm silica showed smaller mesopore distribution compared to the 120nm silica. The ceramic fibres have no pores. As mentioned in Section 4.3.1, this analysis was not performed on zeolite NaA, as the smaller micropores of the NaA zeolite cannot be accessed by nitrogen at 77K due to cation pore blockage.

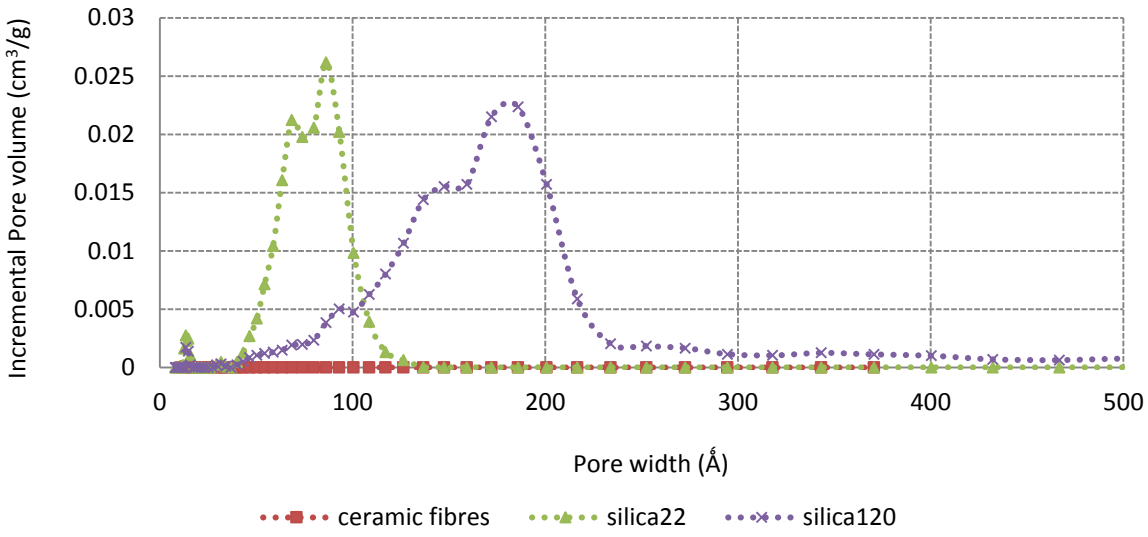

Figure 4.10: Pore size distribution of the inorganic materials in the sheet structure performed using N_2 adsorption measurement

4.4 Mercury Porosimetry

Mercury porosity measurements were done on all the samples to find the relation between synthesis conditions and the porosity created in the structure due to the synthesis conditions. This section details how the measurement and analysis were carried out and the results

obtained from this technique. The results have been divided into different pore size ranges to examine variations due to different synthesis conditions.

4.4.1 Introduction

Mercury porosimetry produces fundamental data which is the volume of mercury intruded into the pores of the sample as a function of applied pressure*[53]*. Pore diameters ranging from 0.003µm to 360µm can be assessed using mercury porosimetry techniques.

Mercury does not wet most substances and will not penetrate pores by means of capillary action. In order for mercury to enter pore spaces, pressure has to be applied *[41]*. The pressure required for mercury to penetrate a pore is inversely proportional to the pore opening size. The behaviour of a non-wetting liquid in an inundated porous object is described by the Washburn equation*[41]* which is given below

$$D = \frac{-2\gamma \cos\theta}{P} \qquad [4.1]$$

where D is the diameter of a cylindrical pore, γ is the surface tension of mercury, θ is the contact angle mercury forms against the solid and P is the applied pressure.

The pores are rarely perfectly cylindrical and pore width is given as the available distance between two opposite walls. Porosity is defined as the ratio of volume of pores to the volume occupied by the solid. There are mainly two different types of pores and they are open pores and closed pores. Open pores can further be divided into interconnected pores, blind pores and through pores. Open pores have access to the surface and these pores can be measured by the mercury porosimetry techniques. Closed pores are cavities that have no connection to the surface and cannot be measured by this technique. Blind pores have a single connection to the surface, interconnected pores are connected to other pores and through pores are open from both sides of the solid material*[111]*.

The method works in such a way that at low pressures, the larger pores are first filled and then as pressure is increased, the smaller pores get filled up*[41]*. This is in reverse to gas adsorption measurements where the smaller pores are filled first followed by the larger pores. Since this is the case, with some blind pores that have narrow necks and open into a larger cavity, the mercury source will have the volume behind the neck register as the porosity with the diameter of the neck.

4.4.2 Measurement Technique

For the mercury porosimetry measurements, the samples were degassed as described for adsorption measurements. Mercury porosimetry was measured using a Micromeritics Autopore III. The degassed sample was placed in the penetrometer sample cup and sealed. The penetrometer was introduced to the low pressure analysis port where the sample was evacuated and mercury was allowed to fill the accessible space within. Following the low pressure analysis, high pressure analysis was conducted up to 400MPa to fill the macro and mesopore space. Using the scanning mode of operation, a cumulative intrusion vs pore diameter curve was obtained. The starting components present in the final structure are incompressible, hence the structure can be compressed only by fracture of the sample. In order to check whether the fracture had occured, the intrusion and the extrusion curves were compared and the extrusion curves lay very close to the intrusion curves. They did not completely overlap the intrusion curves because of the bottlenecks which meant the mercury could not be removed fully from the sample*[112]*. In case of fracture, the mercury intrusion increases rapidly at the pressure at which fracture occurred and a large difference is observed between the intrusion and extrusion curves.

4.4.3 Analysis Technique

Statistical analysis of the mercury pore size data was carried out using SPSS software package and these results are provided in Section 4.4.4 and Table 4.1. The raw data from the

mercury porosimetry data was used to find the pore volume across the entire range from 4-50,000nm. These results were then used to find the mean values for every variable in every range and the statistical significance was tested using *p*-value analysis. If the *p*-values were less than 0.05, then the results in that range showed that there was a major significance in the use of those variables. On the other hand, if the *p*-value was greater than 0.1, then the results showed no difference from the use of the variables. The results have been given for individual variables with main effects and some interaction effects. The porosity ranges have been divided into the mesoporous range (4-50nm) and the macroporous range (> 50nm). The macroporous range has been further divided into 50-500nm, 500-5000nm and 5000-50,000nm ranges. The variables affecting the total pore volume will be discussed. The variables are the same as those described in Section 3.5 and the factors used in the analysis are the high and low limits for each variable.

4.4.4 Mercury Porosimetry Results

The complete data set for the mercury porosity measurements for two different samples with the division of the pore size range are shown in Figure 4.11. These two samples were chosen to highlight a few differences in porosity measurements of the different samples. The results are discussed for each variable such as ceramic weight: zeolite weight, heating rate, silica concentration, silica particle size, zeolite particle size and pulp type. The porosity range where any significant differences have been observed are reported for that variable. A mean pore value table has also been provided to give an understanding of the more significant variables for creating structures of required porosity.

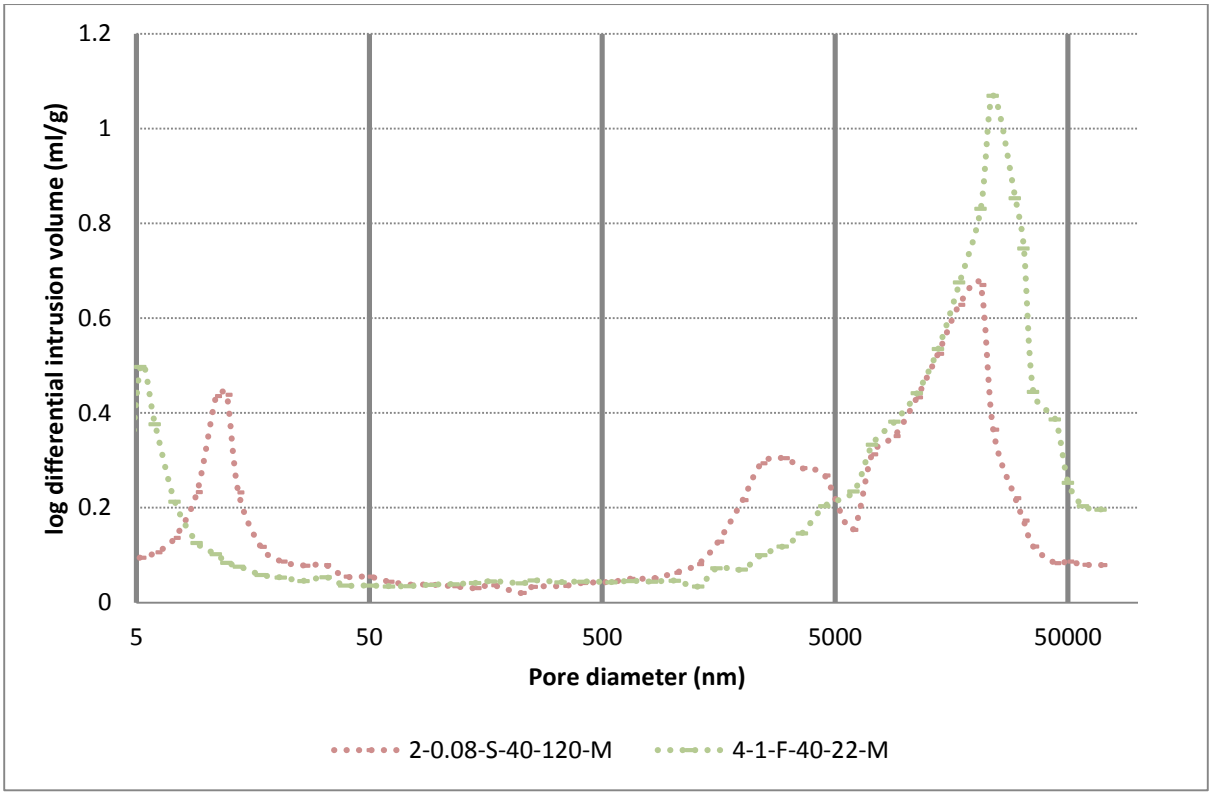

Figure 4.11: Complete data set for mercury porosimetry measurements with the division showing each pore size range

4.4.4.1 Mean pore volumes

Table 4.1 shows the mean pore volumes for all the factors in the different size ranges. The variables that are in bold have statistical significance. Virtually all of the variables studied have an impact on the mesoporous size range. In addition, the major variable that affects most of the porous range is the silica concentration. These variables are studied in the decreasing order of significance from Section 4.4.4.2-4.4.4.7.

Table 4.1: Mean pore volume from mercury porosity measurement for the mesoporous and macroporous regions for the laminate structures obtained from statistical analysis of porosity results

Variables	Factors	4-50nm	50-500nm	500-5000nm	>5000nm	cumulative
Ceramic fibre: zeolite weight	0.08:1	**0.171**	0.11	0.138	**0.732**	1.151
	1:1	**0.149**	0.078	0.109	**0.953**	1.288
Heating rate	Fast	**0.152**	0.088	0.121	0.878	1.237
	slow	**0.168**	0.1	0.126	0.807	1.202
Silica concentration	20	**0.14**	0.118	**0.156**	**1.118**	**1.532**
	40	**0.179**	0.07	**0.091**	**0.567**	**0.907**
Silica Particle size	22	**0.168**	0.076	0.124	0.763	1.13
	120	**0.152**	0.112	0.123	0.922	1.309
Zeolite particle size	micron	**0.135**	**0.033**	**0.16**	0.832	1.16
	nano	**0.184**	**0.155**	**0.086**	0.853	1.279
Pulp Type	Kraft	0.158	0.089	0.116	0.913	1.275
	TMP	0.162	0.099	0.131	0.772	1.164

Pore volume ml/g

4.4.4.2 Initial Silica Concentration

The statistical analysis performed using p-value analysis showed that silica concentration was the most important experimental variable controlling the porosity. Silica concentration had a statistically significant effect on porosity in all regions except the 50-500nm range.

In all regions, except the mesoporous region, higher silica concentration is associated with lower porosity. Mesoporosity is mainly caused by the presence of silica particles; hence having more silica gives rise to more mesopores. Figure 4.12 shows the effect of using different silica concentration quite clearly for Exp 2 and 5 where Exp 2 has a high silica concentration and Exp 5 has a low silica concentration.

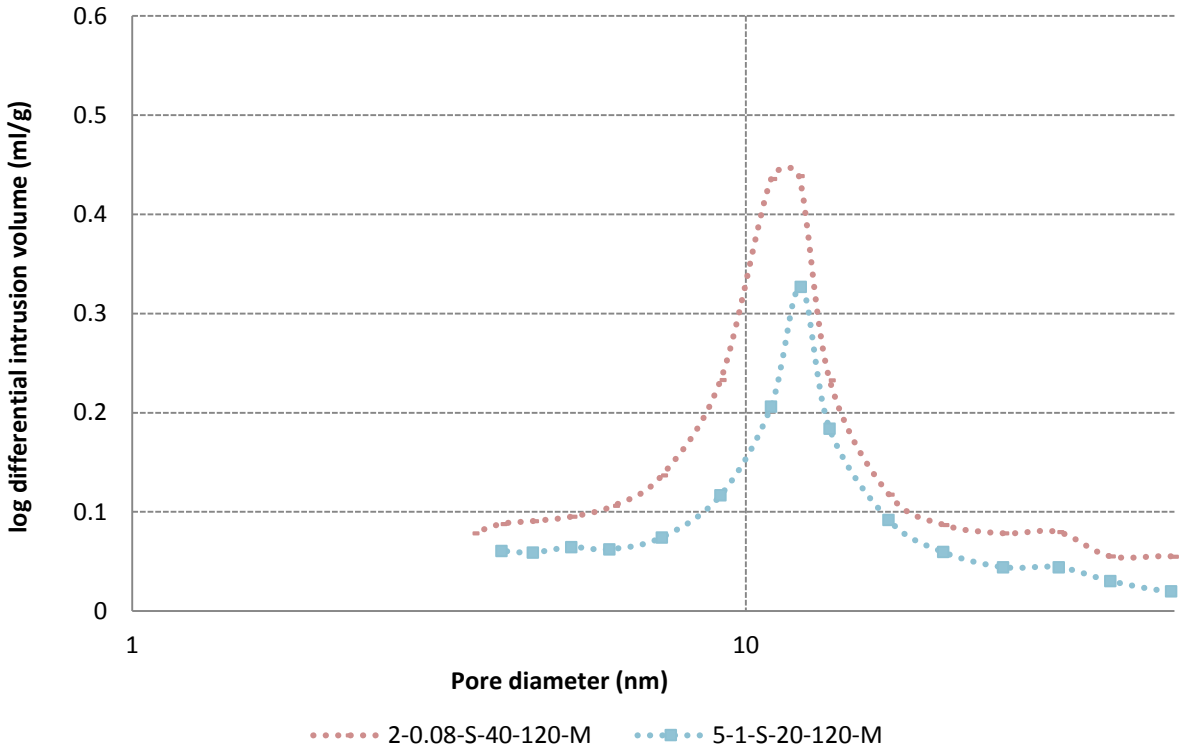

Figure 4.12: Log differential intrusion volume curves in the mesoporous range showing different silica concentrations

Although there is no main effect caused by silica concentration, there is an interaction effect with zeolite particle size in the region 50-500nm and 500-5000nm which is explained in Section 4.4.4.3. But as can be expected, 40wt% silica samples have lower porosity than 20wt% silica samples. Above 5000nm as well, 40wt% silica samples have lower porosity than 20wt% silica samples. In this range, the size of the zeolite particle does not play a role. The decrease in porosity with increasing silica concentration across a number of regions leads to an overall effect in the cumulative pore volume where two distinct "families" of cumulative pore volumes can be seen, corresponding to the two silica levels as shown in Figure 4.13. With varying silica concentration, the final weight of the sample varies. 20wt% silica sheets have a weight of 5g and are about 1.1mm thick while 40wt% silica sheets have a weight of 6.67g and are about 1.4mm thick. This shows that the 40wt% silica sheets are

denser and have more packing than 20wt% silica sheets which corresponds to their reduced porosity.

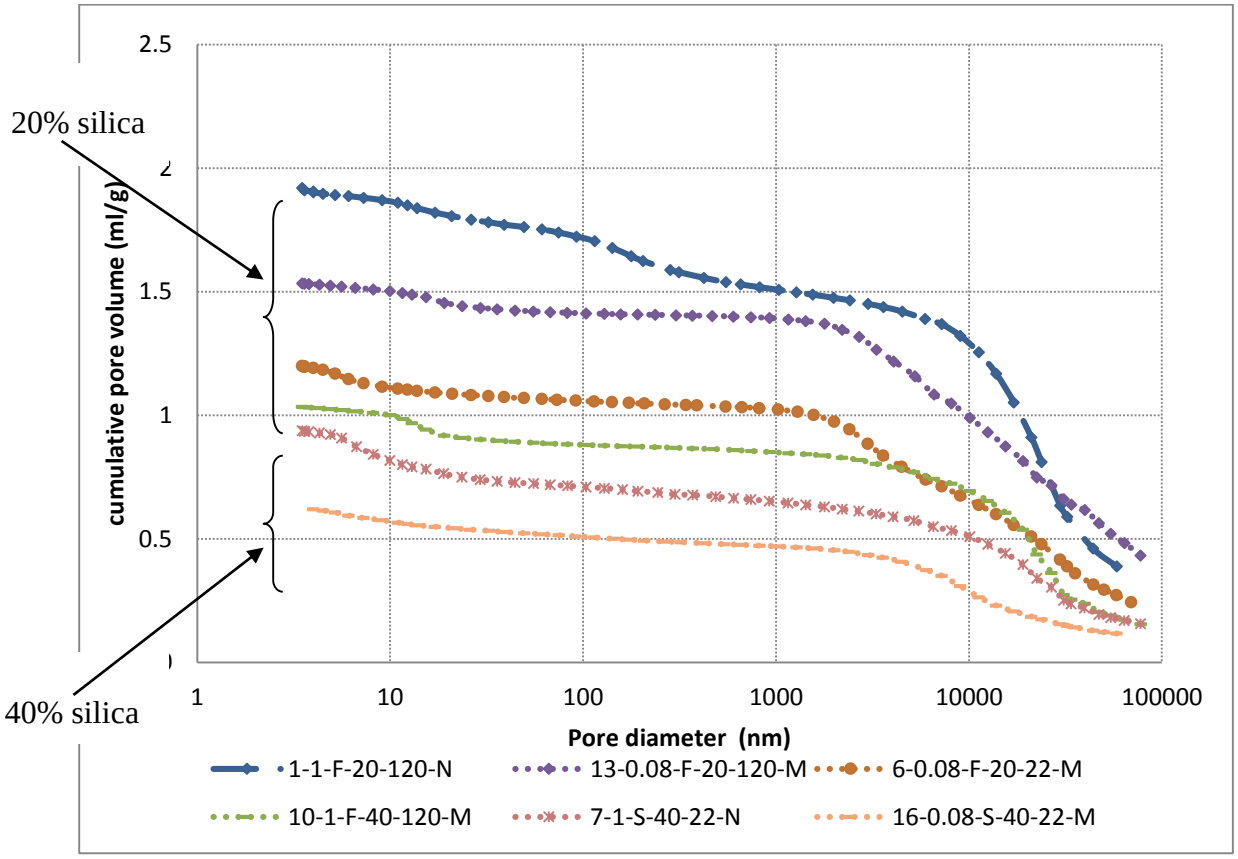

Figure 4.13: Cumulative pore volume to show the two families of curves for 20wt% and 40wt% silica

4.4.4.3 Zeolite particle size

The effect of zeolite particle size is felt from the mesoporous range to 5000nm. The mesoporous range also has an interaction effect with ceramic: zeolite weight. In the mesoporous range, higher nano zeolite content is associated with more pores due to the interaction effects of ceramic: zeolite weight and zeolite particle size. The presence of mesopores is attributed to the size and packing of the nano zeolite with silica rather than interaction with any other component as shown in Figure 4.14a and 4.14b where the interaction between the nano zeolite and silica against micron zeolite and silica is shown.

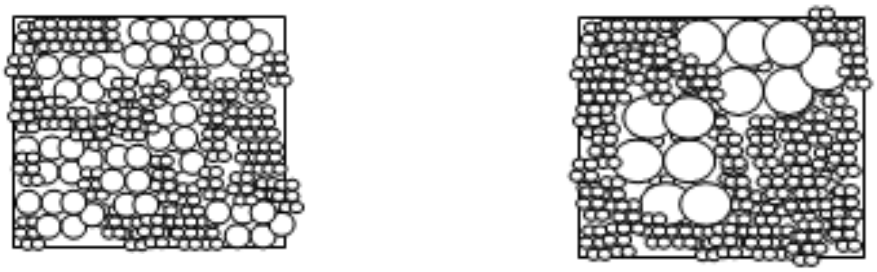

a b

Figure 4.14: a) Interaction of nano zeolite and colloidal silica b) Interaction of micron zeolite and colloidal silica

In Figure 4.15, the mesopores for Exp 1, 2, 8 and 10 have been shown. Exp 2 and 10 have micron zeolite and have sharp peaks due to the presence of mesoporous silica. The micron zeolite does not interact with the silica to cause mesopores, therefore there is only an individual effect. But with Exp 1 and 8, nano zeolite is present which shows a tail in the curve due to the interaction with the silica. This broadening of the peak is shown above 20nm.The larger pore volume for Exp 8 is due to the larger nano zeolite content which leads to more interaction with the silica, creating more pores in this region.

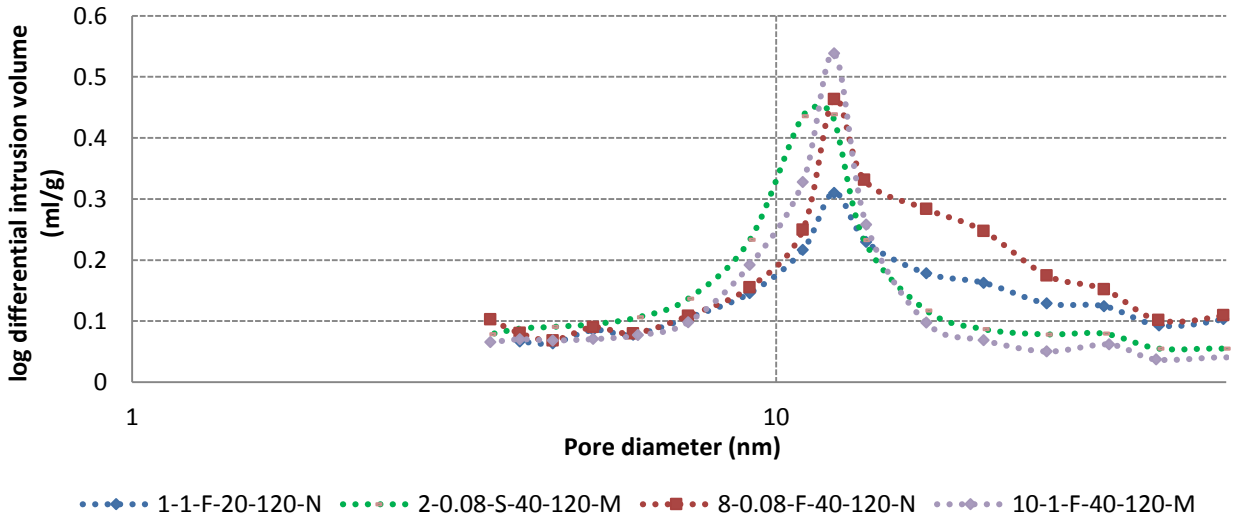

Figure 4.15: Log differential intrusion volume curves in the mesoporous range to show differences in interaction between micron and nano zeolite laminate structures with colloidal silica

In the 50-500nm range, having nano zeolite creates porosity. The nano zeolite particles have a varying size range from 300-500nm and their packing with the silica creates pores of about 150nm. The effect of the micron zeolite particles is observed between 500nm and 5000nm. These particles are 1-2µm in size and have cubic shapes. Their packing creates pores of about 3-4µm. For both these regions, having more silica produces a more tightly packed structure, which thereby reduces porosity. Figure 4.16 shows pore size distribution from 50-5000nm for nano zeolite samples compared against micron zeolite samples and the reduced porosity for higher silica content. Exp 1 and 8 have nano zeolite thereby exhibiting pores in the 50-500nm range with Exp 1 having lower initial silica content in the solution which shows more pore volume as compared to Exp 8. Exp 2 and 5 have micron zeolite which exhibits pores in the 500-5000nm range with Exp 2 having higher initial silica content which shows less pores as compared to Exp 5.

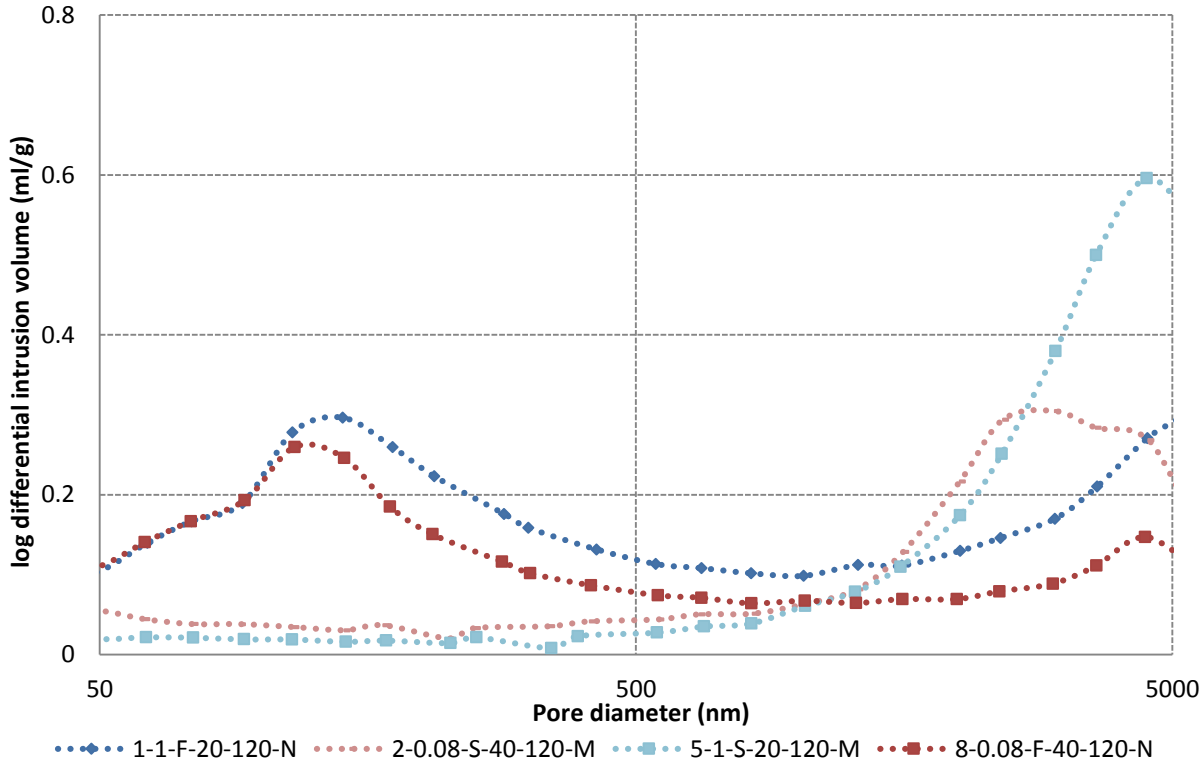

Figure 4.16: Log differential intrusion volume curves in the 50-5000nm range to highlight the differences between using differing amounts of silica and differing sizes of zeolite

4.4.4.4 Ceramic weight: Zeolite weight

The ratio of ceramic weight to zeolite weight only affects the mesopores and the very large macropores of over 5000nm. The mesoporous range has an interaction with the zeolite particle size and is discussed in Section 4.4.4.3.

Macropores above 5000nm are affected by ceramic weight: zeolite weight ratio. Here, having more zeolite creates less pores. Above 5000nm, having a lower ratio of ceramic weight: zeolite weight reduces the pore size. This is because with more zeolite, the particles are more likely to fill the gaps, thereby reducing pore volume when compared to the ceramic fibres which entangle with each other. This is shown schematically in Figure 4.17a and b where Figure 4.17a shows the sample having equal amount of ceramic and zeolite. Figure 4.17 shows the sample having higher zeolite content thereby reducing the pore area above 5000nm.

a b

Figure 4.17 a) Figure showing arrangement for a sample where ceramic weight: zeolite weight is 1:1 b) Figure showing arrangement for a sample where ceramic weight: zeolite weight is 0.08:1

Figure 4.18 shows the 5,000-50,000nm range of the same experiments shown in Figure 4.15. As described, Exp 1 and 10 have low zeolite but high ceramic content, which is responsible for large pore volume as compared to Exp 2 and 8 with high zeolite content.

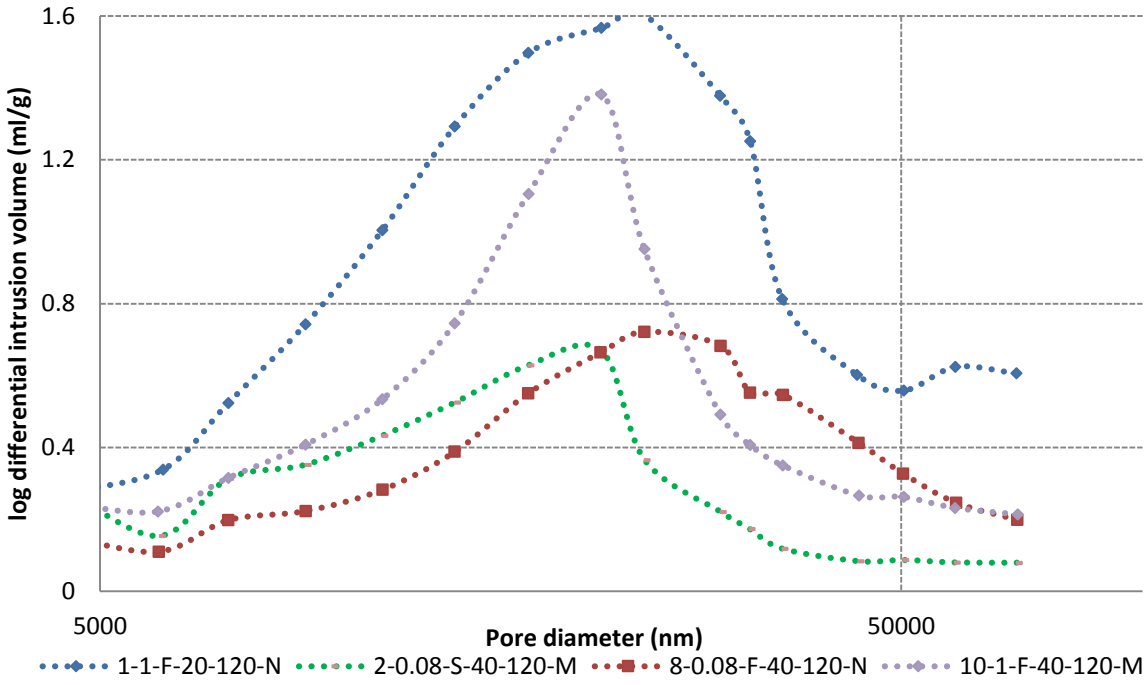

Figure 4.18: Log differential intrusion volume curves for the pores above 5000nm for differing ratios of ceramic: zeolite weight

4.4.4.5 Silica Particle size

Silica particle size is statistically significant only in the mesoporous region. 22nm silica shows a lower pore size and higher pore volume than 120nm silica. The pore size for the 22nm silica is between 5-10nm while the pore size for the 120nm silica is between 10-20nm. This pore size is caused by the packing of the silica particles. The 22nm size particles have a uniform particle size distribution that gives rise to a pore size distribution between 5-10nm, while the 120nm silica has a varying particle size distribution. This leads to a lower pore size distribution, mostly between 10-20 nm, than would be expected from the nominal particle size. Figure 4.19 also shows the pore size distribution of 22nm and 120nm silica obtained from N_2 adsorption measurements using liquid N_2 which is compared with samples 4 and 10 which have 22nm and 120nm silica, respectively, in the mesoporous range. The overlap of the graphs shows good agreement between the two measurement techniques. 22nm silica also

has a higher pore volume when compared to the 120nm silica, this is because the 120nm silica, having varying particles size, can get the smaller particles in between the pores created by the larger particles thereby reducing pore volume when compared to the silica particles that are monodisperse.

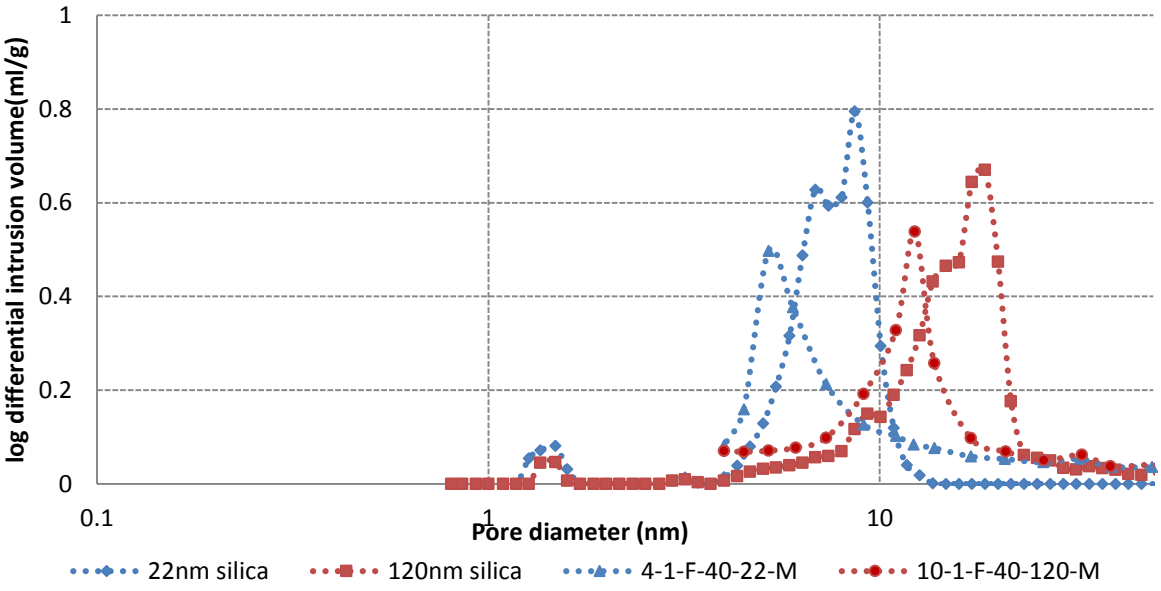

Figure 4.19: Log differential intrusion volume curves in the mesoporous range for 22nm and 120nm silica and laminate structures with 22nm and 120nm silica

4.4.4.6 Heating rate

Heating rate only affects the mesoporous range for the samples having 20wt% silica content. This is an interaction effect with the initial silica concentration. Fast heating has less porosity than slow heating. No other pore size range is affected by heating rate.

4.4.4.7 Pulp Type

There was no statistically significant effect of pulp type. The lack of sensitivity of pulp type is due to the very similar dimensions of the pulp fibres. If the dimensions of the pulp fibres are extremely different this would be expected to affect the region above 5000nm as the

removal of pulp is responsible for this region. Hence, fibres of extremely different dimensions were compared to check if porosity in the laminate structure changed due to this difference. Figure 4.20 shows the laminate structure created from Micro fibrillated cellulose (MFC) and kraft pulp. The MFC fibres were obtained from Daicel chemicals and have fibres below 1µm in diameter. As expected, the kraft fibres which have larger fibres when compared to the MFC fibres have larger macropores when compared to MFC fibres.

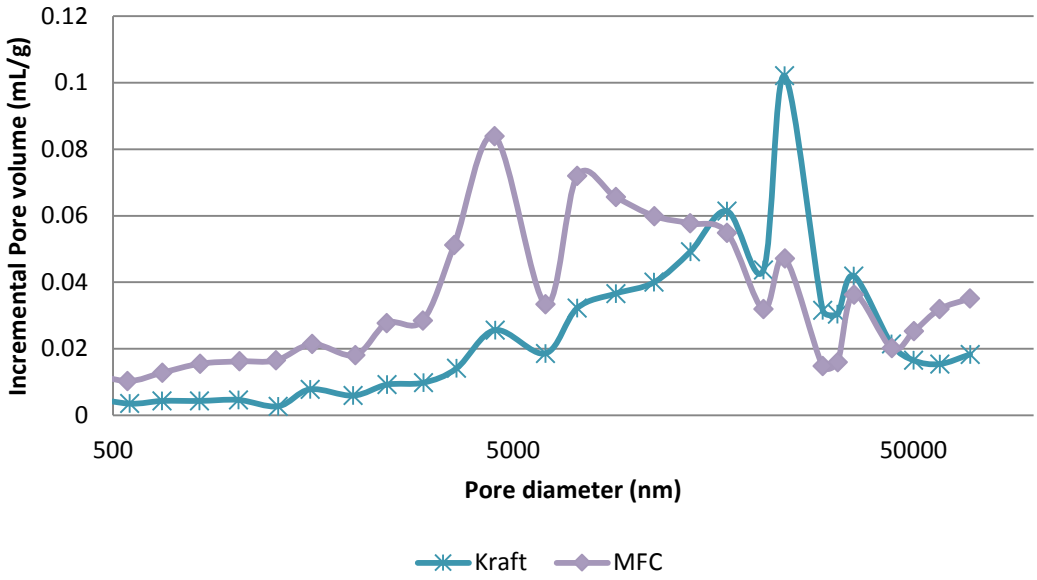

Figure 4.20: Pore size distribution above 500nm for the laminate samples with kraft fibres and MFC fibres

4.4.4.8 Summary of Mercury Porosimetry results

The mercury porosimetry results show that the initial silica concentration is responsible for the major porosity differences between the structures with high and low silica content. These structures having different silica contents can be classified into two families of curves with the high silica content structures having lower porosity than the structures with low silica content. The SEM images are also in agreement with the mercury porosity results. Structures having different zeolite particle sizes have porosity in different sizes ranges with laminate samples having nano zeolite showing porosity in the range 50-500nm, while laminate

structures with micron zeolite have porosity in the range 500-5000nm. Structures having varying ceramic to zeolite weight ratios also have higher porosity for laminate structures with higher ceramic content when compared to higher zeolite content in the sheets. Silica particle size has an effect on porosity only in the mesoporous range with laminate structures having 22nm silica showing pores between 5-10nm and 120nm silica showing pores between 10-20nm. Lastly, although pulp type did not produce any differences in porosities between the different samples in the partial factorial experimental design, using a very different size of pulp will definitely show differences in porosity as shown by using Microfibrilated cellulose instead of Thermo Mechanical and Kraft pulp.

Figure 4.21 shows a schematic of the laminate samples showing the different synthesis conditions, which affect the porosity of the laminate sheet. Figure 4.21a shows a sample with 20wt% silica and a high ratio of ceramic to zeolite particles. Figure 4.21b shows a sample with 20wt% silica and a low ratio of ceramic to zeolite particles. Both these images show the pulp spaces are not properly formed and that the silica has fallen into these spaces. Figure 4.21c shows a sample with 40wt% silica and a high ratio of ceramic to zeolite particles. Figure 4.21d shows a sample with 40wt% silica and a low ratio of ceramic to zeolite particles. Both these images show well formed spaces left behind by fibres. All the other components are also labelled in the images.

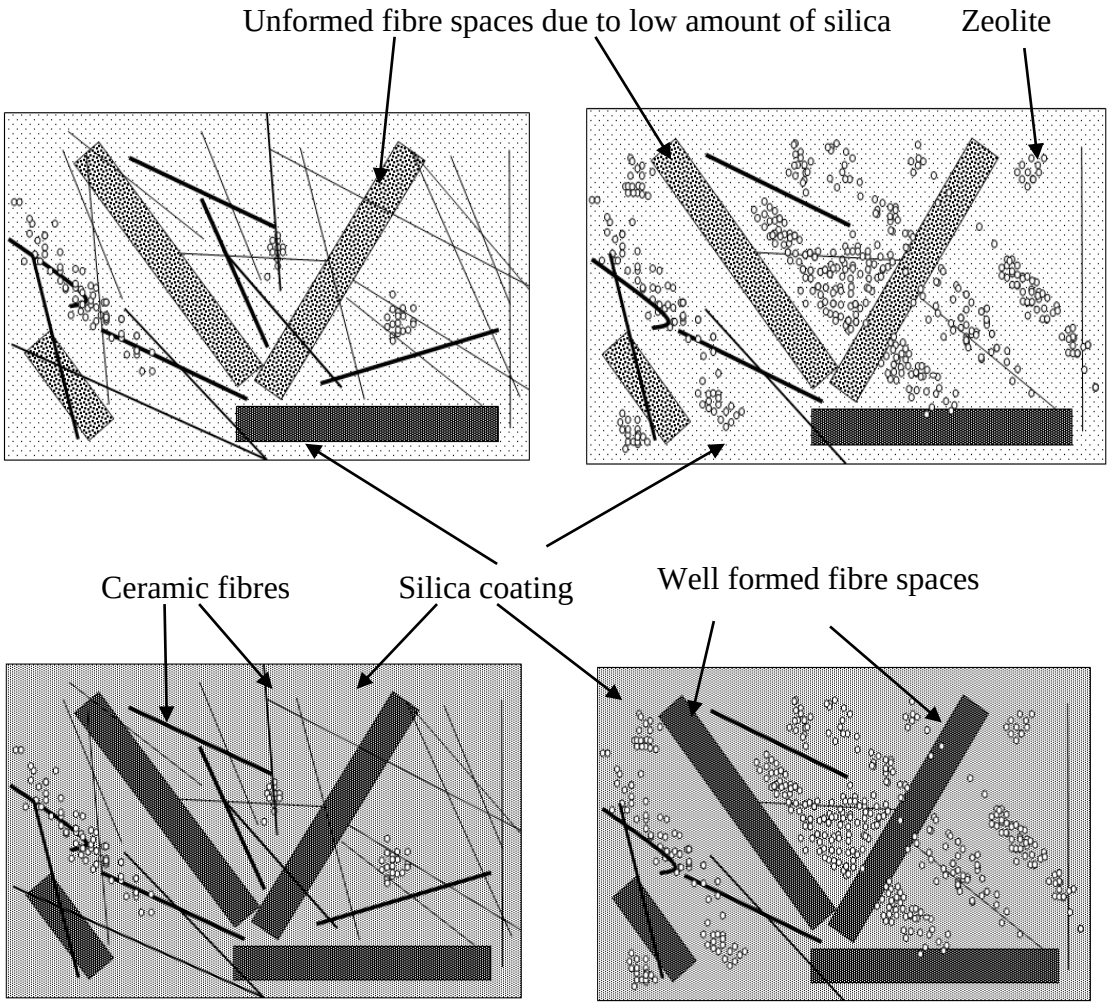

Figure 4.21: Schematic diagrams a) 20wt% silica and high ceramic fibres to zeolite weight ratio b) 20wt% silica and low ceramic fibres to zeolite weight ratio c) 40wt% silica and high ceramic fibres to zeolite weight ratio d) 40wt% silica and low ceramic fibres to zeolite weight ratio.

4.5 Conclusion

This section has shown the relationship between synthesis conditions and the structure of laminate sheets using SEM imaging and mercury porosimetry measurements. Each of the synthesis condition is responsible for its own porous network allowing for tuning the porosity

in the structure. In broad terms, the silica particle size is responsible for mesoporosity, the nano zeolite for porosity between the 50-500nm, the micron zeolite for porosity between 500-5000nm and the ratio of ceramic fibre weight to zeolite weight affects the range between 5000-50,000nm with most of the porosity in this range coming the sacrificial burning of pulp fibres. The initial silica concentration is responsible for overall porosity in the laminate structure. The SEM images show that the laminate structures have good network connectivity due to the voids left behind by the fibres which act as transport channels for the gas thereby having the potential to enhance the mass transfer kinetics during adsorption. Hence, it has been shown that the laminate pore structure across a wide size range can be engineered. With the porosity measurements completed, other characteristics have to be determined so an optimal structure for gas adsorption can be created. Chapter 5 deals with the testing the strength and the rate of adsorption of the laminate structure.

This page is intentionally blank

Chapter 5

Novel Characterisation Techniques for Assessment of Laminate Structured Adsorbents

This page is intentionally blank

5.0 Novel Characterisation Techniques for Assessment of Laminate Structured Adsorbents

5.1 Introduction

As discussed in Section 4.1, it is necessary to optimise different properties of the adsorbent structure to obtain the required adsorbent performance. Papermaking techniques have been chosen to reduce the cost of preparation of the adsorbent structure and also increase the adsorbent loading when compared to other non-particulate adsorbent structures. Since the preparation method can be applied to any zeolite, the separation performance can be enhanced by choosing the appropriate zeolite for the corresponding application. Voidage in the structure has been characterised by applying gas adsorption and mercury porosimetry techniques as outlined in Chapter 4. Other properties of adsorbent structures of importance to their performance are mechanical strength, mass transfer kinetics, pressure drop and dispersion characteristics. The last two properties, pressure drop and dispersion will be considered in Chapter 7 which discusses breakthrough testing of the adsorbent structures. This chapter considers the mechanical strength and mass transfer characteristics.

Since the adsorbent structures are made using papermaking techniques, strength measurement techniques similar to paper strength measurement were considered for testing the mechanical performance of the laminate structures. It is important to note that these structures although made using papermaking techniques, do not have the same flexibility and strength characteristics as paper and therefore standard techniques used to test paper strength may not be relevant for adsorbent structures. It was therefore necessary to find or develop an appropriate mechanical strength measurement technique which would provide meaningful data related to the method of failure and the handling conditions which an adsorbent structure would undergo.

In addition to good mechanical strength, the adsorbent structures will also be used to adsorb CO2 under rapid cycling conditions. Hence the rate of mass transfer to and from the gas and adsorbent structure is important. Measurement of the CO_2 adsorption kinetics was therefore undertaken as a useful metric of structure performance. The rate of adsorption was measured using Micromeritics ASAP 2010 gas adsorption analyser at different gas pressures.

5.2 Available Strength Measurement Tests

As mentioned in Section 5.1, strength measurement techniques used for paper strength testing were initially considered. These tests are described in Section 5.2.1. Section 5.2.2 describes strength tests used for other poly crystalline materials. The problems associated with these tests for the laminate samples prepared are also discussed and the argument for a new strength measurement technique is presented which is subsequently described in section 5.3.

5.2.1 Tensile Strength

Tensile strength is generally used in paper strength measurement. Tensile strength measurement techniques are used to measure the tensile breaking strength using a constant rate of elongation apparatus. The tensile strength can be described using stress- strain graphs where the x-axis is a measure of tensile strain or length of elongation of the sample. Strain is a dimensionless quantity which is defined as the change in length divided by the original length of the strip. The y-axis is a measure of tensile stress which is the tensile force applied to the sample ends divided by the cross sectional area of the paper strip. The test can also be used to derive the Young's Modulus which determines stiffness. The Young's Modulus is determined by the initial slope of the stress-strain curve*[113]*.

The standard for paper testing is given by Tappi Method T-494, which specifies the use of a constant rate of elongation equipment to determine tensile strength, stretch, tensile energy absorption and tensile stiffness. Tensile strength is used to determine the strength of paper or

board from factors such as fibre strength, fibre length and bonding. An unsuccessful attempt was made to use this method to test the strength of the laminates using an Instron tester. The major problem encountered with the testing was in gripping the sample with pneumatically operated jaws. The initial attempts saw the sample failing when clamping pressure was applied. Next, adhesive tape was used to protect the jaw contact area. This allowed the sample to be gripped, but tensile tests invariably failed at the jaw, which means that the measured values cannot be used. The samples are highly particulate, with relatively few ceramic fibres and no pulp fibres remaining after calcining. Since tensile testing measures fibre strength and fibre-fibre bonding, it was concluded that the samples are too fragile to test using conventional tensile testing.

Other paper strength measurement techniques such as zero span testing were considered but these tests also required some form of clamping the sheet. The tests which did not require clamping such as ring crush test requires the sheet to be flexible, which these sheets were not.

5.2.2 Other Mechanical Tests used for Polycrystalline Materials

Other mechanical tests were also considered apart from strength measurements used in the paper industry. These tests are generally used for polycrystalline materials and it was thought that these tests could be adapted to the laminate structure. These are the 3-point bending test and the Hardness test.

5.2.2.1 3-point bending test

Bending tests are generally used for brittle and fragile samples and the stress state varies along the specimen from compression to tension. The 3-point bending test places the sample on two supports and one force is applied on the centre of the specimen. This test was unsuccessful as many of the samples were too weak to be loaded in such a manner and also large amounts of sample were required for this test*[114]*.

5.2.2.2 Hardness test

A hardness test uses an indentor tip pressed into a flat sample under load. Hardness is then defined as the ratio of applied force to the surface of imprint of the indentor*[114]*. This test was performed on some laminate structures. The samples that were stronger cracked at a particular force and created crack lines running through the entire sample. It was difficult to identify the indentation marks. When the weaker samples were tested, the indentor was easily pushed through the sample, even at the lowest indentation load available, and again the indentor marks were difficult to identify. Hence this test did not provide very useful results.

5.3 Design of a New Strength Measurement Test

As discussed in Section 5.2, the available strength measurement tests were hard to perform on the laminate samples due to various reasons. Hence it was necessary to develop a new method for measuring the strength of the laminate structures. This measurement method need not be an absolute strength measure but only a comparative measure between the different structures. The measurement method also needs to be useful in selecting a structure which will have enough strength for the required purposes. The structure needs to have enough strength to allow manual handling of the structure till it is placed inside containment for PSA cycling. Hence considerations will have to be made for the gas flow loads the sample will face during pressure swing adsorption. Hence a method has to be determined which would closely resemble the motions the sample would be put through during pressure swing adsorption.

A vibratory sieve was considered for use as a strength measurement tool for the laminate structures. The motions undergone by the sample in the vibratory sieve will be harsher compared to what the sample will face due to gas flow and pressure swing adsorption.

5.3.1 Vibratory Sieve

A Ro-Tap Test Sieve Shaker (Model *RX-29)* was used for strength measurement testing. This is a common industrial test sieve shaker to measure particle size and size distribution in samples. It uses a rotating movement and tapping action. A stack of sieves from the larger holed sieves to the smaller holed sieves are placed in decreasing order of size with a solid pan at the bottom to catch any dust. The mechanical rotating action with the tapping action on the top allows the particles to move through the sieve for a set amount of time. Figure 5.1 shows a Ro-Tap sieve shaker*[115]* with all the different components labelled.

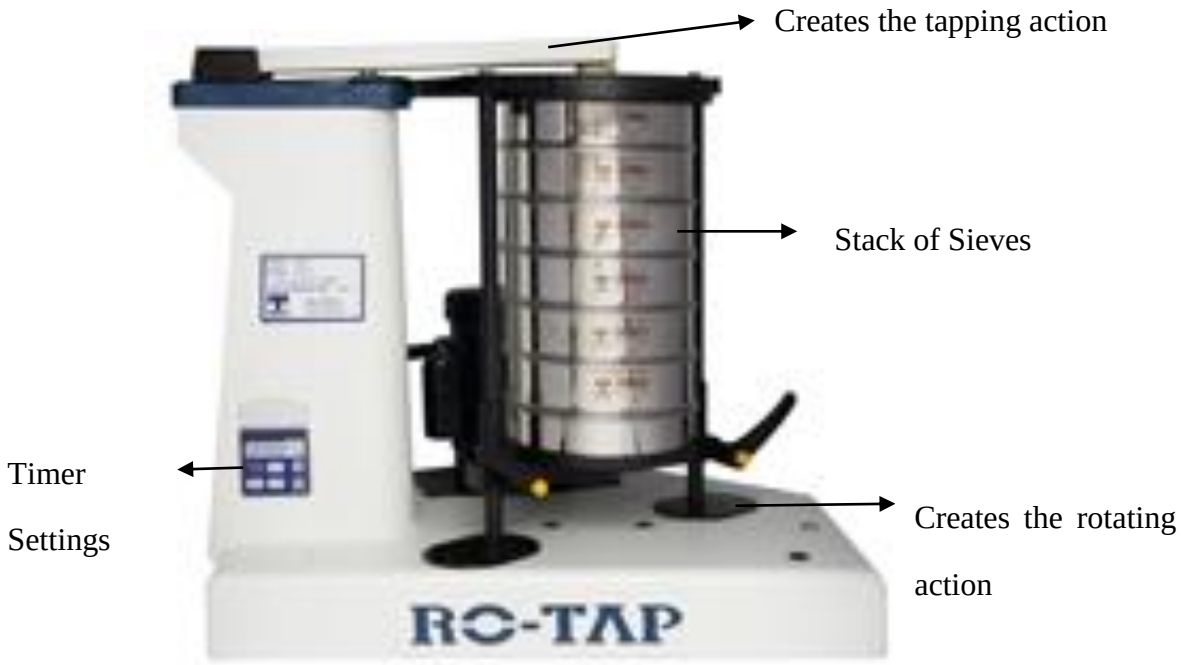

Figure 5.1: A Ro-Tap Test Sieve Shaker*[115]*

5.3.2 Strength Measurement Methodology of Laminate Structure

A 5cm x 5cm square calcined laminate sample was used to perform strength measurements from the experiments in the partial factorial table. The initial sample weight was recorded. Only one sieve was used as any of the particles that separate from the structure is dust and need not be sieved further and this sample was placed on a sieve with 1 mm openings, with a

solid pan at the bottom. This assembly was locked into place in the Ro-Tap. The Ro-Tap is not used conventionally for strength testing and usually receives a powdered sample for sieving. The timer was set for two minutes of the rotating and tapping action. During this time, any particles which were not well attached to the structure easily fell off and were sieved through. At the end of two minutes, the weight was recorded of the sample which was on top of the 1mm sieve. This was repeated every two minutes until 10 minutes had passed and the weight was recorded. The sieving was then continued in ten minute steps until half an hour and then in fifteen minute steps for a further half an hour and the weight on top of the 1mm sieve was recorded at the end of every interval. In total, the test was conducted for one hour for every sample. The recorded weights over the entire hour were then converted to a percentage of the initial weight and plotted on Matlab. A curve fitting tool was used with the decay function

$$y = 100 + a(1 - \exp(cx)) \quad [5.1]$$

where the values for a and c were used as fitting parameters. a gives the final weight proportion that the sample loses and c is the degradation rate. Both these variables are important to quantify the strength of the sample.

5.4 Strength Results

A similar statistical analysis as performed for the pore size distribution was done for the strength measurements. Table 5.1 shows the mean strength values for all the variables from the partial factorial design. The values in bold have a statistical significance and only these variables are discussed in the following sections.

As can be seen from Table 5.1, the strength is affected by the reinforcement and binding agents. The samples that had more binding and reinforcement materials were stronger and their mode of breakdown was very different from the samples that had more adsorbent. The

stronger samples lost their strength through surface powdering, some samples fragmented into large pieces but a majority of the structure was retained while the very weak samples completely lost their overall laminate structures and broke down into the starting materials. This is discussed in more detail along with the results.

Table 5.1: Mean values of final weight loss (a) and inital degradation rate (c) as representatives of laminate strength measurements

Variables	Factors	a	c
Ceramic fibre weight: zeolite weight	0.08:1	**-59.6**	-0.22
	1:01	**-25.2**	-0.08
Heating rate	Fast	-47.4	-0.15
	slow	-37.5	-0.16
Silica concentration	20	**-57.9**	**-0.26**
	40	**-27.0**	**-0.05**
Silica Particle size	22	-43.1	-0.14
	120	-41.8	-0.16
Zeolite particle size	micron	**-26.9**	-0.11
	nano	**-57.9**	-0.20
Pulp Type	Kraft	-37.5	-0.17
	TMP	-47.4	-0.13

The breakdown of the structures can be categorized into four modes:

1. Surface powdering but structure preserved: These structures have micron zeolite or nano zeolite with large quantities of both the reinforcement and sintering agents or have micron zeolite with large quantities of either one of the reinforcement or sintering agents. An image showing the preserved structure of the samples under this mode of breakdown after one hour of sieving is shown in Figure 5.2a.

2. Fluffy structure but structure preserved: These structures have nano zeolite and have more reinforcement agent (ceramic fibres). Figure 5.2b shows an image of a sample after the fluffy part of the sample is removed due to the sieving. Although the structure is preserved, there is

only a bare minimum of the sample left and the sample has a reduction in thickness due to material lost.

3. Fracturing of sample into pieces: These structures also have nano zeolite and have more binding agent (colloidal silica). Figure 5.2c shows the fractured pieces of the sample where the larger parts of the sample remained on the sieve after sieving.

4. Complete breakdown of structure to starting components: These structures have low reinforcement and binding agent. The structures with nano zeolite show complete breakdown almost immediately after starting the test while the structures with micron zeolite show complete breakdown towards the end of the test. Not much sample remains after the sieving is performed. Very little fluffy material can be obtained after sieving and this is shown in Figure 5.2d.

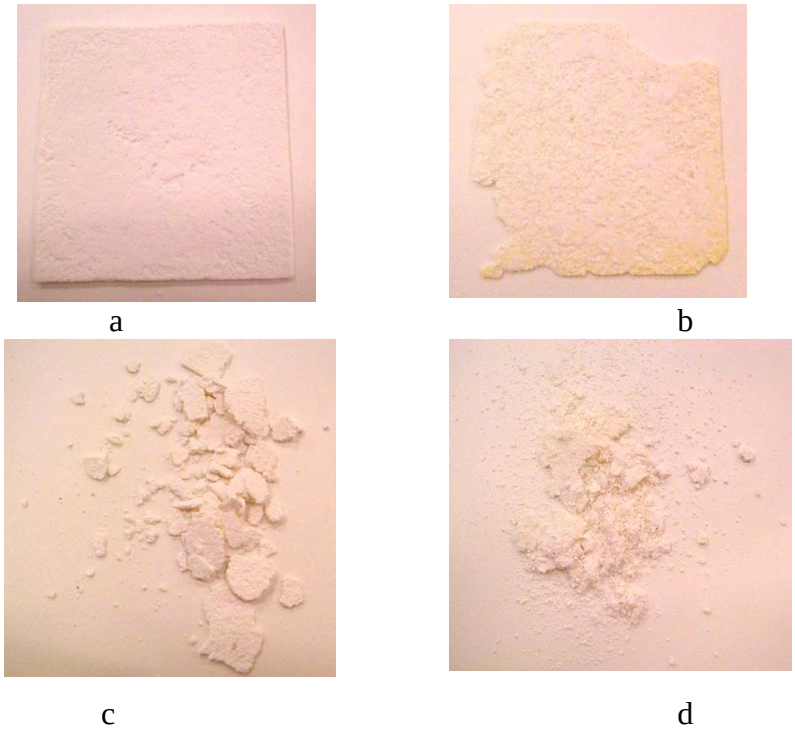

Figure 5.2: Images showing the different breakdown modes of the different laminate structures after the sieving is complete a)Surface powdering but preserved structure b)Preserved structure after the fluffy part is removed c)Fragmented structure d)Complete breakdown of structure

The strength results are affected by the final weight loss (a value) and the degradation rate (c value). Examples of some of the components affecting strength are shown in Figure 5.3. The initial silica concentration is the most important variable that affects strength as it is the silica used that acts as a binding agent between the different components of the sheets. Exp 13 and 16 in Figure 5.3 have differing silica concentration. Exp 16 has a higher silica concentration and therefore feels the effect of sintering/binding to other silica particles, zeolite particles and to the ceramic fibres more strongly which gives it a higher strength as compared to Exp 13. Having higher silica content generally provides a strong structure with the breakdown of the structure happening through surface powdering and the loss of material is slow. In some instances however, where the ceramic content is low and the structure has nano zeolite, the structure breaks down to pieces immediately after strength measurement, but the pieces are too large to fall through the sieve. Hence the broken pieces are retained and can still be used for strength measurement.

The other variables that affect the final weight loss are ratio of ceramic weight to zeolite weight and zeolite particle size. Exp 2 and 4 in Figure 5.3 have varying ceramic weight: zeolite weight. Exp 4 has more ceramic which means that the sample has more fibres holding the structure together thereby increasing strength as compared to Exp 2 which has more particles. The effect of ceramic weight to zeolite weight is more pronounced in structures which have nano zeolite and low silica concentration, with a high concentration of ceramic fibres. These structures are very fluffy and have more loss of material through surface powdering but maintain an intact structure. Lastly Exp 3 and 6 have different zeolite particle sizes. Exp 6 is stronger as it has larger sized zeolite particles. The samples with smaller zeolite particles require more silica to adhere the particles together than the samples with larger zeolite particles. Hence the samples with larger zeolite particles are stronger. The nano zeolite samples also showed dusting, as larger flocs were formed during preparation and the formation was worse than samples that had micron zeolite. As explained, the structures with nano zeolite are the ones that show a greater chance of losing strength quickly. The only

structures with micron zeolite that lose strength easily are the structures that have low reinforcement and low binding agent. The nano zeolite structures on the other hand can only be saved if they posses high amount of sintering and binding agent.

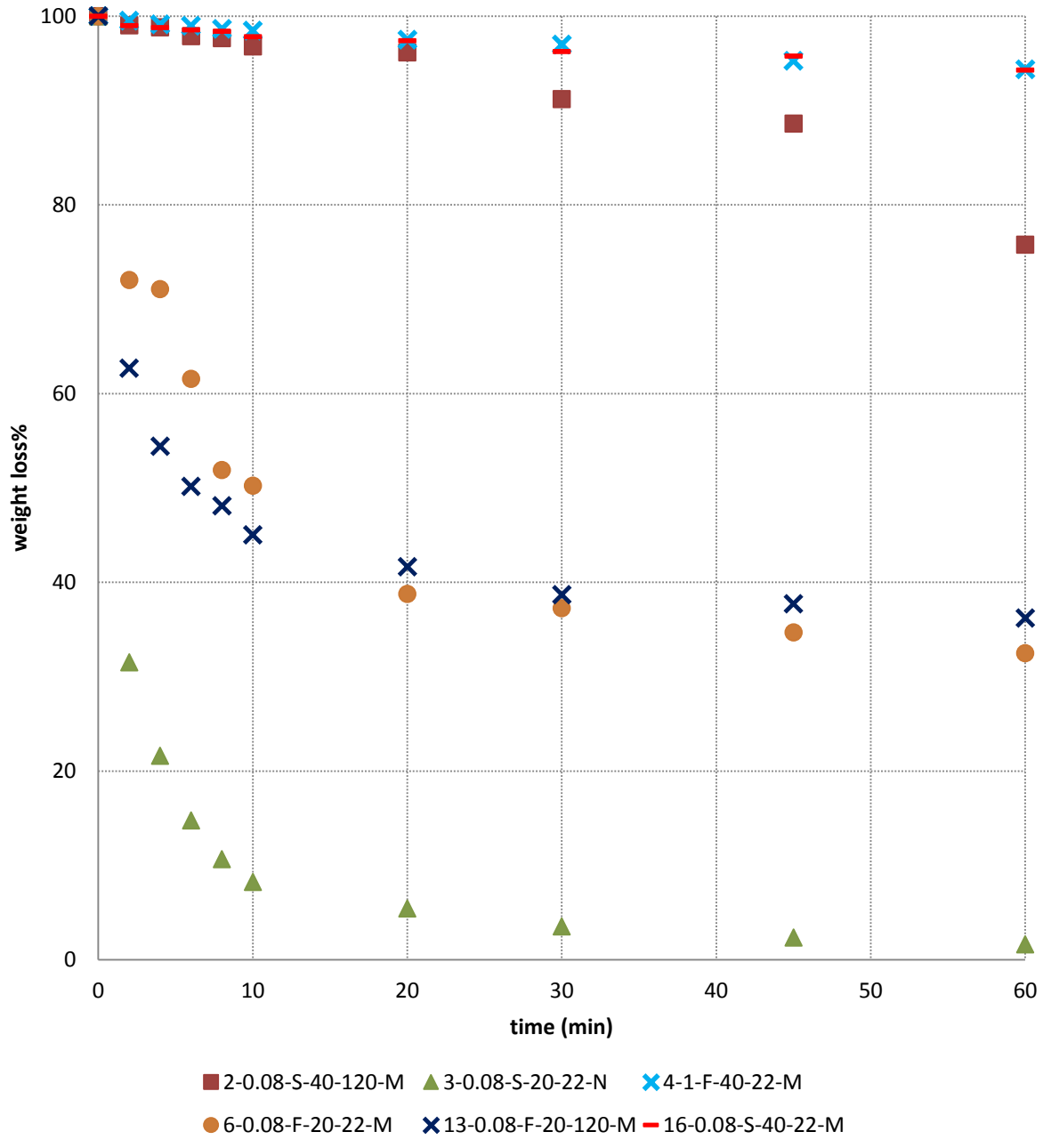

Figure 5.3: Strength measurements for laminate samples comparing the different silica concentration, ceramic to zeolite weight ratio and zeolite particle size

To show the effect of silica concentration, ceramic to zeolite weight ratio and zeolite particles size, the individual results of all the samples plotting the final weight reached against the degradation rate are shown in Figure 5.4. 5.5 and 5.6 respectively. Figure 5.4 shows the samples with differing silica concentration. The structures with 40wt% silica have very low degradation rate and most of the samples have a very high final weight % reached when compared to the samples with 20wt% silica. Next the samples are shown in Figure 5.5 but highlighting the differences between high and low ceramic to zeolite weight ratio. The structures having 1:1 ceramic to zeolite weight ratio have most of the samples achieving a higher final weight reached when compared to the samples that have 0.08:1 ceramic to zeolite weight. Lastly, the differences between nano and micron zeolite is highlighted for the same results in Figure 5.6. Again, most of the micron zeolite show a high final weight reached when compared to the nano zeolite samples.

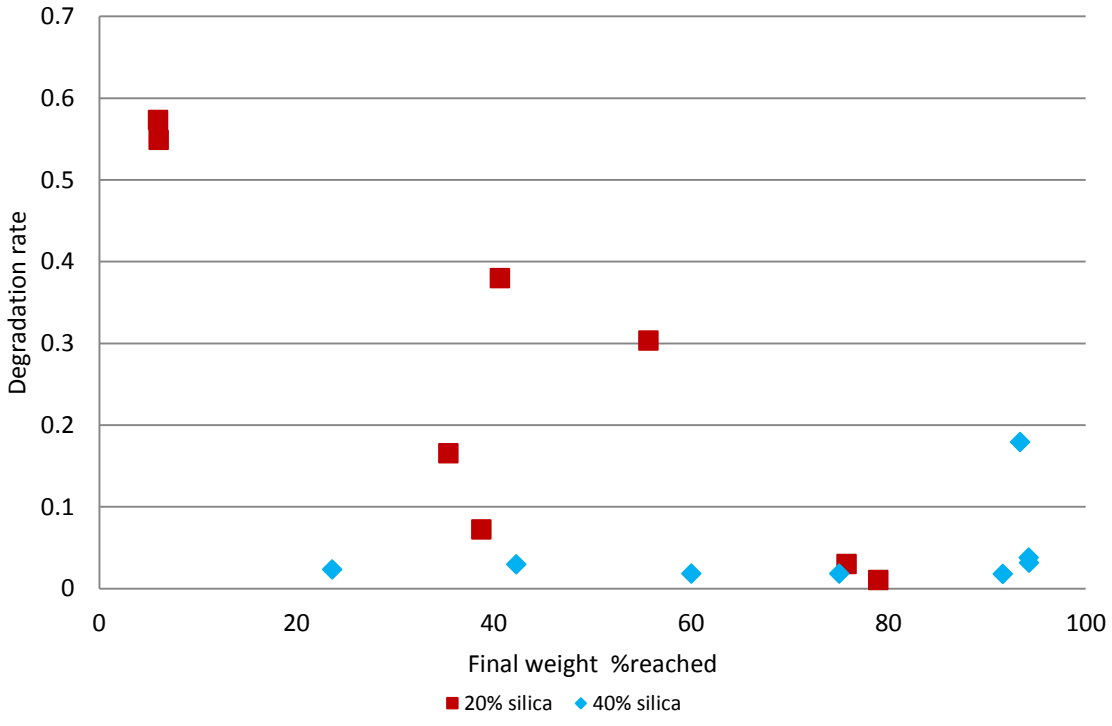

Figure 5.4: Final weight % reached against degradation rate for all samples highlighting their different silica concentration.

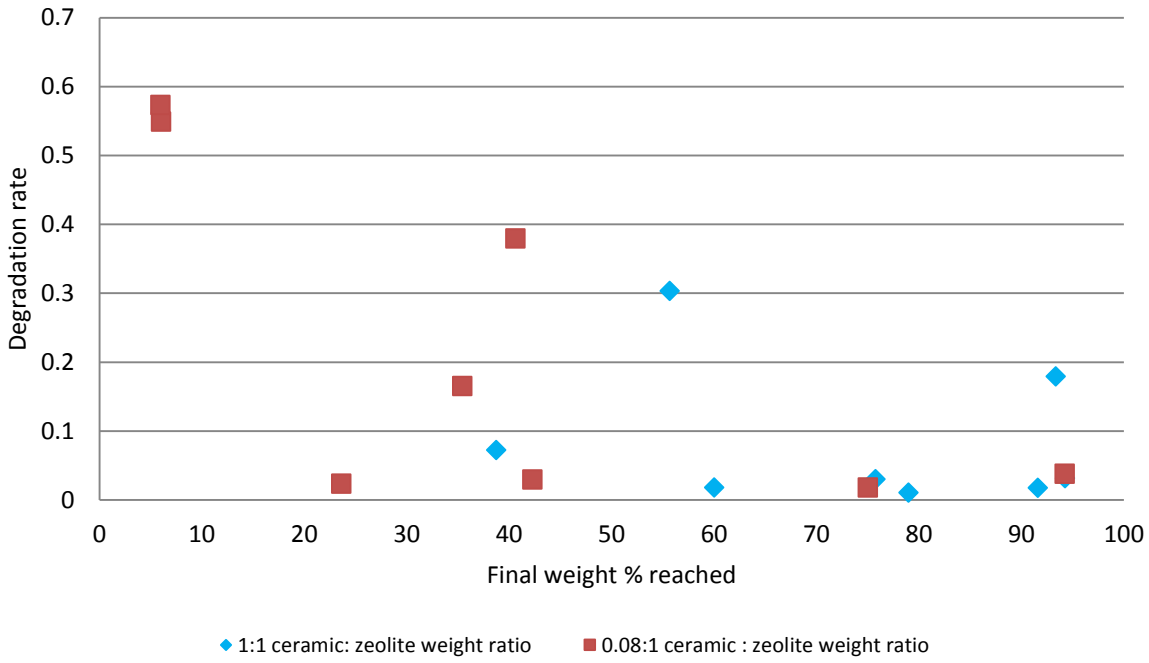

Figure 5.5: Final weight % reached against degradation rate for all samples highlighting their different ceramic to zeolite weight ratio.

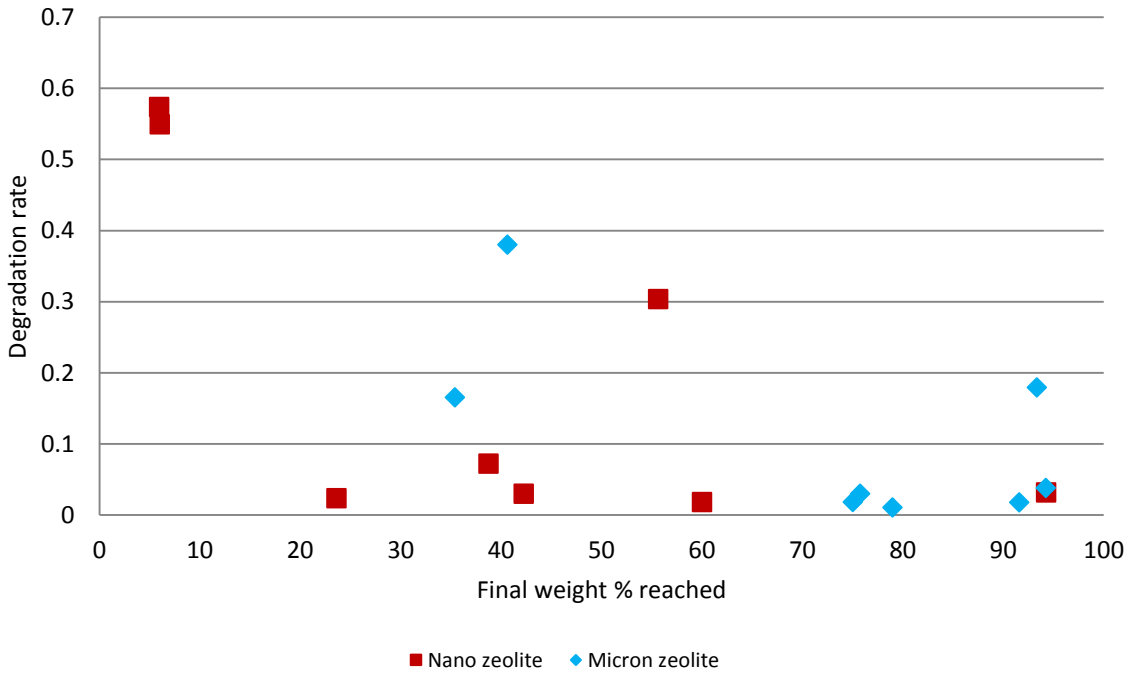

Figure 5.6: Final weight % reached against degradation rate for all samples highlighting their different zeolite particles sizes.

The strength measurements show that structures with micron zeolite have adequate strength when having one of the high factors for either the sintering agent or binding agent. Hence structures with 40-55wt% micron zeolite can easily be made for breakthrough testing and they are expected to have enough strength to last through the process. On the other hand, structures with nano zeolite need to have high factors for both the sintering and binding agents to be useful for breakthrough testing.

5.5 Rate of Adsorption Measurements

The rate of adsorption measures how quickly or slowly a sample adsorbs a dose of gas. An analysis of the rate of adsorption of a material at one or more relative pressures can reveal information about the accessibility of the pore area to the probe molecule, and how energetically the surface collects and holds the gas. The rate of adsorption is related to diffusion of the probe molecules into pores, hence, an analysis of the rate of adsorption as a function of relative pressure reveals much about the pore throat shape and tortuosity.

The rate of adsorption in a porous adsorbent is generally controlled by transport within the pore network rather than by intrinsic kinetics of sorption at the surface. Pore diffusion may occur by several different mechanisms depending on pore size, sorbate concentrations and other conditions*[116]*.

For a given molecule, the effective diffusion coefficient depends on the accessible porosity, pore organisation, friction with the pore wall and adsorption kinetics*[117]*. The rate of adsorption of each adsorbent is often assumed to be independent of the presence of other adsorbents and can be tracked by accounting for the loading of each adsorbent in the mixture*[118]*. Hence the amount of zeolite in the laminate samples can be tracked by the loading of zeolite in each adsorbent structure and rate of adsorption also assesses the role of silica in the laminate structure on slowing the carbon dioxide molecules in reaching the zeolite pores.

For kinetic measurements, the particles at the external surface behave completely different from the bulk material*[41]*. The zeolite laminate structures provide easy accessibility to the zeolite particles because of the high internal porosity of the structure which provides different kinetics to the materials in their bulk form. The high internal porosity of the structure can improve the kinetics of the laminate sheet.

5.5.1 Rate of adsorption in Zeolite & Zeolite Structures

In zeolites, which have micropores, the diffusing molecule never escapes the force field of the adsorbent's surface and transport occurs by an activated process involving jumping between adsorption "sites". Such a process is called surface diffusion. Commercial adsorbents however consist of small microporous crystals combined to form a macroporous structure. Such adsorbents offer two distinct diffusional resistances to mass transfer: micropore resistance of the adsorbent crystals or microparticles and macropore diffusional resistance of the adsorbent structure. The relative importance of micropore and macropore resistances depends on the ratio of the diffusional time constants which varies widely depending on the systems and the conditions*[24]*.

5.5.2 Measurement Method

The rate of adsorption was measured on the Micromeritics ASAP 2010 gas adsorption analyzer using the "rate of adsorption" mode. The sheet structure was broken into pieces to fit into the glass tube used on the Micromeritics ASAP 2010 instrument. This sample was then degassed by heating slowly to 350°C and holding it for 10 hours under vacuum. The sample was then cooled to room temperature and analysis was performed using carbon dioxide as the adsorptive gas. The analysis was performed at 273K using an ice-water mixture. The ASAP 2010 uses a fixed volume method for dosing. It doses the sample and records pressure change per dose vs. time. The gas dose volume was selected as $2cm^3/g$ and the time interval to

measure the change in pressure during adsorption was selected as 0.1s for all the samples. This pressure history is then converted to actual amount adsorbed.

5.5.2.1 Analysis Method

The sample starts at an initial pressure (the equilibrium value from the previous data point) and initial loading, as calculated by the instrument. The dosing manifold is then pressurised to some pressure P_0. The valve is then opened and the gas flows from the dosing manifold to the sample and the dosing pressure P is recorded as a function of time. This set up is shown in Figure 5.7.

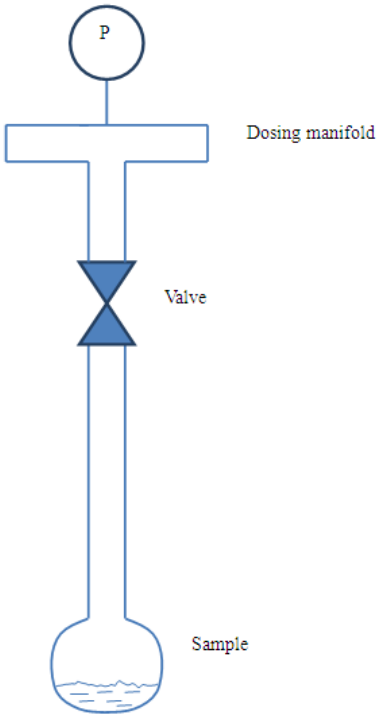

Figure 5.7: Dosing of Manifold gas to sample in ASAP 2010.

The rate of adsorption of gas into the adsorbent ($\frac{dn}{dt}$) can be written according to the linear force driving model as:

$$\frac{dn}{dt} = k\,(n_{eq}(P) - n) \qquad [5.2]$$

With the pressure, P changing, the equilibrium amount of adsorption (n_{eq}) will also change as it is a function of P. The variable k represents the overall linear driving force constant which is the rate of adsorption at the target Pressure. The value n represents the instantaneous adsorption loading on the sample. Since changing pressure causes a change in the equilibrium amount of adsorption, this makes the fitting difficult. However, by adopting the trapezoidal rule for integration, this equation can be solved explicitly for instantaneous loading at a future time. Integrating over the time interval t to $t + \Delta t$ gives:

$$\int_t^{t+\Delta t} \frac{dn}{dt} dt = \int_t^{t+\Delta t} k\,(n_{eq}\,(P) - n)\,dt \qquad [5.3]$$

Solving this equation gives:

$$n(t + \Delta t) - n(t) = k \int_t^{t+\Delta t} (n_{eq}\,(P) - n) dt \qquad [5.4]$$

Applying the trapezoidal rule to the right hand integral gives:

$$n(t + \Delta t) - n(t) = \frac{k}{2}\,[(n_{eq}\,(P) - n)_{t+\Delta t} + (n_{eq}(P) - n)_t]\Delta t \qquad [5.5]$$

The equilibrium amount of adsorption can be calculated from the pressure using an isotherm model such as the dual-site Langmuir model, the equation for which is given in Section 5.5.3. Rearranging and solving for $n\,(t + \Delta t)$ gives:

$$n\,(t + \Delta t) = \frac{\frac{k\Delta t}{2}[n_{eq}(t+\Delta t) + n_{eq}(t)] + n(t)[1 - \frac{k\Delta t}{2}]}{1 + \frac{k\Delta t}{2}} \qquad [5.6]$$

By implementing this equation, $n\,(t + \Delta t)$can be solved at each successive time step and the k value giving the best fit can be determined for each target pressure (from 5 to 70mm Hg) in every sample. The target pressure above 70mm Hg was not used for analysis as the adsorption occurred too quickly to get useful results.

The k values are then plotted on a graph against Pressure and the k value at 30mm Hg was chosen for statistical analysis to determine which variables had any statistical significance.

30mm Hg was used as this is close to the midpoint between 5 and 70mm Hg and also by this point, the slope of the curve between pressure vs rate of adsorption becomes very clear.

5.5.3 Rate of Adsorption Results

As mentioned in Section 5.5.2.1, the equilibrium amount of adsorption is first fitted using the dual-site Langmuir model given by

$$n_{eq} = \frac{m_1 b P_{eq}}{1+bP_{eq}} + \frac{m_2 d P_{eq}}{1+dP_{eq}} \quad [5.7]$$

where n_{eq} is the equilibrium amount adsorbed, m_1 and m_2 are the maximum adsorbed amount, P_{eq} is the gas pressure corresponding to the equilibrium amount adsorbed and b and d are adsorption constants. Using this equation, a curve fitting was done on one sample between equilibrium amount adsorbed and the corresponding pressure as shown in Figure 5.8 in order to obtain m_1 m_2, b and d After 200 mm Hg, the fitting does not overlay the experimental data. But the rate constant is obtained from the pressure range 5-70mm Hg and this fits the data very well as shown in Figure 5.9.

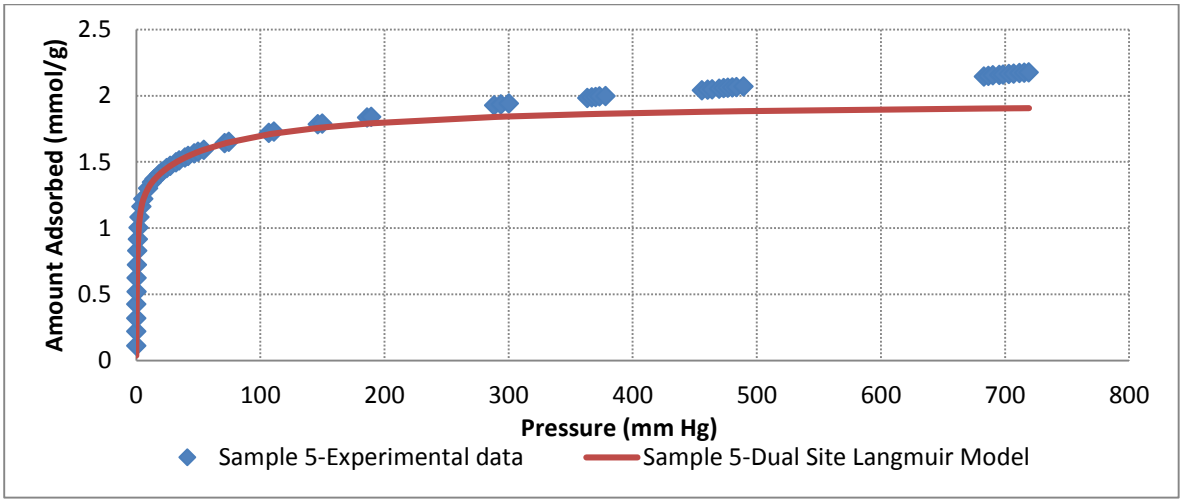

Figure 5.8: Comparison of Langmuir dual site model against experimental data for equilibrium amount adsorbed against the corresponding pressure for the entire range of data.

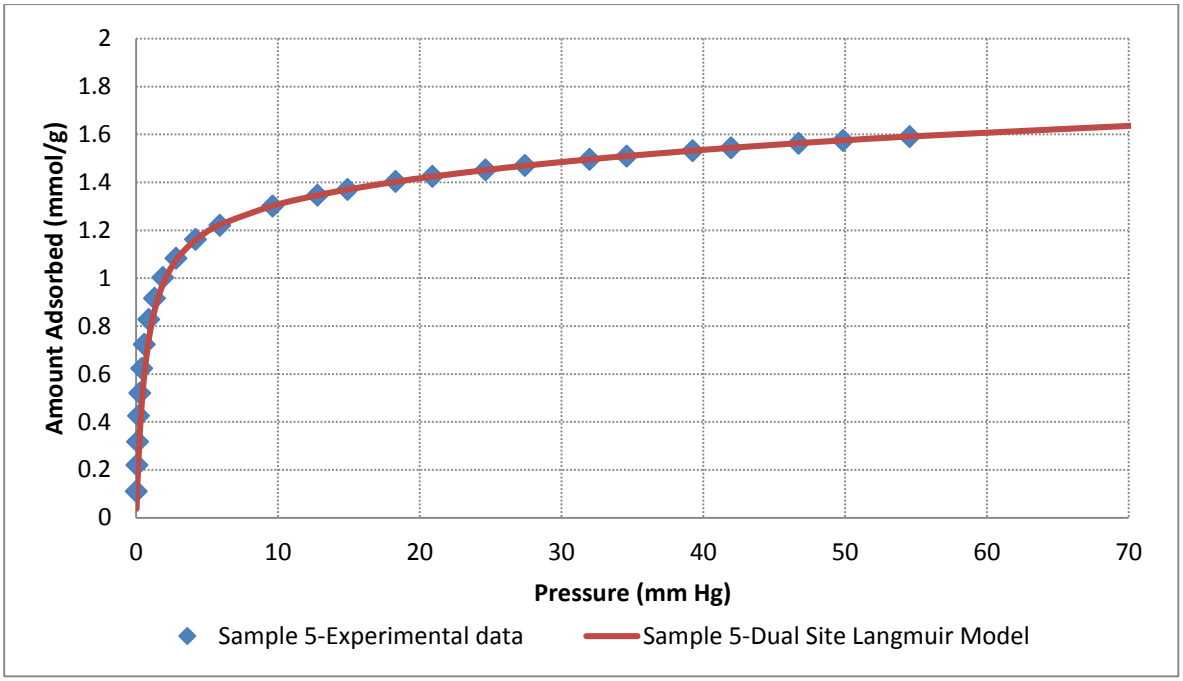

Figure 5.9: Comparison of Langmuir dual site model against experimental data between the pressure ranges 0-70mm Hg

The *k* values for each of the 16 samples from the partial factorial design in Table 3.1 were calculated according the analysis method as outlined in Section 5.5.2.1 by plotting the time at which the adsorption occurs against the instantaneous amount adsorbed. The *k* values were also compared against the micron powder sample and nano powder samples of zeolite A as well as zeolite A beads. Figure 5.10 shows how well the analysis method works to fit against the measured data for nano zeolite at a target pressure of 36mm Hg. Figure 5.11shows the *k* values for micron and nano zeolite A and the zeolite A beads. The pressure range used for *k* value measurement is from 5-70mm Hg. The *k* value increases with increasing pressure showing that the adsorption kinetics increases with increasing pressure.

The rate of adsorption or the *k* value calculated from eqn 1 in Section 5.5.2.1 actually represents the diffusion rate constant and the slope of the isotherm. The micron and nano zeolite A powders have very similar rates of adsorption. The maximum amount of adsorption of nano zeolite is lower than micron zeolite and this has been taken into account while

calculating the k values of nano zeolite. Also, the amount of zeolite in the beads has been taken into account for the calculation of k values by adjusting the k values according to the loading of the zeolite. It was expected that the nano zeolite would have better kinetics than its micron zeolite counterpart, but Figure 5.11 showed no differences between the two samples.

It was necessary to understand why particle size showed no difference in the kinetics of adsorption and also to check whether packing played a bigger role in kinetics which had overshadowed the difference in kinetics due to particle size changes. To understand the effect of compaction of the structure on kinetics, the rate of adsorption of micron zeolite A was carried out under three different conditions. The first one has the micron zeolite powder in a bulb like sample holder with a rod in the middle, the second had the micron zeolite powder in thin tube with no bulb and the third was the same thin tube with a rod in the middle. The images for the three different conditions are shown in Figure 5.12. The micron zeolite powder in a bulb like tube had the highest kinetics, followed by the micron zeolite in a thin tube without the rod and lastly the micron zeolite in a thin tube with the rod in the centre had the lowest kinetics. This is shown in Figure 5.13. Hence, the kinetics are intrinsically related to the packing of the structure. The micron zeolite powder in the bulb like tube was not compacted and had more exposed surface at the top. With the thinner tube, the exposed surface became less and with the thinner tube with the rod in the middle, the zeolite powder became highly compacted which increased the time taken for adsorption. For all the samples, the tube with the bulb at the end and rod was used and this was the general measurement method. In powder form for the nano and micron zeolites, the gas has to flow through a bulk material to reach the individual particles and therefore the size of the zeolite particle has no effect on the rate of adsorption. The beads have a lower rate of adsorption as compared to the powder forms due to its compacted structure. Hence, the diffusion limitation was due to macropores.

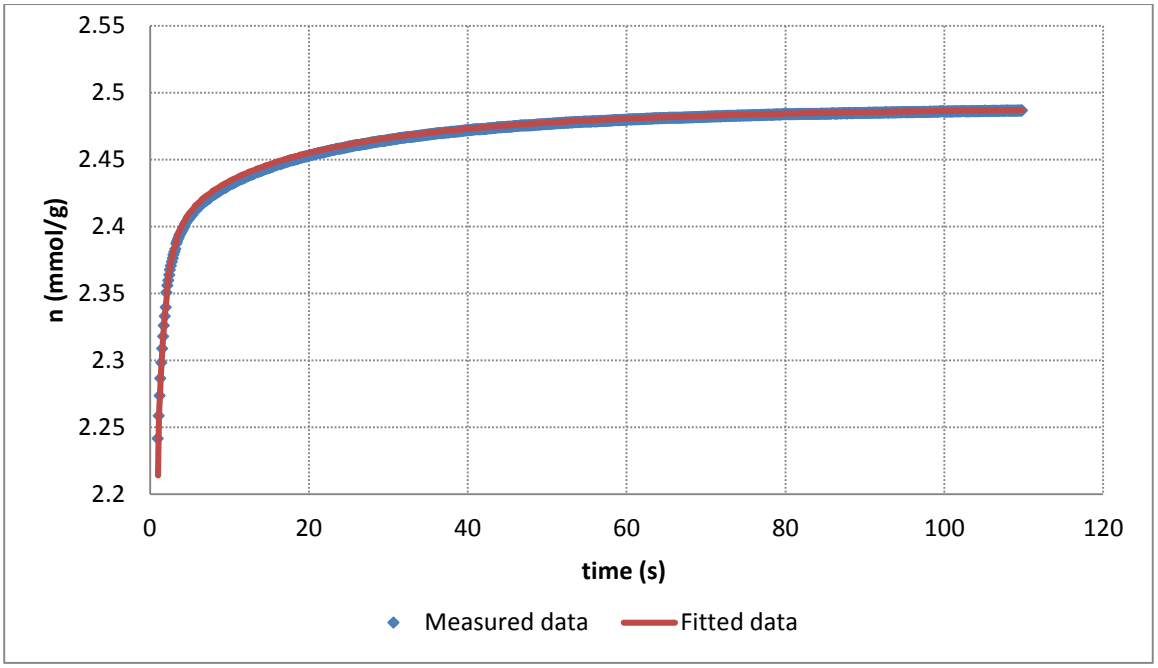

Figure 5.10: *k* value determination for nano zeolite powder by fitting the instantaneous adsorbent loading against the calculated adsorbent loading at a target pressure of 36mm Hg

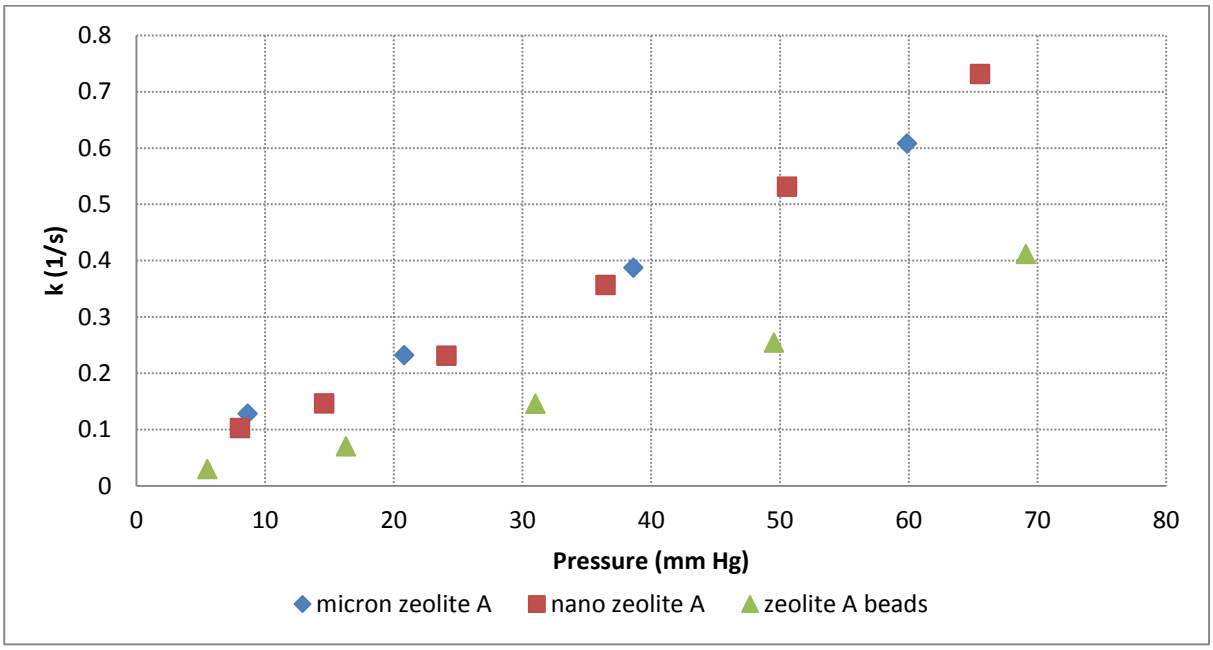

Figure 5.11: *k* values for micron and nano zeolite A powder compared against zeolite A beads in a pressure range of 5-70mm Hg.

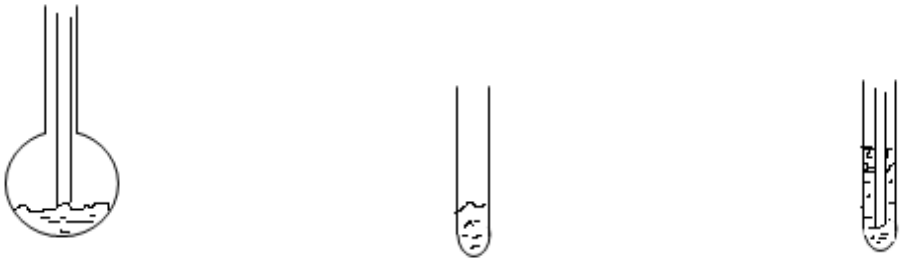

Figure 5.12: Conditions for powder sample analysis using ROA a) Tube with a bulb and rod b) Narrow tube c) Narrow tube with rod

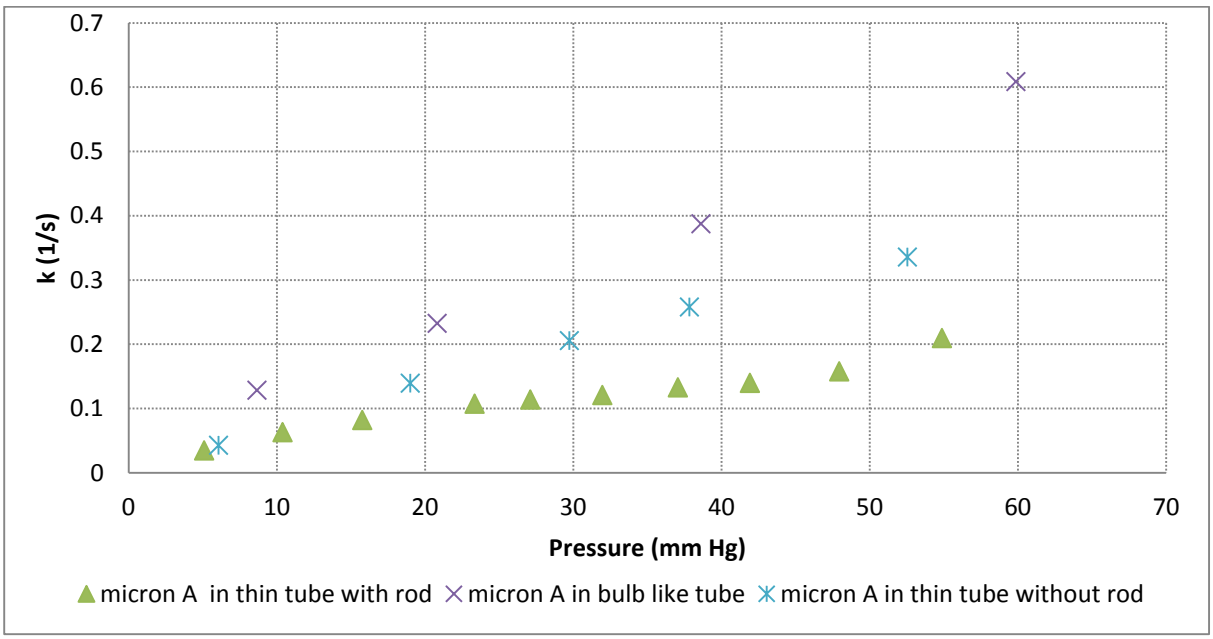

Figure 5.13: *k* values for micron A powder held in different tubes in a pressure range of 5-70mm Hg.

The rates of adsorption of some samples are shown in Figure 5.14. These samples are compared against the powder micron and nano samples. Surprisingly, the powder samples gave lower rates of adsorption when compared to the laminate structures. This could be attributed to the fact that the laminate structures are more open and all the zeolite is very easily accessible when compared to the bulk powder samples. Also, the amount of ceramic weight to zeolite weight ratio plays a part in the kinetics measurement. Without accounting

for the amount of zeolite or the presence of nano zeolite, all the laminate structures show faster adsorption rate when compared to powder samples or beads. But, accounting for the presence of nano zeolite and the amount of zeolite in the structure gives rise to Figure 5.15. Normalising for presence of nano zeolite was done by adjusting for the difference in the amount of CO_2 adsorbed for the nano zeolite powder and the micron zeolite powder due to amorphous material in the nano zeolite powder and normalising for the weight of zeolite is done by adjusting for the wt% of zeolite in the structure. Here the presence of nano zeolite gives rise to *k* values larger than the powder samples and having micron zeolite give rise to kinetics less than powder samples, to show clearly that the size of the zeolite particles affects the kinetics of adsorption when present in the laminate structure. It was expected that the silica concentration would also affect the kinetics. In the SEM images observed in Section 4.2.2, it was shown that having more silica creates a denser structure and so it was anticipated that it might take longer to reach the zeolite particles but there was no real difference between the samples that had 20wt% silica and 40wt% silica as shown in Figure 5.16.

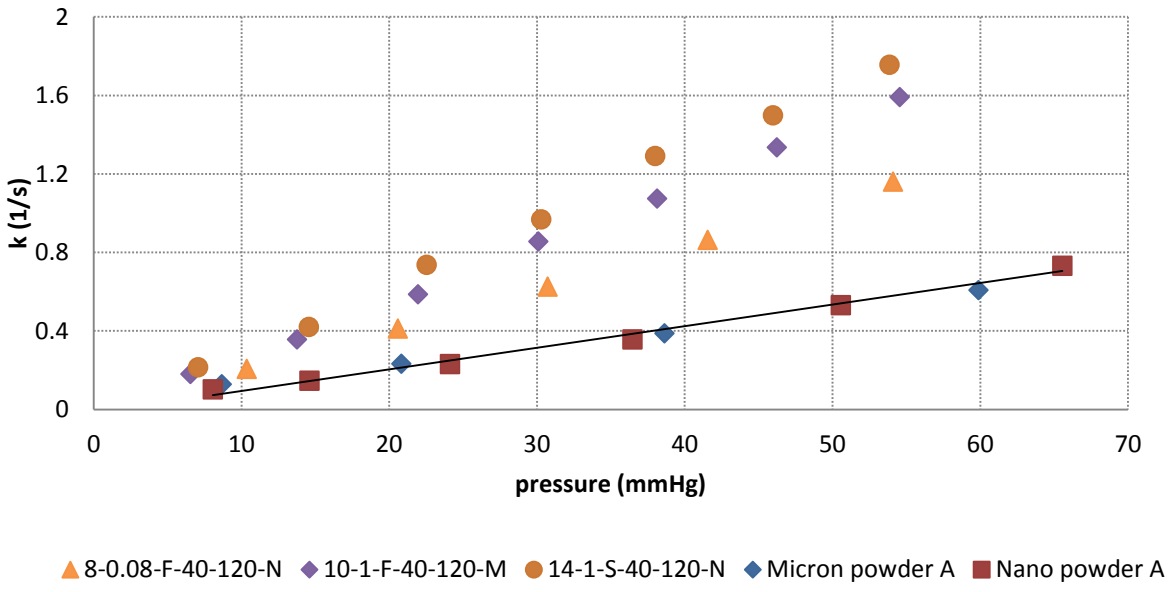

Figure 5.14: *k* values for some laminate samples compared against micron and nano powder samples

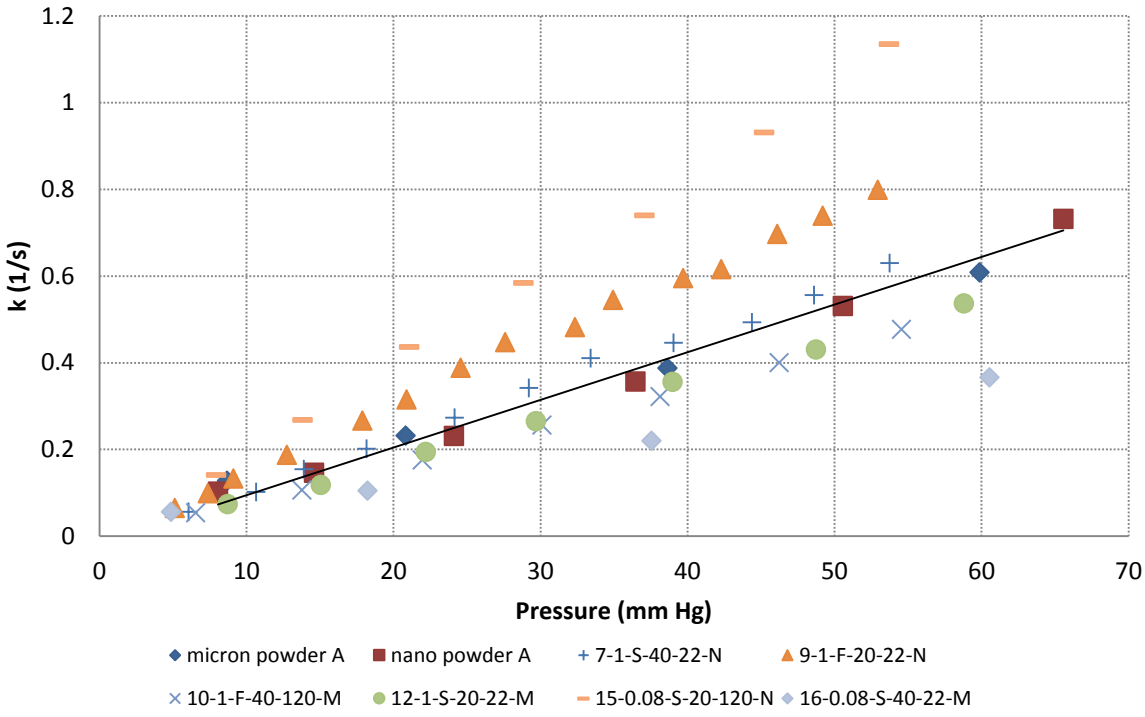

Figure 5.15: Adjusted *k* values for samples that contain nano and micron zeolite in the laminate structures compared against micron and nano powder samples

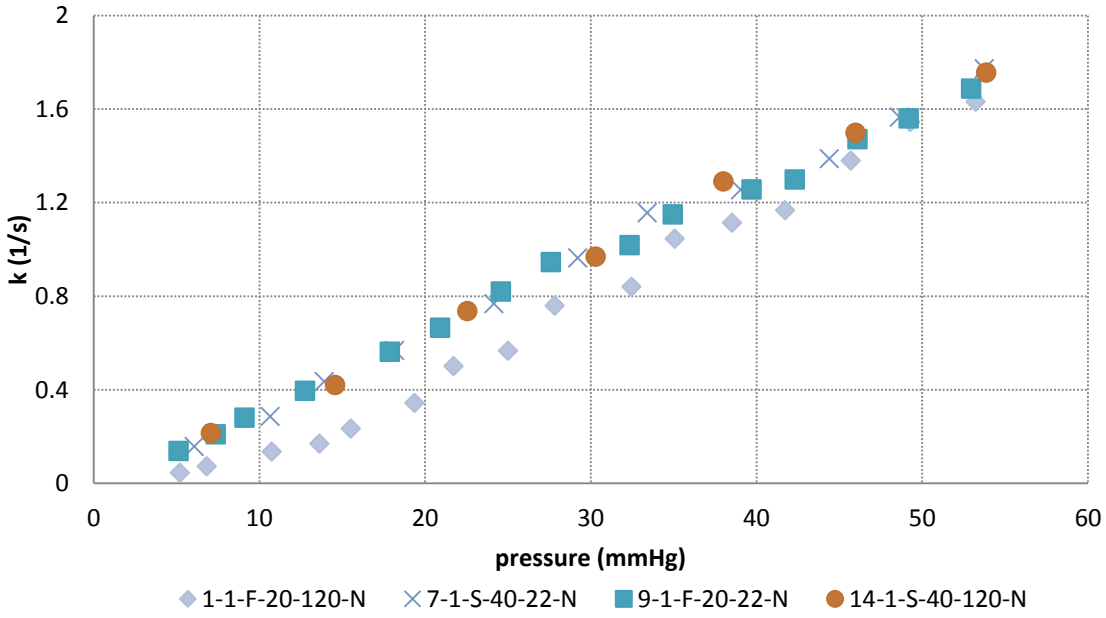

Figure 5.16: *k* values for laminate samples comparing the amount of silica present in the samples

For statistical analysis, the *k* values at 30mm Hg were chosen and the analysis was performed to assess the *p* value which assesses the statistical significance of the variables. The *k* values obtained initially were used without normalising for the amount of zeolite in the laminate structure. The mean values for the rate constants are shown in Table 5.2. As seen from this table, the ceramic weight to zeolite weight ratio and the zeolite particle size play a significant role in the kinetics. These values are highlighted in bold. Accounting for the amount of zeolite, only the zeolite particle size has any significance in kinetic measurements as shown in Table 5.3.

Table 5.2: Mean values of rate constant *k* at 30mm Hg

Variables	Factors	*k* values
Ceramic fibre weight: zeolite weight	0.08:1	**0.488**
	1: 1	**0.818**
Heating rate	Fast	0.613
	slow	0.693
Silica concentration	20	0.639
	40	0.667
Silica Particle size	22	0.644
	120	0.662
Zeolite particle size	micron	**0.498**
	nano	**0.808**
Pulp Type	Kraft	0.618
	TMP	0.688

Table 5.3: Mean values of adjusted rate constant *k* at 30mm Hg

Variables	Factors	*k* values
Ceramic fibre weight: zeolite weight	0.08:1	0.353
	1: 1	0.316
Heating rate	Fast	0.305
	slow	0.364
Silica concentration	20	0.375
	40	0.294
Silica Particle size	22	0.340
	120	0.330
Zeolite particle size	micron	**0.215**
	nano	**0.454**
Pulp Type	Kraft	0.316
	TMP	0.353

5.6 Conclusion

Novel characterisation techniques have been used to understand which variables play a significant role in strength and kinetics of the laminate structures. The laminate structures have different properties when compared to paper materials and other polycrystalline materials and hence required a new method for strength measurement using vibratory sieving. It can be quite clearly seen that for structures with micron zeolite, having more of either the reinforcement agent or the sintering agent creates laminate structures with enough strength for use in breakthrough measurement. This means that micron zeolite laminate structures with between 40-55wt% zeolite can be made. For the nano zeolite laminate structures, a large amount of both the reinforcement agent and the sintering agent have to be used to create structures with adequate strength. Hence only structures with 30wt% nano zeolite can be made for breakthrough testing. Comparing the kinetics of the different laminate structure, having nano zeolite in the laminate structures is shown to improve the rate of adsorption of

the laminate structures. On the whole, the laminate structures have better adsorption rates when compared to the beads or powder forms of the zeolite and this property will show marked improvement with mass transfer rates during breakthrough operation.

Chapter 6

Synthesis-Characteristics Relationships

This page is intentionally blank

6.0 Synthesis – Characteristics Relationship

6.1 Introduction

Chapters 4.0 and 5.0 deal with the characterisation of zeolite laminate structures created using the compositions listed in Table 3.1. The porosity, strength, zeolite loading and kinetics of the structures have been established and the variables that play an important role in significantly improving or diminishing these characteristics have been statistically determined. This chapter deals with the synthesis- characteristics relationship of the zeolite laminate structures. In order for the structure to be useful for carbon dioxide adsorption, the structure is expected to have high loading, high mass transfer kinetics, high strength and high porosity. The results discussed in the Chapters 4 and 5 show that improving individual characteristics will not result in an overall optimal structure as certain variables that enhance particular characteristics work unfavourably for other characteristics. So the creation of a zeolite laminate structure will require optimisation of the various characteristics as shown in Figure 6.1. As mentioned in Section 5.1, cost and separation performance have been dealt with by choosing papermaking techniques and zeolites respectively. Pressure drop and dispersion characteristics will be dealt with in Chapter 7 and further improvements to these characteristics will be considered in Chapter 8. Hence a clearer picture will emerge by bringing together all the results from characterisation and determining which synthesis variables are the most important in the manufacture of zeolite laminate structures and how these variables can be manipulated in obtaining an optimal zeolite laminate sheet structure.

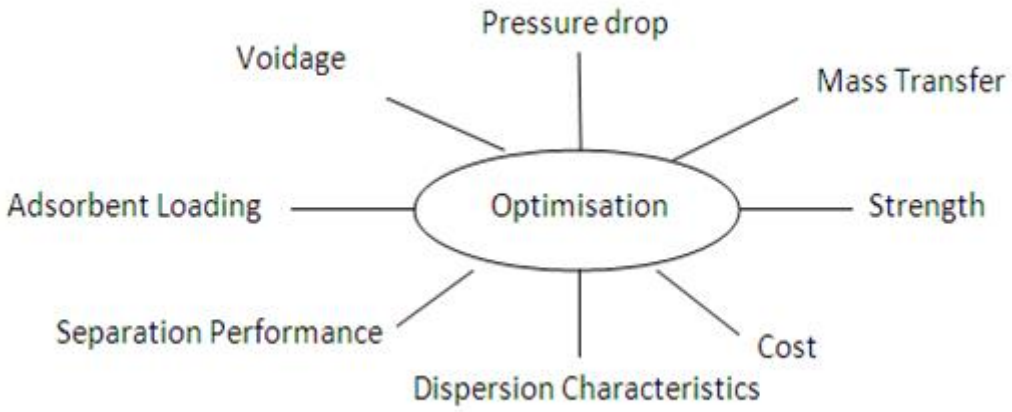

Figure 6.1: Trade-off between different characteristics of structured adsorbents

6.2 Results from Characterisation Experiments

The mean values from all the characterisation experiments done so far are shown in Table 6.1. The mean values of the variables that have any statistical significance are shown in bold. In the following sections, the statistical significance of the important variables for the characteristics determined is considered more in detail.

Table 6.1: Mean values for porosity, strength, kinetics and loading for the high and low factors for the six different variables with the bold values showing statistically significant variables

Variables	Factors	4-50nm	50-500nm	500-5000nm	>5000nm	cumulative	a	c	k (1/s)	Zeolite Loading
Ceramic fibre:	0.08:1	**0.171**	0.11	0.138	**0.732**	1.151	**-59.62**	-0.222	**0.488**	**0.645**
zeolite weight	1: 1	**0.149**	0.078	0.109	**0.953**	1.288	**-25.212**	-0.084	**0.818**	**0.35**
	Fast	**0.152**	0.088	0.121	0.878	1.237	-47.35	-0.146	0.613	0.498
Heating rate	slow	**0.168**	0.1	0.126	0.807	1.202	-37.481	-0.16	0.693	0.497
Silica	20	**0.14**	0.118	**0.156**	**1.118**	**1.532**	**-57.868**	**-0.261**	0.639	**0.57**
concentration	40	**0.179**	0.07	**0.091**	**0.567**	**0.907**	**-26.964**	**-0.046**	0.667	**0.425**
Silica Particle	22	**0.168**	0.076	0.124	0.763	1.13	-43.069	-0.142	0.644	0.498
size	120	**0.152**	0.112	0.123	0.922	1.309	-41.763	-0.164	0.662	0.497
Zeolite particle	micron	**0.135**	**0.033**	**0.16**	0.832	1.16	**-26.888**	-0.105	**0.498**	0.497
size	nano	**0.184**	**0.155**	**0.086**	0.853	1.279	**-57.944**	-0.201	**0.808**	0.498
	Kraft	0.158	0.089	0.116	0.913	1.275	-37.455	-0.172	0.618	0.497
Pulp Type	TMP	0.162	0.099	0.131	0.772	1.164	-47.376	-0.134	0.688	0.498
				Pore volume ml/g			Strength		Kinetics	Adsorbent Loading

The critical variables are given in bold in Table 6.1, as determined by *p*-value testing. These are initial silica concentration, ceramic: zeolite weight and zeolite particle size. The less important variables are heating rate, silica particle size and pulp type. Initially the important variables are discussed followed by the less significant variables.

6.2.1 Critical Variables

Most of the optimisation of the different characteristics can be completed by choosing either the high or the low factors of these critical variables. The best factors for these variables are discussed in the Section 6.2.1.1 to Section 6.2.1.3.

6.2.1.1 Initial Silica Concentration

Initial silica concentration is one of the most important variables which has an effect on almost all characteristics except the rate constant and the porosity in the size range between 50-500nm. High porosity, strong structures and high loading can be achieved by varying silica concentration. The samples with 20wt% silica have higher porosity for all pore sizes above 500nm and also have higher zeolite loading. Having 40wt% silica gives greater porosity in the mesoporous range and increases the overall strength of the structure as these structures have low degradation rate and less loss of material. Again choosing the low or high factor of this variable has to be done in combination with other variables to give a more optimal structure. Since the samples with 20wt% silica have higher porosity in the 5000-50,000nm range, these samples are expected to have lower pressure drop in breakthrough tests and this is discussed in Section 7.3.2.

6.2.1.2 Ratio of Ceramic fibre weight to zeolite weight

The ratio of ceramic fibre weight to zeolite weight is responsible for mesoporosity, the porosity between 5000-50,000nm, the final weight reached in strength measurements, the rate constant for kinetic measurements and it also affects the amount of zeolite in the laminate structure. The positive aspect of having a low ratio of ceramic fibre weight to zeolite weight

is that there are more pores in the mesoporous range and a high zeolite loading but this is detrimental in the porous range between 5000-50,000nm, strength and kinetic measurement. Strength will increase as the ratio of ceramic fibre weight to zeolite weight increases. It is also expected that having more pores in the range between 5000-50,000nm would be useful for lowering the pressure drop, which is tested in Section 7.3.2. Since the low and high factors of this variable have both disadvantages and advantages for different areas in the characterisation techniques, choosing which factor to use will depend more collectively on the other variables.

6.2.1.3 Zeolite Particle Size

Zeolite particle size is very important below 5000nm size range and for strength and rate constant measurements. Using nano zeolite particles increases the porosity below 500nm due to the pores created by the arrangement of these particles and their interaction with silica and also increases the rate constant kinetics while using micron zeolite increases porosity in the 500-5000nm range and also increases the strength of the structure as there is not much loss in the final weight of the structure. But nonetheless, the overall kinetics of the structure is improved no matter which zeolite particles are used when compared to beads or even the powder forms, as the laminate structure exposes the zeolite particles to gas flow. Although Table 6.1 shows no significant differences in adsorptive capacity caused by the use of different zeolite particle sizes, the structures with nano zeolite had amorphous material which means that their CO_2 adsorptive capacity is reduced when compared to the structures with micron zeolite. The nano zeolite particles are also obtained via a more complicated synthesis route as opposed to the micron zeolite particles which are available off the shelf, which makes the nano zeolite particles a much higher cost option than the micron zeolite particles. Again there are both positive and negative effects on different characteristics by the use of the high and low factors of this variable. Hence the choice of the high or low factor must be made in accordance with the other variables being selected and the availability of the zeolite particle size.

6.2.2 Less important Variables

Heating rate, silica particle size and pulp type are the secondary variables as they either have no significance or limited significance in any of the statistical tests. Hence the choice of the high or low factor is based mostly on convenience.

6.2.2.1 Heating rate

Heating rate has no effect on any other variable except porosity and only in the mesoporous range. This effect is also only an interaction effect with the 20wt% silica having fewer pores after fast heating than with slow heating. Choosing slow or fast heating rate therefore depends completely on the time and energy input available during the preparation process of the laminate structure. Hence it will be easier to use the fast heating method for the preparation of the zeolite laminate structure.

6.2.2.2 Silica Particle Size

With silica particle size, using 22nm silica gives more pores in the mesoporous range than 120nm silica. Since there is not much difference in using either of the silica, any silica particle size can be used but the 22nm silica has a more uniform particle size, hence it is suggested that this silica be used.

6.2.2.3 Pulp Type

The pulp type has no effect on any of the characteristics and this loss of sensitivity might be due to the very similar dimensions of the pulp fibres. Hence more work has to be done with different fibre dimensions as varying fibre dimensions creates pores of different dimensions as shown in Figure 4.20. But with the current pulps of kraft or TMP fibres used in the partial factorial design, any pulp type might be used.

6.2.3 Optimisation of the structure

With the discussion of all the variables, it becomes necessary to trade off the effect of the variables to arrive at an optimum structure. The heating rate, silica particle size and pulp type have no major effect on the laminate structures created, hence any of their low or high factors can be used for laminate structure preparation. For the other three variables, which are the ratio of ceramic fibre weight to zeolite weight, initial silica concentration and zeolite particle size, each factor will have both positive and negative effects on the final properties. These positive and negative effects are given in Table 6.2. Hence it is necessary to determine what is required of the structure being created.

Table 6.2: Pros and Cons of using the high and low factors of the critical variables

Variable	Factor	Reduces	Increases
Initial Silica Concentration	20wt% silica	-Pores in the mesoporous range -Overall strength	- Pores above 500nm - Zeolite Loading
	40wt% silica	-Pores above 500nm - Zeolite loading	-Pores in the mesoporous range -Overall strength
Ceramic weight : Zeolite weight ratio	0.08:1	-Pores between 5000-50,000nm -Final weight reached in strength -Rate of adsorption	-Pores in the mesoporous range -Zeolite Loading
	1:1	-Pores in the mesoporous range -Zeolite Loading	-Pores between 5000-50,000nm -Final weight reached in strength -Rate of adsorption
Zeolite Particle Size	Micron sized zeolite	-Pores between 4-500nm -Rate of adsorption -Cost of preparation	-Pores between 500-5000nm - Final weight reached in strength -Zeolite Loading
	Nano sized zeolite	-Pores between 500-5000nm - Final weight reached in strength -Zeolite Loading	-Pores between 4-500nm -rate of adsorption -Cost of preparation

The structure being created is required to have adsorbent loading better than current non-particulate structures and have lower pressure drop and high mass transfer rate when compared to commercial adsorbents such as beads, while retaining sufficient strength to avoid disintegration.

Current non-particulate structures have a zeolite loading less than 37wt% of zeolite in the final structure*[71, 119]* and the laminate structures from the partial factorial design having a loading of 40wt% and higher will therefore be more effective when compared to the other non-particulate structures. All the laminate structures still have a lower loading when compared to beads as the highest loading the laminate structures have is 74wt% zeolite as opposed to 85wt% zeolite for the beads. So in terms of loading, structures with 40wt% zeolite i.e. structures having 1:1 ratio of ceramic fibres to zeolite weight and 20wt% silica and structures with 55wt% zeolite i.e. structures having 0.08:1 ratio of ceramic fibres to zeolite weight and 40wt% silica can be used for breakthrough testing. In terms of strength, these structures with 40-55wt% zeolite will have adequate strength and can be breakthrough tested for the micron zeolite samples but not for the nano zeolite samples. To test the nano zeolite samples, structures having 30wt% nano zeolite have to be used as structures with higher zeolite content will have serious dusting issues. Also the structures with nano zeolite are less cost effective which make these samples less useful for breakthrough testing. Hence the structures that will be used for breakthrough testing are micron zeolite laminate samples that have either 0.08:1 ceramic to zeolite weight ratio and 40wt% silica or 1:1 ceramic to zeolite weight ratio and 20wt% silica. This way the positive and negative factors of both these variables i.e is the ceramic weight to zeolite weight ratio and initial silica concentration can be observed for breakthrough testing and no matter which of these structures are chosen for future work, they will have a higher loading when compared to other non particulate structures.

Chapter 7

Performance of Laminate Structures

This page is intentionally blank

7.0 Performance of Laminate Structures

7.1 Introduction

Zeolite powder if placed directly in a packed bed reactor for adsorbent purposes will result in a very large pressure drop and have fluidization issues. Hence, the zeolite powder is made into beads or pellets to be used for industrial applications. These structures still result in high pressure drop and depending on the size of the beads, they might have fluidisation issues. If the beads are large, they have low pressure drop but increased mass and heat transfer resistance due to the long transfer paths along the radius of the beads which results in lowering the performance of the adsorption process*[71]*. This is discussed in Section 2.6. Hence, there is a need to create alternate structures which have better performance than beads. These alternate structures like monoliths, foam, laminate and fabric structures have their own pros and cons when compared to the beads. The main drawback of these structures is that the zeolite loading when compared to beads is very low.

The laminate structures created using papermaking techniques have higher loading than other non-particulate structures and are expected to have better breakthrough performance than beads in terms of pressure drop and mass transfer characteristics because of the shorter path length for mass and heat transfer. The challenges of the laminate structures for breakthrough testing are to pack the structure in an appropriate manner to reduce the risk of channelling through the structure. The geometrical shape the laminate structure is packed in also plays an important role in gaining a superior structure to a packed bed of beads.

The largest single sheet, allowing for trimming of the edges, that can be made using the Moving Belt Sheet former is a 20cm x 20cm square sheet. Hence this size was used for the preparation of a laminate structure for breakthrough testing. The optimised results from the partial factorial design discussed in Section 6.2.3 were used to select the composition of the

sheets and the breakthrough properties of the sheets were measured and compared with commercial beads. Other forms of deliberate spacing were introduced to the sheet structures and compared to the structures without spacing. Spacing helps aid the gas flow through the structure by providing better transport paths to active sites, thereby reducing pressure drop.

The breakthrough testing for the laminate structures prepared using papermaking techniques was undertaken with carbon capture technology in mind and for this reason CO_2/N_2 mixtures were tested. Flue gas mixtures contain between 5-20% CO_2 in a gas mixture. Here, a dry gas mixture of 15% CO_2 in N_2 was used to test the performance of the laminate structures.

In addition to the CO_2 breakthrough data, pressure drop data was also measured. During a breakthrough experiment, the mixture is fed to the adsorbent bed and the CO_2 is adsorbed from the inlet gas by the adsorbent. The time for breakthrough and the shape of the breakthrough curve are important characteristics for determining the operation of an adsorption column*[120]*. The Mass Transfer Zone (MTZ) is the portion of the bed of adsorbent where the adsorbate is being adsorbed. The MTZ moves from inlet towards the outlet as the adsorbent at the inlet becomes saturated*[120]*. Figure 7.1*[120]* shows the movement of the MTZ in an adsorbent bed and the resulting breakthrough curve. The breakthrough curve shows the shape of the MTZ in the time domain at the exit of the bed. A numerical simulation of the breakthrough was also performed to infer the effective diffusivity of the adsorption column for the beads and the laminate structures. The numerical simulation method is discussed in Section 7.2.4.

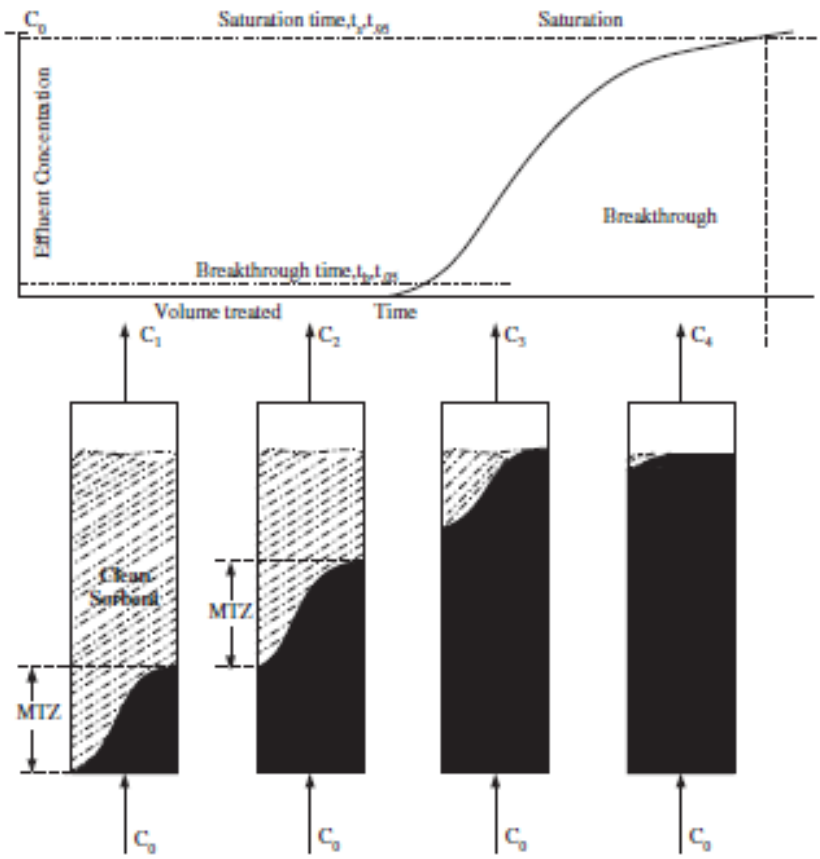

Figure 7.1: Movement of mass transfer zone and the resulting breakthrough curve*[120]*

7.2 Structure and Equipment for Breakthrough testing

This section describes how the laminate structure created using papermaking methods was prepared for breakthrough testing and the equipment and methodology used for testing purposes.

7.2.1 Structure Preparation

The laminate structure formation procedure is as given in Section 3.3. The sheets for the partial factorial design in Table 3.1 were prepared from zeolite NaA. For breakthrough testing purposes, the sheets were prepared using micron zeolite NaX. Zeolite NaX has been found to be most suitable for CO_2 capture due to its high working capacity, low purge requirement and equilibrium selectivity*[70]*. Zeolite NaX was not used for sheet preparation

of the partial factorial design because the design in Table 3.1 required nano zeolite structures which were very difficult to form with zeolite 13X. From Section 6.2.7, structures with 40wt% or 55wt% zeolite loading were selected for breakthrough testing. These structures are expected to give good loading of zeolite when compared to other non-particulate structures. Although the loading in these structures is lower than beads, the overall performance of these structures needs to be tested against beads to give a comparative assessment. Structures having 40wt% zeolite loading have 1:1 ratio of ceramic fibres to zeolite weight and 20wt% silica in them and have more porosity when compared to structures with 55wt% zeolite loading which has 0.08:1 ratio of ceramic fibres to zeolite weight and 40wt% silica. The sheets prepared from the MBSF are cut exactly to a size of 20cm x 20cm.

Once the sheets were dry, they were coated with silica as discussed in Section 3.5.2. The wet sheet was then wrapped around a hollow capped steel rod of length 19cm and diameter 1 cm. The rod is shorter when compared to the length of the sheet because if the rod was too long, it could block the gas flow into the adsorbent structure. The sheet was tightly wrapped around the rod and then fired at 650°C according to the fast heating procedure described in Section 3.5.5, so the structure was preserved. Figure 7.2 shows an image of a rolled laminate structure before and after firing. After the oven was switched off and the oven cooled to below 200°C, the rolled laminate structure was carefully removed from the furnace.

Depending on the thickness of these structures, the diameters of the laminate structures can vary widely. Hence a single diameter tube could not be made for breakthrough testing. In consideration of these different diameters and to have a close fit to prevent channelling of gas between the sides of the tube and the structure, a heat shrink tube was used to wrap around the outside of the laminate structure. A heat gun was used to shrink the heat shrink tube to fit it to the outer shape of the laminate structure. In order to complete the structure and fit the column to the testing equipment, two fittings (CF connector female Gyrolok 316 6.3mm OD x 15NPT) were used on either side of the adsorption column. The fittings had the inner thread removed and were smoothed until the inner diameter was 2.1 cm. The fitting was attached to

the heat shrink tube using a silicone sealant. The silicone sealant was allowed to dry for at least 24 hours before handling. The adsorption column (Figure 7.3) was then attached to the breakthrough testing equipment. The final dimensions of the laminate structure was 20cm in length and the outer diameter of the heat shrink tube was between 1.9cm and 2.1cm

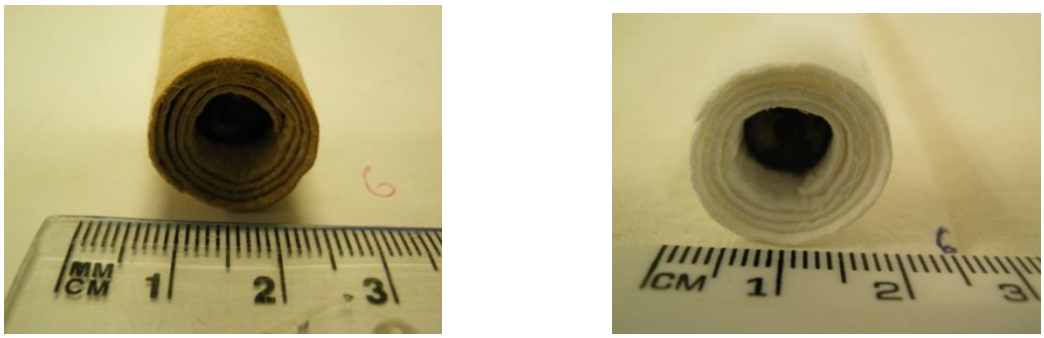

A B

Figure 7.2: A) Laminate structure prepared for adsorption before firing B) Laminate structure prepared for adsorption after firing.

Figure 7.3: Adsorbent column for breakthrough testing

To achieve variable spacing for gas flow through the structure, several alternate configurations were produced. In one configuration, the sheet was pressed using a metal plate (welded with 304 mesh stainless steel), to create parallel channels running in the structure, directly following the coating of the sheet with silica. The welded mesh has wires in two

layers with one layer having wires running in the vertical direction and the other layer having wires running in the horizontal direction. Hence pressing with the laminate sheets with the welded mesh only creates channels running in one direction. Since the spacing is large, it was pressed two or three times to create equal spacing in the structure. The wires of the mesh were spaced 2.5cm apart, as shown in Figure 7.4a. Hence the mesh was indented on the silica coated sheet either two times, creating spaces 1.25cm apart (Figure 7.4b), or three times creating a channel spacing of 0.83cm (Figure 7.4c).

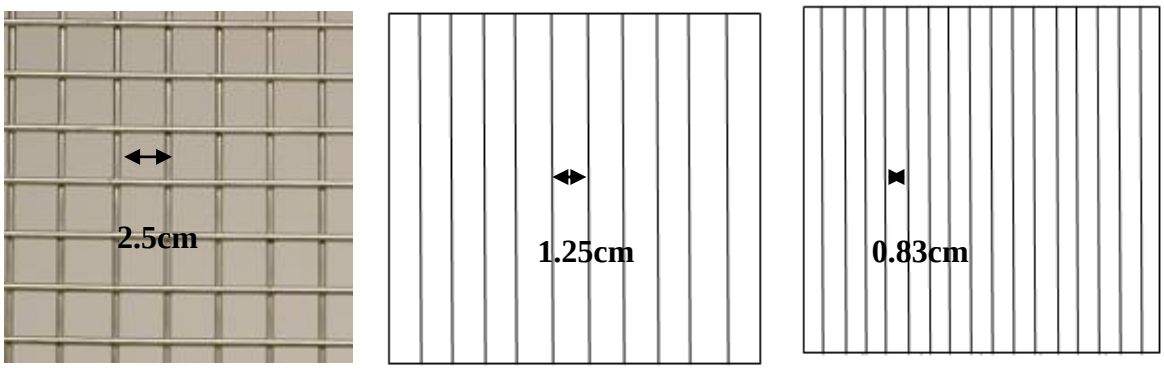

Figure 7.4: a) Image of wire mesh showing spacing at 2.5cm b) Diagram of indenting wire mesh two times on the sheet showing spacing of 1.25cm and c) Diagram of indenting wire mesh three times on the sheet showing spacing of 0.83cm

An additional configuration to create channels was to wrap the structure with a woven stainless steel mesh of thickness 100µm to create flow through the structure. The method by which this structure was created is shown in Figure 7.5 and the laminate structures before and after firing are shown in Figure 7.6. These structures create spacing between sheets in the range of 0.12-0.16mm.

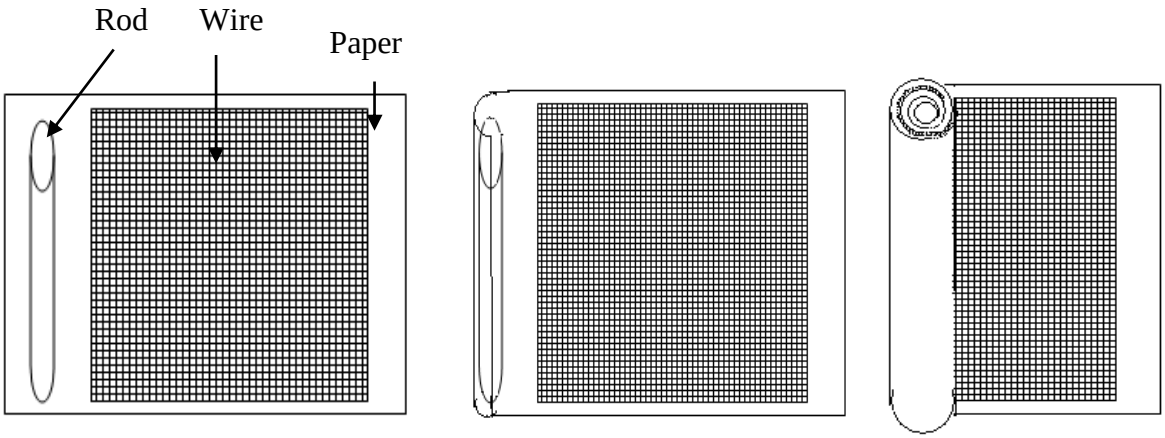

Figure 7.5: Method of creating laminate structure with spacing using wire mesh

A B

Figure 7.6: A) Laminate Structure with wire before firing B) Laminate Structure with wire after firing

Table 7.1 shows all the laminate samples that were prepared for breakthrough testing.The flow rate used to test the samples was 250ml/min unless otherwise stated.

Table 7.1: The preparation conditions of the samples used for breakthrough testing.

No	Amount of 13 X (g)	Amount of ceramic fibres (g)	Amount of silica (wt%)	Conditions
1	18.5	1.5	40	no spacing
2	18.5	1.5	40	no spacing
3	10	10	20	no spacing
4	10	10	20	no spacing
5	10	10	20	no spacing
6	18.5	1.5	40	parallel lines, 1.25 cm spacing
7	18.5	1.5	40	parallel lines, 0.83 cm spacing
8	18.5	1.5	40	wire
9	18.5	1.5	40	wire
10	10	10	20	wire
11	10	10	20	wire

7.2.2 Beads

The beads used for comparison against the laminate structures are APG III beads obtained from UOP containing zeolite 13X. The beads are 2mm in diameter. These beads were packed in a stainless steel column of height 7.5cm and inner diameter 2.24cm. When packed in the column, the beads weighed 18.5g.

7.2.3 Testing Equipment

The schematic of the testing apparatus is shown in Figure 7.7. The pressure regulator, needle valve, rotameter and buffer tank are all present to ensure stable flow and pressure inside the system. The adsorbent column prepared, as described in Sections 7.2.1 or 7.2.2, was initially

purged using pure N_2 gas to remove any contaminants from the structure. A gas stream containing 15% CO_2 and 85% N_2 was fed to the adsorbent column at 1.05bar and room temperature. The CO_2 concentration at the exit was measured using a CO_2 analyser (Servomex 1440) and the experiment was run using Advantech GeniDaq software. During industrial operation, the flow would be stopped or diverted when CO_2 concentration was detected at the exit of the column but for breakthrough testing, the experiment was conducted until saturation was reached, which is when the CO_2 concentration at the exit of the column reached the same CO_2 concentration as the inlet of the column. The exit concentration from the CO_2 analyser as a function of time gives the breakthrough data. The pressure drop between the inlet and the exit of the breakthrough column was also measured using pure N_2 gas at different flow rates for the sample.

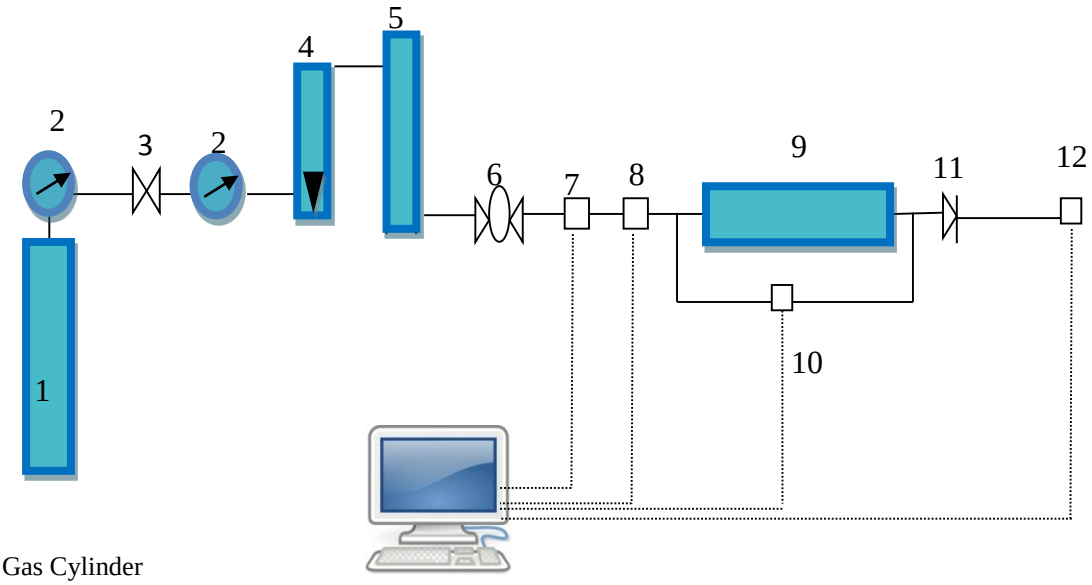

1 Gas Cylinder
2 Pressure Regulator
3 Needle Valve
4 Rotameter
5 Buffer Tank
6 Ball Valve
7 Pressure Transducer
8 Mass Flow Meter
9 Adsorption Column
10 Pressure Drop
11 Check Valve
12 CO_2 Analyser
13 Computer

Figure 7.7: Layout of Breakthrough testing apparatus

7.2.4 Numerical Breakthrough simulation

For the numerical breakthrough simulation, adsorption isotherms were obtained according to the method described in Section 4.3 using a Micromeritics ASAP 2010. Isotherms of pure CO_2 and N_2 were measured at temperatures of 0°C, 20°C and 40°C. The dual site Langmuir model was fitted to the isotherms according to the equation

$$n_i = \frac{m_{1i} b_i P_i}{1+b_i P_i} + \frac{m_{2i} d_i P_i}{1+d_i P_i} \quad [7.1]$$

And

$$b_i = b_{0i} \exp(-\frac{Q_{1i}}{RT}) \quad ; \quad d_i = d_{0i} \exp(-\frac{Q_{2i}}{RT}) \quad [7.2]$$

Where n_i is the amount of component i adsorbed (mol/kg); m_{1i}, m_{2i} are the maximum amount adsorbed of component i (mol/kg), P is the gas pressure (kPa), b_i and d_i are adsorption constants (1/kPa), T is the temperature (K), R is ideal gas constant and Q is the heat of adsorption (J kmol). These parameters are listed in Appendix II for the different samples in Table 7.1.

The adsorption characteristics of binary gases in an adsorbent column with either laminar structures or beads was analysed and estimated using numerical breakthrough simulation. The assumptions made during this simulation were that the feed gas was ideal i.e the temperature and pressure of the gas are close to ideal conditions, that there was no axial dispersion, the pressure at the exit of the bed was constant during the entire experiment, and the mass transfer can be modelled using the linear driving force model.

The laminate structures were modelled assuming a rectangular shape and then mapped into a series of cylindrical shapes, used for the current laminate structures. Hence adjustments have to be made when entering the data, as width and number of sheets in the column are required which is obtained from the inner and outer diameter of the circular laminate structures and

the total mass of the laminate structure. The width is calculated as shown in Figure 7.8, where the average circumference around the cylinder is used to calculate the width of the rectangle. The thickness of each of the layers in the circular structure is the same as the thickness of the sheets in the rectangular setting and the number of layers is adjusted until the mass of the structure is equal to the measured mass of the structure. Also, it is difficult to obtain the spacing between the layers and this is obtained by calculating the pressure drop from the Hagen-Poiseuille equation by adjusting the spacing width until the pressure drop matches the experimentally observed values.

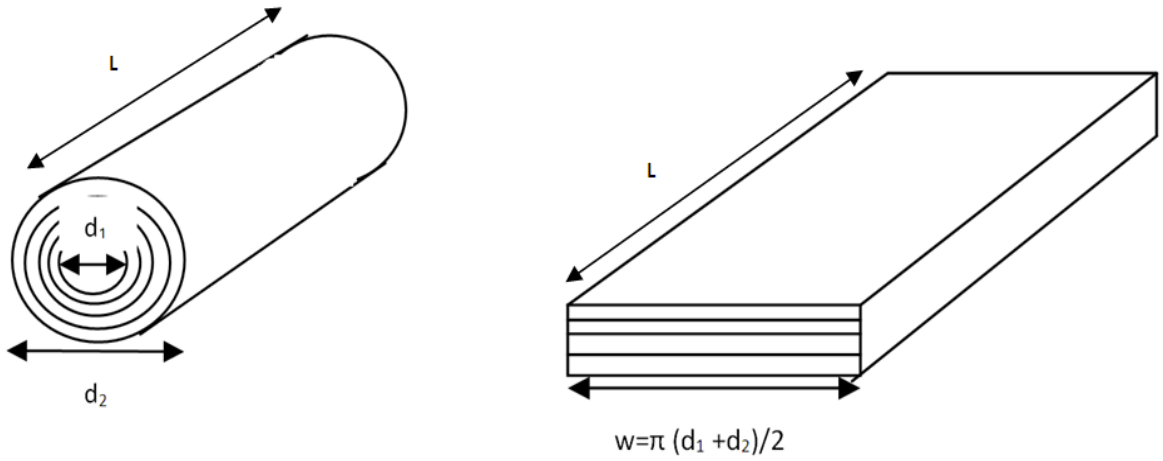

a b

Figure 7.8: Dimensions of actual "swiss roll" (a) used in modelling the rectangular simulated laminate structure (b)

The model is based on conservation of mass, energy, momentum and constitutive relationships for kinetics and equilibrium. The mass balance for an adsorbate in the gas phase irrespective of geometry can be described as follows:

$$\frac{\partial C_i}{\partial t} + \left(\frac{1-\epsilon_b}{\epsilon_b}\right)\rho_{ads}\frac{\partial n_i}{\partial t} = -\frac{\partial u C_i}{\partial z} \qquad [7.3]$$

where i represents the adsorbate component in the binary mixture, C_i is the concentration of component i (gmol/cm^3), t is time (s), ϵ_b is the bed voidage (does not include the voids in the adsorbent), z is the bed length (cm), ρ_{ads} is the adsorbent density (g/cm^3), n_i is the loading of component i in the adsorbent (gmol/kg) and u is the interstitial velocity (cm/s).

The energy balance equation assuming the adsorbent and gas phase are in local equilibrium is:

$$\rho_{bed} C_{ads} \frac{\partial T}{\partial t} - \rho_{bed} \sum_{i=1}^{2} q_i \frac{\partial n_i}{\partial t} - \rho_{bed} Q_{gen} = -C_{gas} \frac{\partial (uCT)}{\partial z} - \frac{4h_w}{D}(T - T_w) \quad [7.4]$$

where ρ_{bed} is the bed density (g/cm^3), T is the temperature (K), C is total gas concentration (gmole/cm^3), C_{ads} is the adsorbent heat capacity, C_{gas} is the gas heat capacity, h_w is the heat transfer coefficient from the bed to the wall and T_w is the wall temperature. The isosteric heats q_i are determined from the Clausius-Clapeyron equation applied to the adsorption isotherms.

The linear driving force model based on solid diffusion was used to determine the rate of adsorption

$$\frac{\partial n_i}{\partial t} = k_i (n_i^* - n_i) \quad [7.5]$$

For a packed bed: $k_i = \frac{15 D_{ei}}{R_p^2}$ [7.6]

where $R_p$is the average diameter of the beads and D_{ei} is the effective diffusivity parameter.

For a laminate structure: $k_i = D_{ei} * l$ [7.7]

The only unknown parameter is therefore effective diffusivity which is determined by fitting the simulated breakthrough curve to the experimental breakthrough data.

Pressure drop can be calculated using the Hagen-Poiseuille equation for laminate structures which is

$$\Delta P = \frac{12\mu UL}{\epsilon_b w^2} \quad [7.8]$$

where ΔP is the pressure drop in Pa, μ is the viscosity of the gas mixture in Pas, L is the bed length in cm, U is the interstitial velocity in (cm/s), w is the spacing between the sheets in cm and ϵ_b is the bed voidage.

Pressure drop for the beads was calculated by using the Ergun equation

$$\Delta P = \frac{150\mu\, v_0 L_b}{\Phi_b^2 D_p^2}\frac{(1-\epsilon)^2}{\epsilon^3} + \frac{1.75\,\rho v_0^2 L_b(1-\epsilon)}{\Phi_b D_p \epsilon^3} \quad [7.9]$$

Where ΔP is the pressure drop in Pa is, $L_b$is the packed bed length in cm, v_0 is the superficial velocity of the gas mixture in cm/s, ϵ is the bed void fraction, D_p is the average diameter of the beads in cm, ρ and μ is the density and viscosity of the gas mixture in g/cm^3 and Pas respectively and Φ_b is the sphericity of the beads.

The set of mass and energy balance equations was solved using the finite volume method to discretise the equations in the axial domain to produce a set of ordinary differential equations in the time domain. These equations were solved with the MATLAB integrator ode15s, a backward differentiation formula (BDF) also known as Gear's method, used for stiff sets of differential equations.

7.3 Results

The effective diffusivity and pressure drop of various laminate samples were collected by performing CO_2 breakthrough experiments. As mentioned in Section 7.2.3, all the runs for breakthrough testing were performed at 250mL/min, unless otherwise stated.

A representative set of experimental breakthrough data collected is shown for illustrative purposes in Figure 7.9 with the breakthrough gas concentration on the y-axis and the time taken to reach the breakthrough gas concentration on the x-axis. In this case the data is

provided for laminate structure number 3 in Table 7.1. A blank experiment was also performed and this was the breakthrough data collected for an empty tube instead of the adsorption column. The breakthrough curve for the blank run is very sharp and indicates all dispersion observed from the successive runs is due to mass transfer resistance and/or velocity distribution in the channels of the sample. This also justifies the plug-flow assumption. In order to correct the results for sample delay time, the results for the blank run are subtracted from the raw data of the sample run. Hence only the effect of adsorption created by the sample is shown.

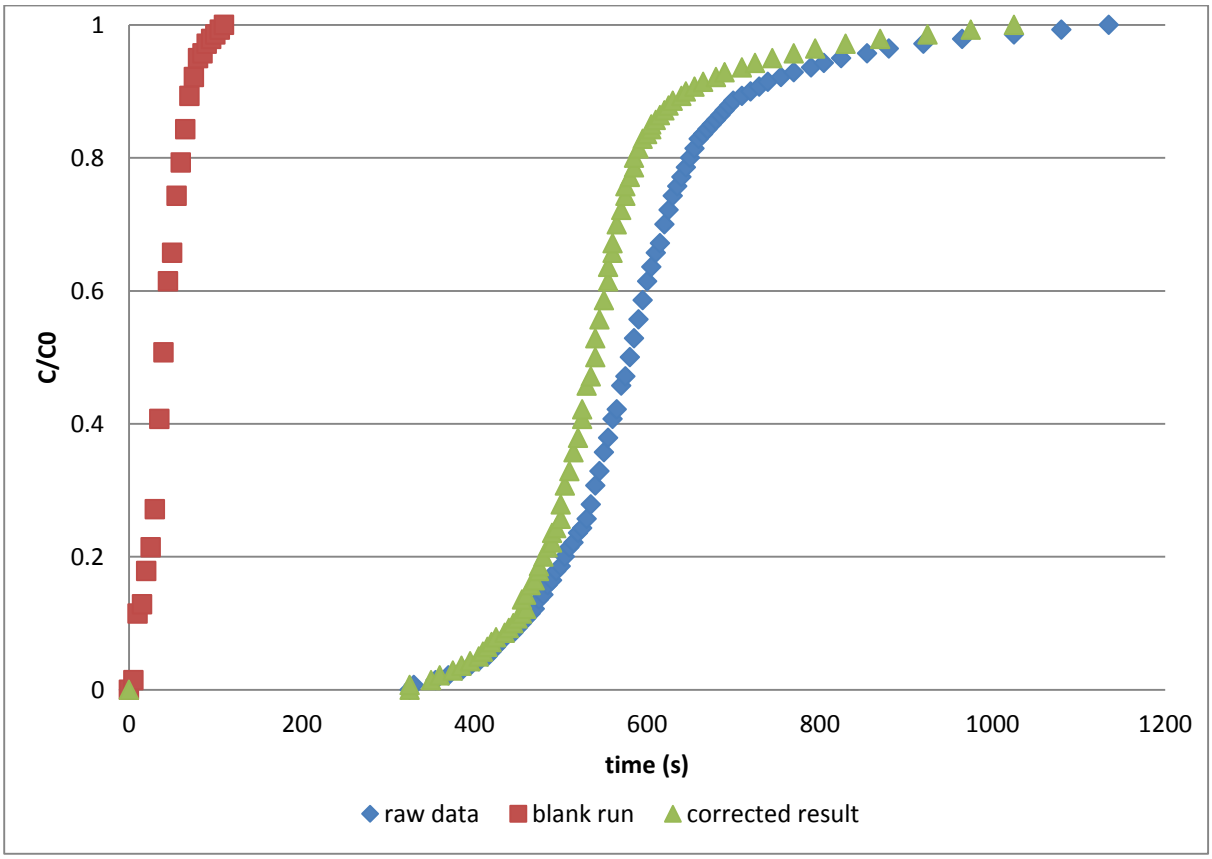

Figure 7.9: Breakthrough profiles of blank run with no sample and raw experimental data and the corrected data of laminate structure number 3 from Table 7.1

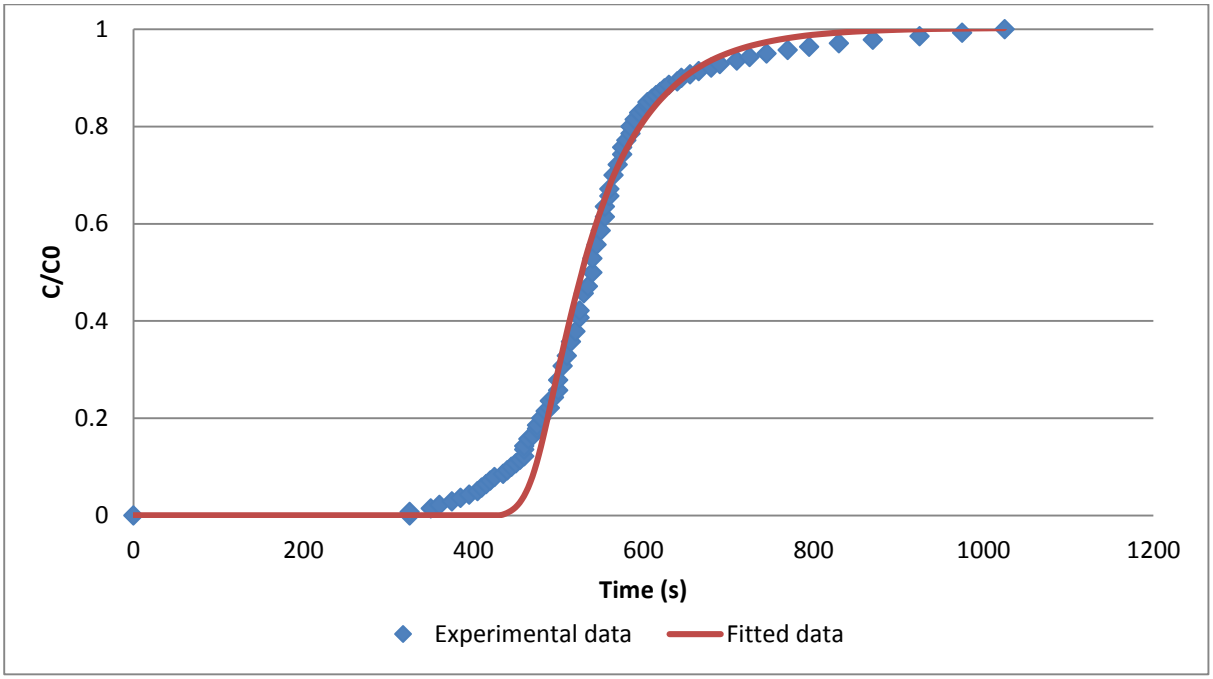

Figure 7.10: Comparison of the experimental (symbols) and simulated (solid) breakthrough profiles of laminate structure number 3 from Table 7.1

The corrected breakthrough profile obtained previously was then fitted to a simulated breakthrough curve using the numerical breakthrough simulation discussed in Section 7.2.4, by changing the effective diffusivity. The corrected experimental curve and the fitted curve are shown in Figure 7.10. The effective diffusivities for all the samples were obtained by fitting the simulated data to the experimental data shown in Appendix II. The sum of square errors was calculated between the experimental and simulated data and the effective diffusivity that gave the minimum sum of square errors was chosen as the effective diffusivity of the sample. The graph showing the sum of square errors against effective diffusivity for the sample from Figure 7.10 is shown in Figure 7.11. As shown in Figure 7.10, the initial section of the breakthrough curve does not match the fitted data. This is because, the channelling or dispersion within the structure has not been accounted for within the numerical simulation and this could cause the gas to exit more quickly. But, nonetheless, the breakthrough curve matches the simulated curve well and the effective diffusivity can be determined.

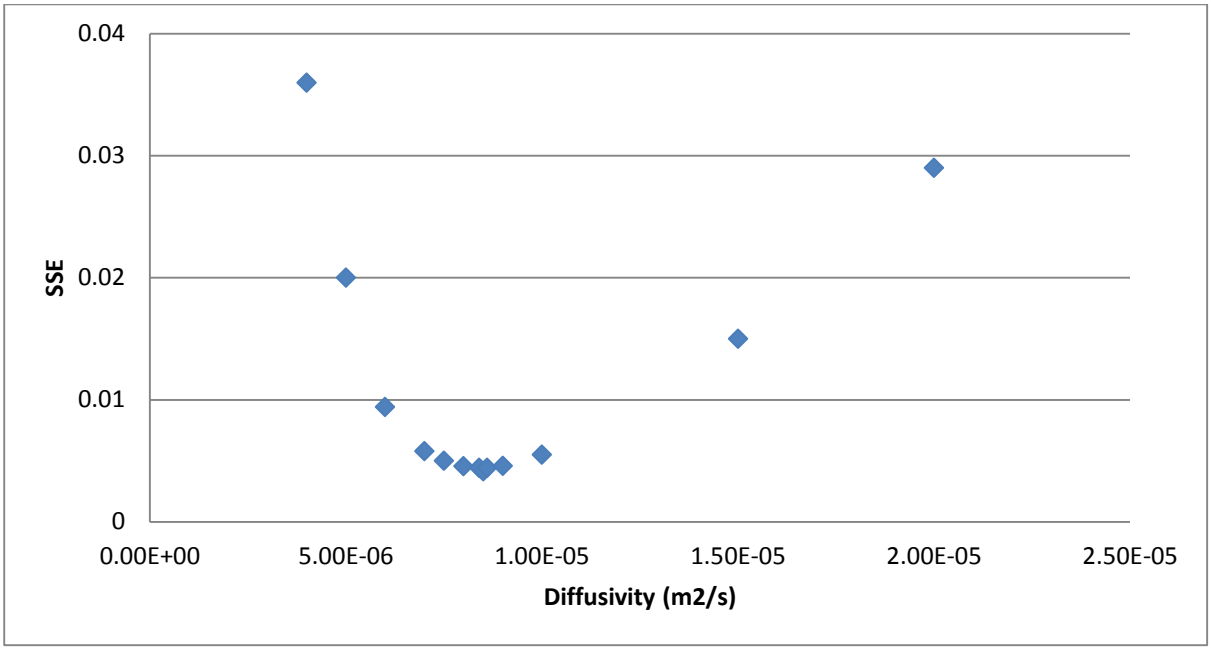

Figure 7.11: Sum of square errors against effective diffusivity for laminate structure number 3 from Table 7.1

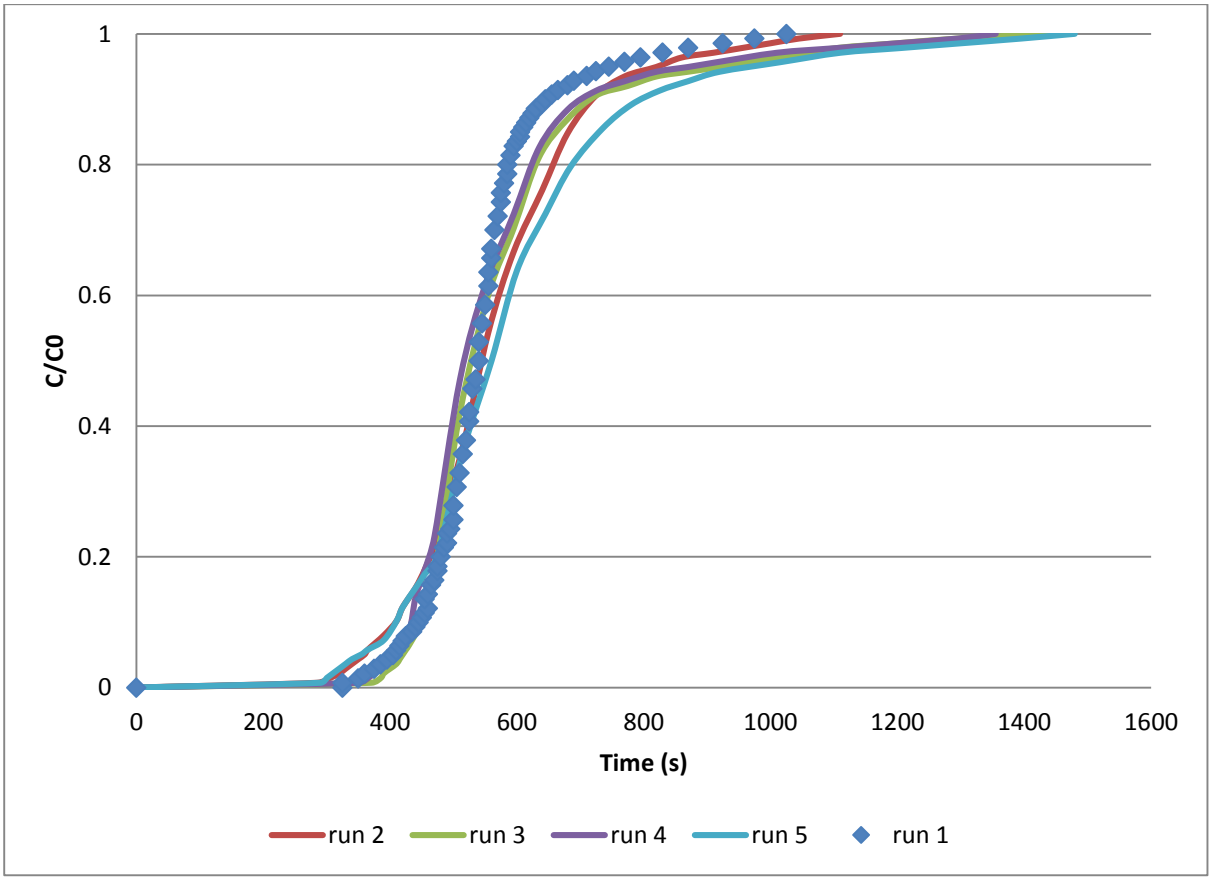

Figure 7.12: Breakthrough repeats of laminate structure number 3 from Table 7.1

Figure 7.12 shows the repeatability of the breakthrough runs using the laminate structures. In total, 5 breakthrough experiments were completed at the same flow rate of 250ml/min for the same laminate structure number 3. The first breakthrough experiment for run 1 is shown using dotted points while the breakthrough experiments after that are shown using solid lines. The effective diffusivity for all the breakthrough experiments are shown in Table 7.2. The first breakthrough experiment shows the highest effective diffusivity. The effective diffusivity decreases slightly after the first breakthrough experiment is performed. Hence, these results show good repeatability within the same sample. The average effective diffusivity is therefore $6.3\pm1.4 \times 10^{-6} m^2/s$.

Table 7.2: Effective diffusivity of repeat breakthrough experiments of laminate structure number 3 from Table 7.1

Breakthrough experiment	Effective diffusivity $(x10^{-6})m^2/s$
1	8.63
2	5.25
3	6.55
4	5.75
5	5.35

7.3.1 Effect of Flow rate

The same laminate structure (Number 2 from Table 7.1) was subjected to three different flow rates to see the effect of varying flowrates on effective diffusivity. Figure 7.13 shows the breakthrough profiles at different flow rates of 250ml/min, 400ml/min and 560ml/min for the Laminate structure number 2 from Table 7.1. As expected, at a higher flowrate of 560 ml/min, the breakthrough occurred earlier as the bed saturated quicker with CO_2 compared to

a lower flow rate of 250ml/min. For the highest flowrate, the mass transfer zone moves more quickly and the mass transfer coefficient should be higher because of higher Reynold's number*[121]*. The effective diffusivities for the varying flow rates were calculated and are shown in Figure 7.14. The effective diffusivities show that they are the independent of flow rate for the same sample although the effective diffusivity at 250ml/min is slightly lower than the effective diffusivities at 400ml/min and 560ml/min. Although the effective diffusivity at 250ml/min is lower, the upper bounds of the 95% confidence intervals of the effective diffusivity at 250ml/min comes in the same range as the lower bounds of the 95% confidence interval of the effective diffusivity at 400ml/min. This shows that the mass transfer in the structure is affected only by the internal structure or porosity and not by external factors such as flow rate.

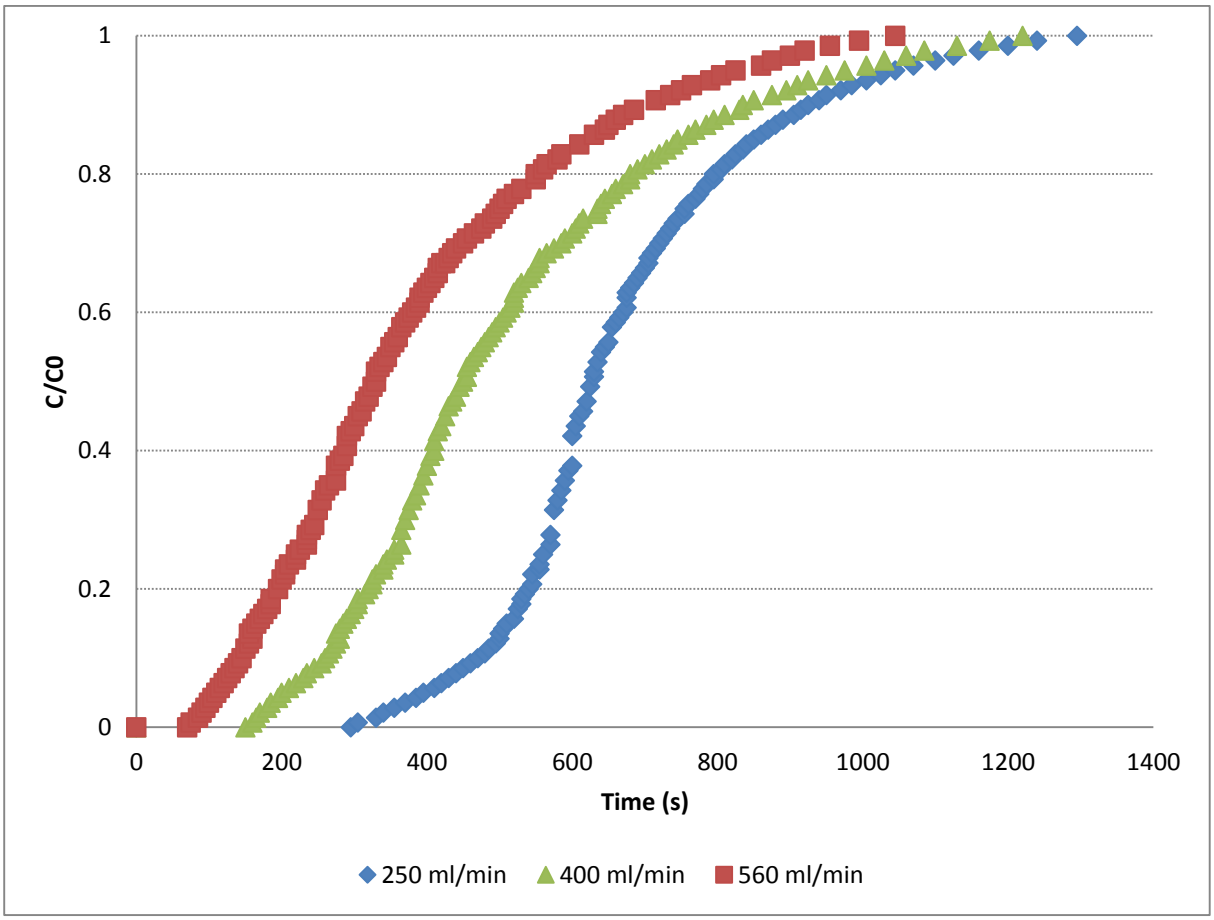

Figure 7.13: Effect of flow rate on breakthrough profiles of same laminate structure number 2

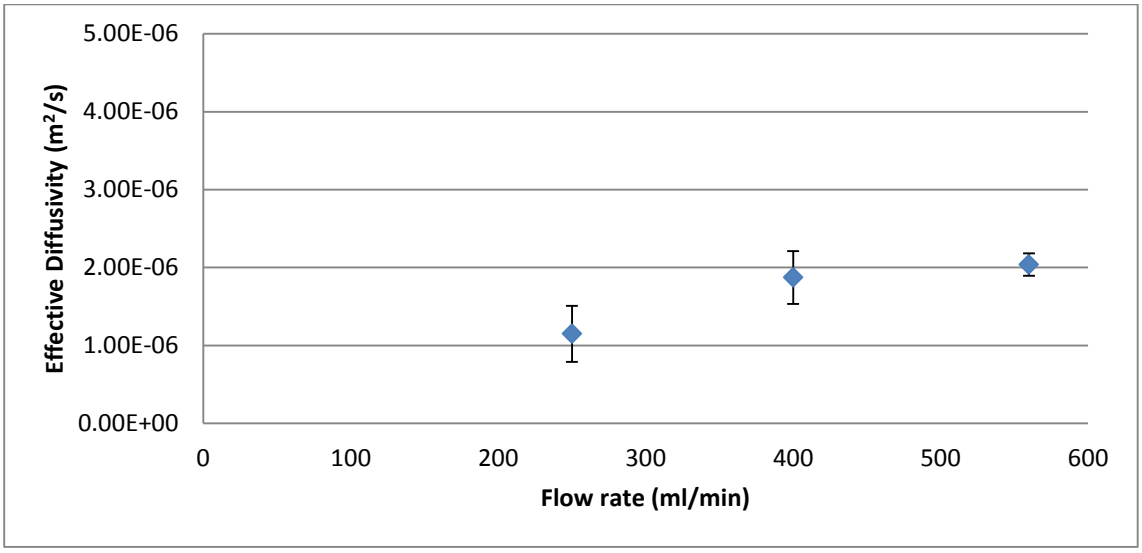

Figure 7.14: Effective diffusivities plotted against flow rate for laminate structure number 2 from Table 7.1

7.3.2 Effect of Porosity

Figure 7.15 shows the breakthrough profiles of two laminate structures number 1 and 3 from Table 7.1, created with different levels of porosity for the same flow rate of 250ml/min. The sample with high porosity (Laminate structure number 3) is created with 20wt% silica and the sample with low porosity (Laminate structure number 1) is created with 40wt% silica. As explained in Section 4.4.4.3, the internal porosity is mostly dependent on the silica concentration with samples containing 20wt% silica having more pores than the samples containing 40wt% silica. It is clear from Figure 7.15, that the sample containing 20wt% silica has a sharper breakthrough front than the sample containing 40wt% silica. Having a narrow MTZ is advantageous because this reduces the energy costs associated with regeneration while also making efficient use of the adsorbent as there is a greater degree of utilisation of the bed*[122]*. From the results, the structures with 20wt% silica are able to have gas flow through the structure and reach the zeolite active sites without difficulty. The time required for breakthrough which is the time required to reach 5% of the final CO_2 concentration in the mixed gas is 405s for the high porosity structure and 395s for the low porosity structure.

Hence both these structures have similar breakthrough time but the saturation time, which is the time taken to reach 95% of final CO_2 concentration in the mixed gas is 745s for the high porosity structure (Laminate structure number 3 from Table 7.1) and 1045s for the low porosity structure (Laminate structure number 1 from Table 7.1) . Both these samples have different amounts of zeolite with the high porosity structure having less zeolite than the low porosity structure but it can be quite clearly seen that the low porosity structure has a more dispersed shape when compared to the structure which has high internal porosity.

Although the structures have varying amount of zeolite, the active amount of zeolite in the sheet is reduced due to the preparation method of the adsorption rig. After the structure has been calcined, the sample was placed in a heat shrink tube and had the fittings attached to it using the silicone sealant. The silicone sealant requires 24 hours of drying before the sample could be used for breakthrough testing. During this time, no further precaution was taken to forbid the entry of water into the structure in room temperature conditions. This reduces the active zeolite for adsorption of CO_2. Hence the amount of zeolite for adsorption in the laminate structure is less than the amount of zeolite present in the laminate structure.

Porosity not only affects the breakthrough profile but also the pressure drop characteristics. The pressure drop of the laminate structures is compared against a column of beads as described in Section 7.2.2 in Figure 7.16. The pressure drop increases linearly with flow rate. The beads have lower pressure drop when compared to the laminate structures. The high porosity structure (Laminate structure number 4 from Table 7.1) also has a lower pressure drop when compared to the lower porosity laminate structure (Laminate structure number 1 from Table 7.1). The high porosity laminate structure has a pressure drop about 2 to 5 times higher than the beads and the low porosity laminate structure has a pressure drop about 5 to 7 times higher than the beads. Hence in terms of breakthrough profile, effective diffusivity and pressure drop and comparing only the laminate structures, the high porosity laminate structure is much more efficient and increasing porosity plays an important role in improving

breakthrough characteristics. Figure 7.17 shows the effective diffusivities of laminate structures and beads compared against their pressure drop.

The manual issues arising during winding the laminate structure cause small inconsistencies in the effective diffusivities and pressure drop of the laminate structures. Nevertheless, a pattern can be observed for structures made under similar conditions. If the structure has channelling due to inefficient winding, then there is more dispersion and the structure will have lower pressure drop and lower effective diffusivity. This can be seen from the densities of the different structures. In general the low porosity structures have a higher density than the high porosity structures. Comparing within the similarly prepared structures for example, the laminate structures number 4 and 5, laminate structure number 4 has a lower density and a lower pressure drop when compared to laminate structure number 5. But it can still be seen that even with the inefficiencies of winding, the high porosity structures are much more efficient in terms of breakthrough characteristics. The high porosity laminate structure with low pressure drop (Laminate structure number 5) still has higher effective diffusivity than the low porosity structures and the high porosity structure with high effective diffusivity (Laminate structure number 4) has lower pressure drop than the low porosity laminate structure making these structures more suitable for adsorption. These structures have also been compared against the effective diffusivity and pressure drop of beads. The beads have lower effective diffusivity and lower pressure drop when compared to the high porosity laminate structures. Hence, it becomes a matter of selecting which characteristic needs to be sacrificed to obtain the required results.

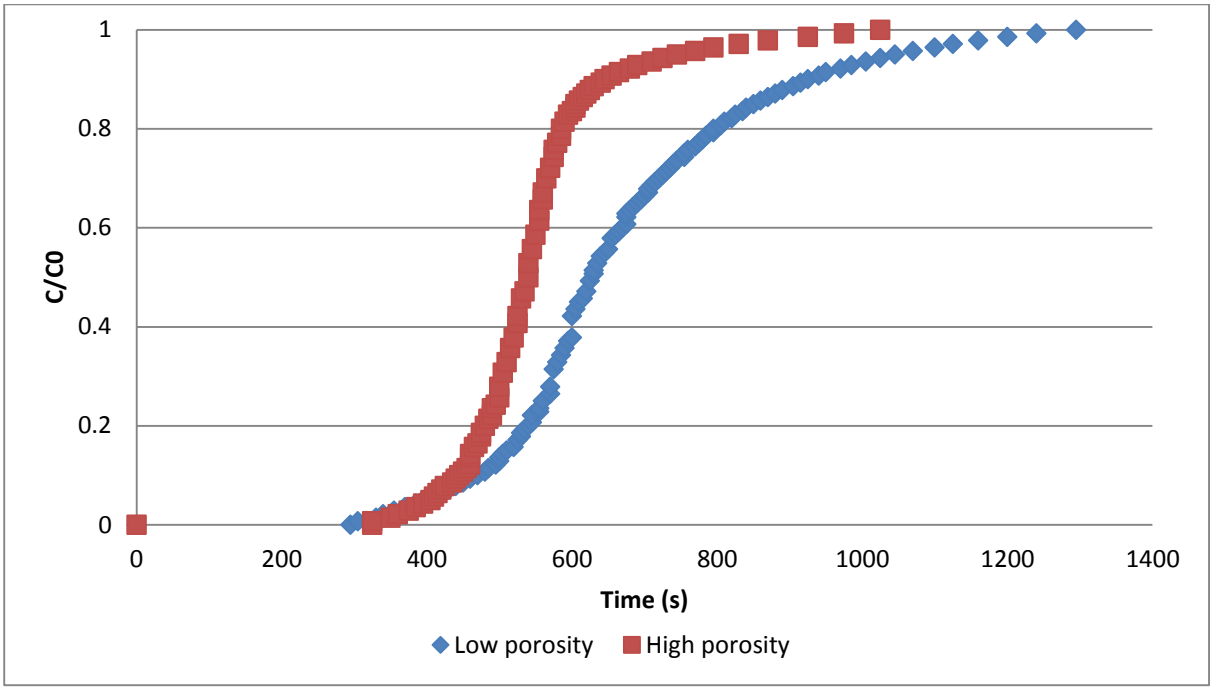

Figure 7.15: Effect of porosity on breakthrough profiles

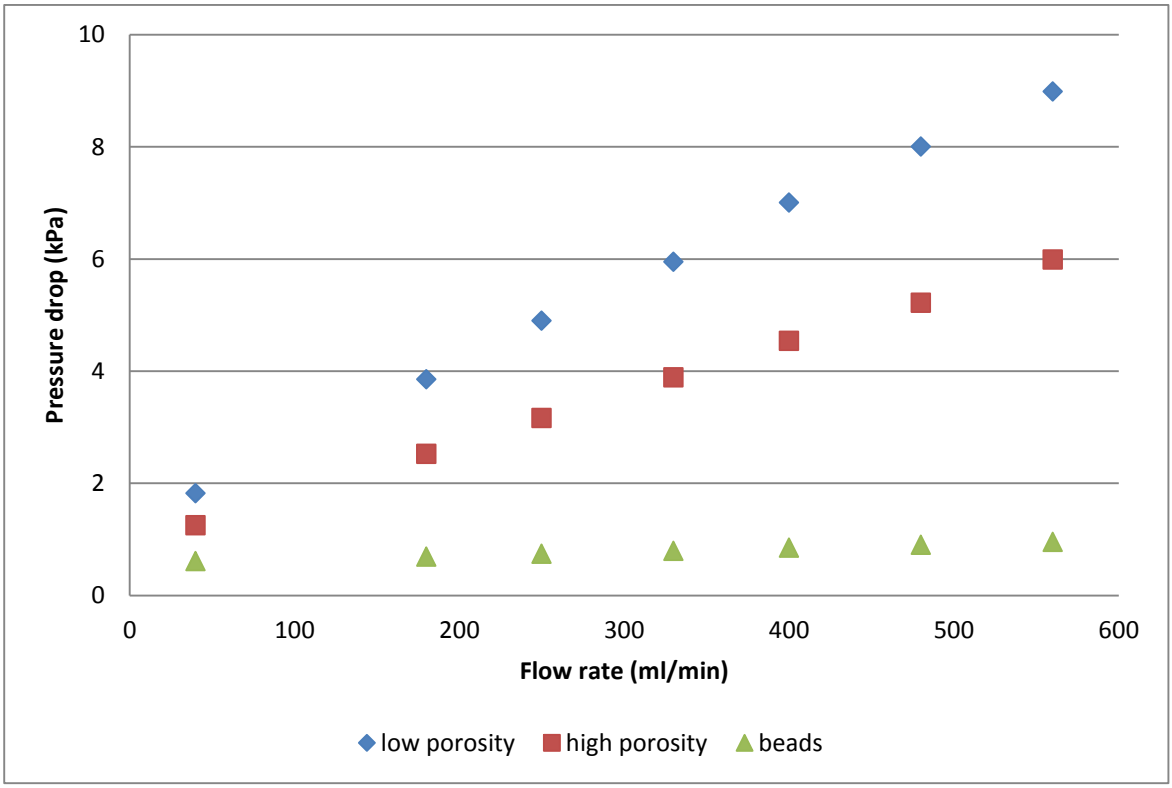

Figure 7.16: Effect of porosity on pressure drop for laminate structures compared against beads

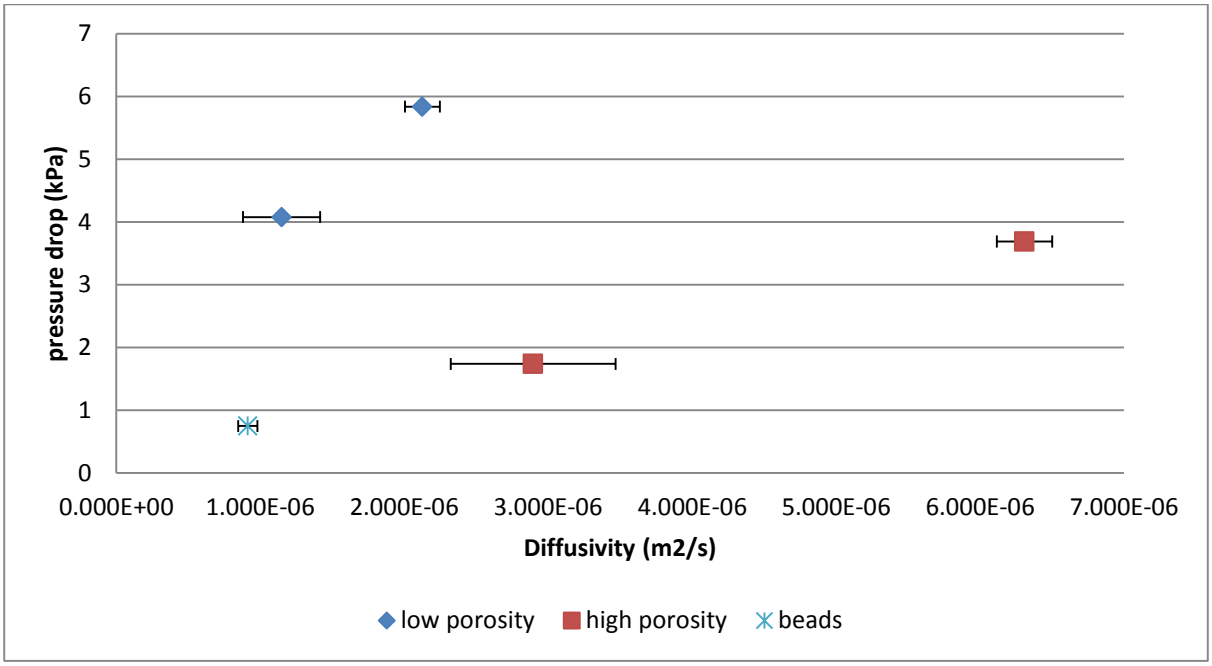

Figure 7.17: Effective diffusivity against pressure drop for structures containing different internal porosities and beads

7.3.3 Channel creation by indents from a metal plate

Figure 7.4 gives an overview of this method of creating indents on the laminate samples. These indents were done on the low porosity sheets as the indentation marks pack the sheet even more densely thereby reducing porosity even further. It was hoped that creating channels for guiding the gas flow would help improve the efficiency and performance of these laminate structures.

The breakthrough profiles and the pressure drop data shown in Figure 7.18 through a plot of effective diffusivity against pressure drop. The pressure drop shown for all the structures is at 250ml/min. Both the channelled structures created with the indents (Laminate structure number 6 and 7) have higher pressure drop and lower effective diffusivities than the structures without channels or beads, meaning that their performance is inferior to the other laminate structures. This could be because after the indents are formed, the structures are rolled to create the structures shown in Figure 7.2A, while the sheet is still wet to create the

template from which the wood fibres are burnt. While winding the structure into a "swiss roll", pressure was applied to keep the rolled structure tight and this might have reduced the depth of the channels created by the indents. This makes these structures much denser, thereby making these structures even less porous when compared to the low porosity structures (Laminate structure 1 and 2) which thereby drops the breakthrough performance of the structure with indent marks. Both these structures have similar values in terms of pressure drop and effective diffusivity, which is worse than the structures without spacing showing that this method of creating spacing does not create useful laminate structures for gas adsorption. Therefore, other methods of directing better gas flow paths have to be considered to improve the breakthrough performance of the laminate structures and make them more competitive with fixed beds packed with beads.

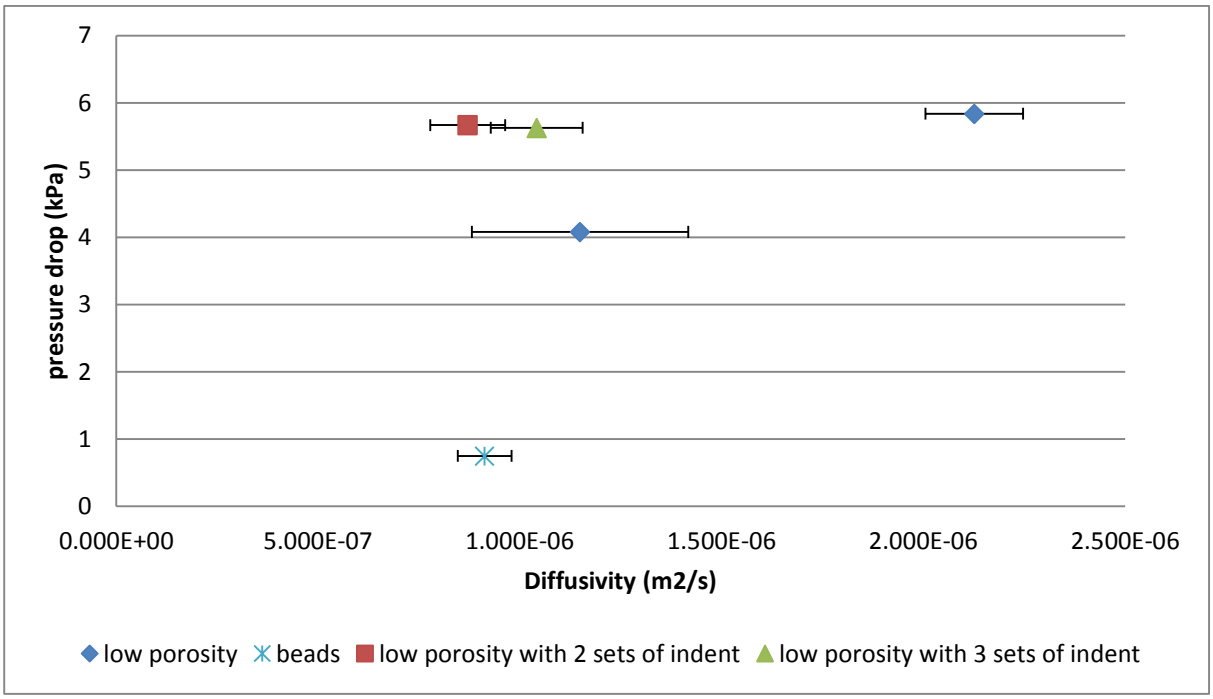

Figure 7.18: Effective diffusivity against pressure drop for structures containing channels created by indents against structures without channels and beads

7.3.4 Effect of creating spacing using wires in the laminate structures

To improve on the channels created by using the indentation of a metal plate, stainless steel wires were used to create spacing between the layers of the structure. Figure 7.5 shows the method creating laminate structures with wire between the layers of the structure and Figure 7.6 shows the laminate structure created by this method. As mentioned in Section 7.2.1, the wires were wrapped with the structure to create spacing between the rolls of the structure. The wires are very difficult to control as they are not as flexible as the laminate structure and do not take on and hold the shape of the "swiss roll". Hence controlling the rotation of the wire during the manufacturing process is very complicated. The wires unlike the indents created by the metal plate do not affect the density of the sheet structure but create large spaces for gas flow. Figure 7.19 shows the pressure drop across the laminate structure for different flow rates. The structures with the wires in them (Laminate structures number 8 and 10) have very low pressure drop similar to the beads when compared to the laminate structures without wires. Figure 7.20 shows the effective diffusivities of different laminate structures plotted against the pressure drop at 250ml/min for all the structures. The effective diffusivities of the structures with low porosity and wire (Laminate structures number 8 and 9) are similar to the effective diffusivities of the structures with low porosity without wires (Laminate structures number 1 and 2) while the pressure drop of the structures with the wire is much lower than those of the structures without wire. The same is true for the structures with high porosity with wire (Laminate structure number 10 and 11) and without the wire (Laminate structures number 4 and 5). As can be seen from the figures, the structures with the wire either have similar performance to or better performance than beads. The structures with low porosity and with the wire have similar effective diffusivity and pressure drop when compared to beads while the structures with high porosity and wire have lower pressure drop (in one case) and much higher effective diffusivity when compared to the beads, showing that these structures have better breakthrough performance than beads. This is very promising

although the problem of obtaining reproducibility between structures must still be overcome. Hence other means of producing spacing or channels for gas flow need to be considered for producing laminate structures that can compete with traditional fixed beds containing beads.

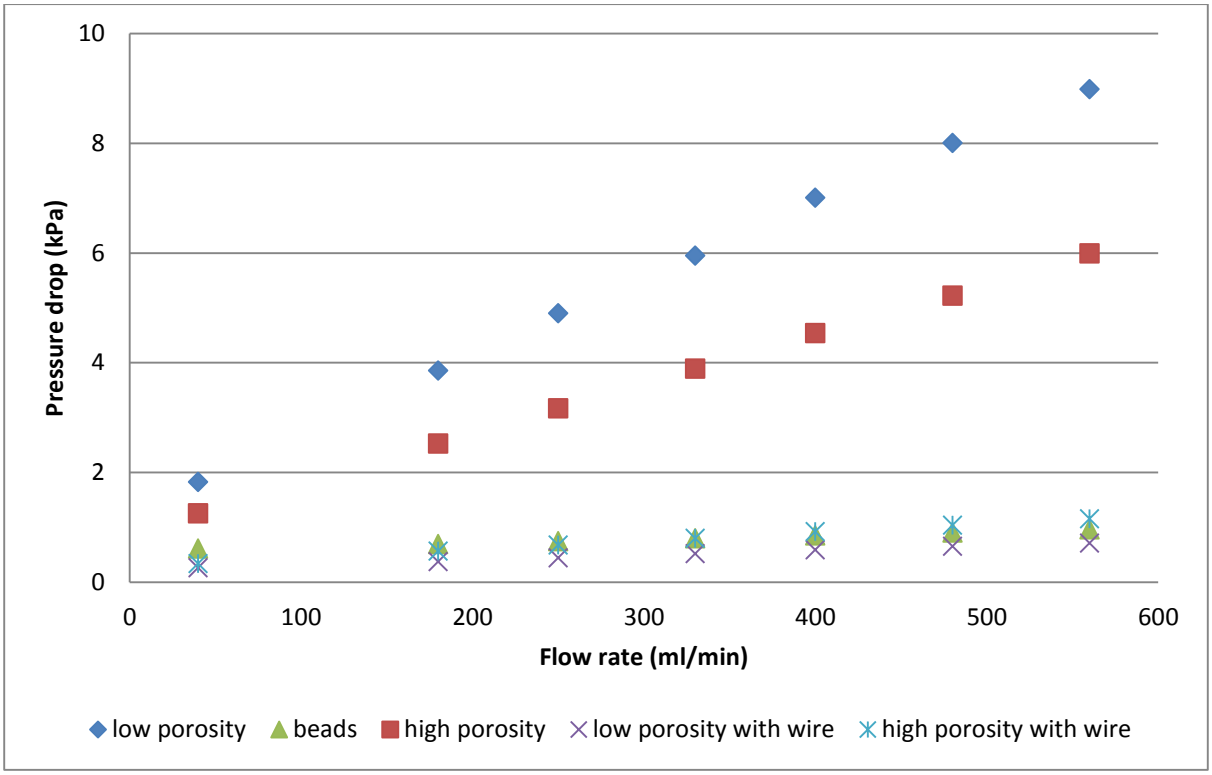

Figure 7.19: Effect of creating spacing using wire and without wires on pressure drop compared against the pressure drop of beads

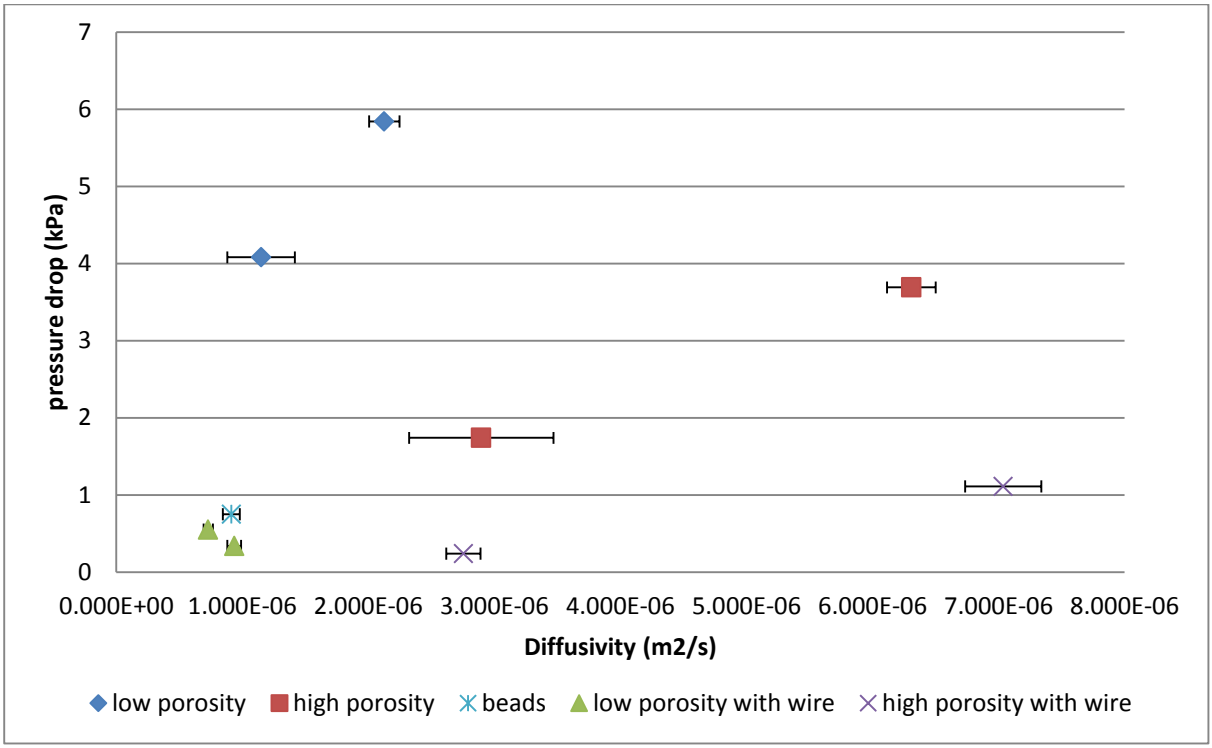

Figure 7.20: Effective diffusivity against pressure drop for structures containing spacing created by wire against structures without spacing and beads

7.4 Conclusion

Zeolite laminate structures for breakthrough testing were prepared using different methods to create spacing in the structure and give breakthrough properties superior to beads. The performance of these laminate structures was evaluated using CO_2 adsorption and compared against 13X beads. The laminate structures have issues with reproducibility as the winding of the structure is done manually but an idea of how the structure performs can still be obtained from the current structures. Flow rate does not affect the effective diffusivity of the structures. Structures with high porosity give higher effective diffusivity and lower pressure drop and therefore show better performance than low porosity structures. Creating channels on the structures with indents is not a very useful technique because the channels are lost during winding and the structure is made denser which increases the pressure drop. Lastly, using the wire to create spacing for gas flow works well by reducing the pressure drop and

giving structures that have much better performance than beads but this method is very difficult to reproduce and needs further improvement. The overall conclusion is that the laminate structures prepared using papermaking techniques for use in gas separation by adsorption are competitive alternatives to traditional beads in terms of pressure drop and effective diffusivity properties.

Chapter 8

Creation of Parallel Surface Channels Using AKD Printing

This page is intentionally blank

8.0 Creation of parallel surface channels using AKD printing

8.1 Introduction

The best structures from the partial factorial design gave a comparatively good performance in terms of pressure drop and breakthrough front when compared to commercial beaded structures. If flow channels could be made to run across these structures to better control the gas flow path, the performance of these structures is expected to improve. As mentioned in Section 2.8, a parallel channel adsorbent structure will have more advantages when compared to the laminate structures without channels. These structures should have faster adsorption kinetics and lower pressure drop due to the identical and regular channels. There are many methods to create channels such as deposition and embossing on the laminate structures but the method should improve the performance of the structure.

As discussed in Section 7.3.4, channelled structures were produced by creating indents using a metal mesh. These structures had higher pressure drop and lower effective diffusivity when compared to the laminate structures without channels. As explained previously, the process of indenting the sheet to produce the channels made the structure denser. This made it difficult for the gas to reach the zeolite in the sheet, thereby decreasing diffusivity and rate of mass transfer. In addition, the sheets are wet with silica while the indents are made. Rolling up the sheets to create the breakthrough samples then partially destroyed the channels that had been created. Hence the pressure drop was also not reduced. Clearly this method of creating channels did not work well and would create difficulty during mass production.

The focus of the work in this chapter is thus to look at alternate ways of patterning the sheet surfaces to create channels. The key advance in the work reported here is the recognition that the laminate structures that have been discussed in Chapters 3 and 7 derive their strength

from the sintering of the colloidal silica nanoparticles with the zeolite and ceramic fibre components at a temperature of 650°C, which also removes the water from the zeolite. Thus if it is possible to prevent the penetration of the colloidal silica into an area, then the sheet structure at that point will disintegrate during oven treatment, creating voids. This could potentially be achieved by selectively making parts of the sheet hydrophobic to inhibit the movement of the colloidal silica suspension into the sheet at that point.

The pulp and paper industry uses paper sizing agents, either added to the bulk of the sheet or on the surface, to impart hydrophobicity to a sheet*[123]*. Some of the internal sizing agents are alkyl ketene dimer, rosin and alkyl succinic anhydride. One of the most commonly used chemicals is Alkyl ketene dimer (AKD) because the sizing effect happens during neutral to slightly basic conditions*[124]*. The sizing agents are immobilised onto cellulose fibres via an esterification reaction as given below in Figure 8.1.

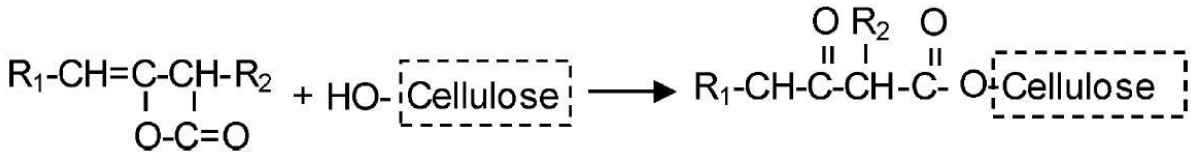

Figure 8.1: The esterification reaction of the sizing agents on cellulose fibres

The four membered lactone ring in AKD reacts with nucleophiles to form β-keto ester bond with cellulose which is the primary reaction for AKD sizing of paper. The covalent bond immobilises and orients the hydrophobic tail outward, away from the paper surface*[125]*. This sizing reagent creates hydrophobic surfaces with contact angle between 110-125° with water.

Our attention was drawn to the possibilities of using AKD as there have been a recent series of studies in which microfluidic patterning has been applied to paper sheet surfaces by printing AKD dissolved in heptane using an adapted ink jet printer by Li et al*[126, 127]* The

challenges to be overcome were to create a sheet which was able to be printed and a sheet surface which could be made hydrophobic.

8.2 Preparation of Channelled Laminate Sheet using AKD printing

None of the sheets prepared according to the partial factorial design in Table 3.1 in Section 3.5 were able to be used for printing. The sheet must have enough ceramic fibres to hold together after firing but also not have too many ceramic fibres as the sheet would be too thick and cause issues with running the sheet through a printer. In addition, the zeolites used in the work of this thesis are hydrophilic and AKD does not react with zeolite to give a hydrophobic surface. Hence the maximum amount of zeolite and the time taken to create the smallest floc size that can create hydrophobicity in the sheet structure has to also be determined.

8.2.1 Determination of Amount of Ceramic content to create AKD printed laminate structures

The amount of ceramic content in the sheet must first be determined before preparing the sheets. The amount of pulp was kept constant at 100gsm. Several sheets were made with varying concentrations of ceramic fibres from 1.5g to 8g for a 22cm x 22cm sheet. This is equivalent to sheets having between 30 to 165gsm of ceramic fibres. No zeolite was used in this preparation method. In the partial factorial design of Table 3.1 in Section 3.5, the ceramic content varied between 30gsm and 200gsm for the low and high factors. Hence, even using the largest value of 165gsm is lower than 200gsm of ceramic fibres from the partial factorial design. These sheets were coated with 20wt% colloidal silica and fired to see if the structure would retain its strength. A ceramic fibre content of 6.5g was selected for the sheet forming process. If more ceramic fibres were used, then the sheets were thick and therefore would cause printing issues as the sheets became more board-like and the printer was unable to feed

the sheets for printing. Less ceramic content showed complete breakdown of the sheet with 20wt% silica as discussed in Section 5.4 from using low ceramic content and low weight percent of silica.

8.2.2 Determination of the amount of Zeolite content in the Printed Laminate Sheet Structure

In order to determine the optimal amount of zeolite for the AKD printing on the laminate structure, many sheets were created with differing amounts of zeolite while the ceramic and pulp content were kept constant at 6.5g and 4.84g dry weight, respectively, per sheet. The zeolite content was varied between 2g to 20g The sheets from the partial factorial table 3.1 in Section 3.5 on the other hand had zeolite weights of either 10g or 18.5g. The amount of CPAM used for preparation of the sheets was kept constant at 5mg CPAM/g zeolite with a stirring time of 15 minutes, from the results in Section 3.4.2. The varied amount of zeolite in the sheets is shown in Figure 8.2. The floc size and the increasing surface coverage of the sheets can be seen. The floc sizes are mostly similar but with increasing zeolite content, there is less exposed fibre surface. Hence, there will come a point when there is not enough fibre surface for the cellulose sizing effect to occur. These sheets were then tested for their ability to be made hydrophobic by adding drops of AKD solution to the sheet surface.

The AKD solution was prepared by mixing 2%v/v AKD with n-heptane solvent. Drops of AKD solution were then placed on the dried sheet and cured in an oven at 105°C for 40 minutes. The AKD is a wax like substance at room temperature and a temperature greater than 40°C removes the solvent and melts the AKD to enhance the cross-linking effect to produce a hydrophobic surface. The sheets were then cooled to room temperature and deionised water was applied to the sheet surface.

It was found that a laminate sheet with a maximum loading of 8g zeolite gave a sharp distinction between hydrophilic and hydrophobic regions. This distinction between the

hydrophilic and hydrophobic regions is essential during the silica coating process of the printed sheet.

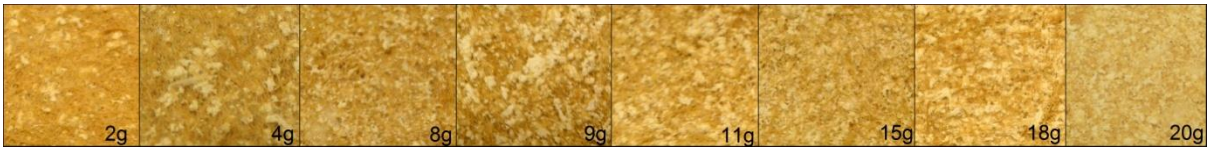

Figure 8.2: Optical Images showing increasing content of zeolite in laminate structures

Next the stirring time for cationic polyacrylamide with the zeolite needs to be determined. 8g of zeolite was used for all these experiments and the images for the different stirring times are shown in Figure 8.3. It can be seen from Figure 8.3 that increasing the stirring time reduced the size of the flocs and gave a more even dispersion of the flocs through the laminate structure. It was found that a stirring time of 30 minutes was appropriate as this resulted in zeolite flocs which were finer and also gave the most even dispersion throughout the laminate sheet. Having a stirring time less than 30 minutes gave a more uneven dispersion with a larger floc size and this would lead to difficulty in retaining the hydrophobic channels in the sheet where the zeolite flocs lie directly across the channels. Hence a zeolite weight of 8g with a CPAM stirring time of 30 minutes was chosen for preparation of laminate structures for parallel channel printing.

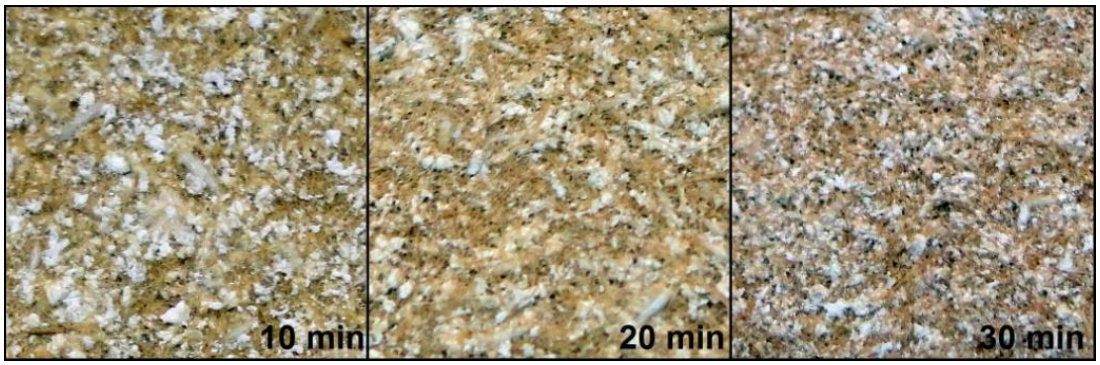

Figure 8.3: The effect of stirring time of CPAM and zeolite on floc size and dispersion

Thus the amount of zeolite and ceramic were determined for the final sheet preparation process. From here the zeolite laminate formation procedure is the same as description in Section 3.3.2 until the wet sheet is dried in the humidity controlled room.

The final structure for parallel channel printing was of size 22cm X 22cm. 8g of micron zeolite was flocculated using 5mg/g zeolite for 30 minutes. This flocculated zeolite was added to a dispersed 100gsm (4.84g dry weight) pulp and 135gsm (6.5g) ceramic fibre slurry. This slurry was then used for the sheet forming process as discussed in Section 3.3.2 for the preparation of parallel channel laminate structures,

8.2.3 Testing for creation of hydrophobicity on the laminate structures

It was necessary to check if the AKD printing method would actually work and give the desired results of creating a parallel patterned laminate adsorbent. Hence AKD was initially dropped onto the laminate structure created from Section 8.2.2. These sheets were cured in an oven at 105°C for 40 mins. Colloidal silica was then coated on these sheets. The results of this test are shown in Figure 8.4. Image A, shows the hydrophobicity created by patterning the structure with droplets on one sheet and creating hydrophobicity on an entire portion of another sheet after coating will colloidal silica. Image B, shows the same samples after they have been fired at 650°C. It can be clearly seen that most of the places where the AKD has spread have not maintained their strength and collapsed as the silica has not reached the hydrophobic areas. In some hydrophobic areas, the structure has not completely collapsed and is held together either because the ceramic fibres have held together or because the colloidal silica has managed to penetrate into some portion of the structure. Hence this was a good method to check the successful application of printing hydrophobic channels.

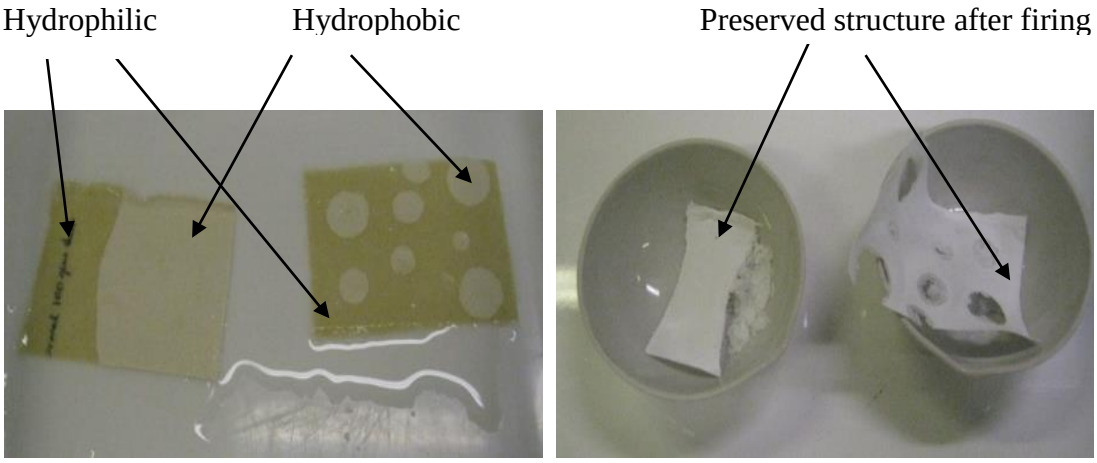

Figure 8.4: Test showing successful application of the creation of hydrophobic sections in laminate sheet A) Image shows sheets having hydrophobic patterns soaked in Colloidal silica B) Image shows the same sheets fired with patterns still present.

8.2.4 AKD printing on the Laminate Sheet

For the printing process, the side for printing must first be chosen. The side of the sheet stuck to the wire is the bottom side of the sheet. Images showing both the top and bottom side of the paper structure are shown in Figure 8.5. The bottom side of the sheet has many ceramic fibres and larger zeolite flocs. Hence this side of the sheet is more uneven. The ceramic fibres as seen in Figure 3.4A have bulbous heads and long tails. The heads tend to sink to the bottom of the sheet during the sheet forming process. Therefore, the top side of the sheet was chosen for the printing process.

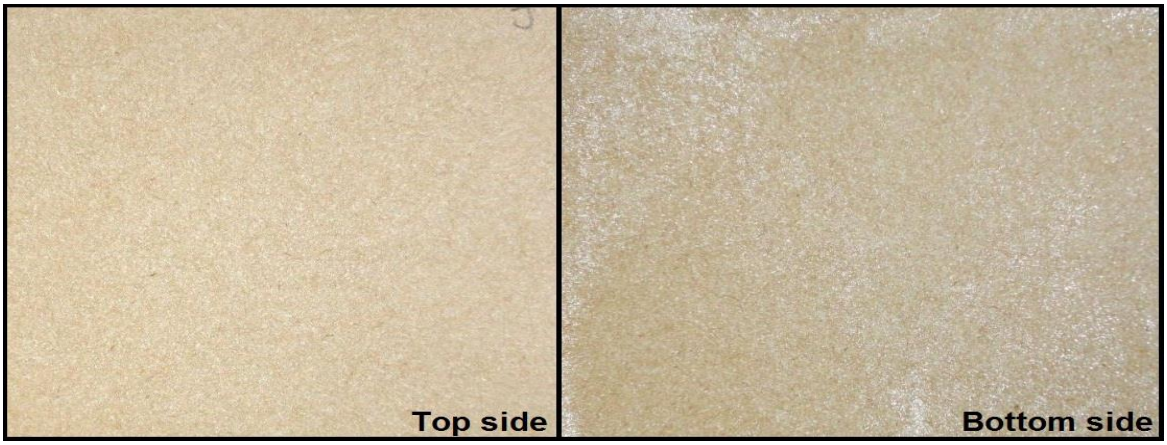

Figure 8.5: Image showing the two sidedness of the zeolite laminate paper

After preparation, the 22cm x 22cm sheet was then cut to 20cm x 20cm to be within the dimensions of an A4 sheet of paper. This sheet was then pasted onto the centre of an A4 sheet of paper, so the printer was easily able to pick up the paper. A 2%(v/v) solution of AKD in n-heptane was prepared. The magenta cartridge in the Canon inkjet printer (model number iP 3600) was emptied and filled with the 2%(v/v) AKD solution. Templates of different channel dimensions of solid print with different widths between the channels were prepared with the magenta filling where the AKD should be printed. To check if the printing process was occurring correctly, a thin black outline was given to the channels. The print quality was set to a high standard to achieve maximum definition. An image of laminate sheet emerging from the printer is shown in Figure 8.6. The channels in the sheet emerging from the printer are 1mm in width and have 1mm spacing.

Figure 8.6: Laminate sheet emerging from the inkjet printer

Even while the sheet was emerging from the printing process, the smell of the AKD on the sheet was clear. This sheet was then placed in a laboratory oven at 105°C for 40 minutes. Once the sheet was cured, the sheet was coated using either 20wt% or 40wt% 22nm colloidal silica and then calcined in a furnace at 650°C. Figure 8.7 shows an AKD printed sheet after calcination. The sheet has been cut to a width of 5cm and has 1mm channels and 1mm spacing between the channels.

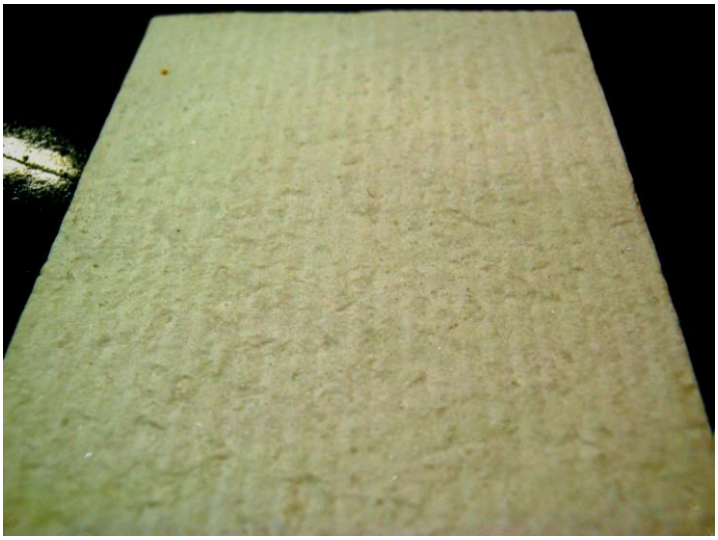

Figure 8.7: Parallel channel printed laminate structure after calcination at 650°C

8.3 Analysing the Dimensions of the Hydrophobic channels from the Inkjet Printer

It was necessary to determine the resolution of the channel width, depth and spacing between channels for the printing process. The inkjet printer only prints on one side of the paper surface and the AKD penetrates some distance into the sheet. This penetration distance is quite small due to the quick evaporation of the hydrocarbon solvent. For a given sample, printer and printing tone, the penetration distance is fixed and hence only the channel widths and spacing can be altered.

A range of channel widths and spacing between channels were first tested. Channels widths of 0.5mm, 1mm and 2mm were printed with spacing between channels of 0.5mm, 1mm and 2mm, as shown in Figure 8.8. The cured sheet was coated with water to check for hydrophilic/hydrophobic resolution. It was found that channels with a width of greater than 1mm showed good resolution between hydrophilic (wet) and hydrophobic (dry) areas. When the spacing or channel width was less than 1mm, the channels were discontinuous in terms of hydrophilic/hydrophobic boundaries. Also in some instances where zeolite flocs were found on the surface where printing was supposed to take place, the silica would cover the floc, thereby making the hydrophobic layer less distinguishable. Hence a channel width of 1mm was chosen with different spacing widths. This is the smallest channel width that gives good resolution and a greater amount of small channels was preferred to aid gas dispersion through the sheet.

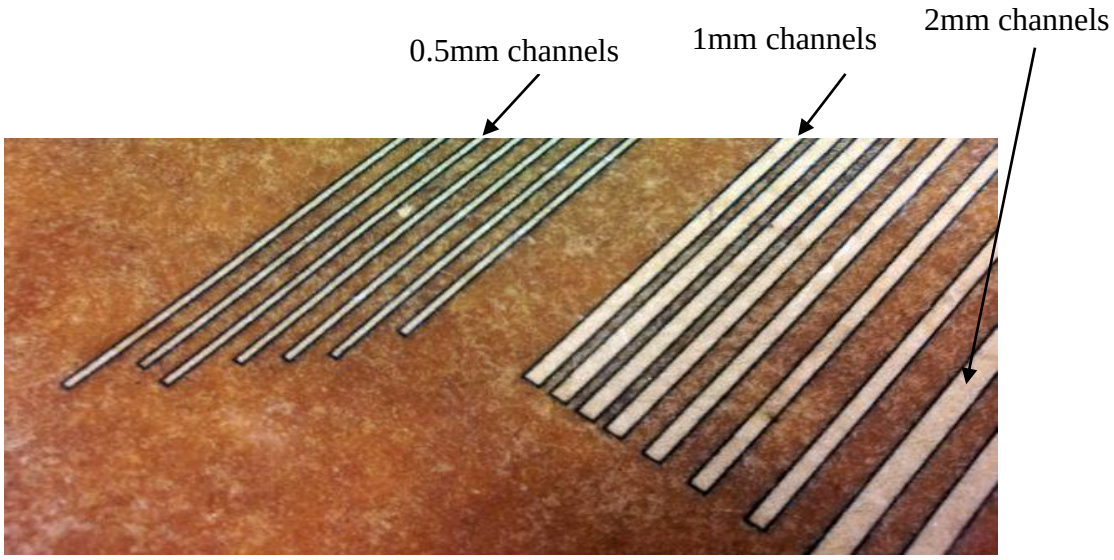

Figure 8.8: Different channel widths with different spacing distances between channels showing hydrophilic (wet)/hydrophobic (dry) resolution

8.3.1 SEM Imaging to determine channel dimensions

The Phenom desktop SEM was used to view the final printed laminate structure after calcination at 650°C. More details about the Phenom SEM can be found in Section 4.2.1.1. The largest length that can be measured using the desktop SEM is 500µm but the channel widths are 1mm. Hence it is necessary to overlay images to be able to view the channels. SEM images of two laminate samples prepared in a similar manner with differing concentration (wt%) of silica coating are shown. Figure 8.9 shows a schematic diagram of the locations that were imaged in order to find the dimensions of the channels created by hydrophobic printing. These locations were:

1. A top view of the sheet showing channel width
2. A cross sectional view across the channels showing both channel width and channel depth
3. A cross sectional view along the channel showing channel depth

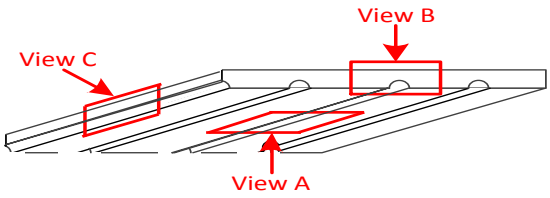

Figure 8.9: Sample views taken to determine channel dimensions

Two different silica concentrations were used to create parallel channel laminate adsorbent structures. Samples with 40wt% colloidal silica create structures with low porosity and high strength while structures with 20wt% colloidal silica create structures with high porosity and low strength. Since the structures prepared for printing have the necessary amount of ceramic fibres for minimum strength requirements, the amount of colloidal silica can be either 20wt% or 40wt%.

8.3.1.1 Channels Dimensions for Sample with 40 wt% Silica

The top view (View A) is shown for a sample with 40wt% colloidal silica in Figure 8.10. From the image, it can be seen that the channels are well preserved from the printing stage to after firing the sheet. There is excellent distinction between the channels created and the spaces between the channels. The centre of the image shows the ceramic fibres not coated by the silica. This is the channel, which is a darker and a bare region with only the fibres running across the space. The edges of the image show where the hydrophilic region had existed and where the silica coating has penetrated the structure. This region is dense and it is difficult to see underneath this layer. The width of the channel was also measured and found to be close to 1mm.

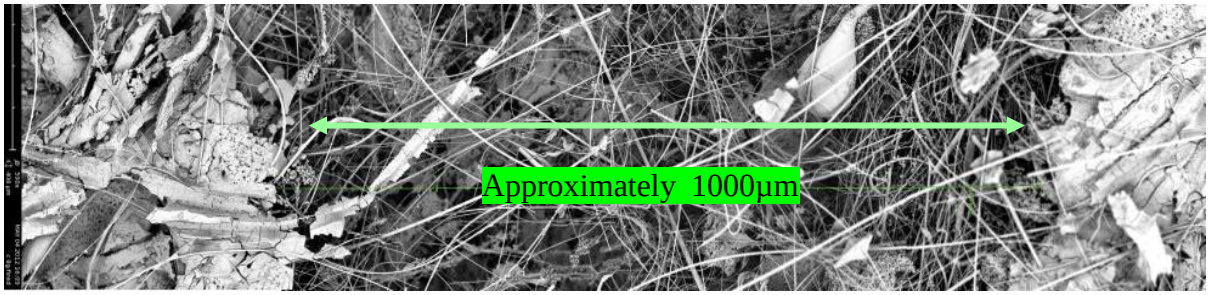

Figure 8.10: Top view of channel in a sample coated with 40wt% colloidal Silica

Figure 8.11 shows the cross sectional view across the channels (View B) of the parallel channel laminate structure coated with 40wt% silica showing both channel depth and channel width. The channels created do not have a change in depth but instead have sections where the silica is covering the ceramic fibres and zeolite flocs and then have channels where there is no silica present. Hence the perceived difference in depth is due to absence of silica in the regions where hydrophobicity was created. Since the silica is coated on both sides of the sheet, the silica penetrates the sheet from the side where the channels are not printed. Therefore, if the depth of the channel needs to be measured, it would be the depth till the layer where the silica is not covering the channel. Showing this view was difficult as cutting through the channels damaged some of the silica coating and this is made more apparent from Figure 8.11 where the silica coating is not continuous, as would be expected. However, this figure clearly shows the difference in depth and the presence of well maintained channel width and channel spacing.

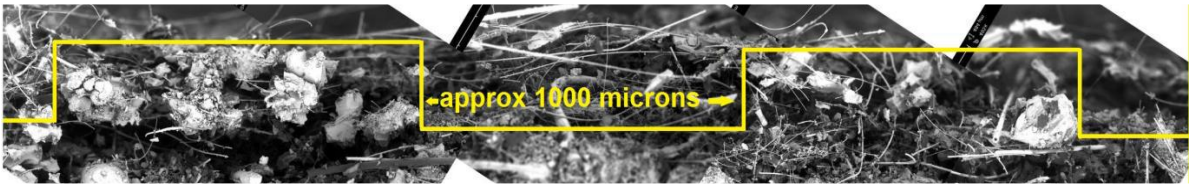

Figure 8.11: Cross sectional view across the channels of a sample coated with 40wt% silica

The cross sectional view along the channel length (View C) of the parallel channelled laminate adsorbent with 40wt% silica is shown in Figure 8.12. This cross-sectional view was taken by cutting along the length of a channel. The upper region of the image is the side of the sheet where no printing took place and hence is completely coated with silica. The lower part of the image shows the channel with no silica present and also gives an idea of how deep the channel is. The channel depth for a parallel channel laminate adsorbent structure coated with 40wt% silica was measured to be between 100- 150µm.

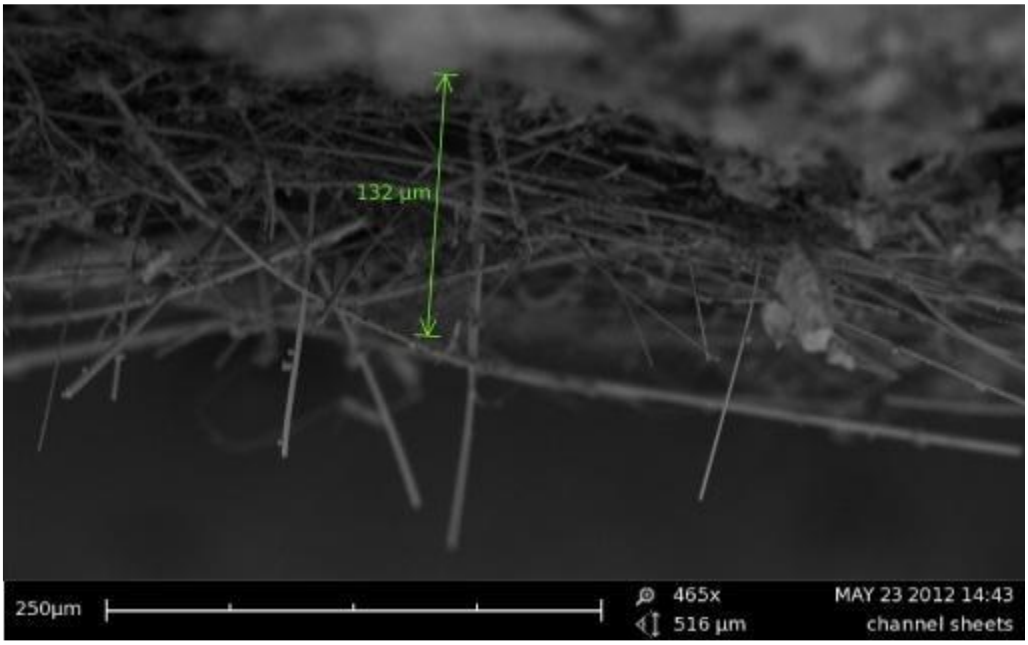

Figure 8.12: Cross sectional view along the channel of a sample coated with 40wt% silica

8.3.1.2 Channel Dimensions for Sample with 20wt% silica

Again, the top view of the sample coated with 20wt% silica is shown in Figure 8.13. This image shows one channel in the centre and two sections of the spacing between the channels on either side of the channel with a couple more channels on the edges of the image. Again, there is excellent distinction between the channels created and the spaces between the channels. The areas where the channels were printed are darker and barer with mostly ceramic fibres filling those regions. The denser regions that have the silica covering them are the spaces between the channels. The template for printing this sheet of paper had a channel width of 1mm and the spacing between the channels was also 1mm. This can be clearly seen from Figure 8.13. Hence the dimensions of the channel were clearly preserved. On the extreme right of the image, in the dark space, there is some silica covering a zeolite floc. This, as mentioned before, is because the zeolite floc is at the surface of the paper where the printing has occurred. The zeolite surface cannot be cured to create hydrophobicity and hence

although this region is meant to be hydrophobic, the presence of the zeolite floc has reduced the distinction between channel and non-channel area in this region.

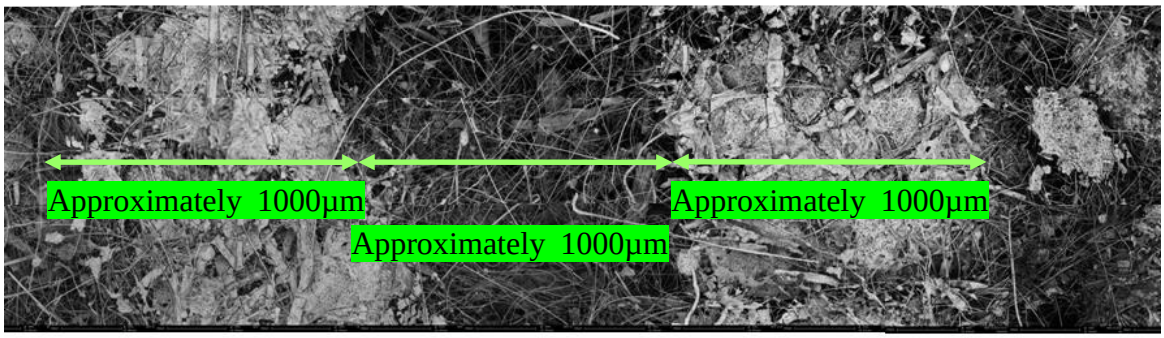

Figure 8.13: Top view of channel of sample coated with 20wt% silica

View B was not taken for a laminate structure with 20wt% silica because as mentioned in Section 8.3.1.1, this view was difficult to capture even for a sample that had 40wt% silica. As discussed in section 5.4, the amount of silica present in the sample is very indicative of strength, with samples having more silica, having more strength. Hence measurement of depth of the channel in this sample was carried out from View C which is the cross section of the sample along the length of the channel. This view is shown in Figure 8.14. Similar to the sample with 40wt% silica, the upper region of the image is the side of the sheet where no printing took place and hence is completely coated with silica. The lower part of the image shows the channel with no silica present and also gives an idea of how deep the channel is. The channel depth for a parallel channel laminate adsorbent structure coated with 20wt% silica was measured to be between 220-280µm. This channel depth is larger than that of the sample with 40wt% silica, because the silica penetration is not as deep from the side where printing has not taken place, because of the lower amount of silica. Hence structures with 20wt% silica, have deeper channels when compared to samples with 40wt% silica.

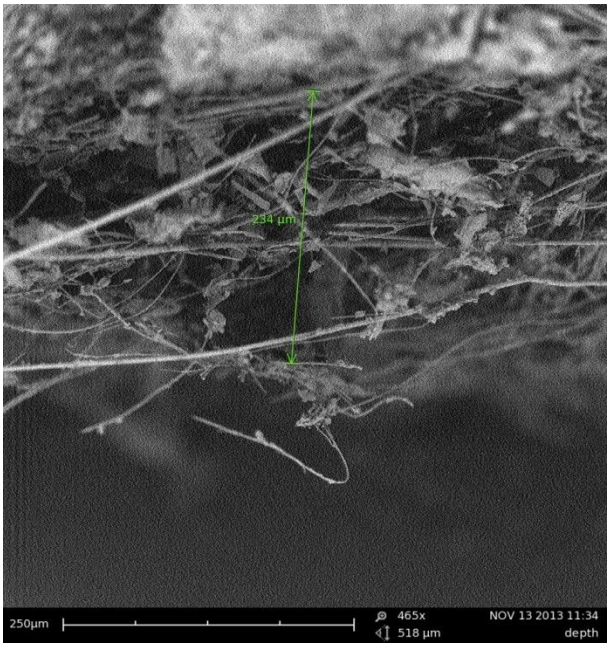

Figure 8.14: Cross section view along the length of a channel of a sample coated with 20wt% silica

Parallel channel printed structures with either 20wt% or 40wt% colloidal silica can be created using the method described in Section 8.2. The SEM images very clearly show that the width and spacing between the channels is the same as the AKD printed surface showing that the channels are preserved. The structures having 40wt% colloidal silica have lower porosity and lower channel depth when compared to structures having 20wt% colloidal silica. These structures are very promising and their breakthrough results are discussed in Section 8.4.

8.4 Breakthrough testing of parallel channel printed laminate structure

The performance of the parallel channel printed laminate structure was tested using breakthrough testing. The sample was prepared according to the method described in Section 8.2 and the breakthrough testing apparatus was set up according to the method described in Section 7.2. The breakthrough profiles and pressure drop of the laminate structures are compared in Sections 8.4.1-8.4.3. Since the laminate structure created for printing has

different concentration of zeolite and ceramic fibres in comparison to the laminate structures prepared from Table 3.5.7.1, a sheet with the same composition as the other printed structures was also prepared without printing channels for comparison against structures with channels. All the structures, therefore, had the same starting amount of zeolite and their breakthrough properties can be compared against one another.

Four different structures were created for breakthrough performance testing. The first structure as stated in the previous paragraph did not have any channels printed and was coated with 20wt% silica. The second structure had 1mm channels with 1mm spacing and was coated with 20wt% silica. The third structure had 1mm channels with 2mm spacing and also coated with 20wt% silica. The last structure had 1mm channels with 1mm spacing and was coated in 40wt% silica.

8.4.1 Breakthrough profiles of printed parallel channel laminate structures

Figure 8.15 shows the breakthrough profiles of the four laminate structures described in Section 8.4. These breakthrough profiles were obtained at a flow rate of 250ml/ min. The structures with 20wt% silica show better breakthrough profiles when compared to the structure with 40wt% silica. As described in Section 4.4.4.2, samples with 40wt% silica have lower porosity than samples with 20wt% silica but even with the channels the breakthrough profile has not improved when compared to the structure with no channels and 20wt% silica. For all the samples with 20wt% silica, the structure with no channels has the most dispersed breakthrough profile, as expected, and the structures with the 1mm channels and 2mm spacing between the channels have the most favourable breakthrough profile out of all four laminate structures.

The breakthrough width for the samples was calculated by finding the time between 5% of final adsorbing gas concentration and 95% of final adsorbing gas concentration from the

breakthrough curve. This was found to be 280s, 300s, 305s and 545s for the samples with 1mm channel width, 2mm spacing and 20wt% silica, 1mm channel width, 1mm spacing and 20wt% silica, no channels and 20wt% silica and 1mm channel width, 1mm spacing and 40wt% silica, respectively. The time taken to reach 50% of final concentration of adsorbing gas was found to be 255s for all four samples, which shows that all four samples have the same amount of zeolite. The effective diffusivities for these breakthrough profiles were found by fitting these simulated curves using the numerical breakthrough model from Section 7.2.4. These results are discussed in Section 8.4.3. The breakthrough runs of the same samples were performed at higher flow rates of400ml/min and 560ml/min and these curves are shown in Figure 8.16. Even at the higher flow rates, the same pattern is observed.

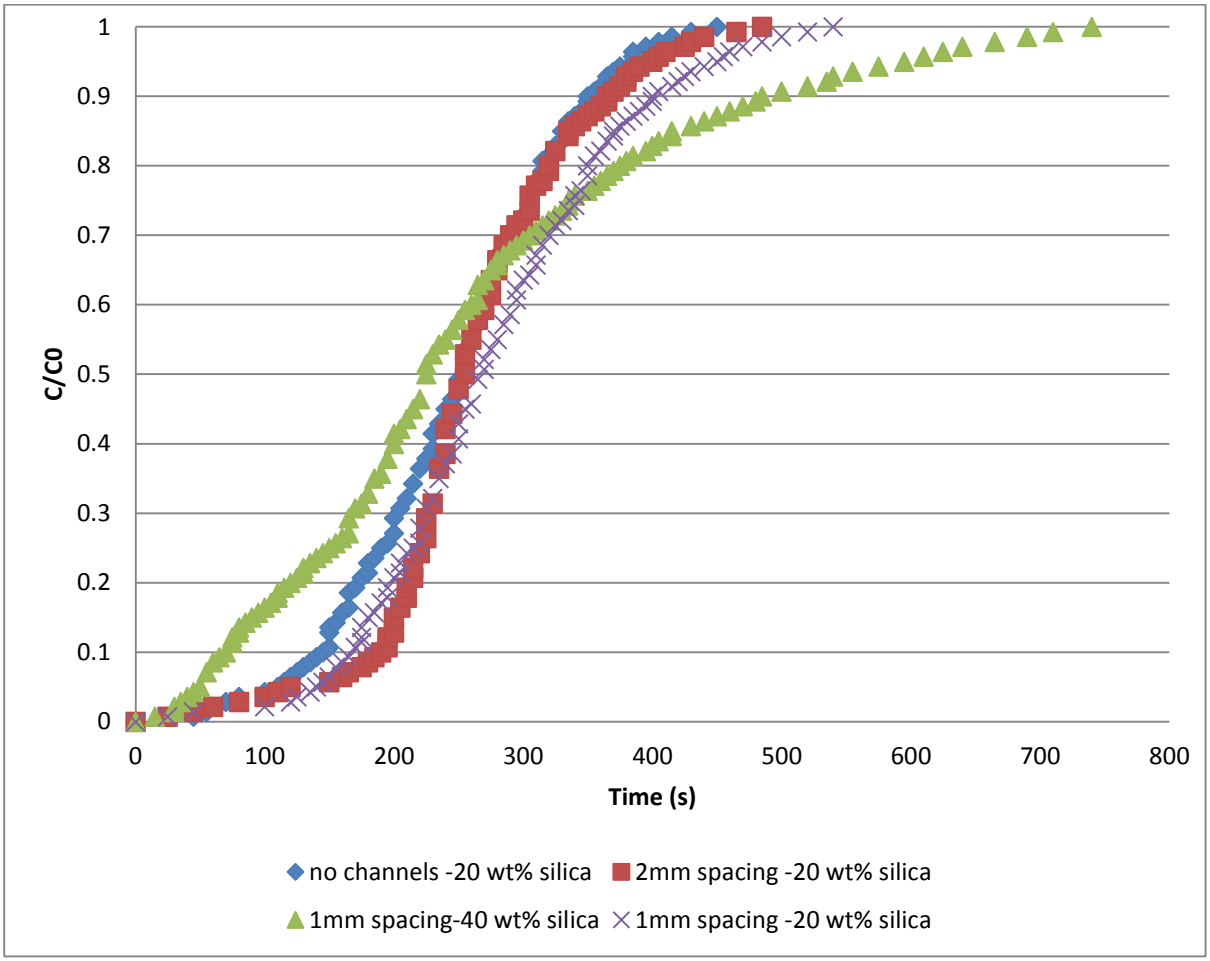

Figure 8.15: Breakthrough profiles at 250ml/min of laminate structures created via AKD printing

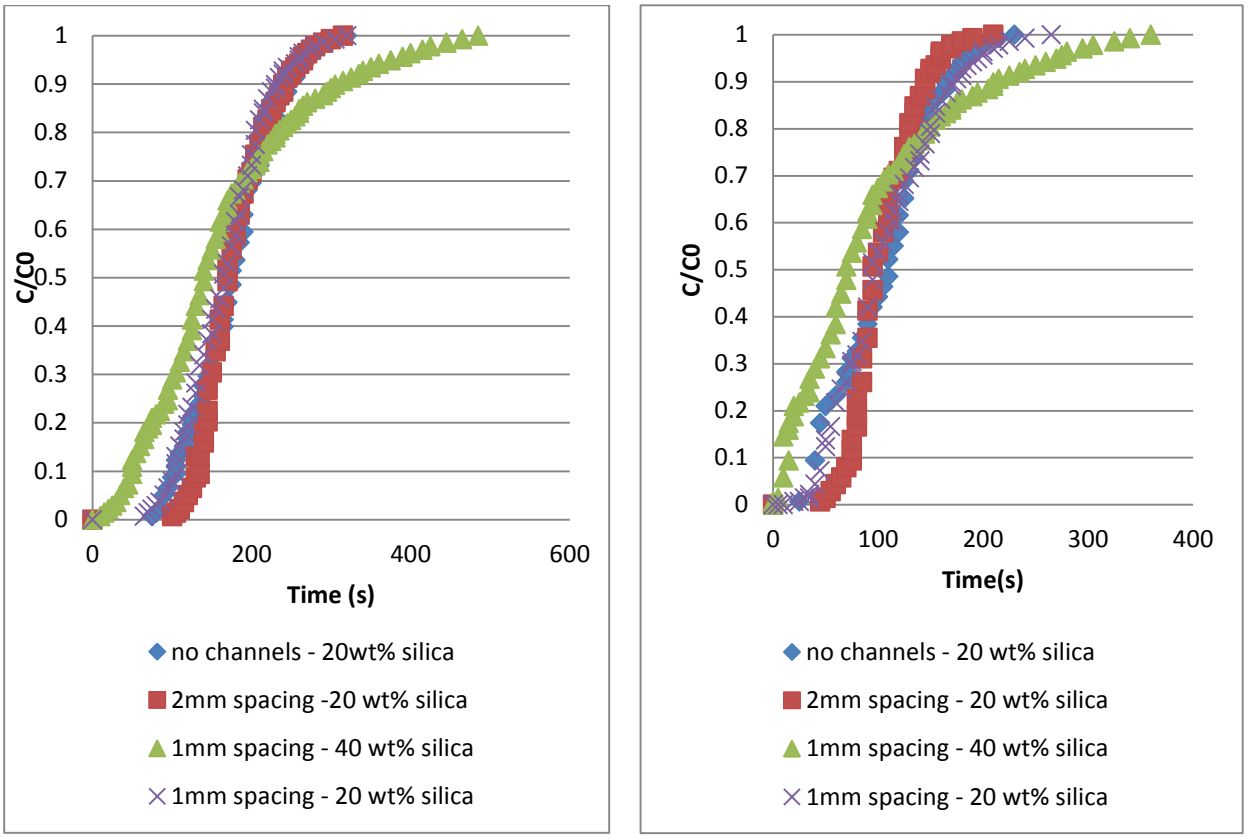

Figure 8.16: Breakthrough profiles at a)400ml/min and b)560ml/min of laminate structures created via AKD printing

8.4.2 Pressure drop measurements

The pressure drop measurements across the laminate adsorbent structures discussed in Section 8.4 are shown in Figure 8.17 for various flow rates of gas. The results were not quite as expected. The structure with no channels printed on it had the highest pressure drop, but all these structures had a lower pressure drop than any of the structures from the partial factorial table 3.5.7.1. This could be because the structure created here had a lower overall inorganic content when compared to the structures from the partial factorial design and this has increased the porosity of this structure. In comparison to the structure with no channels and 20wt% silica, the laminate structure with 1mm channels, 2mm spacing between channels and 20wt% silica has slightly lower pressure drop which shows that adding the parallel gas flow channels at such an increased spacing has not significantly improved the pressure drop

across the structure. Compared to both these samples, the laminate samples with 1mm channels widths and 1mm channel spacing have lower pressure drops for coating with either 20wt% or 40wt% silica.

It is expected that the sample with 40wt% silica should have higher pressure drop because the depth of the channels created by coating the samples with 40wt% silica is lower than the depth of the channels created by coating the samples with 20wt% silica and also, in general, the samples with 40wt% silica had lower porosity than samples coated with 20wt% silica. Although the pressure drop across both these samples with 1mm channel widths and 1mm channel spacing is the same, the breakthrough profiles for both these samples show that the gas was not evenly dispersed in the sample with 40wt% silica. This suggests that the sample with 40wt% silica had significant gas channelling in the structure which has given the same pressure drop as the sample with 20wt% silica but has significantly lowered the effective diffusivity of the sample.

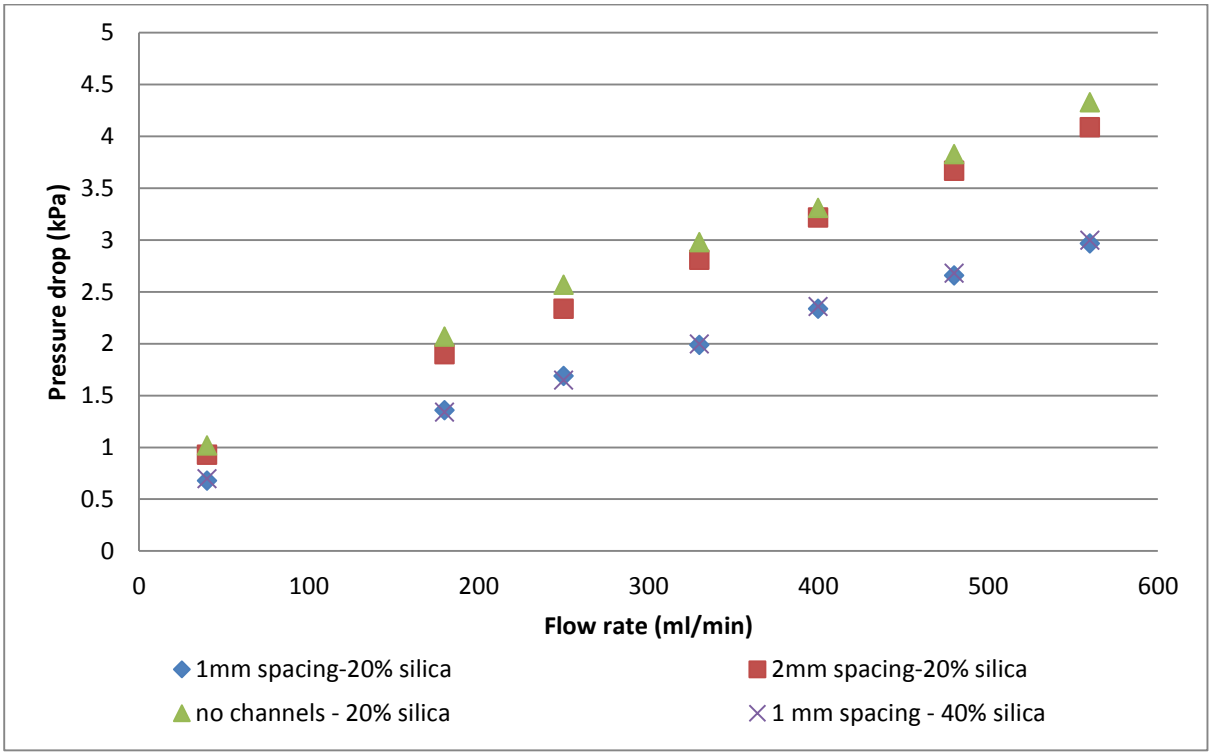

Figure 8.17: Pressure drop measurements across laminate structures created via AKD printing for different flow rates

8.4.3 Effective Diffusivity and Pressure drop measurements

The effective diffusivity was calculated using simulated breakthrough curves from numerical modelling described in Section 7.2.4. These values for the laminate structures both printed and not are plotted against the pressure drop across the laminate structures at a gas flow of 250ml/min in Figure 8.18. These values have also been compared against beads, as discussed in Section 7.2.2. The best adsorbent structure would give very high effective diffusivity values while maintaining a low pressure drop and a sharp breakthrough curve. The laminate structure which was not printed on has almost the same effective diffusivity but a much higher pressure drop when compared to the laminate structure with 1mm channels and 1mm spacing and 20wt% silica. The sample with 40wt% silica has the same pressure drop but lower effective diffusivity when compared to the same sample but with 20wt% silica. Hence, it is a matter of choosing between the sample with 1mm channel, 1mm spacing and 20wt% silica or 1mm channels, 2mm spacing and 20wt% silica which have lower pressure drop and lower diffusivity compared to higher pressure drop and higher diffusivity respectively.

The beads have the lowest effective diffusivity values but also have the lowest pressure drop across the column. But all of these structures have lower pressure drop and higher effective diffusivity when compared to the structures shown in Section 7.3.2 and Section 7.3.3, hence making these structures created via hydrophobic patterning highly favourable for further consideration as suitable adsorbent structures. These structures have slightly higher pressure drop when compared with samples with wires in between the layers, shown in Section 7.3.4, but their effective diffusivity is much higher. Also, the presence of proper parallel channels should create less chance of channelling and more chance for the gas to reach all the zeolite present in the structure when compared to a structure with wire, as proper channels better aid gas flow. These structures created via hydrophobic printing have zeolite loading of 39.4wt% and 46wt% for the samples with 40wt% and 20wt% silica, respectively. This loading is slightly lower than laminate structures manufactured from the partial factorial design, where

the loading was either 40wt% or 55wt%. However, the breakthrough properties show that this reduction in loading has had only negligible effect, as balanced with the reduction in pressure drop and increase in effective diffusivities produced by the channels created in these structures.

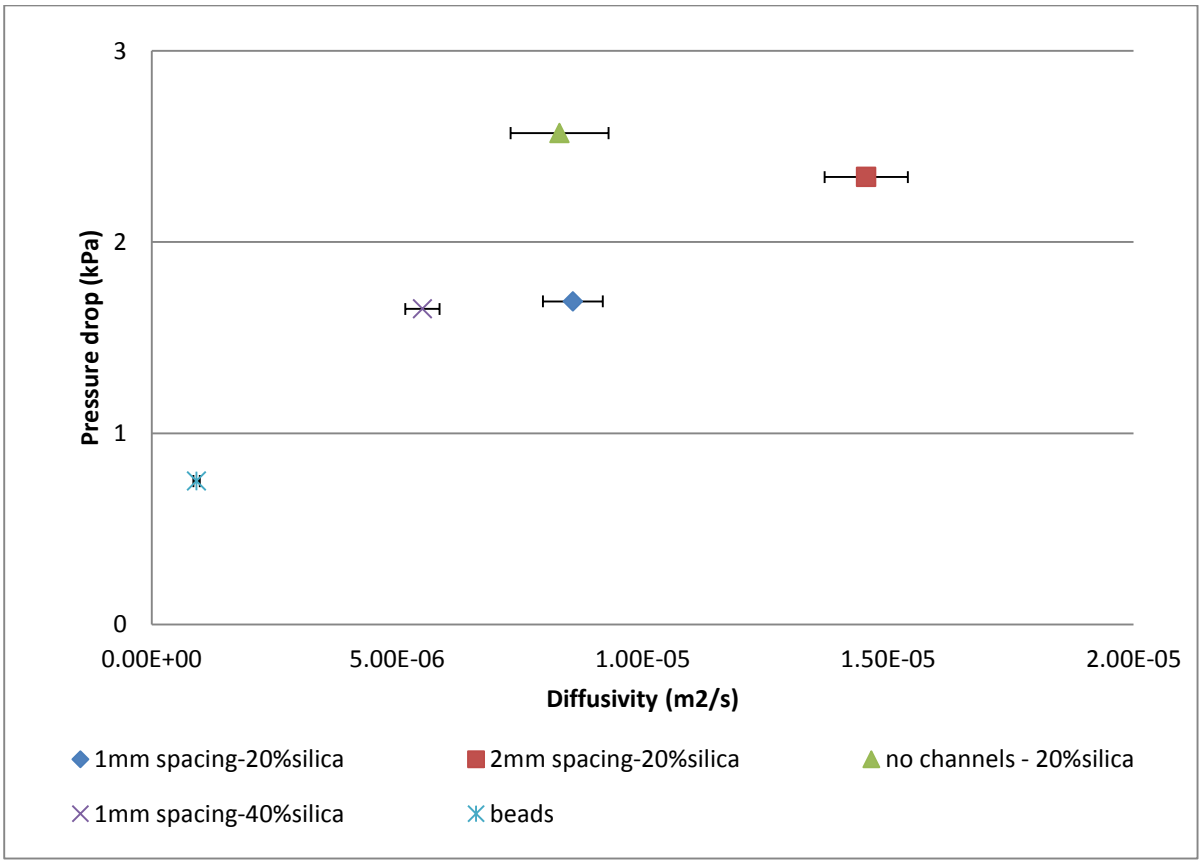

Figure 8.18: Pressure drop vs Effective Diffusivity for printed parallel laminate structures compared against beads

8.5 Conclusion

This chapter has shown that creating channels for gas flow through producing hydrophobic patterning via printing has reduced pressure drop, increased effective diffusivity and reduced the breakthrough curve width when compared to the laminate structures without channels. The laminates with channels also have higher diffusivity than conventional zeolite beads, although at the cost of a higher pressure drop.

The papermaking method was investigated for the work in this thesis for creating laminate structures due to the ease of mass production and lower costs of manufacture. The additional use of inkjet printing to create hydrophobic channels allows for a process that can be scaled very easily for industrial applications.

This page is intentionally blank

Chapter 9

Conclusions and Recommendations for Future Work

This page is intentionally blank

Chapter 9: Conclusions and Recommendations for Future Work

9.1 Conclusions

A simple and cheap papermaking technique has been successfully used to create laminate structured adsorbents. This technique used a minimum of materials and, through the papermaking process, reproduced many of the properties of commercial paper machines. This should make the scale up procedure straightforward. It was also found that none of the properties of the starting materials was affected due to processing during synthesis. A partial factorial design was found to be a good method to determine which synthesis variables affected the different characteristics of porosity, kinetics of adsorption and strength. The adsorption capacity of the laminate structured adsorbents can be found by measuring the carbon dioxide adsorption isotherms of the laminate structures against the zeolite powder as all the adsorption capacity of the structures results from the zeolite.

The mercury porosimetry results show that the initial silica concentration while making the sheet structures is the most important variable during synthesis that affects the porosity of the laminate structures. Having a low silica concentration of 20wt%, gave a more porous structure when compared to having 40wt% silica. Furthermore, each of the synthesis variables affected porosity in the structure at different levels, thereby making porosity tuneable. A novel method was developed to measure the strength of the laminate structures using a vibratory sieve. The strength results show that increasing the amount of ceramic fibres and silica concentration increases the strength of the structure. The presence of nano zeolite increased dusting and reduced retention; hence, the structures with micron zeolite were favoured. The most important variable that increased the strength of the laminate structures was again the initial silica concentration. This is because the structure with 40wt%

silica had more binding material in their structures when compared to structures with lower silica content. This is important because while the structure with different silica content had varied weight, it was only the ratio of reinforcement agent which was varied with the zeolite amount in the structure.

The kinetics of adsorption of carbon dioxide was also measured to characterise the zeolite laminate structures. The results show that the structures that had smaller zeolite particles exhibited faster kinetics. This is expected as having a smaller zeolite particle size allows the gas to reach the interior of the cell more quickly. But it was unexpected that the laminate structures showed better rate of adsorption when compared to powder samples. This was because the surface of the powder is more exposed than the bulk powder. With the laminate structures, almost all the zeolite particles are at the surface, which allows faster kinetics. From all the various characteristics analysed, it was found that the structures having between 40-55 wt% zeolite showed the best characteristics for breakthrough testing using carbon dioxide.

A solution was found to create an adsorbent column for the laminate structures of varying sizes using a heat shrink tube. The results from breakthrough performance testing show that the structures with higher porosity created using 20wt% silica have better performance in terms of effective diffusivity and pressure drop when compared to structures with lower porosity. In comparison to beads, the structures with high porosity have three to six times greater diffusivity but they have also have two to four times higher pressure drop. Considering the methods of improving the performance of the laminate structures by creating proper gas flow pathways, the use of the wire on high porosity structures with 20wt% silica, showed promising results. These results show that the structures with the wire in them have the same effective diffusivity as the structures without the wire but the pressure drop is lowered by four times. This means that the high porosity laminate structures with wire spacing show better performance than beads as their effective diffusivity has increased by three to six times while their pressure drop is almost equal. The laminate structures still have

issues with reproducibility as they are produced using manual methods but in an industrial setting, these issues should be minimal. The structures with wires will have difficulty being reproducible in an industrial setting as the thin metallic wire and the paper sheet cannot be wound together easily. Hence, other means to reproducibly manufacture laminate sheets with gas flow channels are required for consistent results.

To improve on the methods used to produce effective gas flow channels on the laminate structures, the hydrophobic printing technique was utilised. This method produced parallel flow channels as gas flow passageways. The results for effective diffusivity and pressure drop varied depending on the spacing distance between the channels and the initial amount of silica coating. These structures had better performance when compared to structures with no channels and the same amount of silica. Structures with 1mm spacing had the same effective diffusivity as structures with no channels and their pressure drop was 1.5 times lower than the structures with no channels. The structures with 2mm spacing had 1.5 times higher effective diffusivity and slightly reduced pressure drop when compared to structures with no channels. Hence, the hydrophobic printing technique was successfully used to create laminate structures with parallel channels. This method can be easily controlled for the scale up of laminate structure production methods. This results show that the laminate structures produced using papermaking methods are competitive alternatives to structured adsorbents like beads because they show high effective diffusivity, low pressure drop and better adsorption capacity when compared to other non-particulate structures.

9.2 Recommendations for Future Work

1. The breakthrough testing of the structures for carbon dioxide capture had many issues with reproducibility due to the manual production methods. Hence, it is suggested to use machine rolling so the spacing in the rolled structure is tighter and the results from the analysis are more consistent.

2. The use of nano zeolite for structured laminates increases adsorption kinetics but nano zeolites were not tested for breakthrough performance. It would be interesting to see the role of nano zeolite in breakthrough testing and nano zeolite 13X would provide good results for comparison of similar sheets as micron zeolite 13X.

3. It is recommended to perform cyclic testing of laminate sheet structures to see how the sheets perform in cyclic testing conditions.

4. The printed sheets can be further investigated by producing deeper channels with increased definitions and changing the printing designs to create different patterns and seeing their effects on the pressure drop and effective diffusivity of the sheet structures during breakthrough performance.

5. Finally, it is recommended to investigate the scale up performance of the laminate structures in a pilot plant during production and operation as structured adsorbents for carbon dioxide capture.

References

(1) Abu-Khader, M., - Recent progress in CO_2 capture/sequestration: A review, *Energy Sources, Part A: Recovery, Utilization and Environmental Effects*, **28**(14):1261-1279 (2006).

(2) Bárcia, P.S., Ferreira, A., Gascon, J., Aguado, S., Silva, J.C., Rodrigues, A.E., and Kapteijn, F., - Zeolite Beta membranes for the separation of hexane isomers, *Microporous and Mesoporous Materials*, **128**(1-3):194-202.

(3) Breck, D.W., - **Zeolite molecular sieves: structure, chemistry and use**, New York : Wiley(1974).

(4) Breck, D.W., Eversole, W.G., Milton, R.M., Reed, T.B., and Thomas, T.L., - Crystalline Zeolites. I. The Properties of a New Synthetic Zeolite, Type A, *Journal of the American Chemical Society*, **78**(23):5963-5972 (1956).

(5) Cecchini, J.P., Serra, R.M., Barrientos, C.M., Ulla, M.A., Galván, M.V., and Milt, V.G., - Ceramic papers containing Y zeolite for toluene removal, *Microporous and Mesoporous Materials*, **145**(1–3):51-58 (2011).

(6) Chabot, B. and Loranger, E., - Potentials of zeolite materials in the production of value-added papers, *International Paper and Coating Chemistry Symposium, Proceedings,* p 37-41 (2003).

(7) Coutinho, D. and Balkus, K.J., - Preparation and characterization of zeolite X membranes via pulsed-laser deposition, *Microporous and Mesoporous Materials*, **52**(2):79-91 (2002).

(8) Du, X. and Wu, E., - Porosity of microporous zeolites A, X and ZSM-5 studied by small angle X-ray scattering and nitrogen adsorption, *Journal of Physics and Chemistry of Solids*, **68**(9):1692-1699 (2007).

(9) Dunne, S.R., - Industrial Gas Phase Adsorptive Separations, **Zeolites in Industrial Separation and Catalysis**, Wiley-VCH Verlag p. 273-305, (2010).

(10) Funk, C.V. and Lloyd, D.R., - Zeolite-filled microporous mixed matrix (ZeoTIPS) membranes: Prediction of gas separation performance, *Journal of Membrane Science*, **313**(1-2):224-231 (2008).

(11) Holmes, S.M., Schmitt, M., Markert, C., Plaisted, R.J., Forrest, J.O., Sharratt, P.N., Garforth, A.A., Cundy, C.S., and Dwyer, J., - Zeolite A Membranes for Use in Alcohol/Water Separations: Part I: Experimental Investigation, *Chemical Engineering Research and Design*, **78**(8):1084-1088 (2000).

(12) Hu, C.-C., Liu, T.-C., Lee, K.-R., Ruaan, R.-C., and Lai, J.-Y., - Zeolite-filled PMMA composite membranes: influence of coupling agent addition on gas separation properties, *Desalination*, **193**(1-3):14-24 (2006).

(13) Kawamura, K., Aoike, N., Fumitoshi, N., and J, T., - Effects of natural zeolite filler on tracking in paper phenolic laminate, *Conference of electrial insulation and dielectric phenomena*, Institute of Electrical and Electronics Engineers (IEEE) Virginia, USA. , p. 527-532, (1990).

(14) Kazemimoghadam, M. and Mohammadi, T., - Preparation of NaA zeolite membranes for separation of water/UDMH mixtures, *Separation and Purification Technology*, **47**(3):173-178 (2006).

(15) McCusker, L., - International Zeolite Association, vol. 2012, http://www.iza-online.org/default.htm, (2012).

(16) Mumpton, F.A., - La roca magica: Uses of natural zeolites in agriculture and industry, *Proceedings of the National Academy of Sciences of the United States of America*, **96**(7):3463-3470 (1999).

(17) Pires, J., de Carvalho, M.B., Ribeiro, F.R., and Derouane, E.G., - Carbon dioxide in Y and ZSM-20 zeolites: Adsorption and infrared studies, *Journal of Molecular Catalysis*, **85**(3):295-303 (1993).

(18) Sakai, H., Tomita, T., and Takahashi, T., - p-Xylene separation with MFI-type zeolite membrane, *Separation and Purification Technology*, **25**(1-3):297-306 (2001).

(19) Dyer, A., - **An Introduction to Zeolite Molecular Sieves** vol. 14, John Wiley & Sons Ltd.(1989).

(20) Yin, X., Wang, J., Chu, N., Yang, J., Lu, J., Zhang, Y., and Yin, D., - Zeolite L/carbon nanocomposite membranes on the porous alumina tubes and their gas separation properties, *Journal of Membrane Science*, **348**(1-2):181-189.

(21) Yin, X., Zhu, G., Wang, Z., Yue, N., and Qiu, S., - Zeolite P/NaX composite membrane for gas separation, *Microporous and Mesoporous Materials*, **105**(1-2):156-162 (2007).

(22) Rezaei, F. and Webley, P., - Structured adsorbents in gas separation processes, *Separation and Purification Technology*, **70**(3):243-256.

(23) Berk, Z., - Chapter 12 - Adsorption and Ion Exchange, in Berk, Z., (Ed.) **Food Process Engineering and Technology** 2ed, Academic Press, San Diego, p. 311-327, (2013).

(24) Shivaji, S. and Alan, L.M., - Gas Separation by Zeolites, **Handbook of Zeolite Science and Technology**, CRC Press, (2003).

(25) Thomas, W.J. and Crittenden, B., - Chapter 1 - The development of adsorption technology, in Thomas, W.J. and Crittenden, B., (Eds.) **Adsorption Technology & Design**, Butterworth-Heinemann, Oxford, p. 1-7, (1998).

(26) Rezaei, F. and Webley, P.A., - Optimal design of engineered gas adsorbents: Pore-scale level, *Chemical Engineering Science*, **69**(1):270-278 (2012).

(27) Sy, A., - Special issue on: Accounting for global warming, *Critical Perspectives on Accounting*, **19**(4):431-434 (2008).

(28) Brouillette, F., Chabot, B., Morneau, D., and Daneault, C., - Effect of physico-chemical conditions on the properties of zeolite microparticles used in pulp and paper applications, *Microporous and Mesoporous Materials*, **70**(1-3):51-56 (2004).

(29) Quanchang, Z., Mingdi, S., Changlu, D., Huarui, Y., Qixing, Z., and Zhiguo, Z., - Use of Clinoptilolite in Paper Industry as Filler of Paper, *Studies in Surface Science and Catalysis*, **24**(C):531-538 (1985).

(30) Grönfors, J., - Use of fillers in paper and paperboard grades, Tampere University of Applied Sciences (2010).

(31) Ichiura, H., Kuboto, Y., Wu, Z., and Tanaka, H., - Preparation of zeolite sheets using a papermaking technique. Part 1 Dual polymer system for high retention of stock components, *Journal of Materials Science*, **36**:913-917 (2001).

(32) Sawada, J., Alizadeh-Khiavi, S., Roy, S., and Kuznicki, S. High Density Adsorbent structures.*US Patent 20050129952* (2005).

(33) Florides, G.A. and Christodoulides, P., - Global warming and carbon dioxide through sciences, *Environment International*, **35**(2):390-401 (2009).

(34) Alexiadis, A., - Global warming and human activity: A model for studying the potential instability of the carbon dioxide/temperature feedback mechanism, *Ecological Modelling*, **203**(3-4):243-256 (2007).

(35) Dutta, P.K. and Radner, R., - A strategic analysis of global warming: Theory and some numbers, *Journal of Economic Behavior & Organization*, **71**(2):187-209 (2009).

(36) Honjo, K., - R&D for technology to solve global warming, *Journal of Materials Processing Technology*, **59**(3):218-220 (1996).

(37) Kaya, Y., - The role of CO_2 fixation in the strategy for mitigating global warming, *Studies in Surface Science and Catalysis*, vol. 153, p. 555-560, (2004).

(38) Figueroa, J.D., Fout, T., Plasynski, S., McIlvried, H., and Srivastava, R.D., - Advances in CO_2 capture technology--The U.S. Department of Energy's Carbon Sequestration Program, *International Journal of Greenhouse Gas Control*, **2**(1):9-20 (2008).

(39) Feng, B., An, H., and Tan, E., - Screening of CO_2 adsorbing materials for zero emission power generation systems, *Energy and Fuels*, **21**(2):426-434 (2007).

(40) Olajire, A.A., - CO_2 capture and separation technologies for end-of-pipe applications - A review, *Energy*, **35**(6):2610-2628.

(41) Webb, P.A. and Orr, C., - **Analytical methods in Fine Particle Technology**, Micromeritics, United States of America (1997).

(42) Pini, R., - Interpretation of net and excess adsorption isotherms in microporous adsorbents, *Microporous and Mesoporous Materials*, **187**:40-52 (2014).

(43) Stadie, N.P., Murialdo, M., Ahn, C.C., and Fultz, B., - Anomalous Isosteric Enthalpy of Adsorption of Methane on Zeolite-Templated Carbon, *Journal of the American Chemical Society*, **135**(3):990-993 (2013).

(44) Stancheva, K.A., Bogdanov, B.I., and Georgiev, D.P., - Synthetic zeolites. structures, classification, properties, synthesis, industrial and environmental applications, *Oxidation Communications*, **34**(4):792-811 (2011).

(45) Kulprathipanja, S., - Aspects of Mechanisms, Processes, and Requirements for Zeolite Separation, **Zeolites in Industrial Separation and Catalysis**, Wiley-VCH Verlag p. 203-228, (2010).

(46) Grande, C.A. and Rodrigues, A.E., - Electric Swing Adsorption for CO_2 removal from flue gases, *International Journal of Greenhouse Gas Control*, **2**(2):194-202 (2008).

(47) Carr, D.A., Lach-hab, M., Yang, S., Vaisman, I.I., and Blaisten-Barojas, E., - Machine learning approach for structure-based zeolite classification, *Microporous and Mesoporous Materials*, **117**(1-2):339-349 (2009).

(48) McCusker, L.B. and Baerlocher, C., - Zeolite structures, **Studies in Surface Science and Catalysis**, vol. 168, p. 13-37, (2007).

(49) Thomas, W.J. and Crittenden, B., - Chapter 2 - Adsorbents, in Thomas, W.J. and Crittenden, B., (Eds.) **Adsorption Technology & Design**, Butterworth-Heinemann, Oxford, p. 8-30, (1998).

(50) Sayari, A., Belmabkhout, Y., and Serna-Guerrero, R., - Flue gas treatment via CO_2 adsorption, *Chemical Engineering Journal*, **171**(3):760-774 (2011).

(51) Krishna, R. and van Baten, J.M., - A comparison of the CO2 capture characteristics of zeolites and metal–organic frameworks, *Separation and Purification Technology*, **87**(0):120-126 (2012).

(52) Cheung, O., Bacsik, Z., Liu, Q., Mace, A., and Hedin, N., - Adsorption kinetics for CO_2 on highly selective zeolites NaKA and nano-NaKA, *Applied Energy*, **112**:1326-1336 (2013).

(53) Webb, P.A., -An Introduction to the Physical Characterisation of Materials by Mercury Intrusion Porosimetry with Emphasis on Reduction and Presenetation of Experimental Data, Micromeritics Instrument Corp, (2001).

(54) Meier, W.M. and Baerlocher, C., - Zeolite Type Frameworks: Connectivities, Configurations and Conformations, in Baerlocher, C., Bennett, J.M., Depmeier, W., Fitch, A.N., Jobic, H., Koningsveld, H., Meier, W.M., Pfenninger, A., and Terasaki, O., (Eds.) **Structures and Structure Determination**, vol. 2, *Molecular Sieves*, Springer Berlin Heidelberg, (1999).

(55) Flanigen, E.M., Broach, R.W., and Wilson, S.T., - Introduction, **Zeolites in Industrial Separation and Catalysis**, Wiley-VCH Verlag p. 1-26, (2010).

(56) Yang, R.T., - Zeolites and Molecular Sieves, **Adsorbents: Fundamentals and Applications**, John Wiley & Sons, New Jersey, p. 157-190, (2003).

(57) Baerlocher, C., McCusker, L., and Olson, D.H., - **Atlas of Zeolite Framework Types**, Elsevier(2007).

(58) McCusker, L.B., Liebau, F., and Englehardt, G., - Nomenclature of structural and compositional characteristics of ordered microporous and mesoporous materials with

inorganic hosts (IUPAC recommendations 2001): Physical chemistry Division commision on colloid and surface chemistry including catalysis, *Microporous and Mesoporous Materials*, **58**(1):3-13 (2003).

(59) - Alibaba.com, vol. 2012, http://www.alibaba.com/trade/search?fsb=y&IndexArea=product_en&CatId=&SearchText=natural+zeolite+powder, Ed., (2012).

(60) - Alibaba.com, vol. 2012, http://www.alibaba.com/trade/search?fsb=y&IndexArea=product_en&CatId=&SearchText=TiO2, Ed., (2012).

(61) Song, D., Dong, C., Ragauskas, A., and Deng, Y., - Filler Engineering for Energy Savings and Improved Paper Properties, *Tappi PaperCon Conference* p(2009).

(62) Reynolds, W.R. and Williford, C.W., - Zeolite and clay-mineral induced resistivity in simulated reservoir sand, *Journal of Petroleum Science and Engineering*, **5**(2):163-172 (1991).

(63) Fertu, D.I.T. and Gavrilescu, M., - Application of natural zeolites as sorbents in the clean-up of aqueous streams, *Environmental Engineering and Management Journal*, **11**(4):867-878 (2012).

(64) Kallo, D. and Sherry, H.S., - **Occurrence, properties and utilization of natural zeolites. Papers from the 2nd international conference, 1985**, Budapest : Akadémiai Kiadó(1988).

(65) Georgiev, D.P., Bogdanov, B.I., Angelova, K., Markovska, I., and Hristov, Y., - Synthetic zeolites -Structure, Classification, Current trends in zeolite synthesis a review, *International Science Conference,* (2009).

(66) Petrov, I. and Michalev, T., - Synthesis of Zeolite A: A Review, *Scientific Works of the University of Ruse*, vol. 51, http://conf.uni-ruse.bg/bg/docs/cp12/9.1/9.1-5.pdf, Bulgaria, (2012).

(67) Broach, R.W., - Zeolite Types and Structures, **Zeolites in Industrial Separation and Catalysis**, Wiley-VCH Verlag p. 27-59, (2010).

(68) Porcher, F., Dusausoy, Y., Souhassou, M., and Lecomte, C., - Epitaxial growth of zeolite X on zeolite A and twinning in zeolite A: structural and topological analysis, *Mineralogical Magazine*, **64**(1):1-8 (2000).

(69) Inui, T., Okugawa, Y., and Yasuda, M., - Relationship between properties of various zeolites and their carbon dioxide adsorption behaviors in pressure swing adsorption operation, *Industrial & Engineering Chemistry Research*, **27**(7):1103-1109 (1988).

(70) Mosca, A., Hedlund, J., Ridha, F., and Webley, P., - Optimization of synthesis procedures for structured PSA adsorbents, *Adsorption*, **14**(4-5):687-693 (2008).

(71) Mosca, A., Hedlund, J., Webley, P.A., Grahn, M., and Rezaei, F., - Structured zeolite NaX coatings on ceramic cordierite monolith supports for PSA applications, *Microporous and Mesoporous Materials*, **130**(1–3):38-48 (2010).

(72) Jaramillo, E. and Chandross, M., - Adsorption of Small Molecules in LTA Zeolites. 1. NH_3, CO_2, and H_2O in Zeolite 4A, *The Journal of Physical Chemistry B*, **108**(52):20155-20159 (2004).

(73) Reed, T.B. and Breck, D.W., - Crystalline Zeolites. II. Crystal Structure of Synthetic Zeolite, Type A, *Journal of the American Chemical Society*, **78**(23):5972-5977 (1956).

(74) Kim, C.H., Cho, S.H., and Park, W.P.O., - Inhibitory effect of functional packaging papers containing grapefruit seed extracts and zeolite against microbial growth, *Appita Journal*, **58**(3):202-207 (2005).

(75) McCusker, L.B. and Baerlocher, C., - Chapter 3 Zeolite structures, in Bekkum, v.H., Flanigen, E.M., Jacobs, P.A., and Jansen, J.A., (Eds.) **Studies in Surface Science and Catalysis**, vol. Volume 137, Elsevier p. 37-67, (2001).

(76) Moreno-Castilla, C. and Pérez-Cadenas, A., - Carbon-Based Honeycomb Monoliths for Environmental Gas-Phase Applications, *Materials*, **3**(2):1203-1227 (2010).

(77) - Sorbead India, vol. 2013, http://www.indiamart.com/sorbeadindia/latesttradeoffer.html.

(78) Hubbe, A.M., - How do retention aids work?, *Papermakers Conference,* Tappi, (1988).

(79) Gill, R.A., - Tappi- Introduction to Wet End Chemistry: Fillers for papermaking, Norcross, U.S.(2005).

(80) Klass, P.C. and Sikora, D.M. High performance natural zeolite microparticle retention aid for papermaking.*United States Patent US 7201826 B2* (2007).

(81) Ivanov, K., Gruber, E., Schemp, W., and Kirov, D., - Possibilities of using zeolites as filler and carrier for dyestuffs in paper, *Das Papier*, **50**(7):456-460.

(82) Ivanov, K., - Aging of Paper filled with zeolite, *Wochenblatt Fier Papierfabrikation*, **126**(16):739-741 (1998).

(83) Rock, L.S. Pigment system for paper.*United States Patent US4752341* (1988).

(84) Huang, X., Shen, J., and Qian, X., - Filler modification for papermaking with starch/oleic acid complexes with the aid of calcium ions, *Carbohydrate Polymers*, **98**(1):931-935 (2013).

(85) Gamelas, J.A.F., Lourenço, A.F., Xavier, M., and Ferreira, P.J., - Modification of precipitated calcium carbonate with cellulose esters and use as filler in papermaking, *Chemical Engineering Research and Design*.

(86) Ovenden, C. and Xiao, H., - Flocculation behaviour and mechanisms of cationic inorganic microparticle/polymer systems, *Colloids and Surfaces A: Physicochemical and Engineering Aspects*, **197**(1–3):225-234 (2002).

(87) Ko, S., Pekarovic, J., Fleming, P.D., and Ari-Gur, P., - High performance nano-titania photocatalytic paper composite. Part I: Experimental design study for TiO_2 composite sheet using a natural zeolite microparticle system and its photocatalytic property, *Materials Science and Engineering: B*, **166**(2):127-131 (2010).

(88) Daneault, C., Sain, M., and Grondin, G., - The modified zeoilte in waste paper recycling: shows promise to chelate metals and stabilize peroxide in repulping process, *Pulp and Paper Canada*, **99**(7) (1998).

(89) Shen, J., SONG, Z., QIAN, X., and Zhang, Y. Method for the preparation of acid-tolerant calcium carbonate fillers and filled paper based on high-lignin-content deinked pulp derived from recycled newspaper.*US Patent 20120111520 A1* (2012).

(90) Chabot, B. and Loranger, E., - Potentials of zeolite materials in the production of value added paper, *5th international paper and coating chemistry symposium,* Pulp and Paper Technical Association of Canada, p 37-41 (2003).

(91) Daneault, C., Chabot, B., and Thibodeau, J., - Calcium ion removal by a synthetic zeolite in the manufacture of mechanical grade papers, *Pulp and Paper Canada*, **106**(3) (2005).

(92) Ichiura, H., Okamura, N., Kitaoka, H., and Tanaka, H., - Preparation of zeolite sheet using a papermaking technique; Part 2: The strength of zeolite sheet and its hygroscopic characteristics, *Journal of Materials Science*, **36**:4921-4926 (2001).

(93) Ichiura, H., Nozaki, M., Kitaoka, T., and Tanaka, H., - Influence of uniformity of zeolite sheets prepared using a papermaking technique on VOC adsorptivity, *Advances in Environmental Research*, **7**(4):975-979 (2003).

(94) Yoo, Y.J., Kim, H.S., and Han, M.H., - Toluene and Methyl Ethyl Ketone adsorption behavior of the adsorption system using honeycomb adsorption rotor, *Separation Science and Technology*, **40**(8):1635-1651 (2005).

(95) Cecchini, J.P., Serra, R.M., Ulla, M.A., Zanuttini, M.A., and Milt, V.G., - Enhancing Mechanical Properties of Ceramic Papers Loaded with Zeolites using Borate Compounds as Binders, *Bioresources*, **8**(1):313-326 (2013).

(96) Ichiura, H., Kitaoka, T., and Tanaka, H., - Preparation of composite TiO_2-zeolite sheets using a papermaking technique and their application to environmental improvement: Part I Removal of acetaldehyde with and without UV irradiation, *Journal of Materials Science*, **37**(14):2937-2941 (2002).

(97) Ichiura, H., Kitaoka, T., and Tanaka, H., - Removal of indoor pollutants under UV irradiation by a composite TiO_2-zeolite sheet prepared using a papermaking technique, *Chemosphere*, **50**(1):79-83 (2003).

(98) Ichiura, H., Kitaoka, T., and Tanaka, H., - Preparation of composite TiO_2-zeolite sheets using a papermaking technique and their application to environmental improvement: Part II. Effect of zeolite coexisting in the composite sheet on NO_x removal, *Journal of Materials Science*, **38**(8):1611-1615 (2003).

(99) Ko, S., Fleming, P.D., Joyce, M., and Ari-Gur, P., - High performance nano-titania photocatalytic paper composite. Part II: Preparation and characterization of natural zeolite-based nano-titania composite sheets and study of their photocatalytic activity, *Materials Science and Engineering: B*, **164**(3):135-139 (2009).

(100) Liu, L., Singh, R., Xiao, P., Webley, P., and Zhai, Y., - Zeolite synthesis from waste fly ash and its application in CO_2 capture from flue gas streams, *Adsorption*, **17**(5):795-800 (2011).

(101) Wang, H., Holmberg, B.A., and Yan, Y., - Synthesis of Template-Free Zeolite Nanocrystals by Using in Situ Thermoreversible Polymer Hydrogels, *Journal of the American Chemical Society*, **125**(33):9928-9929 (2003).

(102) Tao, W., Yang, T., Chang, Y., Chang, L., and Chung, T., - Effect of Moisture on the Adsorption of Volatile Organic Compounds by Zeolite, *Journal of Environmental Engineering*, **130**(10):1210-1216 (2004).

(103) Lidén, E., Karlsson, S., and Tokarz, B., - Silica sols as refractory fibre binders, *Journal of the European Ceramic Society*, **21**(6):795-808 (2001).

(104) Oliveira M, Tejado A, and T.G.M, V.d.V., - Effects of fillers on the wet-web strength of paper, *Nordic Pulp and Paper research*, **24**(2):141-147 (2009).

(105) Alince, B. and Bednar, F., - Role of cationic polyacrylamide in fiber-$CaCO_3$ pigment interactions, *Journal of Applied Polymer Science*, **88**(10):2409-2415 (2003).

(106) - Sigma Aldrich - Material Safety Data Sheet, (2014).

(107) Xu, L. and Parker, I., - Simulating the forming process with the moving belt drainage former, *APPITA Annual General Conference*, **1**:169-173 (1999).

(108) Mitchell, C., Parker, I., and Johnston, R., - Development of the Moving Belt Sheet Former/Drainage Tester, *APPITA Annual General Conference,* p 287-292 (2002).

(109) Lönnberg, B., - **Mechanical pulping**, vol. 5, 2nd ed, Finnish Paper Engineer's Association,Tappi and Fapet Oy, Finland (2009).

(110) Fardim, P., - **Chemical Pulping Part 1:Fibre Chemistry and Technology**, vol. 6, 2nd ed, Finnish Paper Engineer's Association, Tappi and Fapet Oy, Finland (2009).

(111) Rouquerol, F., Rouquerol, J., and Sing, K., - Chapter 1 - Introduction, in Rouquerol, F., Rouquerol, J., and Sing, K., (Eds.) **Adsorption by Powders and Porous Solids**, Academic Press, London, p. 1-26, (1999).

(112) Bergins, C., Hulston, J., Strauss, K., and Chaffee, A.L., - Mechanical/thermal dewatering of lignite. Part 3: Physical properties and pore structure of MTE product coals, *Fuel*, **86**(1–2):3-16 (2007).

(113) Caulfield, D.F. and Gunderson, D.E., - Paper testing and strength characteristics, *Paper Preservation Symposium*, Press, T., Ed., TAPPI Press Washington, United States, (1998).

(114) Kruml, T. and Michel, J.-P., - Mechanical testing of materials Ecole des Mines de Nancy, (2005).

(115) Laval Lab Inc, - Ro-Tap Sieve Shakers, (2012).

(116) Thomas, W.J. and Crittenden, B., - Chapter 4 - Rates of adsorption of gases and vapours by porous media, in Thomas, W.J. and Crittenden, B., (Eds.) **Adsorption Technology & Design**, Butterworth-Heinemann, Oxford, p. 66-95, (1998).

(117) Wernert, V., Bouchet, R., and Denoyel, R., - Influence of the structure of mesoporous adsorbents on transport properties, *Microporous and Mesoporous Materials*, **140**(1–3):97-102 (2011).

(118) Webley, P. and Todd, R., - Kinetics of Mixed Adsorbent Systems in Gas–Solid Adsorption, *Adsorption Science & Technology*, **21**(1):9-34 (2003).

(119) Li, G., Singh, R., Li, D., Zhao, C., Liu, L., and Webley, P.A., - Synthesis of biomorphic zeolite honeycomb monoliths with 16 000 cells per square inch, *Journal of Materials Chemistry*, **19**(44):8372-8377 (2009).

(120) Monazam, E.R., Spenik, J., and Shadle, L.J., - Fluid bed adsorption of carbon dioxide on immobilized polyethylenimine (PEI): Kinetic analysis and breakthrough behavior, *Chemical Engineering Journal*, **223**:795-805 (2013).

(121) Mulgundmath, V.P., Jones, R.A., Tezel, F.H., and Thibault, J., - Fixed bed adsorption for the removal of carbon dioxide from nitrogen: Breakthrough behaviour and modelling for heat and mass transfer, *Separation and Purification Technology*, **85**:17-27 (2012).

(122) García, S., Gil, M.V., Martín, C.F., Pis, J.J., Rubiera, F., and Pevida, C., - Breakthrough adsorption study of a commercial activated carbon for pre-combustion CO2 capture, *Chemical Engineering Journal*, **171**(2):549-556 (2011).

(123) Wang, L., - Spreading of AKD and ASA in Early Stage of Paper Sizing, Monash University, (2009).

(124) Walter, H., Albro, S., Albro, T., Ash, N., Baker, C., Barger, S., Barrett, T., Dwan, A., Espinosa, R., Garlick, K., Hamburg, D., Meier-james, B., Munn, J., Nicholson, K., Orlenko, K., and Vitale, T., - Sizing, **Paper Conservation Catalog**, 5 ed, American Institute of Conservation Book and Paper Group, Washingtong DC, (1988).

(125) Lindström, T. and LarssonLind, T., - Alkyl Ketene Dimer (AKD) sizing - a review, *Nordic Pulp and Paper research*, **23**(2):202-209 (2008).

(126) Li, X., Tian, J., Garnier, G., and Shen, W., - Fabrication of paper-based microfluidic sensors by printing, *Colloids and Surfaces B: Biointerfaces*, **76**(2):564-570 (2010).

(127) Li, X., Ballerini, D.R., and Shen, W., - A perspective on paper-based microfluidics: Current status and future trends, *Biomicrofluidics*, **6**(1):- (2012).

This page is intentionally blank

Appendix I-SEM Images

SEM Images of sample having low silica content, high ceramic content with nano zeolite and 22nm silica

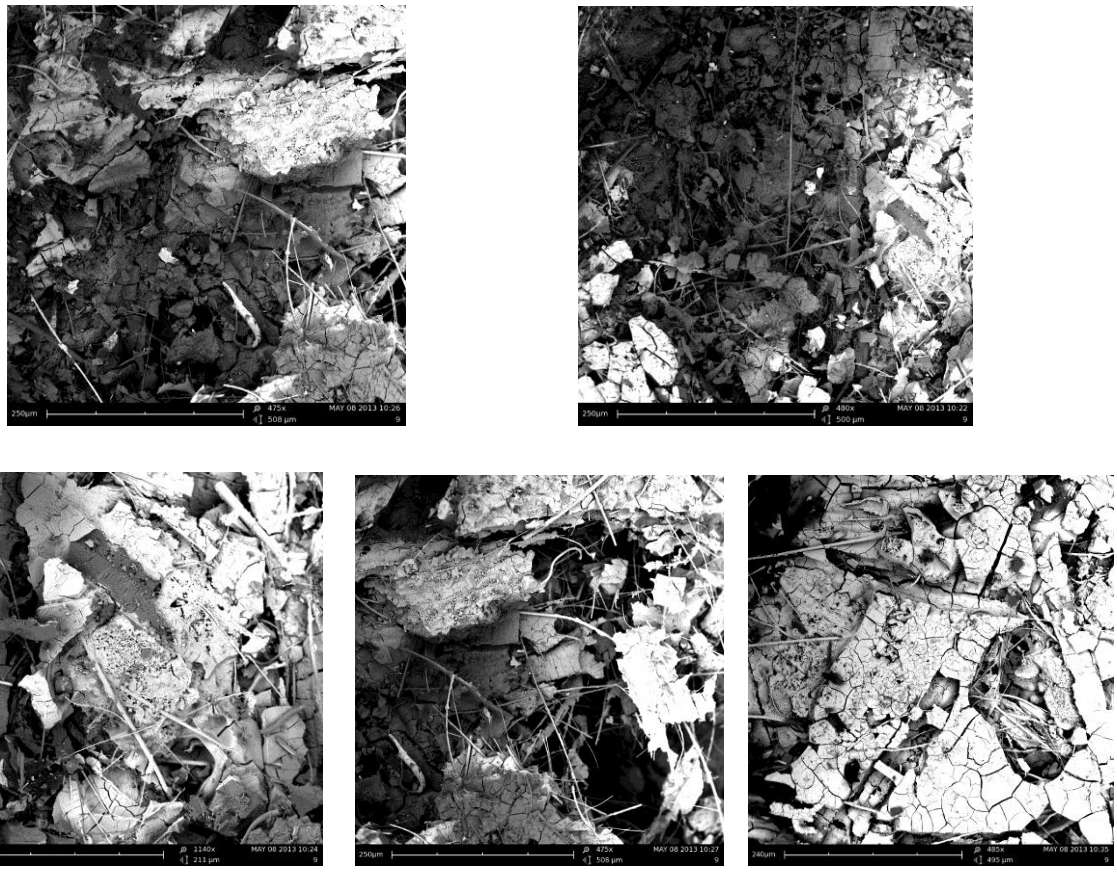

Figure I-1: Sample made from 20wt%, 22nm silica, 1:1 ceramic to nano zeolite with Kraft pulp at a)475X b)480X c)1149X d)475X e)485X showing different sections of the sample

SEM Images of sample having low silica content, high ceramic content, micron zeolite and 22nm silica

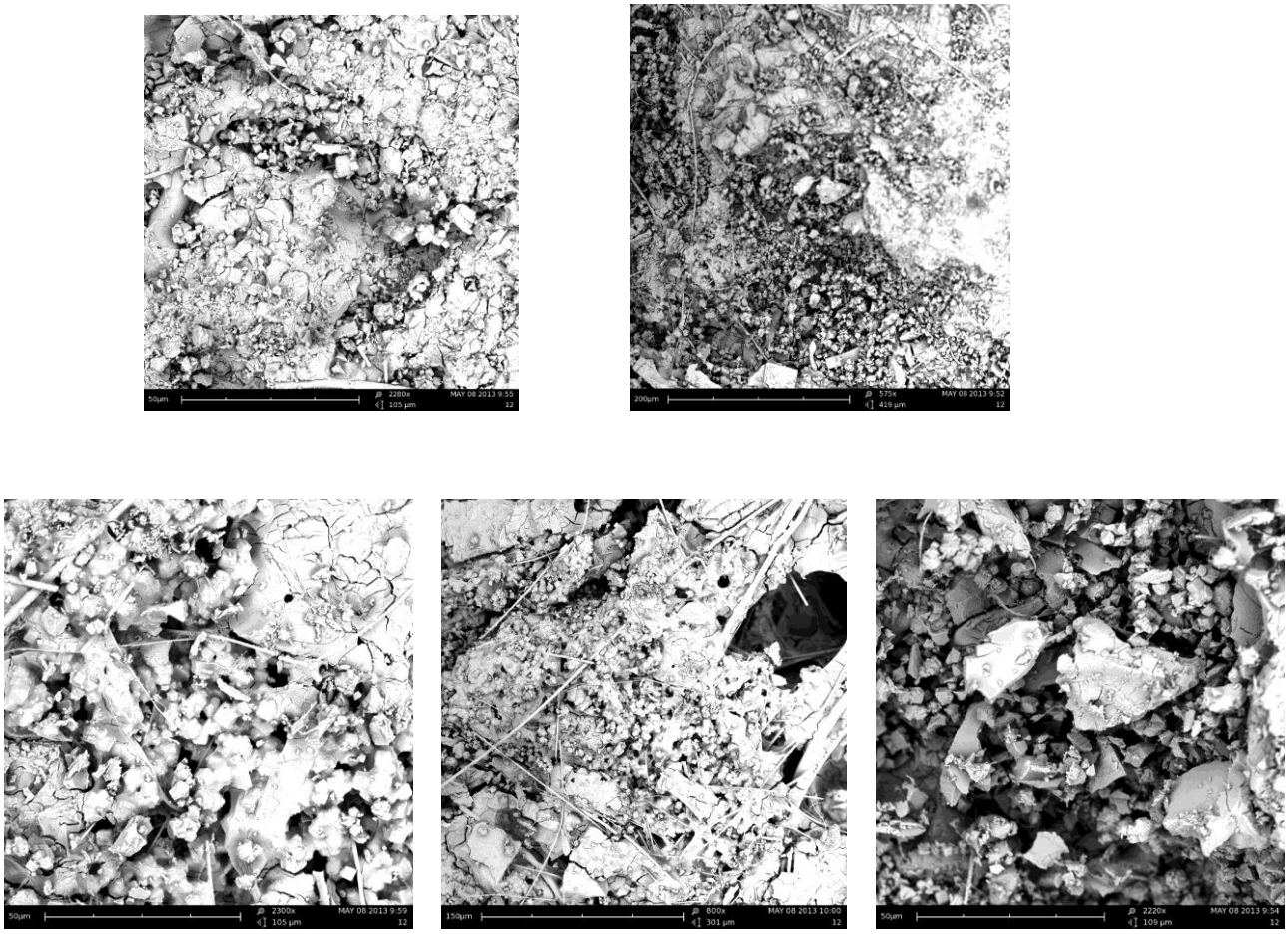

Figure I-2: Sample made from 20wt%, 22nm silica, 1:1 ceramic fibres to micron zeolite and TMP pulp at a)2280X b)575X c)2300X d)800X e)2220X showing different sections of the sample

SEM Images of sample having high silica content, high ceramic content, nano zeolite and 120nm silica

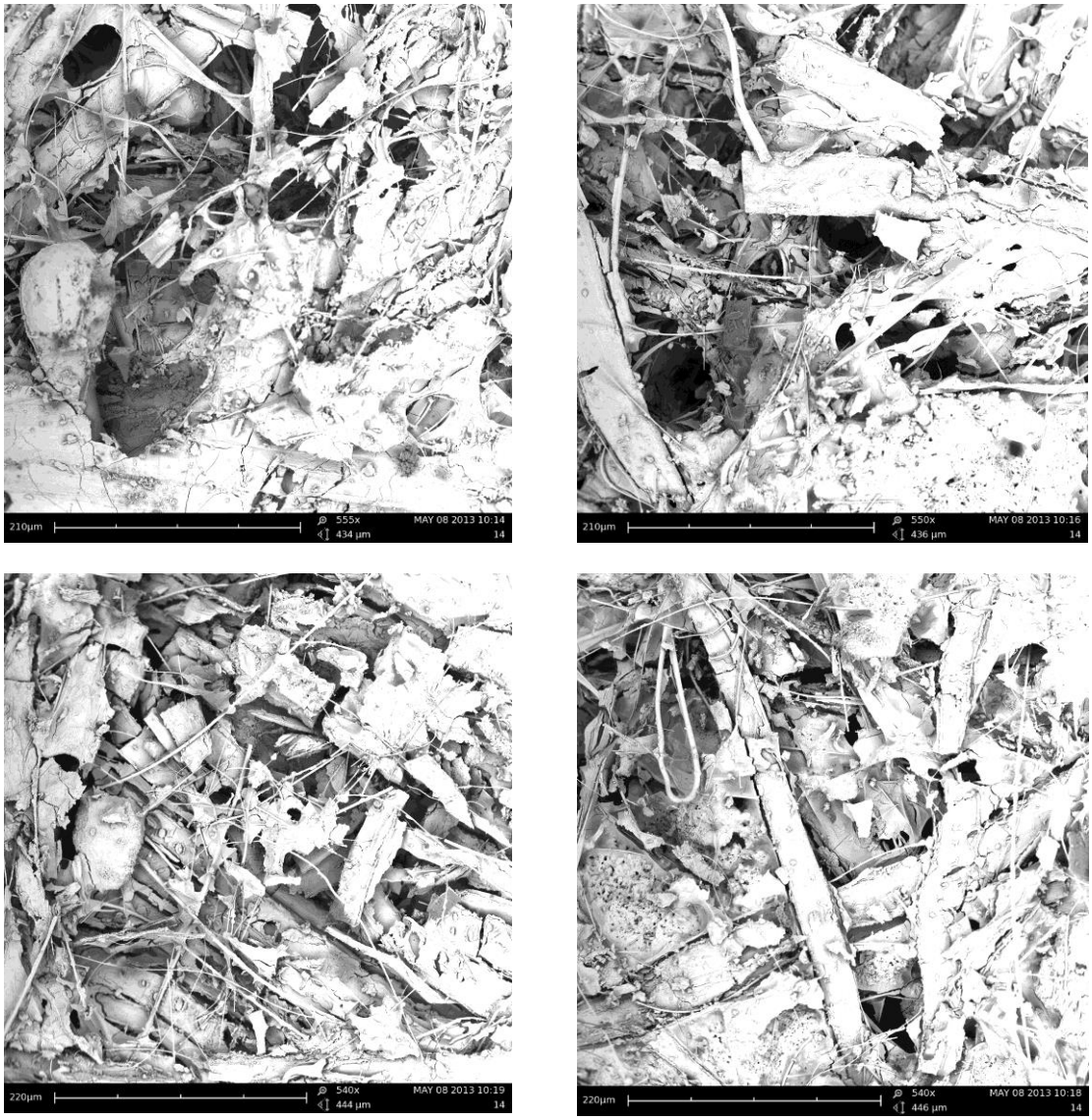

Figure I-3: Sample made from 40wt%, 120nm silica, 1:1 ceramic fibres to nano zeolite and Kraft pulp at a)555X b)550X c)540X d)540X showing different sections of the sample

SEM Images of sample having high silica content, low ceramic content, micron zeolite and 22nm silica

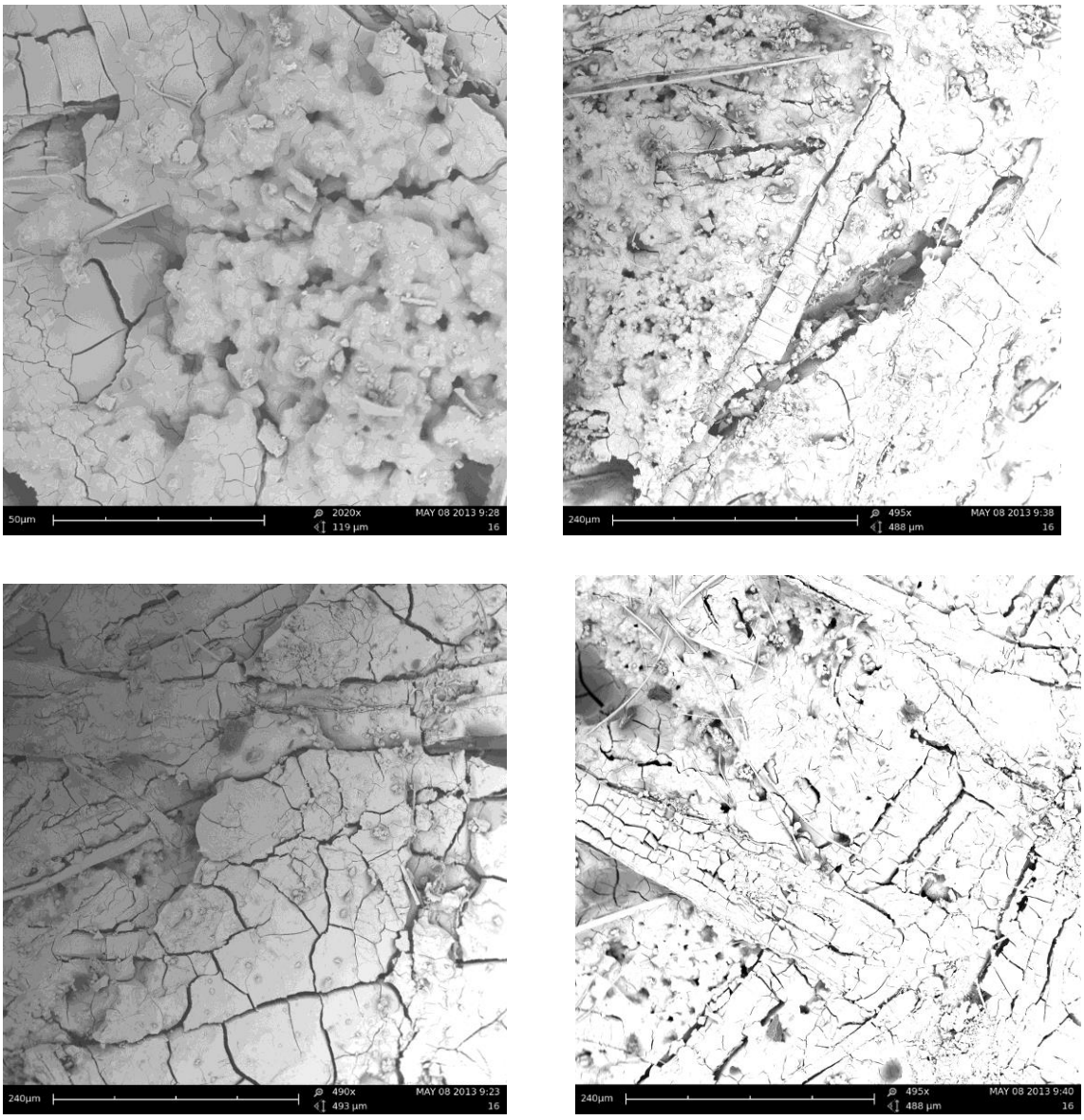

Figure I-4: Sample made from 40et%, 22nm silica, 0.08:1 ceramic fibres to micron zeolite and Kraft pulp at a)2020X b)495 c)490X d)495X showing different sections of the sample

This page is intentionally blank

Appendix II-Breakthrough data

Table II-1: Parameters listed for two different gases for each of the samples in Table 7.1

No	m_1 (CO_2) (mmol/g)	m_2 (CO_2) (mmol/g)	b_1 (CO_2) (1/bar)	b_2 (CO_2) (1/bar)	m_1 (N_2) (mmol/g)	m_2 (N_2) (mmol/g)	b_1 (N_2) (1/bar)	b_2 (N_2) (1/bar)
1	1.1	1.69	1.20E-07	4.51E-07	26.52	0.019	2.28E-04	4.22E-142
2	1.16	1.77	1.20E-07	4.51E-07	27.92	0.02	2.28E-04	4.22E-142
3	0.95	1.55	1.20E-07	4.51E-07	0.19	147.8	2.28E-04	4.22E-142
4	0.65	1	1.20E-07	4.51E-07	15.71	0.011	2.28E-04	4.22E-142
5	0.73	1.12	1.20E-07	4.51E-07	17.62	0.012	2.28E-04	4.22E-142
6	0.93	1.42	1.20E-07	4.51E-07	22.42	0.016	2.28E-04	4.22E-142
7	1.16	1.78	1.20E-07	4.51E-07	28.01	0.02	2.28E-04	4.22E-142
8	1	1.54	1.20E-07	4.51E-07	24.17	0.017	2.28E-04	4.22E-142
9	1.21	1.86	1.20E-07	4.51E-07	29.23	0.021	2.28E-04	4.22E-142
10	0.7	1.07	1.20E-07	4.51E-07	16.84	0.012	2.28E-04	4.22E-142
11	0.88	1.35	1.20E-07	4.51E-07	21.29	0.015	2.28E-04	4.22E-142

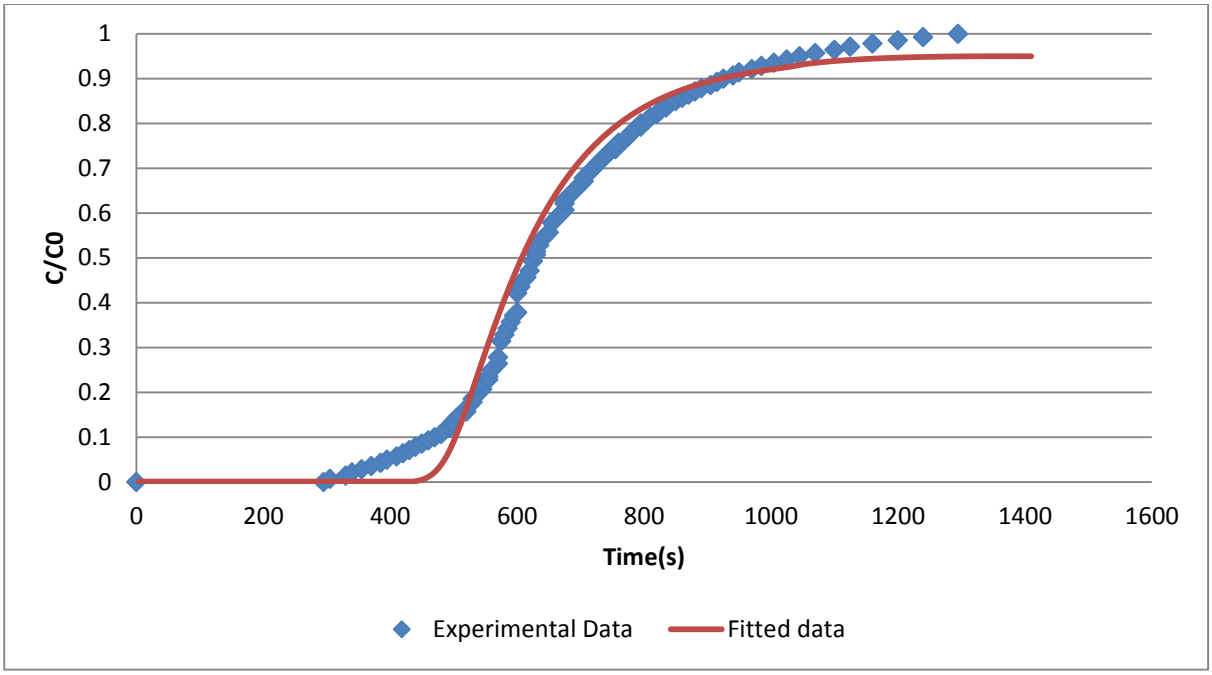

Figure II-1: Comparison of the experimental (symbols) and simulated (solid) breakthrough profiles of laminate structure number 1 from Table 7.1

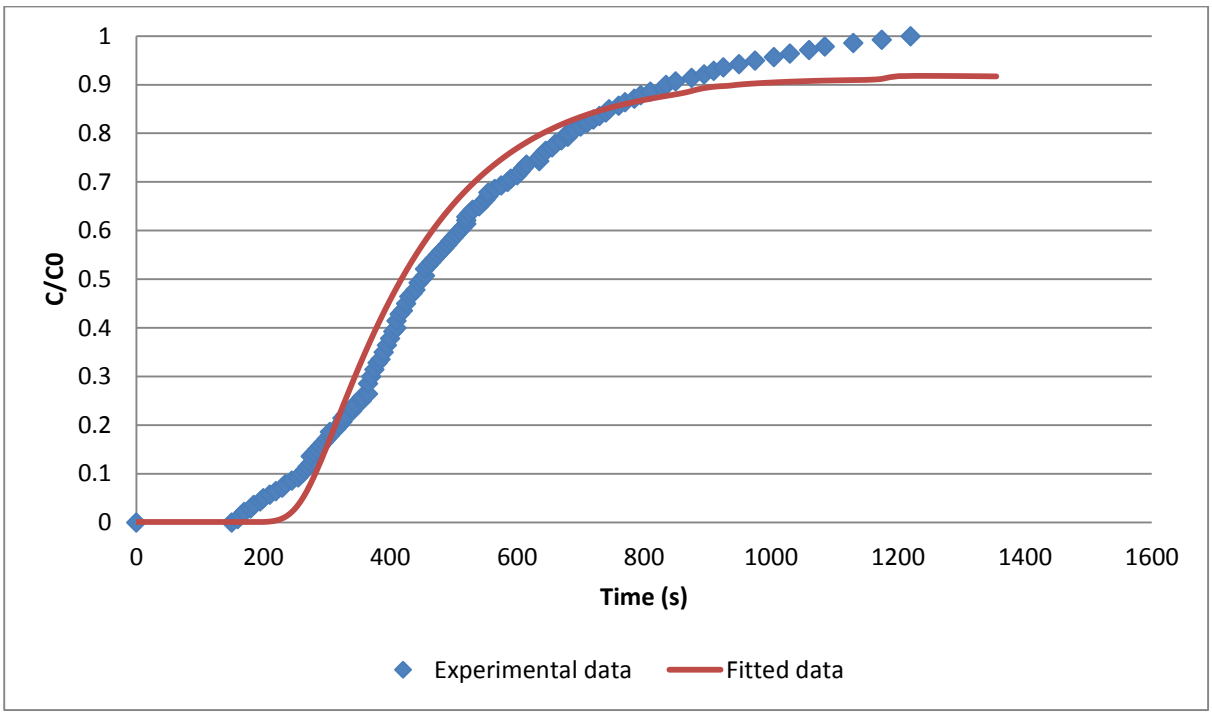

Figure II-2: Comparison of the experimental (symbols) and simulated (solid) breakthrough profiles of laminate structure number 2 from Table 7.1

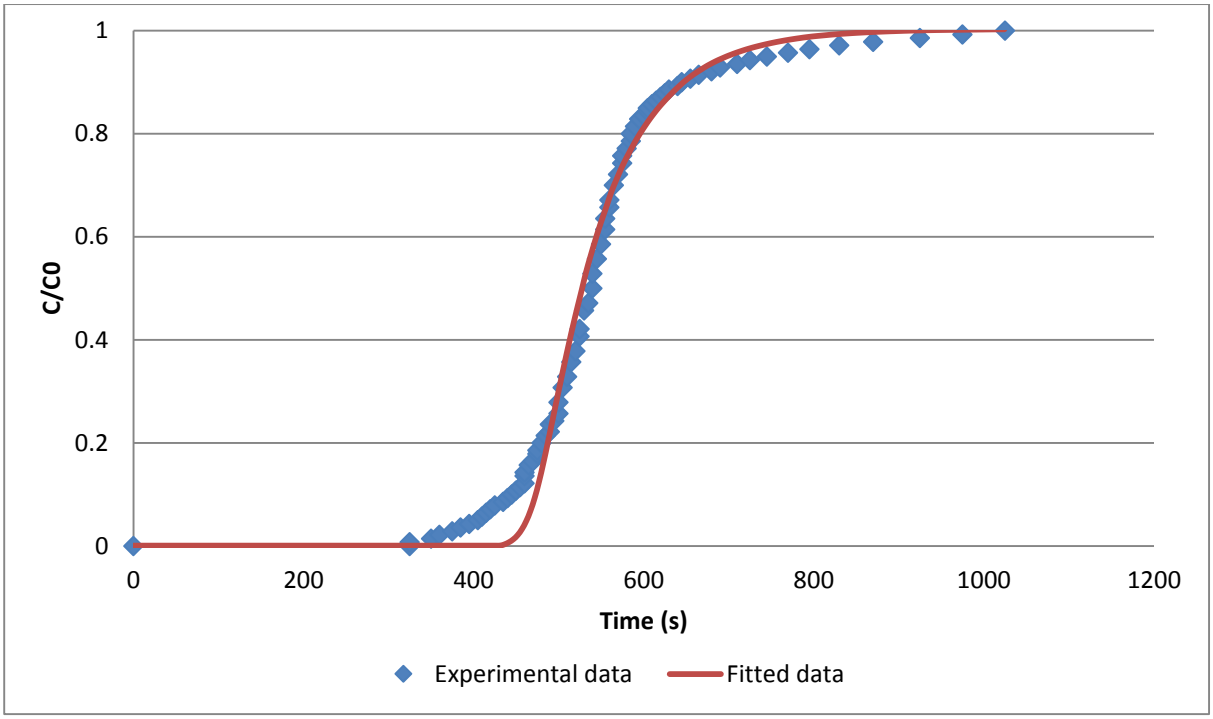

Figure II-3: Comparison of the experimental (symbols) and simulated (solid) breakthrough profiles of laminate structure number 3 from Table 7.1

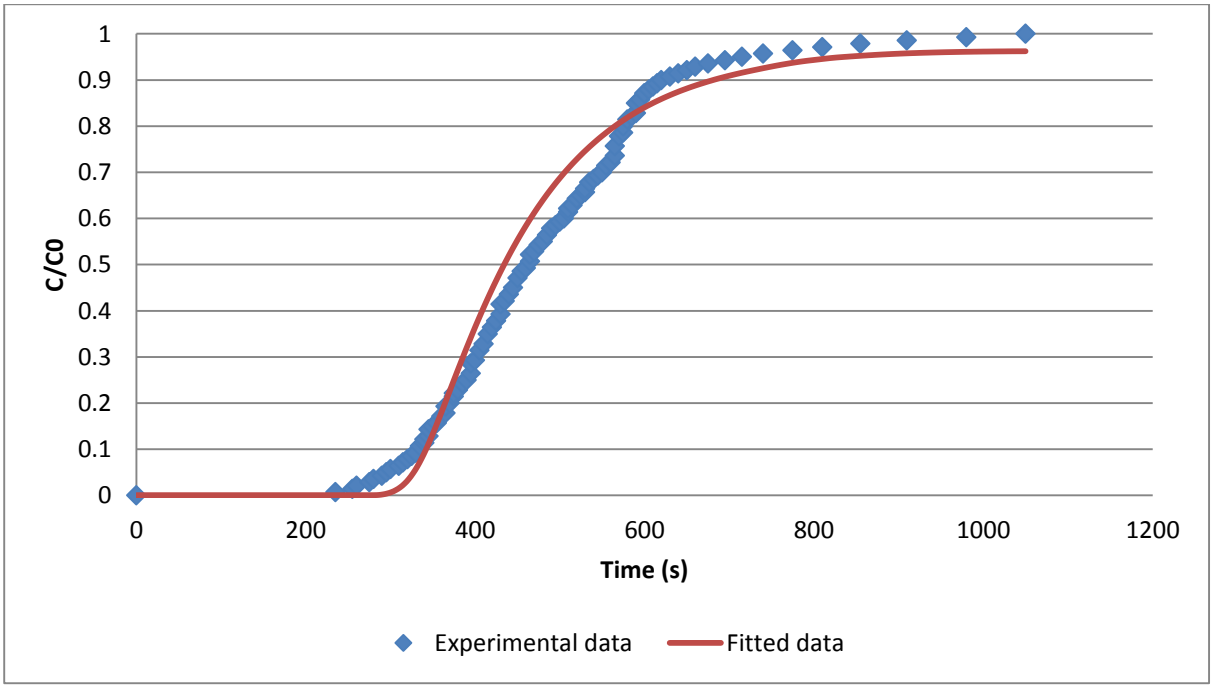

Figure II-4: Comparison of the experimental (symbols) and simulated (solid) breakthrough profiles of laminate structure number 4 from Table 7.1

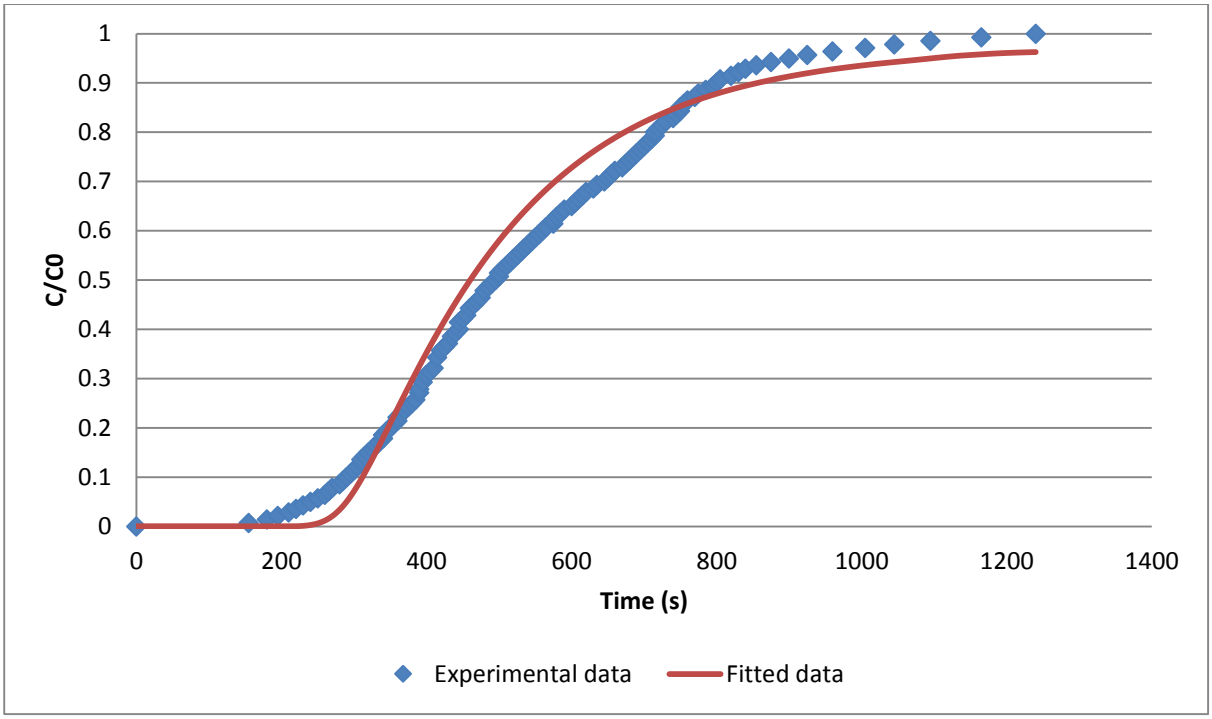

Figure II-5: Comparison of the experimental (symbols) and simulated (solid) breakthrough profiles of laminate structure number 5 from Table 7.1

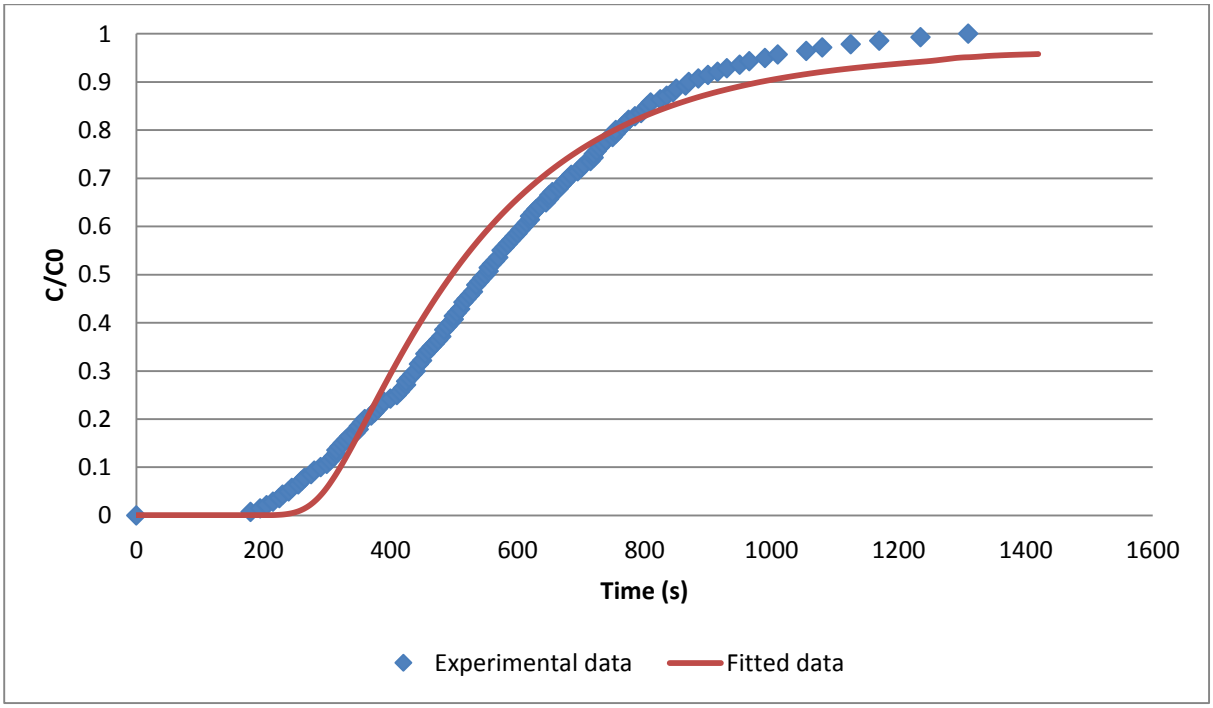

Figure II-6: Comparison of the experimental (symbols) and simulated (solid) breakthrough profiles of laminate structure number 6 from Table 7.1

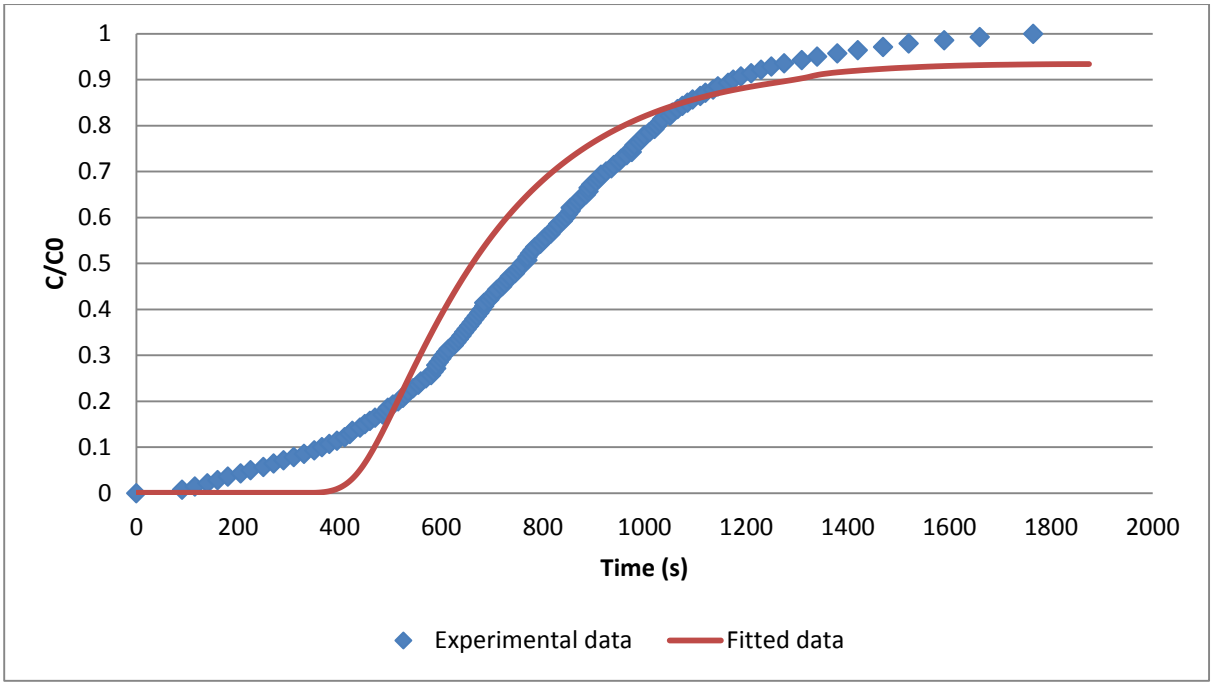

Figure II-7: Comparison of the experimental (symbols) and simulated (solid) breakthrough profiles of laminate structure number 7 from Table 7.1

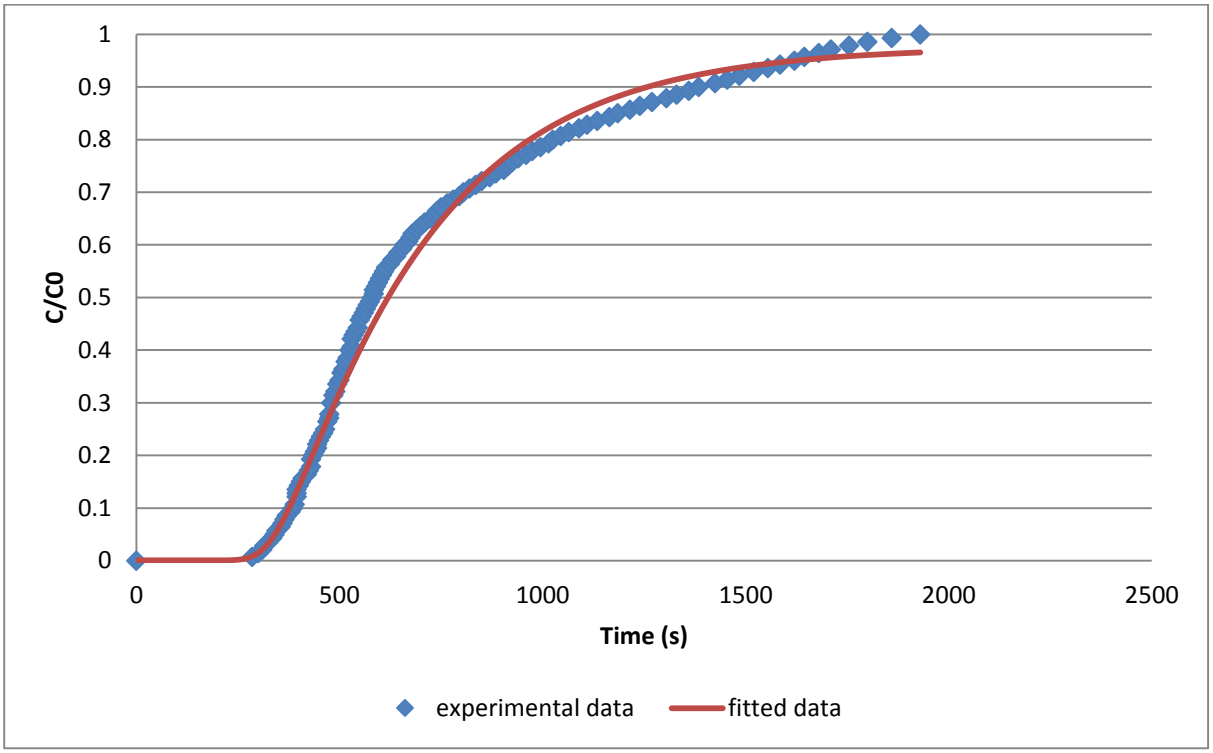

Figure II-8: Comparison of the experimental (symbols) and simulated (solid) breakthrough profiles of laminate structure number 8 from Table 7.1

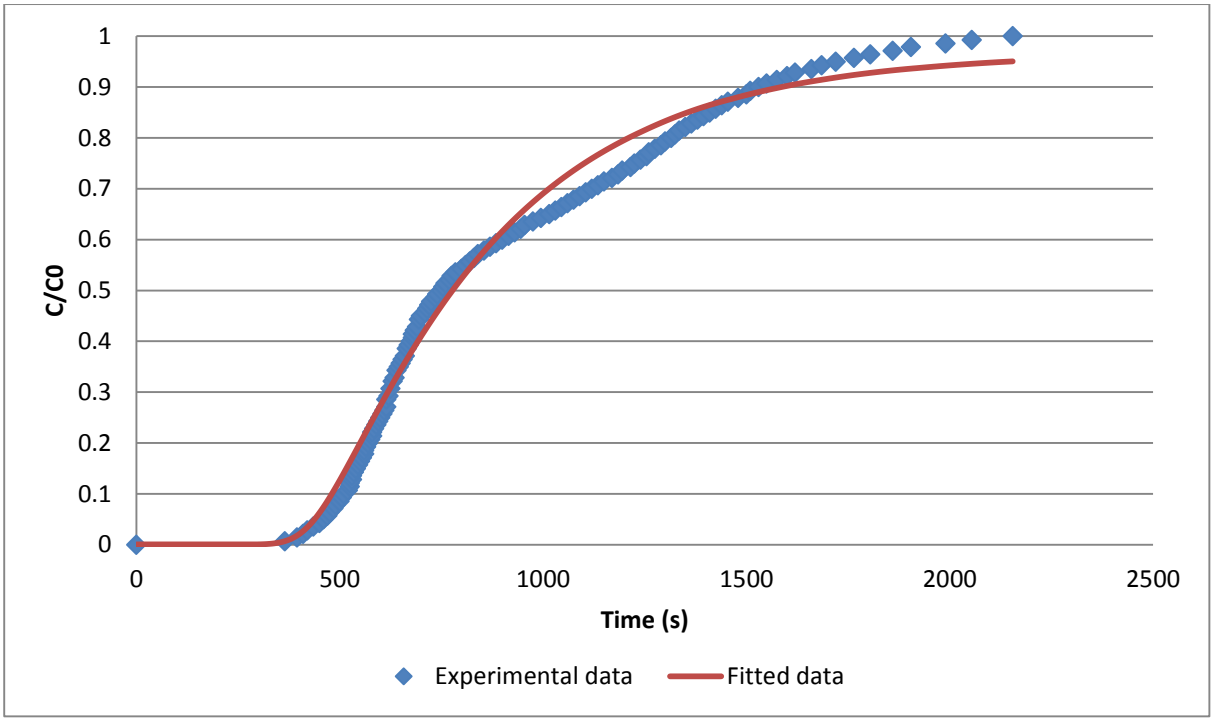

Figure II-9: Comparison of the experimental (symbols) and simulated (solid) breakthrough profiles of laminate structure number 9 from Table 7.1

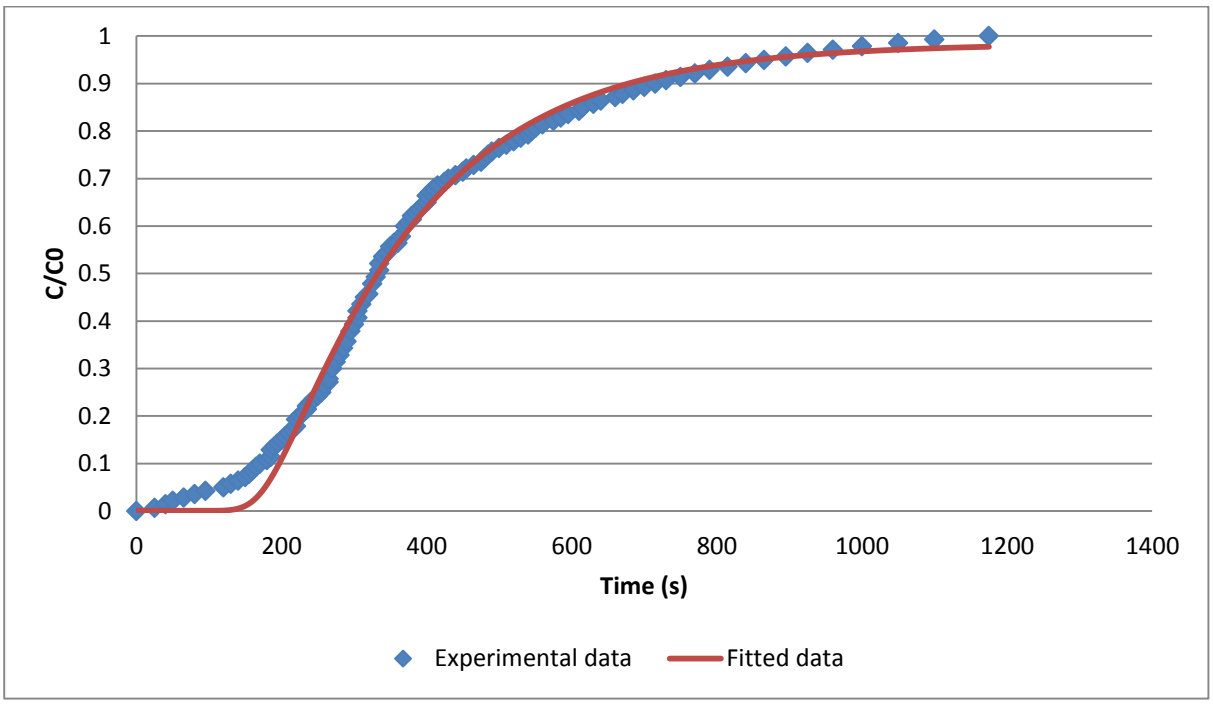

Figure II-10: Comparison of the experimental (symbols) and simulated (solid) breakthrough profiles of laminate structure number 10 from Table 7.1

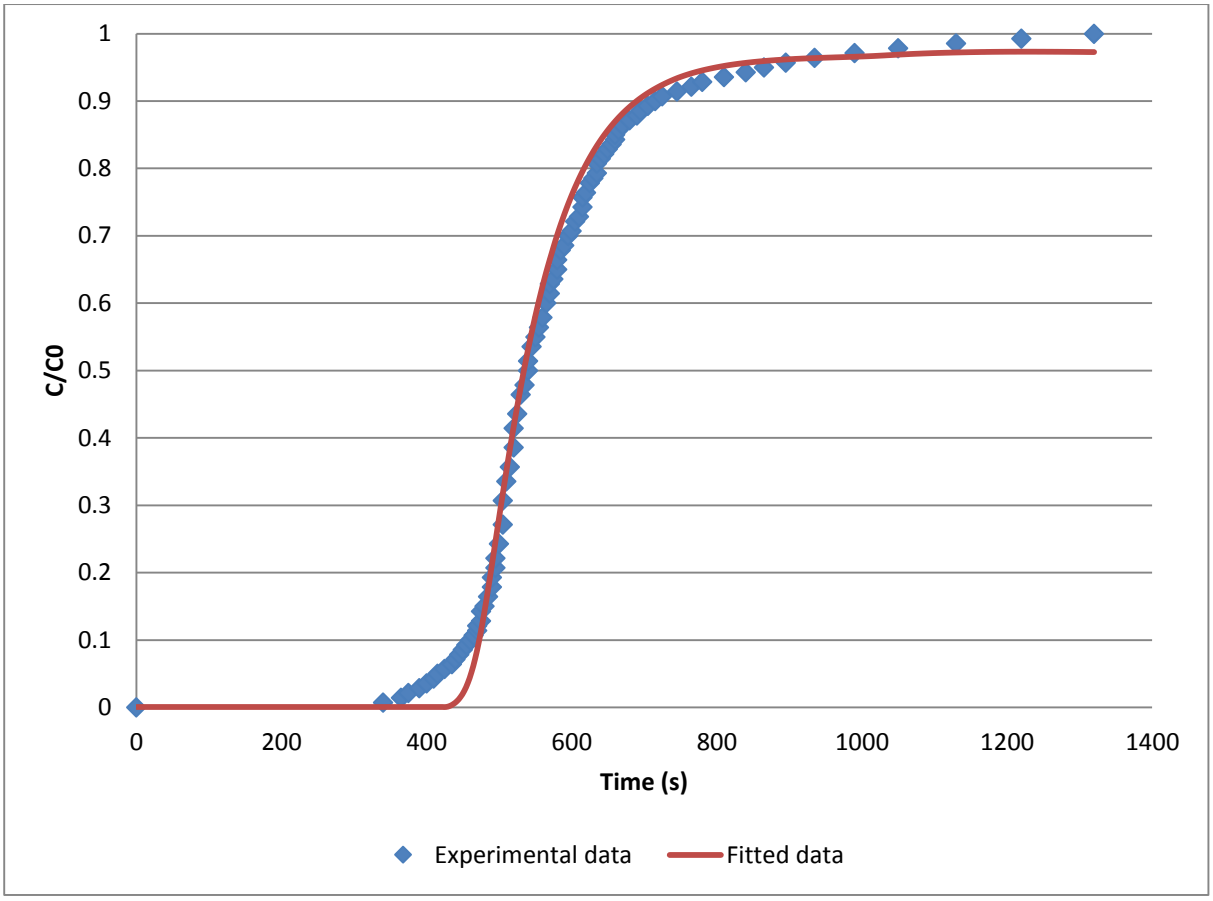

Figure II-11: Comparison of the experimental (symbols) and simulated (solid) breakthrough profiles of laminate structure number 11 from Table 7.1

Appendix III-Relevant Publications

A review on the use of zeolites to create valuable paper products and paper-like adsorbent materials

SIGAPPI NARAYANAN[1], WARREN BATCHELOR[1*] AND PAUL A.WEBLEY[2]
[1]Australian Pulp and Paper Institute (APPI)
Department of Chemical Engineering
Monash University, Clayton, VIC 3800, Australia.
[2]Department of Chemical and Biomolecular Engineering
University of Melbourne, Parkville, VIC 3010, Australia.
*Corresponding author (warren.batchelor@monash.edu)

SUMMARY

Zeolites are used for a range of applications ranging from fillers in paper for bulk, low cost applications to gas adsorbents and catalysts due to their microporous structures and high surface activity. Current adsorption technology uses zeolites in the form of beads or pellets for gas adsorption but has issues relating to increased energy consumption due to high pressure drop as well as low recovery due to mass transfer limitations. Novel non-particulate adsorbent structures have been developed to overcome these problems. These structured adsorbents unfortunately have very low loading of zeolite, thereby limiting their usefulness. In papermaking, zeolites are used as fillers primarily to improve optical properties, bulkiness, printability, and to increase retention at the wet end. This review considers these two varying applications of zeolites. The first part of the review addresses the use of papermaking techniques to prepare zeolite sheet structures using lignocellulosic fibres as a template or substrate. The advantages of such structures along with necessary improvements and further work will be discussed. The second part of the review provides a general overview on the potential use of zeolites as fillers in papermaking for various applications. We also discuss the retention and optical properties when zeolites are used as fillers in laboratory papermaking.

KEYWORDS: Zeolite, Papermaking, Fillers, Zeolite Sheet, High Density Adsorbent Structures

INTRODUCTION

Zeolites are hydrated microporous, silica-oxygen-alumina tetrahedral structures with varying applications in many fields *(1)*. Synthetic zeolites are currently being used in high end applications such as molecular sieves, ion exchangers, adsorbents and catalysts *(2)*. Many more applications in other industries are anticipated with the discovery of larger deposits of natural zeolites. The use of papermaking techniques to create structured adsorbents is an important new area of zeolite application. Current adsorbent structures such as beads and pellets have high mass transfer resistance and pressure drop while pre-formed monolith structures have a high cost associated with their preparation and low adsorbent loading present in the structure. Papermaking is a highly developed field, the methods of which may be used in creating thin, high density adsorbent sheets that will improve mass transfer and have a reduced pressure drop. The preparation of zeolite filled sheets is made much easier as they already play a role in the paper industry as fillers and retention aids in areas where natural zeolite is available in abundance. Zeolite is an unconventional product owing to its characteristic three dimensional channel shape which influences many of its properties. Fillers are used in the pulp and paper industry mainly to reduce production costs, to improve printability and runnability, for mechanical and chemical retention and to improve optical properties *(3)*. While fillers have various benefits, their addition to the pulp slurry impedes other paper properties such as reduction in mechanical strength, stiffness and increase in dusting tendency. The addition of fillers can also increase deposits in the papermaking machine and provide additional components in the white water circulation loop. Zeolites not only work well as fillers but due to their action as adsorbents and ion exchangers, they can be used to create value added paper products and help in dealing with some of the problems associated with fillers. This opens up many avenues for the paper industry to embark upon. In order to be useful as fillers, particle size and shape, size distribution, brightness and surface area are some important characteristics to be considered. As there are more than 200 framework types of zeolites currently known, the necessary zeolite can be chosen from a wide range for the required application. In order to increase the significance of the results from the previous papermaking tests, some laboratory tests have been performed in this study on the retention and optical properties to show zeolite distribution in the sheet structure and their effect on the optical properties of paper.

ZEOLITES

Zeolites are complex, inorganic polymers that have uniformly sized pores of molecular dimensions. They are defined as structures which have aluminosilicate frameworks linked to each other by sharing oxygen atoms with loosely bonded cations and water molecules in extra- framework positions *(4)*. The recent definition however excludes the constraints of composition and comprises any crystalline structure that consists of specific frameworks of linked TO_4 units where T is the tetrahedrally bonded atom in the framework. The TO_4 unit represents the basic building unit. Several basic building units are combined to form a composite building unit which could be simple polyhedral like cubes, hexagonal prisms or cubo-octahedra. A few examples of some composite building units

are shown in Figure 1 *(5)*. The final framework is an assembly of composite building units and the pore sizes range from 0.3 to 20 Å with pore volumes ranging from 0.1 to 0.35 cm^3/g *(6)*.

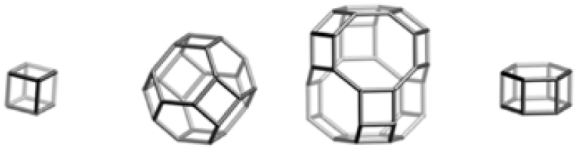

Fig 1: Diagrams of some composite building structures from McCusker*(5)* (a) Double 4-ring, (b) Sodalite cage, (c) Cha, (d) Double 6-ring

Zeolites now include structures that also have Ga, P and Ge as the tetrahedrally bonded atom. Zeolites do not come under an easily definable family of crystalline solids and can be differentiated from denser tectosilicates by the framework density (the number of tetrahedral atoms per 1000 Å) *(7)*. They are primarily classified based on their framework topology (most accepted classification) with distinctive frameworks assigned three letter codes *(8)*. The framework type describes the connectivity of the framework tetrahedral atoms in the highest possible symmetry without reference to chemical composition, dimensions of the channels system, size and shape of pore openings and the type of cation sites available, although all of these properties are very important when determining the properties of the zeolite *(9)*. As of Oct 2011, The International Zeolite Association had 201 framework type codes defined *(5)*.

Zeolites can be naturally occurring or synthesized. Natural zeolites offer only a limited range of atomic structures and properties which prevents large scale use due to stringent product specifications. Synthetic zeolites, on the other hand offer a wide range of properties but have higher cost. The cost of natural and synthetic zeolites is compared against some materials used as fillers in paper industry in Table 1*(10-12)*.

Table 1: Cost comparison of filler materials useful in the paper industry

Material	Cost [$/tonne]
Natural Zeolite	70-200
Synthetic Zeolite	430-500
Clay/PCC	130-150
Titanium dioxide	1000-3000

Natural zeolites are known to occur in very minor quantities in vugs and cavities of basaltic and volcanic rock. Previously, they could not be put to commercial use because of very low occurrence until large, mono-mineralic deposits were found for mining. Zeolites occur in nature as a result of a chemical reaction between volcanic glass and saline water at temperatures between 27 to 55 °C and pH 9 to 10 *(13)*. They are cheap and especially advantageous for bulk applications where the presence of mineral and chemical impurities is accepted to some extent *(14)*. Some of their applications are as fillers in paper, in pozzolanic cements and concrete, in fertilizer and soil as a conditioner, as dietary supplement in animal husbandry, as sorbents or support media for the immobilization of micro-organisms, in the cleanup of aqueous streams for environmental applications and as ion exchangers for cleanup of radioactive waste *(15)*. Some natural zeolites which play a significant industrial role are clinoptilolite, chabazite and mordenite.

Synthetic zeolites have more commercial uses than their natural counterpart due to high purity of product and uniformity of particle sizes. They can be engineered to have many chemical properties and pore sizes with greater thermal stability. Synthetic zeolites can be prepared from silica and alumina as starting materials which are expensive so other cheaper starting materials like clay minerals, coal fly ash, natural zeolites, municipal solid waste, industrial slags and incineration waste are sought after. The use of these precursors decreases the cost of synthetic zeolite and helps mitigate environmental problems *(16)*. Synthetic zeolites have high end applications in industries such as desiccants, adsorbents, molecular sieves, ion exchangers, catalysts and detergent builders. Synthetic zeolites that have significant industrial uses are zeolite A, zeolite X and Y belonging to the Faujasite framework, EMC-2, ZSM-5, and Gismondine.

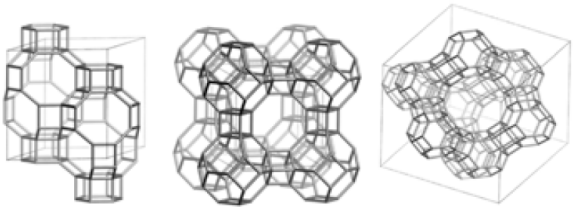

Fig 2: Different zeolite framework types from McCusker*(5)* (a) CHA framework type, (b) LTA framework type, (c) FAU framework type

The empirical representation of aluminosilicate zeolites (most industrially and commercially useful) is $M_{y/n}[(SiO_2)_x(AlO_2)_y].zH_2O$ where M is the charge compensating cation with valency n. These cations belong to the family of alkali and alkaline earth elements. The ratio x/y can have a value of 1 to infinity and z represents the number of water molecules that can be adsorbed or desorbed in the pores *(2)*. The AlO_2 bears a net negative charge which is balanced by an extra-framework univalent cation. The cations and the water molecules occupy the many intracrystalline channels and the interconnected voids present in the framework. These molecules have considerable mobility. Ion exchange thus becomes easy for the cations and the water molecules can be removed reversibly with the application of heat. The host structure has many micropores and voids which account for almost 50% of the crystal volume. The zeolite framework is a little flexible as the size and shape of the pore can change corresponding with the particular guest species present in the pore *(2)*. Figure 2 *(5)* represents different zeolite framework types. In the diagrammatical representation of these frameworks, the nodes represent the T-atoms and the lines represent the oxygen bridges *(9)*. For example, zeolite A of the LTA framework type has a Si/Al ratio of 1 which allows for strict alternation of Si and Al atoms in the structure. In the Faujasite framework, zeolite X has between 96 and 77 Al atoms per unit cell (Si/Al ratio is between 1 and 1.5) and zeolite Y has less than 76 atoms per unit cell (Si/Al ratio is greater than 1.5) *(6)*.

The four arbitrary categories that aluminosilicate zeolites fall into depend on increasing Si/Al composition. They are low, intermediate, high silica zeolites and silica molecular sieves.

Low silica zeolites have a Si/Al ratio of 1 to 1.5, intermediate silica zeolites have a Si/Al ratio of 2 to 5, high silica zeolites have a Si/Al ratio of 10 to 100 and silica molecular sieves have a Si/Al ratio > 100. The low silica zeolites are thermally stable to 700 ^{0}C and they are highly hydrophilic in nature while the silica molecular sieves are thermally stable to 1300 ^{0}C and are hydrophobic in nature *(6)*. With increasing Si/Al ratio, the cation concentration and ion exchange capacity decreases and acidity increases in strength. Low silica zeolites give optimum adsorption properties in terms of capacity, pore size and three dimensional channel systems. Low and intermediate silica zeolites find good use in removal of water from organics and in separation and catalysis of dry streams, while high silica zeolites and silica molecular sieves find use in the removal of organics from water and in separation and catalysis of wet streams *(6)*.

PAPER MAKING TECHNIQUE FOR THE CREATION OF NOVEL STRUCTURED ADSORBENT MATERIALS

The focus of current research occurring within the adsorption field is the improvement in adsorption capacity and selectivity of the adsorbent for the molecule of interest eg. CO_2 adsorption from CO_2/N_2 mixtures. In the context of CO_2 capture, capital cost is directly related to adsorption capacity and selectivity. In particular, system costs are affected by size of the process equipment, available product recovery and the amount of power consumed. These are controlled by parameters such as adsorbent loading per unit volume, mass transfer kinetics, and pressure drop. Improvement of these parameters by varying the adsorbent structures may help reduce system costs *(17)*.

Conventional beads and pellets (Fig. 3 *(18)*) have many limitations in adsorption applications including large pressure drop, increased energy consumption, increased mass transfer resistance, attrition of the zeolite and packing difficulties. In applications like rapid PSA (Pressure Swing Adsorption), the number of limitations increases because of fluidization, fluid friction and specific surface area. Reducing particle size decreases mass transfer resistance for PSA applications but other problems of high pressure drop remains in addition to rapid PSA issues. Other non-particulate, novel structures have been created to eliminate the disadvantages of the conventional beads and pellets. These structures include monoliths (Fig. 4 *(19)*), laminates, foam and fabric structures. In order to replace bead and pellet configurations, these structures must have high mass transfer kinetics, high volume working capacity, and low voidage to create a small sized adsorber and a gas flow path that produces low pressure drop *(17)*.

Fig 3: Pellet and Bead adsorbents from Sorbead India*(18)*

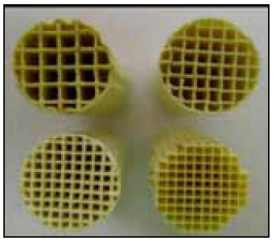

Fig 4: Monolith adsorbent structures from Moreno-Castilla *et al(19)*

Monolithic adsorbents have a continuous body which is supported and have identical channels of different cross-sectional shapes. The main limitation of monoliths is that the density of the adsorbent material available is very low due to the presence of the binder material and support material. Also, not all the adsorbent material is accessible to the adsorbate molecules which flow through the channels. The binder material is essential as it provides an inter-particle network of bridges which bond the adsorbent particles to each other and to the substrate. Without the presence of binder material, the structure is prone to high dust production and has low strength. The fraction of active adsorbent material is decreased by the amount of non-adsorbent material *(20)*.

In order to create monolith structures, extrusion processes have been applied in which the zeolite slurry is extruded through a die. These processes can destroy the porous nature of the zeolite when high extrusion pressures are applied. The rheological properties of a dispersed zeolite slurry make its application in an extrusion process extremely difficult and the extrusion costs can be quiet high. Channel width and wall thickness must be controlled for PSA and rapid PSA application and this becomes very difficult with the extrusion process. Therefore, void space was either very high when narrow wall thickness was needed or the wall thickness became very thick when a small channel height was needed *(20)*. Hence the idea of employing the well established papermaking process to create a large area honeycomb structure was used instead of the extrusion process. The zeolite sheets created by this method are expected to be lightweight, have large surface area, have a homogenous distribution of zeolite, be easy to handle and flexible to process and can have the desired thin, uniform and narrow flow channels. These zeolite sheets can then be transformed to a honeycomb shape and used to remove large quantities of NO_x and SO_x that are present in the flue gases of the power plants or be used in rapid PSA applications *(21)*.

A high density parallel channel laminate adsorbent structure can have advantages compared to conventional and other non-particulate adsorbent structures. This is because voidage can be controlled in these structures by controlling channel width, height and spacing, giving faster adsorption kinetics. Typical flow channel height for adsorbent structures ranges from 200 to 300 µm and these spacers can be created by deposition, printing, extrusion or embossing as a part of sheet fabrication. These structures can also be used in systems where the velocity of the incoming gas exceeds the fluidization of the traditional packed bed or extruded system as the adsorbent particles can be held more rigidly in place *(20)*.

The sheet making process as described by Ichiura *et al* consists of addition of cationic polymer (Poly diallyldimethylammonium chloride, PDADMAC) to the pulp, followed by inorganic fillers which are zeolite Y, glass fibres, ceramic fibres and kaolin and finally the addition of anionic polymer. Once the sheet is formed, it is dipped in colloidal silica and calcined at 700 ^{0}C for 20 minutes *(21)*. A schematic of the sheet forming process is shown in Figure 5. Here the pulp is burnt away and sintering of zeolite particles occur. The final zeolite honeycomb sheets are shown in Figure 6 *(21)*.

Ichiura *et al* report that the use of the dual polymer system showed higher retention of inorganic fillers in the sheet due to the formation of comprehensive flocs. They expect that using only cationic polymer will separate the filler aggregates from the pulp preventing a high retention of zeolite. The pulp fibre

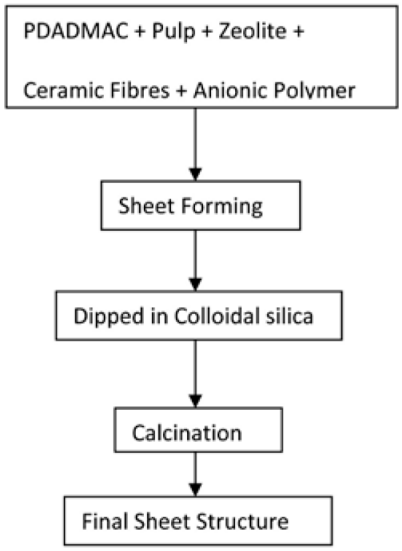

Fig 5: Schematic of sheet forming process

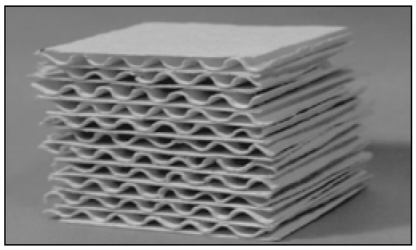

Fig 6: Zeolite honeycomb sheets from Ichiura *et al* (*21*)

was mainly used for reinforcement and for handling of the zeolite sheet to create the honeycomb structure so a pulp content of 5 to 10% was used. Any lower quantity of pulp used made it harder to remove the sheet from the wire. Linter, unbleached softwood kraft and bleached hardwood kraft pulp were compared and linter pulp was the most favourable as the inorganic retention was high when a smaller quantity of pulp was used and the drainage time was also much shorter. From this study, Ichiura *et al* have found that 5% linter pulp, 0.5%PDADMAC and 0.5 to 1% anionic polyacrylamide showed the highest retention and shortest drainage time *(21)*. In a follow-up study by Ichiura *et al (22)*, the sheet strength was evaluated after the internal or external addition of alumina sol. The internal addition method is the addition of alumina sol to the pulp slurry before sheet casting. The external addition method is the dipping of the formed sheet in an alumina sol solution. It was found that the internal addition method proved to be ineffective and the external addition of alumina sol showed a large improvement in sheet strength. Strength was further improved by increasing the content of ceramic fibres from 10% to 24.5%. When tested against beads, the zeolite sheet showed higher initial rate of moisture adsorption making them highly useful in practical applications. A further study by Ichiura *et al (23)*, has shown that sheet uniformity affects the adsorptive performance of the zeolite sheet. Their studies showed that the initial rate of adsorption of the more uniform sheet was much higher than the non-uniform sheet although no comparison was made against zeolite beads. They have also acknowledged that since handsheets were prepared, the drainage was under gravity and therefore the retention was higher and would not be comparable to a commercial paper machine.

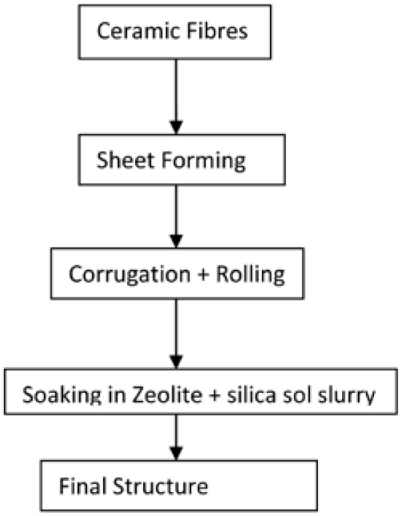

Fig 7: Ceramic rotor preparation method

Yoo *et al (24)* have synthesized a ceramic honeycomb rotor using the papermaking technique. No pulp was used in this preparation. Ceramic fibres were used to prepare a sheet which was then corrugated and rolled to form a honeycomb rotor. The ceramic honeycomb rotor was heat treated at 600 ºC for 5 hours to remove any organic binder. Then the rotor was soaked in a slurry of zeolite ZSM-5 and Y dispersed in silica sol as shown in Figure 7. This method had very low loading of zeolite because zeolite was not used in the sheet preparation process and added only when dipped in a zeolite- silica sol slurry, so there was not much retention of zeolite in the rotor structure. This preparatory method is different from the one described by Ichiura *et al (21, 22)*, the main differences being that pulp and zeolite were not used as a part of the papermaking furnish.

The main drawbacks of these zeolite sheets may be they are weak and brittle. They also powder easily and are difficult to handle. Too many components are added for sheet preparation. The ceramic rotor prepared by Yoo *et al* is more strong and flexible but the amount of zeolite present in the structure is very low. From this previous work it can be seen that there is an optimization between adsorbent content and strength of the sheet. Ichiura *et al* show no comparison against zeolite powder or beads which would give an indication of sheet adsorption properties, while Yoo *et al* show that their structure has less than 30% adsorption capacity of the powder forms

Another zeolite papermaking method is reported by Cecchini *et al (25)* where sheets structures were formed from zeolite NaY, ceramic and cellulose fibres and the dual polymer retention system using the SCAN method. Depending on the end application, only cellulose fibres were used (low temperature

applications) or a mixture of cellulose and ceramic fibres were used (high temperature applications). The high temperature sheets were calcined at 600 °C before being used for toluene removal. The authors report that the sheets containing zeolite have adequate strength before calcination, low air flow resistance and good distribution of zeolite within the thickness of the sheet. A zeolite loading of about 30% has been reported for the structure used in low temperature applications and 50% for the structure used in high temperature applications. Both structures do not show much dispersion in the breakthrough curves. No mention has been made regarding the dusting problem that the calcined structures often face without the addition of sintering agent but the calcined structures are noted to be easy to handle.
A similar sheet making technique to Ichiura *et al* was employed

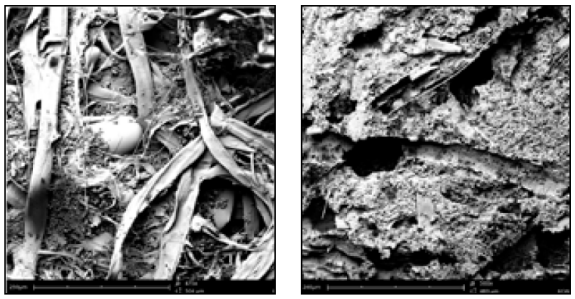

(a) (b)

Fig 8: (a) SEM of as formed sheet (26) (b) SEM of laminate structure after calcinations *(26)*

by Narayanan *et al (26)* with the exception of increased pulp fibres and pre-flocculation of zeolite A particles. The report studied the effect of variation of zeolite size, silica size, pulp type on the pore size distribution within the sheet structure by employing mercury porosimetry techniques. The use of more pulp fibres helped create a porous network for gas flow and hence no corrugation was necessary. The zeolite amount in the sheet ranged from 30 to 50 by wt% and each component used in sheet preparation affected the internal porosity of the sheet. Figure 8a shows the SEM image of zeolite and ceramic fibres filled paper structure and Figure 8b shows the SEM image of the sheet after the addition of silica and calcination. Here the structure of the sheet is preserved even after the removal of fibres by calcination.

PHOTOCATALYTIC APPLICATIONS OF ZEOLITE/TITATINIUM DIOXIDE FILLED LAMINATE STRUCTURES

A variation of the zeolite sheet was prepared by Ichiura *et al (27)*. A composite TiO_2- zeolite sheet was prepared where their combined use results in a synergistic sheet. The zeoliteY works as an adsorbent for VOCs (Volatile Organic Compounds) and the TiO_2 helps in decomposing the VOC to CO_2 by photocatalysis. The composite sheet preparatory method is similar to the zeolite sheet prepared by Ichiura *et al (21)* with the addition of TiO_2 as an inorganic component. The adsorption and decomposition of acetaldehyde was tested on the TiO_2-zeolite sheet. The composite sheet with the help of UV-irradiation decomposed the acetaldehyde after 40 minutes and continued to do so after every run. A TiO_2: zeolite ratio of 1:4 proved to be an optimum value for the continuous removal of acetaldehyde under UV irradiation. This sheet works well when there are dilute pollutants as they can become more concentrated for the photocatalytic action due to the adsorbing action of the zeolite present in the sheet. Further studies by Ichiura *et al (28, 29)* have shown the application of the composite sheets for NO_x, toluene and formaldehyde removal. With NO_x removal, the composite sheets prepared by a slightly different method seemed to produce the best results. In the final step before burning, the sheets were dipped in TiO_2 sol instead of alumina sol. The proposed mechanism of NO_x ($NO + NO_2$) removal from the sheet is that NO was adsorbed by the zeolite, which was then oxidized to NO_2 and then further oxidised to HNO_3 by the TiO_2 in the sol. The HNO_3 is then fixed on the zeolite. Compared to the other sheets that were prepared, the sheet prepared with TiO_2 sol was much faster with the oxidation reaction, and not much NO_2 was generated by this sheet. Toluene and formaldehyde are indoor pollutants and the composite sheet can be placed in the walls and ceilings of the houses where these pollutants are discharged from plywood, particle boards and adhesives from the wallpapers.
Ko *et al (30, 31)* have created a similar TiO_2 photocatalytic paper to Ichiura *et al* where they highlight the effect of zeolite not only for its adsorption of VOC but also for its effect as microparticle retention aid. A different method was considered where using sol-gel synthesis, the TiO_2 nanoparticles were anchored on the zeolite particles. These particles were then used in papermaking to create a composite sheet. This composite sheet was compared with commercial photocatalytic paper and found to perform much better as higher amounts of toluene were removed.
The previous discussion clearly shows the potential of utilizing papermaking techniques in the creation of zeolite laminate structured adsorbents. The next section delves into how zeolites as fillers in papermaking perform similarly to widely used filler systems, hence minimizing any technical barrier to wide scale, low cost production of zeolite laminate structured adsorbents.

ZEOLITE APPLICATIONS IN THE PULP AND PAPER INDUSTRY

Zeolites have many possible applications in pulp and paper processes such as fillers, retention aids and in white water treatment applications.

FILLER APPLICATIONS

Fillers are a necessary addition to paper to reduce production costs, increase printing quality and reduce the use of raw materials. Zeolites are mostly used as fillers for paper in Japan *(32)*. Figure 9 *(33)* shows the distribution of filler use in North America in 2005, where alumino-silicates represent a very small fraction. Research in the potential use of zeolites as fillers has found them useful in the following papermaking applications: i) To improve optical properties of paper as they have high brightness ii) to improve bulkiness and printability iii) to produce specialty papers such as gas filtration, anti-tarnish and photocatalytic papers due to their open structure iv) to increase the co-efficient of friction which can decrease the misfeed to copier machines and v) to reduce print through, which allows them to be used in the production of ultra light-weight coated publication papers and newsprint vi) to reduce problems with pitch and filler deposits due to their ion exchange ability *(34)*.
As described above, zeolites have various properties such as high brightness, open porous structure, controllable particle

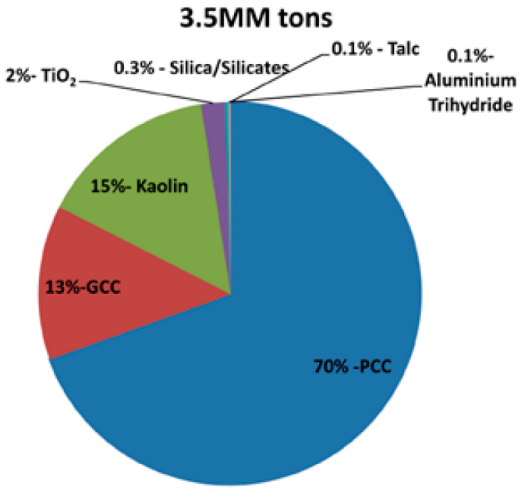

Fig 9: Filler use in North America (2005) *(33)*

size, rheology and hardness which give them the potential to replace traditional mineral fillers like bentonite (clay), GCC (ground calcium carbonate) and PCC (precipitated calcium carbonate). But zeolite filler applications must be carefully chosen as papermaking pH, temperature shocks and high metal concentrations can cause physio-chemical changes that inadvertently affect the zeolite efficiency. Fine paper is manufactured in basic pH of 8-8.5 while mechanical grades are often produced in acidic or neutral conditions. Fine paper manufacturing shows an improvement in sheet formation, retention and optical properties with the use of zeolite fillers as compared to other mineral fillers but this is not the case with mechanical grade paper. In acidic conditions, the zeolite framework is attacked as an exchange of metal cations for hydrogen ions occur and the zeolite material starts dissolving due to dealumination by release of Al^{3+} ions. Once dissolution occurs, this reaction is irreversible. Other effects due to pH variation on zeolite properties include changes to zeta potential and degree of flocculation *(35)*.

Brouillette *et al (35)* demonstrated this effect of pH by measuring conductivity with the addition of HCl. With decreasing pH, neutralization of the zeolite particle occurs and after the isoelectric point (the pH where the streaming potential becomes 0 due to the addition of acid) is reached, dealumination immediately starts occurring. For the zeolites used in this particular study, the isoelectric point occurred between pH 7.2 and pH 7.8 while the clay particles had their isoelectric point occur below pH 5. Hence, zeolite particles are not as stable when there are pH fluctuations in the pulp slurry *(35)* and thus, zeolite is more useful for fine paper production. To be used at low pH, the zeolite surface should be modified to resist dissolution. The zeolite can be made more acid resistant by increasing the salt concentrations as selectivity for the hydronium ions decreases *(35)*.

Klass *et al (34)* in US Patent No:7,201,826 B2 have shown that zeolites (clinoptilolite of size 0.5-2 microns) when used as fillers without retention aids perform admirably when compared against PCC even at high shear rates. Zeolite ash content in the sheet was 4.6% which was 2.5 to 4 times higher than PCC and the sheet formation was more uniform exhibiting improved optical properties. Since the retention of the zeolite was higher, the wet end of the machine was much cleaner. With the zeolite filled paper (45 kg per tonne), no print-through was observed when compared to PCC filled paper (113kg per tonne) which still showed severe print-through. This superior performance indicates that zeolite filled paper would be useful in the production of lightweight coated publication paper.

Quanchang *et al (32)* have mentioned that it is possible to replace talc with zeolite (clinoptilolite) for filler applications in the production of machine glazed paper, writing paper, and newsprint while at the same time reducing production costs. Although the authors claim that in most applications the zeolite filled paper showed better properties than talc, the claim is not supported by the data. Even for experiments where the authors claim that the talc performs better, the results were statistically similar. The major conclusion is that the zeolite-filled paper conformed to the industry standard. The zeolite (clinoptilolite) filled paper had similar whiteness to talc filled paper even though the whiteness of clinoptilolite is much less than that of talc. This is useful to know because talc might be more expensive than clinoptilolite due to its higher whiteness, although the quality of the final paper product is the same. The print quality of the zeolite filled paper was higher than the talc filler paper as shown by increased legibility of the picture and print with no picking and dusting. So in areas where natural zeolite occurs in abundance, zeolite can replace talc without additional equipment or changes to the process being required, therefore without extra cost *(32)*.

Ivanov *et al (36)* have shown that since zeolites have a more open structure than other fillers they can have significant additional benefits when used in filler applications as a carrier for basic dyes. Basic dyes adsorb strongly on zeolites compared to other fillers due to their large surface area as shown in Table 2 *(33)* and reduce the sensitivity of the dye to UV radiation. Zeolites,

Table 2: Specific surface area of different filler types

Filler types	SSA [m^2/g]
Kaolin (hydrous)	10-25
Kaolin (calcined)	15-25
Calcium Carbonate (ground)	2-12
Calcium Carbonate (precipitated)	3-25
Titanium dioxide	7-12
Talc	9-20
Silica, silicates (Zeolites)	45-75

when used as fillers, can also help reduce the effects of aging. Oxidation and hydrolysis reactions that occur due to Cu^{2+}, Mg^{2+}, Fe^{2+} and Fe^{3+} during the process of aging can be neutralized, reducing the loss of brightness within 96 days of artificial aging by approximately 2.5% *(37)*. The same study also showed that using zeolite instead of kaolin increased retention and tensile strength and reduced water uptake.

Unconventional uses of zeolites as fillers include their use in paper phenolic laminates to improve laminate resistance to corrosion when exposed to wet conditions. Paper phenolic laminates are used in printed circuit boards and integrated circuits as insulators, but when exposed to wet conditions they

are affected by electrolytic corrosion. Kawamura *et al (38)* have used zeolite fillers in paper phenolic laminates to increase the resistance to corrosion by improving the tracking failure. They have found that the comparative tracking index increased for copper electrodes with increasing zeolite filler content while there was no change for platinum electrodes.

When very high quality white material that has low abrasion is needed, zeolites can be used in combination with TiO_2. TiO_2 provides very high whiteness thereby improving optical properties. Since TiO_2 by itself is very expensive, other materials need to be added to reduce production costs. Rock *et al (39)* have used zeolite A in combination with TiO_2 to provide paper that has similar brightness and opacity but at lower cost when compared to the use of TiO_2 alone. The brightness of silicates (zeolites), TiO_2 and other fillers are shown for comparison in Table 3 *(33)*. For this application, zeolites must have a crystal size of less than 1 µm and a particle size of less than 3 µm, along with some modifications. These modifications include partial ion exchange and pH adjustment.

Table 3: Filler dry brightness for different filler types

Filler types	% Brightness
Kaolin (hydrous)	78-90
Kaolin (calcined)	90-95
Calcium Carbonate (ground)	80-85
Calcium Carbonate (precipitated)	95-100
Titanium dioxide	98-100
Talc	85-90
Silica, silicates (zeolite)	93-99
Alumina trihydrate	97-100

MICROPARTICLE RETENTION AID

Retention of papermaking components is a very important wet-end operation. High retention levels are required to reduce product loss and pollution thus controlling costs. Many mills are striving to reduce or eliminate their effluent. However, the small sized fines fraction readily drains through the wire and ends up in the white water. This easy drainage of the fines fraction can be reduced by adding a retention aid which enhances the colloidal retention of the fines. The fines or filler particles can form a macroparticle by attaching to each other or by attaching to long fibres thereby increasing their chance of retention. Retention using microparticles is considered to have the greatest impact on small particle retention. Microparticle retention systems include a small highly charged microparticle that is added in addition to the polymer to destabilize the colloidal particle suspension. Different microparticle systems used silica and bentonite clays as they have a high surface area and high surface charge density. Silica microparticles are expensive and the right silica particle must be chosen for differing applications. With bentonite, high purity is required for use as microparticle retention aid. Even though there are other microparticle systems being used, silica and bentonite systems have become standards for microparticle retention comparison systems *(34)*.

Klass *et al (34)* have shown that zeolite (clinoptilolite with particle size 0.5-2 µm) as a microparticle retention aid performs well against microparticle silica when similar quantities were added. This was also true with bentonite as the zeolite performed well even against a larger quantity of bentonite. The use of zeolites as fillers also eliminated the need for a retention aid system.

Ko *et al (31)* have shown that zeolites played an important role as microparticle retention aids in increasing the retention of TiO_2 nanoparticles in the preparation of photocatalytic paper. Compared to using only starch and cationic polymer, the retention of the components with the zeolite was much higher with better formation. This is because instead of fibre-fibre flocculation occurring, fibre-microparticle-fibre flocculation occurs and the microparticle also acts as a supporting substrate for the TiO_2 nanoparticles.

OTHER USES OF ZEOLITES IN THE PAPERMAKING PROCESS

Modified zeolites have shown promise to chelate metals and stabilize peroxide during the repulping process in old newspaper waste recycling. Daneault *et al (40)* have shown that zeolite-supported bleach chemicals can replace the chelants typically used to protect the peroxide from decomposition. Also these zeolite supported chemicals require less alkali and hydrogen peroxide to achieve the required brightness level. The conventional chemicals also perform better when attached to the zeolite thereby enhancing the bleaching performance of peroxide during the deinking process. This better performance creates a better chelating and stabilizing effect and can be attributed to increased contact area of the chemical with the pulp and uniform distribution of zeolite-supported chemical in the pulp. Not only does the zeolite work for the above two processes, the zeolite can also adsorb colloidal particles during bleaching and deinking thereby lowering the dissolved solid content which improves the waste water quality. If all these processes have the potential to work, there are economic gains from using zeolites in the recycling process *(40)*.

Zeolites not only have the ability to adsorb colloidal particles from white water, they also have ion exchange capacity in aqueous streams. Calcium carbonate use as a filler is limited to paper made from chemically pulped fibres with minimal lignin. This is because, when used in lignin containing paper, calcium carbonate causes pulp darkening due to their high alkalinity, which activates the lignin chromophores. When used in acidic conditions for mechanical paper, the calcium carbonate dissolves to generate free calcium ions and CO_2 gas. The free ions continue to react with the dissolved and colloidal substances present in the white water (recycled for environmental purposes) that causes deposits in the paper machine which leads to reduced quality in the final product.

Chabot *et al (41)* have investigated the use of zeolites in the white water to help use calcium carbonate as filler in mechanical grades. Here too, the zeolite 4A has a multifunctional use. It is used for ion-exchange in the white water and as replacement filler (similar brightness effect) when some of the calcium carbonate dissolves. From their investigations, Chabot *et al (41)* observed that increasing the zeolite dosage, increased the ion exchange capacity and the zeolite was unaffected by the dissolved and colloidal substances. Also the zeolite filler was easily retained and the sheet properties were only slightly affected. Brightness of the zeolite filled sheet was high, opacity was reduced, gloss was also slightly higher as this was affected

by the better calendaring response, roughness was about the same while porosity of the zeolite filled sheet was higher giving higher ink penetration during printing. Strength properties were slightly reduced when compared to the PCC filled sheet.

Effects of conductivity, temperature and pH were also studied by Daneault *et al (42)* for the same system. At higher conductivity, the residual free calcium ion concentration was lower but the zeolite efficiency was also lower. Conductivity affects the ion exchange capacity of the zeolite because a higher osmotic pressure develops in the water phase when the sodium ion concentration increases. This increased osmotic pressure makes it difficult for the sodium ion to come out of the cage, thereby lowering the efficiency of the zeolite for ion-exchange. Increasing the temperature increased the performance of the zeolite. Increasing temperature dissociates the surface hydroxyl groups on the zeolite increasing their anionic charge and dehydration makes the calcium ion smaller which allows easy access through the zeolite cages. The effects of pH show that at a higher pH, no free calcium ions are generated while at a lower pH, dissociation of filler is observed. Very low pH affects the efficiency of the zeolite due to acid attack and dissolution of the zeolite framework. Therefore, it can be concluded that this system is safe to use at neutral or slightly acidic conditions.

LABORATORY STUDIES ON RETENTION AND OPTICAL PROPERTIES OF ZEOLITES

METHOD:

Laboratory hand sheets were prepared using the Moving Belt sheet former. Two series of experiments were done.

For the retention experiments, 100 gsm (1 g) never dried unbleached kraft pulp was used to make 10 cm by 10 cm sheets using a Moving belt sheet former. 250 gsm (2.5 g) of zeolite 13X (particle size 2-4 micron) was used for the sheet forming procedure. The zeolite was first flocculated using Cationic Polyacrylamide (CPAM) added at the given concentration for 15 or 30 minutes before addition to the pulp slurry for sheet making. The sheets were then dried to capture images and see distribution of zeolite in the sheet structure. The sheets were later ashed to find zeolite retention in the sheets. A schematic of the procedure is shown in Figure 10. For comparison, sheets were also made with Schaefer Precarb 100S grade PCC with particle size 1±0.2 µm, supplied by Schaefer Kalk. The mechanisms by which CPAM improves retention through electrostatic aggregation of anionically charged particles are discussed in detail by Hubbe *(43)* and the improved performance by filler preflocculation is discussed by Mabee *(44)*.

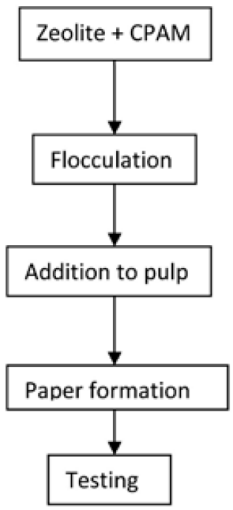

Fig 10: Sheet forming procedure for retention and optical properties

For the measurement of optical properties, 120 gsm sheets were made. Once dried bleached kraft pulp was used for sheetmaking and the sheet size was 22 cm by 22 cm. From the retention experiments, it was found that 5 mg CPAM/ g zeolite with a stirring time of 15 mins gave 100% retention with good distribution of zeolite within the sheet matrix and this quantity and time was used for the papers to measure optical properties. The zeolite content ranged from 0 to 70%. The opacity and reflectance values were measured at 700 nm using the Lorentzen and Wettre Elrepho. Using the reflectance values, the scattering coefficient and the light absorption values can be calculated using the formulae

$$a = \frac{1}{2} * \frac{(R_w - R_b)(1 + R_{w0}R_{b0}) - (R_{w0} - R_{b0})(1 + R_w R_b)}{(R_{b0}R_w - R_{w0}R_{b0})} \quad [1]$$

$$R_\infty = a - \sqrt{a^2 - 1} \quad [2]$$

$$s = \frac{1}{w\left(\frac{1}{R_\infty} - R_\infty\right)} * \ln\left[\frac{(1 - R_{b0}R_\infty)(R_\infty - R_b)}{(1 - R_\infty R_b)(R_\infty - R_{b0})}\right] \quad [3]$$

$$k = \frac{s(1 - R_\infty)^2}{2R_\infty} \quad [4]$$

where R_{w0} and R_{b0} are the reflectance factors for white and black tiles, R_w and R_b are the reflectance factors measured over white and black tiles respectively and s and k are light scattering and light absorption coefficients respectively.

RETENTION RESULTS

Figure 11 shows the sheets made from changing CPAM concentration and stirring time. Unbleached pulp was used in order to pick up visually the effects of filler distribution within the sheet. With immediate addition, large clumps are formed which reduces good sheet formation. With large concentration of CPAM, the pulp also agglomerates creating badly formed sheets. Increasing stirring times, greatly improves sheet formation and concentration of either 2 mg CPAM/g zeolite with 30 minute stirring time, or 5 mg CPAM/g zeolite for either 15 or 30 mins stirring time show the best formation with good distribution of small zeolite flocs.

Retention results (Fig. 12) show that with CPAM addition the retention is increased to more than 80% with 5 mg CPAM/g zeolite showing the highest retention for all stirring times. These retention results were compared to PCC addition to papermaking and required same amount of CPAM as zeolite for highest retention of fillers. From the formation results and

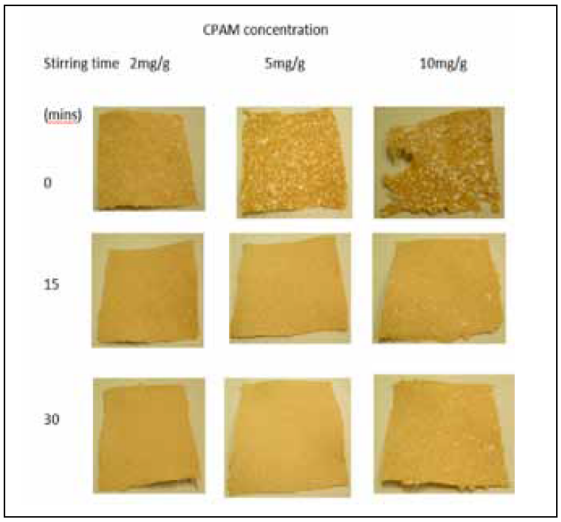

Fig 11: Images of sheets formed by varying CPAM concentration and stirring time

retention experiments a CPAM concentration of 5 mg CPAM/ g zeolite with a stirring time of 15 minutes is suggested. This process had more than 95% retention of zeolite filler. These results show that with the right addition amount of polymers, the zeolite filler can be easily retained with good distribution through the sheet matrix. Depending on the polymer and the size of the zeolite particles, the retention-formation results will vary and have to be determined for each individual situation.

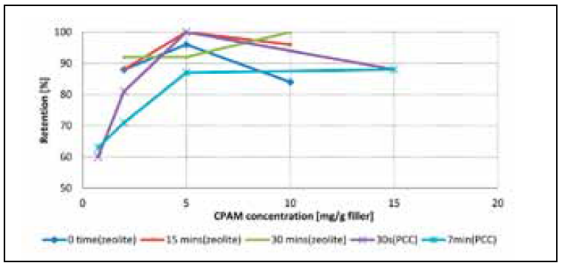

Fig 12: Retention results for varying CPAM concentration and stirring time

RESULTS FOR OPTICAL PROPERTIES:

Figure 13 shows the results for scattering coefficient and light absorption measurements for increasing zeolite weight per cent. Light absorption does not vary with increasing filler content but scattering co-efficient increases as expected with increasing filler content. Hence the paper becomes whiter and more opaque. The opacity was measured between 87 to 90 units increasing slightly with increasing filler content as shown in Figure 14. These results are similar to the findings described in the Filler application section.

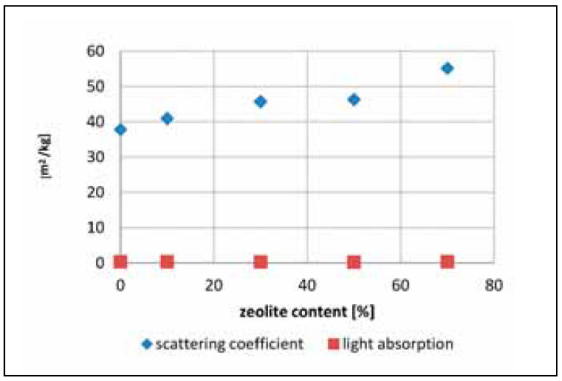

Fig 13: Scattering co-efficient and light absorption for sheets with increasing zeolite content.

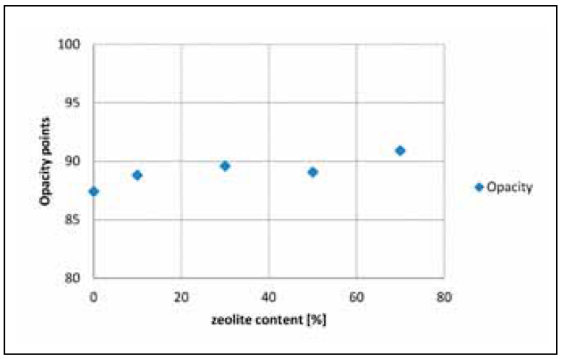

Fig 14: Opacity for increasing zeolite content

CONCLUSION

Although the use of zeolite in the papermaking process and the application of papermaking processes in the construction of novel adsorbents are in their infancy, the purpose of this review has been to gather the various reports so far and consider the potential for further investigations in these areas. It is very interesting to consider that two widely differing materials would provide a range of possibilities by their combination either in application, or by imparting their properties to further developments in the process thereby reducing process costs. Using papermaking techniques for the creation of structured adsorbents is relatively simple and cheap. To improve strength, the amount of binder will need to be increased which will reduce zeolite loading. Also further testing needs to be done on zeolite structures created from papermaking to check how they compare against beads and monoliths in terms of overall system efficiency for adsorption systems. Preparing a composite sheet of TiO_2 and zeolite combines the properties of these two materials in the adsorption and decomposition of various VOCs and NO_x gases with the help of UV irradiation, enhancing the performance of TiO_2 compared to when it is the only component present. This review has also shown that zeolites have a huge potential as fillers and can be used either by themselves or in combination with other fillers for improvements in paper properties. They work very well as microparticle retention aids and as chelating agents. But care must be taken for mechanical grade paper prepared in acidic conditions. Zeolite fillers undergo acid attack and dissolution unless some modifications are made to the zeolite structure to resist acid attack. Laboratory tests provide further evidence that zeolites can be successfully used as fillers to improve optical properties.

REFERENCES

(1) Carr, D.A., Lach-Hab, M., Yang, S., Vaisman, I.I., and Blaisten-Barojas, E., - Machine learning approach for structure-based zeolite classification, *Microporous and Mesoporous* Materials, **117**(1-2):339 (2009).

(2) Breck, D.W., - **Zeolite molecular sieves: Structure, chemistry and use**, New York : Wiley(1974).

(3) Grönfors, J., - Use of fillers in paper and paperboard grades, Tampere University of Applied Sciences http://publications.theseus.fi/bitstream/handle/10024/16226/Gronfors_Jarkko.pdf?sequence=1, (2010).

(4) Olajire, A.A., - CO_2 capture and separation technologies for end-of-pipe applications - a review, Energy, **35**(6):2610.

(5) Mccusker, L., - International zeolite association, Vol. 2012, http://www.iza-online.org/default.htm, (2012).

(6) Kulprathipanja, S., - Zeolites in industrial separation and catalysis Wiley Online Library (2010).

(7) Baerlocher, C., Mccusker, L., and Olson, D.H., - **Atlas of zeolite framework types**, Elsevier(2007).

(8) Mccusker, L.B., Liebau, F., and Englehardt, G., - Nomenclature of structural and compositional characteristics of ordered microporous and mesoporous materials with inorganic hosts (iupac recommendations 2001): Physical chemistry division commision on colloid and surface chemistry including catalysis, *Microporous and Mesoporous Materials*, **58**(1):3 (2003).

(9) Mccusker, L.B. and Baerlocher, C., - Zeolite structures, *Studies in surface science and catalysis*, **168**, p. 13, (2007).

(10) - Alibaba.Com, vol. 2012, http://www.alibaba.com/trade/search?fsb=y&IndexArea=product_en&CatId=&SearchText=natural+zeolite+powder, Ed., (2012).

(11) - Alibaba.Com, vol. 2012, http://www.alibaba.com/trade/search?fsb=y&IndexArea=product_en&CatId=&SearchText=synthetic+zeolite+powder, Ed., (2012).

(12) Song, D., Dong, C., Ragauskas, A., and Deng, Y., - Filler engineering for energy savings and improved paper properties, *Tappi Conf.* http://www.ipst.gatech.edu/faculty/ragauskas_art/technical_reviews/Filler%20Engineering.pdf, Ed.,p (2009).

(13) Fertu, D.I.T. and Gavrilescu, M., - Application of natural zeolites as sorbents in the clean-up of aqueous streams, *Environmental Engineering and Management J.*, **11**(4):867 (2012).

(14) Kallo, D. and Sherry, H.S., - **Occurrence, properties and utilization of natural zeolites. Papers from the 2nd international conference, 1985**, Budapest : Akadémiai Kiadó(1988).

(15) Mumpton, F.A., - La roca magica: Uses of natural zeolites in agriculture and industry, *Proc. National Academy of Sciences of the United States of America*, **96**(7):3463 (1999).

(16) Stancheva, K.A., Bogdanov, B.I., and Georgiev, D.P., - Synthetic zeolites. Structures, classification, properties, synthesis, industrial and environmental applications, Oxidation Communications, 34(4):792 (2011).

(17) Rezaei, F. and Webley, P., - Structured adsorbents in gas separation processes, *Separation and Purification Technology*, **70**(3):243.

(18) Laivins, G.V. and Scallan, A.M., - The mechanism of hornification of wood pulps, *Trans. of the Tenth Fundamental Research Symp.*, PIRA International, p 1235 (1993).

(19) Moreno-Castilla, C. and Pérez-Cadenas, A., - Carbon-based honeycomb monoliths for environmental gas-phase applications, *Materials*, **3**(2):1203 (2010).

(20) James, S., Khiavi, A., Surajit, R., and Steven, K. High density adsorbent structures.US Patent 20050129952 (2005).

(21) Ichiura, H., Kuboto, Y., Wu, Z., and Tanaka, H., - Preparation of zeolite sheets using a papermaking technique. Part 1 dual polymer system for high retention of stock components, *J. of Materials Sci.*, **36**:913 (2001).

(22) Ichiura, H., Okamura, N., Kitaoka, H., and Tanaka, H., - Preparation of zeolite sheet using a papermaking technique part 2 the strength of zeolite sheet and its hygroscopic characteristics, *J. of Materials Sci.*, **36**:4921 (2001).

(23) Ichiura, H., Nozaki, M., Kitaoka, T., and Tanaka, H., - Influence of uniformity of zeolite sheets prepared using a papermaking technique on VOC adsorptivity, A*dvances in Environmental Research*, **7**(4):975 (2003).

(24) Yoo, Y.J., Kim, H.S., and Han, M.H., - Toluene and mek adsorption behavior of the adsorption system using honeycomb adsorption rotor, *Separation Sci. and Technology*, **40**(8):1635 (2005).

(25) Cecchini, J.P., Serra, R.M., Barrientos, C.M., Ulla, M.A., Galván, M.V., and Milt, V.G., - Ceramic papers containing y zeolite for toluene removal, *Microporous and Mesoporous Materials*, **145**(1–3):51 (2011).

(26) Narayanan, S., Batchelor, W., and Webley, P., - Microporous-mesoporous-macroporous zeolite laminate adsorbents prepared using papermaking techniques, I*ntl. Paper Physics Conf.*,p 74 (2012).

(27) Ichiura, H., Kitaoka, T., and Tanaka, H., - Preparation of composite TiO_2-zeolite sheets using a papermaking technique and their application to environmental improvement: Part i removal of acetaldehyde with and without uv irradiation, *J. of Materials Sci.*, **37**(14):2937 (2002).

(28) Ichiura, H., Kitaoka, T., and Tanaka, H., - Removal of indoor pollutants under uv irradiation by a composite TiO_2-zeolite sheet prepared using a papermaking technique, *Chemosphere*, **50**(1):79 (2003).

(29) Ichiura, H., Kitaoka, T., and Tanaka, H., - Preparation of composite TiO_2-zeolite sheets using a papermaking technique and their application to environmental improvement: Part ii. Effect of zeolite coexisting in the composite sheet on NO_x removal, *J. of Materials Sci.*, **38**(8):1611 (2003).

(30) Ko, S., Fleming, P.D., Joyce, M., and Ari-Gur, P., - High performance nano-titania photocatalytic paper composite. Part ii: Preparation and characterization of natural zeolite-based nano-titania composite sheets and study of their photocatalytic activity, *Materials Sci. and Engineering: B*, **164**(3):135 (2009).

(31) Ko, S., Pekarovic, J., Fleming, P.D., and Ari-Gur, P., - High performance nano-titania photocatalytic paper composite. Part i: Experimental design study for TiO_2 composite sheet using a natural zeolite microparticle system and its photocatalytic property, *Materials Sci. and Engineering: B*, **166**(2):127 (2010).

(32) Quanchang, Z., Mingdi, S., Changlu, D., Huarui, Y., Qixing, Z., and Zhiguo, Z., - Use of clinoptilolite in paper industry

as filler of paper, *Studies in Surface Sci. and Catalysis*, **24**(C):531 (1985).

(33) Gill, R.A., - Tappi- introduction to wet end chemistry: Fillers for papermaking, (2005).

(34) Klass, P.C. and Sikora, D.M. High performance natural zeolite microparticle retention aid for papermaking.*United States Patent US 7201826 B2* (2007).

(35) Brouillette, F., Chabot, B., Morneau, D., and Daneault, C., - Effect of physico-chemical conditions on the properties of zeolite microparticles used in pulp and paper applications, *Microporous and Mesoporous Materials*, 70(1-3):51 (2004).

(36) Ivanov,K.,Gruber,E.,Schemp,W.,andKirov,D.,-Possibilities of using zeolites as filler and carrier for dyestuffs in paper, *Das Papier*, **50**(7):456.

(37) Ivanov, K., - Aging of paper filled with zeolite, *Wochenblatt Fier Papierfabrikation*, **126**(16):739 (1998).

(38) Kawamura, K., Aoike, N., Fumitoshi, N., and J, T., - Effects of natural zeolite filler on tracking in paper phenolic laminate, *Proc. Conf. of Electrial Insulation and Dielectric Phenomena*, p. 527, (1990).

(39) Rock, L.S. Pigment system for paper.*United States Patent US4752341* (1988).

(40) Daneault, C., Sain, M., and Grondin, G., - The modified zeoilte in waste paper recycling: Shows promise to chelate metals and stabilize peroxide in repulping process, *Pulp and Paper Canada*, **99**(7) (1998).

(41) Chabot, B. and Loranger, E., - Potentials of zeolite materials in the production of value added paper, *5th Intl. Paper and Coating Chem. Symp.*:37 (2003).

(42) Daneault, C., Chabot, B., and Thibodeau, J., - Calcium ion removal by a synthetic zeolite in the manufacture of mechanical grade papers, *Pulp and Paper Canada*, **106**(3) (2005).

(43) Hubbe, A.M., - How do retention aids work?, *Papermakers Conf.*, Tappi, p 389 (1988).

(44) Mabee, S.W., - Controlled filler preflocculation - improved formation, strength and machine performance., *Proc. Tappi Papermakers Conf.*, Tappi, (2001).

Original manuscript received 19 December 2012,
revision accepted 11 February 2013